FLORIDA STATE UNIVERSITY

FAMU–FSU COLLEGE OF ENGINEERING

SUSTAINABLE BUILDING SYSTEMS

By

JUSTIN S. KRAMER

A Thesis submitted to the
Department of Mechanical Engineering
in partial fulfillment of the
requirements for the degree of
Master of Science

Degree Awarded:
Fall Semester, 2008

The members of the Committee approve the Thesis of Justin S. Kramer defended on August 27, 2008.

Anjaneyulu Krothapalli
Professor Directing Thesis

Brenton Greska
Committee Member

Juan Ordonez
Committee Member

Kenneth Goldsby
Committee Member

The Office of Graduate Studies has verified and approved the above named committee members.

To my friends and family whose support made this possible.

ACKNOWLEDGEMENTS

I would like to thank Dr. Brenton Greska and Dr. Anjaneyulu Krothapalli for all of their guidance while conducting this research. Without their assistance, this research would not have been possible. Also, I would like to thank Mr. Robert Avant for his help fabricating the experimental setup. I would also like to thank Ms. Shannon Ingersoll for her assistance in running tests. Finally, to Mr. Connor Ross, Mr. Doug Law, and all my colleagues who have provided valuable insights, ideas, and discussions that helped me along the way, I will be forever grateful.

TABLE OF CONTENTS

LIST OF FIGURES

ABSTRACT

This work describes the design, construction and operation of a sustainable building, the Off-Grid Zero Emissions Building (OGZEB), and its subsystems. The OGZEB is a completely solar-powered building that will achieve LEED-NC (Leadership in Energy and Environment Design-New Construction) platinum certification. The 1000 square foot building is partitioned such that 750 square feet is a two bedroom, graduate student style flat with the remaining 250 square feet serving as office space. This arrangement allows the building to serve as an energy efficient model for campus designers in student living and office space. The building also serves as a prototype for developing and implementing cutting edge, alternative energy technologies in both residential and commercial settings. Hydrogen will be used extensively in meeting the energy needs of the OGZEB. In lieu of high efficiency batteries, the excess electricity produced by the building's photovoltaic (PV) panels will be used to generate hydrogen via water electrolysis. The hydrogen will be stored on-site until needed for either generating electricity in a PEM fuel cell stack or combusted in natural gas appliances that have been modified for hydrogen use. Properties of hydrogen combustion were identified and methods were developed through research in order to retrofit natural gas appliances, such as an on-demand hot water heater and cook top. The combustion aspect of the hydrogen energy storage system is unique to the OGZEB.

CHAPTER 1

INTRODUCTION

The current energy forecast shows that the world consumes around 135,633 terawatt-hours of energy per year[4]. In the last twenty-five years of the 20th century, the world energy consumption increased by a steady geometric growth rate of 2%. However, in just the first five years of the 21st century, with heavily populated developing countries undergoing their own industrial revolutions, the world energy rate skyrocketed by 50%[4]. This rapid increase in the need for energy will continue for the foreseeable future and with 87% of the world energy being derived from fossil fuels, the demand for these fuels will continue to dramatically increase[5]. When the current growth rates are applied to the fossil fuel reserves, a drastic problem arises. Figure 1.1 takes the energy content of the remaining fossil fuel reserves and applies anticipated consumption using two possible growth rates, as well as no growth. It is important to consider total energy across all fuel sources because when a source runs out, another will most likely be used to sustain the demand. For example, when the petroleum reserves are exhausted it is likely that coal will be liquefied for use as a fuel. The increases in demand, coupled with the political instability of many fossil fuel producing regions and the fact that fossil fuels are in limited supply, have caused their prices, as well as their derived hydrocarbon fuels, to rise dramatically. The prices of natural gas, propane, gasoline, and diesel have increased 5, 22, 49 and 56% respectively over the past year[6]. In addition, hydrocarbon fuels are not just getting more expensive; they also come with environmentally harmful properties.

The combustion of hydrocarbon fuels to create electricity, power cars, or generate heat for various applications produces "greenhouse" gases, such as CO_2, as can be seen in Figure 1.2. In the atmosphere, these gases allow ultraviolet light to pass through and heat the Earth, but they prevent the reradiated infrared rays from escaping, which is referred to as the

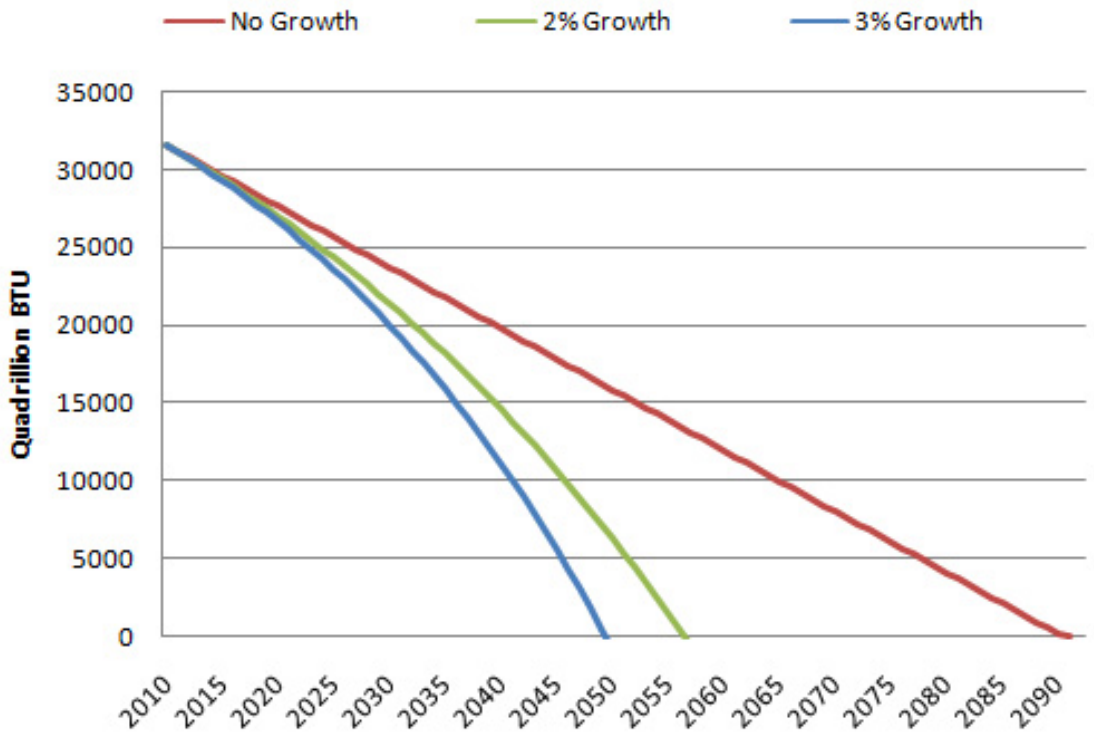

Figure 1.1: Anticipated energy content of natural gas, petroleum and coal reserves over time

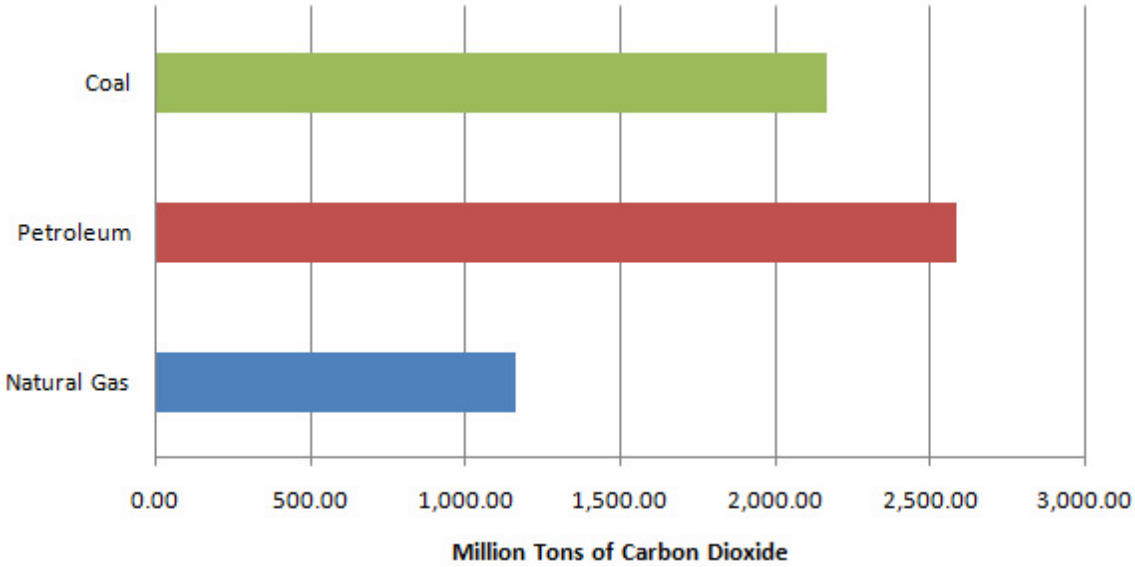

Figure 1.2: Annual CO_2 emissions by fuel type

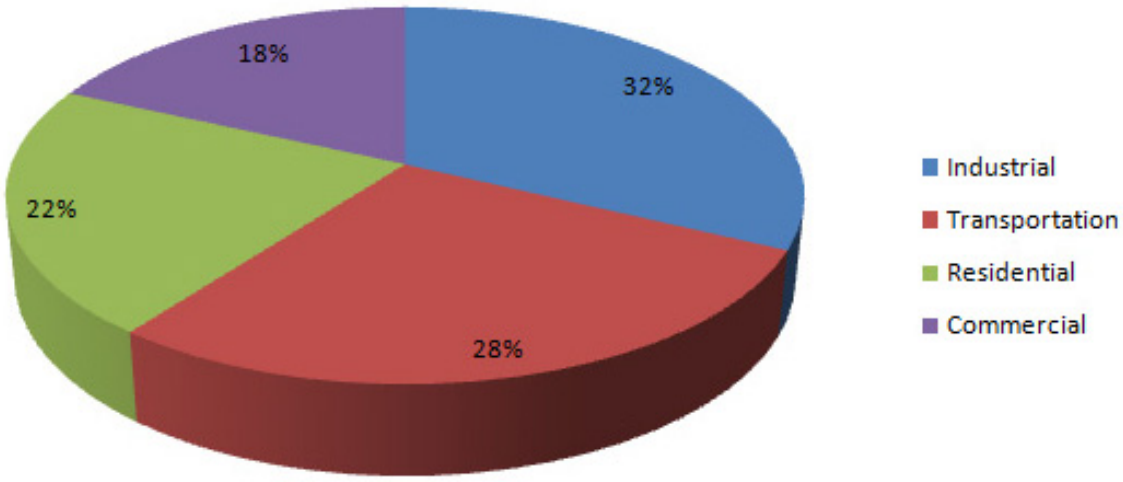

Figure 1.3: US energy consumption by sector[1]

"greenhouse effect." The process of "global warming" occurs when these gases accumulate in the atmosphere, trapping more energy and causing the temperature of the atmosphere to increase. This warming effect, has, and will continue to result in extensive environmental problems[7]. Plants and trees help to maintain atmospheric CO_2 levels but it is being emitted in much larger quantities, thus contributing to global warming. In 2005, it is estimated that the forest sector only absorbed 10% of the United States (US) of America's emissions, leaving 90% to remain in the atmosphere, thus increasing the greenhouse gas levels[8]. These negative impacts on the economy and environment have stimulated research into possible ways to reduce the use of hydrocarbon fuels around the world.

The US, which has less than 5% of the total world population, accounts for 25% of the current global energy consumption. For this reason, the US must develop energy alternatives to replace the combustion of hydrocarbons which include nuclear, wind, solar, and hydroelectric power generation and biofuels. When one examines the US energy consumption by sector, as shown in Figure 1.3, it is apparent that the residential and commercial sectors account for 40% of the total energy consumption. These sectors are essentially comprised of building technologies. Energy consumption for buildings not only requires the operational energy but also the energy required to make the materials and

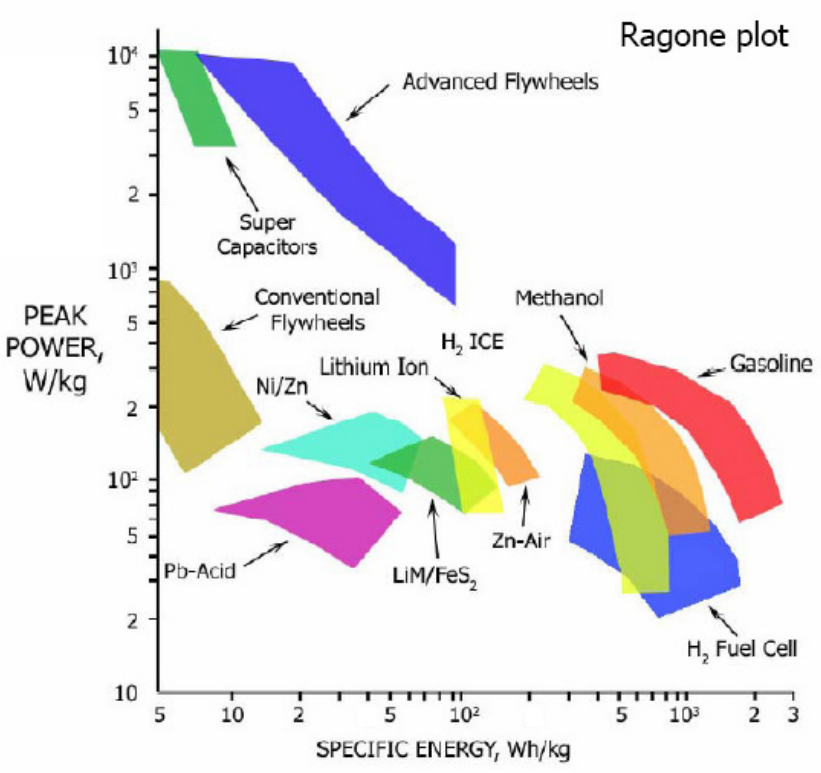

Figure 1.4: Ragone energy storage plot comparing energy densities and energy outputs of various storage mediums[2]

transport them for building assembly; thus making buildings the largest energy consumer. With that in mind, the Off-Grid Zero Emissions Building (OGZEB) was designed and built to reduce the energy consumed by buildings, from construction to operation. The OGZEB is completely independent of the electric grid and uses power generated by photovoltaic (PV) panels to provide all of its energy needs, both electric and thermal.

While the OGZEB possesses many energy efficient features, its energy storage system makes it unique. Off-grid solar systems, like the OGZEB's, require energy storage to provide energy at times when the sun is unavailable. These systems typically use an array of batteries for energy storage, but these are expensive, have limited life span and can present environmental problems. The Ragone plot shown in Figure 1.4 shows that hydrogen used in combustion or fuel cells has a peak power that is similar to that of batteries, but it has a higher specific energy, thus making hydrogen a better option than batteries for an application

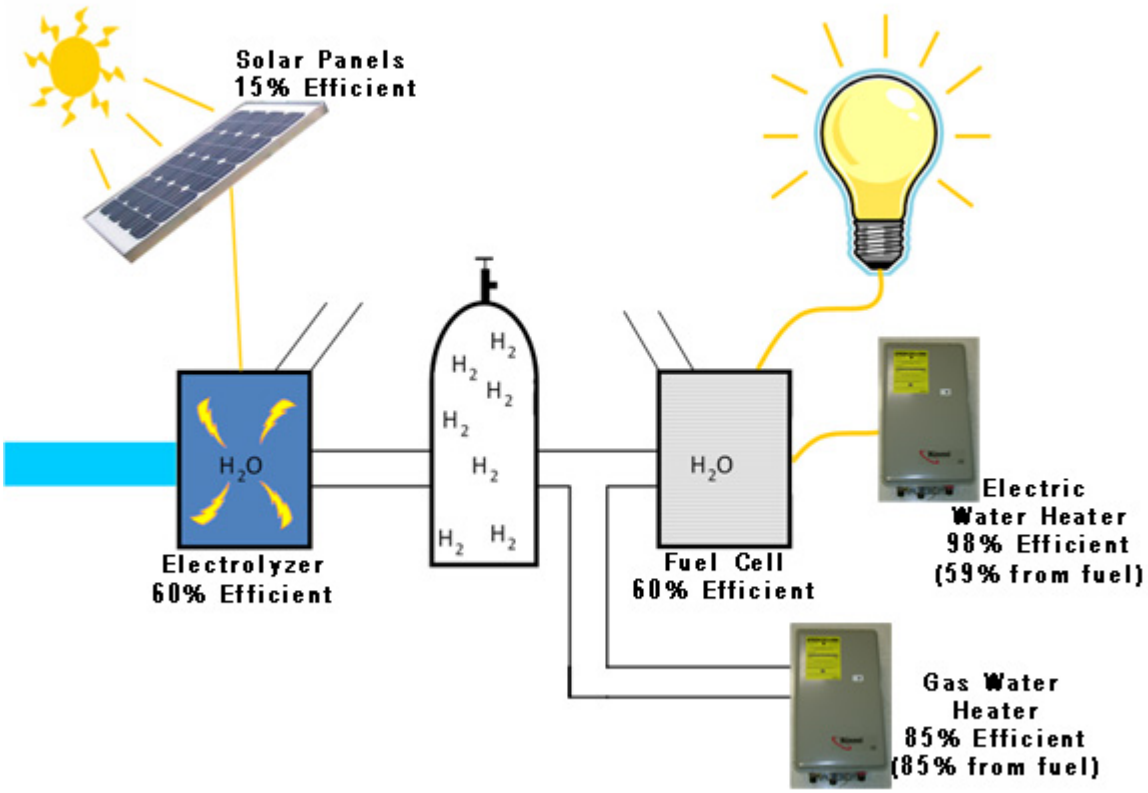

Figure 1.5: OGZEB schematic of energy system

such as a building. The OGZEB energy storage system, shown in Figure 1.5, uses a water electrolysis device, henceforth referred to as an electrolyzer, to convert the excess electricity produced by the PV panels to hydrogen that is then stored onsite. When the sun is unable to provide enough electricity for the OGZEB, hydrogen is supplied to a fuel cell to generate electricity. The concept of a hydrogen energy storage system was demonstrated by the New York Institute of Technology in the 2005 Solar Decathlon, but they only used the hydrogen to power a fuel cell to create electricity, using the electricity to power everything in the house, including heating appliances.

In residential applications, heating appliances account for 42% of the operating energy consumption of a building, as shown in Figure 1.6. Even though residential cooking and

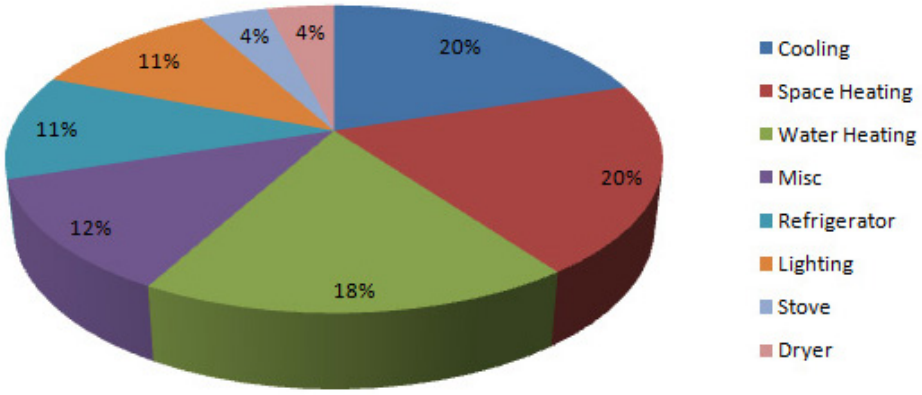

Figure 1.6: Household energy consumption by application[3]

heating are required all day long, they are least required during the peak solar hours. For this reason, only two options are available to consistently meet this need with the off-grid hydrogen storage system, as shown in Figure 1.5. The first is to use a fuel cell to convert the hydrogen back to electricity and then use it in power resistive and/or induction heating. PEM fuel cells, which are the type most commonly found in building applications, typically have an efficiency of 60% based on the higher heating value of hydrogen(140 MJ). With the average efficiency of a conventional electric water heater being around 98%, the combined efficiency of the fuel cell and the electric water heater is 59%. The average efficiency of a gas water heater is around 85%, making it 26% more efficient to directly combust the gas. When the higher efficiency of combustion and greater capacity for combustion to heat water were considered, hydrogen combustion was chosen for appliances that produce heating.

The purpose of the research discussed here was to determine the limitations and benefits of hydrogen combustion and prove that it is a viable solution for providing heat in an off-grid building. The design of the OGZEB will be examined to understand the benefits of its design, as well as to determine which appliances are best suited for hydrogen retrofit. Then hydrogen properties will be examined to develop the resources required to design the optimal retrofit technology. Finally, the hydrogen properties will be used to retrofit certain appliances that are used in the OGZEB.

CHAPTER 2

OFF-GRID ZERO EMISSIONS BUILDING

The Off-Grid Zero Emissions Building (OGZEB) can be categorized broadly under "Sustainable Housing", terminology that incorporates design principles that combine environmental, economic and societal consciousness, thus ensuring the longevity of not only the house but the environment in which the house resides. The design of the OGZEB was guided by a sustainable development framework developed by Parris and Kates[9]. A sustainable development framework was chosen based on a realization that energy concerns and environmental concerns go hand in hand. The emphasis in the present context is providing services to the house in which nature is the source of resources. As a means of measuring the overarching objectives delineated below, the benchmarks for the design, construction and operation of high performance green buildings that are provided by the U.S. Green Building Council[10], under the Leadership in Energy and Environment Design (LEED) New Construction (NC) were used.

Large amounts of materials and energy are typically embedded in the built environment of developed nations. Although energy use in housing has been studied extensively and several efficiency measures have been implemented, the environmental impacts of construction materials and processes have thus far received little attention. However, with the LEED certification system in place, the housing construction industry is slowly adopting environmentally friendly construction materials, processes, activities and designs, thereby reducing the amounts of pollution, waste generation and energy consumption. One example of this process is utilizing local materials that will reduce the energy required to transport these materials.

It is also recognized that the assessment of environmental performance and attainment of environmentally sustainable solutions require the adoption of holistic approaches. The life

Figure 2.1: Conceptual image of the Off-Grid Zero Emissions Building

cycle assessment of a residential building (house) suggests that the energy supply and usage through end use appliances contribute most to the cost. Keeping in mind the sustainability of the different energy technologies and delivered energy, abundantly available sunlight was chosen as the energy resource. The energy production and management is also carried out with no grid connection or any fossil fuel use. In this fashion, the project will achieve most of the characteristics required of sustainable housing.

Constructing a building that met the requirements set forth above involved numerous manufacturing sectors (such as concrete, lumber, flooring), building systems (such as lighting, heating, ventilation and air-conditioning) and service sectors (such as engineering and project management). The OGZEB is a demonstration of the seamless integration of these various sectors. The objective of the project is the design, construction and operation of a 1000 square foot Platinum LEED NC certified building[10], shown in Figure 2.1. The building is partitioned so that 750 square feet is a two-bedroom, graduate style flat with the remaining 250 square feet serving as office space, as seen in Figure 2.2. This arrangement allows for the building to serve as an energy efficient model for campus designers in student living and

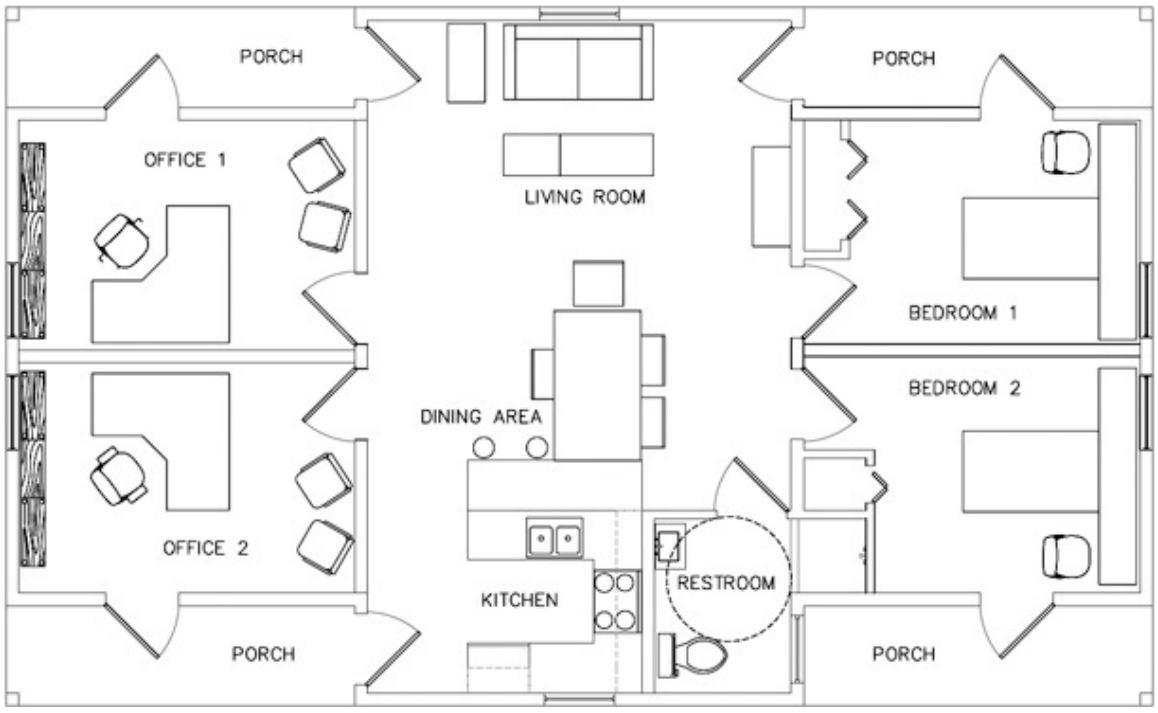

Figure 2.2: OGZEB floor plan

office space.

When approaching a building with such a broad scope, it is critical to assemble a team to tackle the specific issues and goals and insure that all are adequately met. The design and construction of this building encompassed several fields of expertise that are not typically required for the common building. A team of professionals and students was assembled to jointly design the house. The team consisted of a Mechanical Engineer/LEED Accredited Professional (AP), Innovative Architect/LEED AP, Structural Engineer, Electrical Engineer, Civil Engineer, Landscape Architect, Construction Manager and an Interior Designer. An additional Mechanical Engineer, specializing in alternative energy, was included on the team to design the alternative energy systems.

Each member of the team was drawn to the project by their environmental consciousness and desire to learn more about the LEED certification process. The team met on a weekly basis to collaborate on design concepts that would also meet the requirements for LEED points. The LEED point system was reviewed and points to be pursued were identified. The house was then analyzed system by system following the point structure of LEED as a guide,

while never losing sight of the occupants' comfort.

Sustainable design principles call for the design to be specific to the geographic region. Every region has different climatic, environmental and geological limitations and requirements. Being located in Florida requires anticipation of hurricanes, possibility of flooding, excess humidity and specific temperature ranges that must be considered in the design process. Sustainable design also calls for local materials that are either "rapidly renewable" or recyclable, in the true essence of "cradle to cradle" design[11].

In order to create a building that meets the standards of sustainable design it was important to first identify the areas that require focus and consideration while not losing sight of local benefits and limitations. It was extremely important to ensure that the house was not only environmentally friendly but was also livable and comfortable to those residing in it. This consideration does not overlook the fact that certain sacrifices are required but these sacrifices are minimized to ensure that this house is realistic and usable.

It was decided that the best way to handle this task was to split the building into several key topics with subcategories that encompass the majority of the systems, materials and uses of the house. These main topics follow the LEED requirements main point categories: sustainable site, water efficiency, materials and resources, indoor environmental quality, and energy and atmosphere. Each topic was considered separately but never without a mind to the entire building as a complete system or the location of the house.

2.1 Sustainable Sites

LEED requirements strive to return land to nature and preserve the land to ensure the health of the environment. The site that was chosen for this project was formerly a parking lot on the main campus of the Florida State University (FSU). As such it is in a dense community and within walking distance of public transportation and several key community features including healthcare, food, and entertainment. This accessibility reduces the requirement of driving and, in turn, reduces the energy consumption by transportation.

The parking lot was a combination of concrete and asphalt. These non-permeable surfaces were taken up and recycled/reused for LEED credit. On-site parking has been limited to encourage carpooling by the occupants of the building. The parking spaces that were retained used permeable pavers in lieu of concrete. These pavers provide the support that a car needs while allowing rain and plants to permeate the surface. Reserved parking has been designated

for a vehicle that is powered by environmentally friendly alternative energy.

Although the site is not much larger than the footprint of the house, it is landscaped with natural vegetation as dictated by the LEED requirements. Native landscape plants were chosen so that irrigation would be unnecessary, thus saving a considerable amount of water.

Storm water is another major concern with a building. The amount of storm water runoff generated from the site was reduced from the existing conditions by the reduction of the impervious area and addition of native vegetation. This allows for a reduction in the volume of water required to be held and treated. The storm water system is a subterranean system comprised of a corrugated pipe under a gravel bed in a trench that surrounds the house. It collects rain water that flows off the house, retaining it on-site until it permeates into the ground. This allows the earth to filter and treat the water before it reaches the aquifer. There is a pop-off that allows excess runoff to be discharged to the existing watershed during periods of heavy rainfall.

LEED site requirements also consider the roof and its "heat island" effects. Ultraviolet (UV) radiation can pass back through the atmosphere if it is reflected radiation. However, if it is absorbed by a surface it will be converted to infrared radiation. This type of radiation cannot escape the atmosphere and instead results in global warming. By increasing the amount of UV radiation that is reflected instead of absorbed and converted to infrared radiation, the ambient temperature of the environment will be less affected, possibly decreasing global warming. This is accomplished with the use of a reflective or light colored roof, such as the light tan steel roof that was used here. LEED NC requires a Solar Reflective Index (SRI) of greater than 29 for a pitch that is greater than a two foot rise for every twelve feet. The metal roof has an SRI of 46 which means that it greatly reduced the heating of the roof.

The illumination of the site surrounding the building can contribute to light pollution and can cause several ill effects on plant and animal life. By minimizing the light that leaves the house this negative effect on the surrounding habitat can be prevented. Reducing light pollution is as simple as ensuring that no lights point outside causing direct lighting of areas surrounding the house. Exterior flood lights have been avoided and exterior lights in general are used sparingly.

LEED certification also requires the reduction of pollution during construction. This

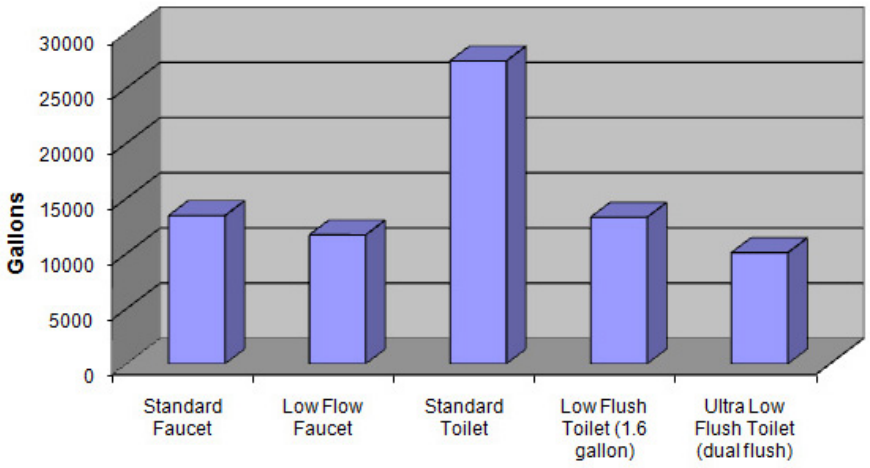

Figure 2.3: Annual water consumption for a family of four

requires the control of airborne dust generation and soil erosion. Silt-fencing was used to prevent erosion. Construction site waste was also minimized and recycled/reused when possible.

2.2 Water Efficiency

Water efficiency in the house was achieved through the use of low flow showers and sinks, and ultra low flush toilets. These fixtures save a significant amount of water throughout the year, as shown in Figure 2.3. The low and ultra low flow fixtures are monitored to ensure that a balance is reached between water savings and comfort of the inhabitants. This reduction of water also saves energy by reducing the amount of water that needs to be heated by the water heater.

2.3 Materials and Resources

Sustainable design requires that materials for the house be local, renewable or recyclable, and environmentally friendly to produce, maintain and dispose of. These principles minimize the environmental impacts of the building materials. The first aspect of the house for material consideration is the foundation. Recycled concrete was chosen for the foundation to prevent the waste concrete from being dumped into landfills.

Certified wood was chosen for most of the floor truss system and interior walls. Certified

wood comes from specific growers that adhere to Forest Stewardship Councils (FSC) Principles and Criteria for wood building components. The certificate is given to growers that adopt environmentally and socially responsible forest management practices. The wood for the OGZEB came from a grower that is within 500 miles of the house site, in accordance with the USGBC's LEED certification.

The exterior walls and roof structure were constructed with structurally insulated panels (SIPs) that are comprised of an expanded polystyrene (EPS) panel sandwiched between two sheets of oriented strand board (OSB). The EPS foam cores used in SIPs are made of mostly air and very little petroleum. "The average SIP home saves nineteen times the energy it took to make the EPS insulation in the first year of installation. The OSB used in SIP skins is made from small, plantation grown trees that can be sustainably harvested. Because engineered wood products use wood more efficient than sawn lumber, it requires less forest acreage to build a SIP home than a conventional wood framed house."[12]

The exterior siding is comprised of recyclable aluminum panels while the interior drywall is gypsum that is green certified and recyclable. The flooring for the house is primarily bamboo, with tile in the bathroom. Bamboo is classified as a rapidly renewable resource based on its rapid growth and, ironically, it is considered a weed in most of the world. It is also a local resource in Florida.

A plan was implemented to reduce the amount of construction waste that ends up in the landfill. For LEED certification 75% of the construction waste must be recycled or reused. This was accomplish by partnering with a construction waste recycling center that provided dumpsters, that upon collection, were sorted and all materials were recycled or reused. This allowed for 100% of the construction waste from the OGZEB to be diverted from the local landfill, reinserting it into the manufacturing process.

2.4 Indoor Environmental Quality

Reducing the impact of the construction process on the environment is necessary not only during construction, but also in the transition from construction to occupancy. A program was implemented to reduce the amount and impact of airborne contaminants resulting from construction on the future occupants of the house. This program included protecting the HVAC system by sealing ductwork during construction to eliminate containments. Absorptive materials, such as gypsum wallboard and insulation, were protected from

contamination by phasing the installation of these products so that they did not absorb contaminants from other phases of construction. This program worked in conjunction with the specification of materials with low toxicity levels, which could impact construction workers and occupants. Prior to occupancy, the HVAC system was used to flush-out any remaining airborne contaminants in the building, thus providing a healthier environment for both construction workers and occupants.

Indoor air quality sensors are used to monitor every aspect of the comfort and conditions of the house. Humidity and temperature are controlled to ensure that the design meets the requirements of the Solar Decathlon for comfort while other levels, such as CO_2, CO, hydrogen, and other organic gases, are monitored for safety. This system provides real-time data that can be observed via the Internet.

2.5 Energy and the Atmosphere

2.5.1 Energy Generation and Storage

The first section of the Energy and Atmosphere LEED category is the process in which the house acquires energy. The house is powered exclusively by the sun in the form of photovoltaic (PV) panels and solar thermal heat absorption. The PV panels directly convert sunlight into electricity at an efficiency ranging from 10%-15% but they are typically expensive with a long payback period. However, in the process of converting the sun's energy to electricity there are no CO_2 emissions and no adverse effect on the atmosphere. Although PV technology was discovered in 1839 and the first solar cell was made in 1941, until recently it was not widely enough accepted to develop the true economy of scale required to make it a viable product. There are companies that are implementing processes and designs that will drastically reduce the cost of these panels. The dependence on PV panels to power the house, as well as LEED certification, required the team to maximize the energy efficiency of individual components of the house.

The house uses a six kilowatt (kW) PV array. A similar array has been assembled at the FSU College of Engineering and has been characterized as to its electricity production. The array produces 7.1 megawatt hours of electricity per year, an amount that more than covers the energy consumption of the OGZEB due to its energy efficient design. The roof is also designed specifically for solar panels. The roof's pitch is 7-12, providing a

30 degree inclination for the solar panels, thus matching the latitude angle and optimizing their performance.

When designing an off-grid house, an energy storage system must be selected that can take excess electricity not immediately used by the house and store it for night hours and cloudy conditions. The typical storage system is a rather large and expensive array of batteries. However, the energy storage system for the OGZEB is a hydrogen based system. The first step of the hydrogen energy storage system is the electrolysis of water with excess electricity from the solar panels. A new catalyst has been developed at FSU that greatly improves the efficiency of water electrolysis while also allowing for the use of less expensive metals for the electrodes. With the ability to use inexpensive materials, like stainless steel, for the electrodes, the capital cost of electrolysis devices will drop significantly. The hydrogen that is generated will be stored in a tank until electricity is needed. Upon demand, the hydrogen will be released to a fuel cell where it will mix with the oxygen in the air, thus creating water and electricity. Hydrogen will not only be converted to electricity but will also be burned when heating is required. This system will not suffer from the limited life of batteries and the chemicals required for the catalyst are nonpolluting. In fact, the chemicals that are used are considered by the EPA to be safe enough to pour down a household drain.

2.5.2 Energy Use

Energy efficiency was first analyzed to ensure the minimum amount of electricity would be required to provide a comfortable living environment. When considering efficiency, each "energy consumer" in the house was carefully evaluated with different options considered for each item in order to reduce the amount of energy required.

The first system considered was the heating, ventilation and air conditioning (HVAC) system, which is the largest energy consumer in most houses. A variable speed, closed loop, ground source heat pump was selected because it consumes half the energy of the traditional air source heat pump. Ground source heat pumps employ a standard refrigeration cycle to transfer heat from the conditioned space to the ground using water as a heat transfer medium. The selected system consists of a residential grade heat pump having an Energy Efficiency Ratio (EER) of 30, a water pump, and a closed-loop polyethylene pipe system was used. The piping system can be either run down a series of wells or shallow-buried around the site. A vertical geothermal system that consists of three interconnected loops. Each loop

consists of three vertical bores that extend to an average depth of 22 meters (72 ft), was installed because the truncated site did not allow enough length for a horizontal installation.

Although this is a very efficient system, several alterations have been made to the house to minimize the drain of the HVAC system on available power supplies. The first alteration was an improvement of the actual envelope of the house over traditional houses. Insulation with a high resistance (R) value reduces the losses by the house, thus requiring a smaller load on the HVAC system and saving energy. SIPs were chosen for their high R-value foam and lack of studs, which prevents direct conduction of heat into or out of the house. The thickness of the SIPs was also important. A 152.4 mm (6 in) thickness (R24) was chosen for the walls and an 203.2 mm (8 in) thickness (R30) for the roof. These R-value ratings are misleading for comparison with common wood frame construction due to the fact that the studs of a wood frame wall have a different R-value than the insulation. Typically the R-value is 1.4 per 25.4 mm (1 in) of the stud compared to that of 3.14 per 25.4 mm (1 in) of fiberglass insulation. The typical 152.4 mm (6 in) wall has an actual R-value of 16.37 instead of 17.27, the typical assumption. Taking the studs into account, the SIPs wall is 32% more efficient than the R16.37. SIPs also seal better than the average stick built house. This seal reduces air infiltration by 95%, as can be seen in Figure 2.4. Air infiltration allows for the unwanted escape of conditioned air from the house, increasing the load on the HVAC system. Also, windows account for a large part of heat transfer in the house. Double Pane, Low E windows were chosen because of their high insulating properties.

The OGZEB was also designed in the traditional "cracker style" of Florida. Cracker houses optimize the characteristics of Florida living to provide the most livable solution for the climate of the region. This type of design involves high ceilings, as well as porches and overhangs. The high ceilings allow for hot air to rise and escape through high windows in the hot summer months while the porches provide shade, cooling the air and creating a convective air flow in the house. Overhangs were also designed to optimize the sun throughout the year. The sun has a 60 degree average inclination with a variation of ± 23.45 degrees depending on the season. Overhangs were designed such that they produced an angle of 30 degrees with the wall of the house about the base of the window, where the house is one leg, the bottom of the window is the vertex and the line created the bottom of the window and the tip of the overhang, as seen in Figure 2.5. This overhang provides shade in the summer and direct light in the winter.

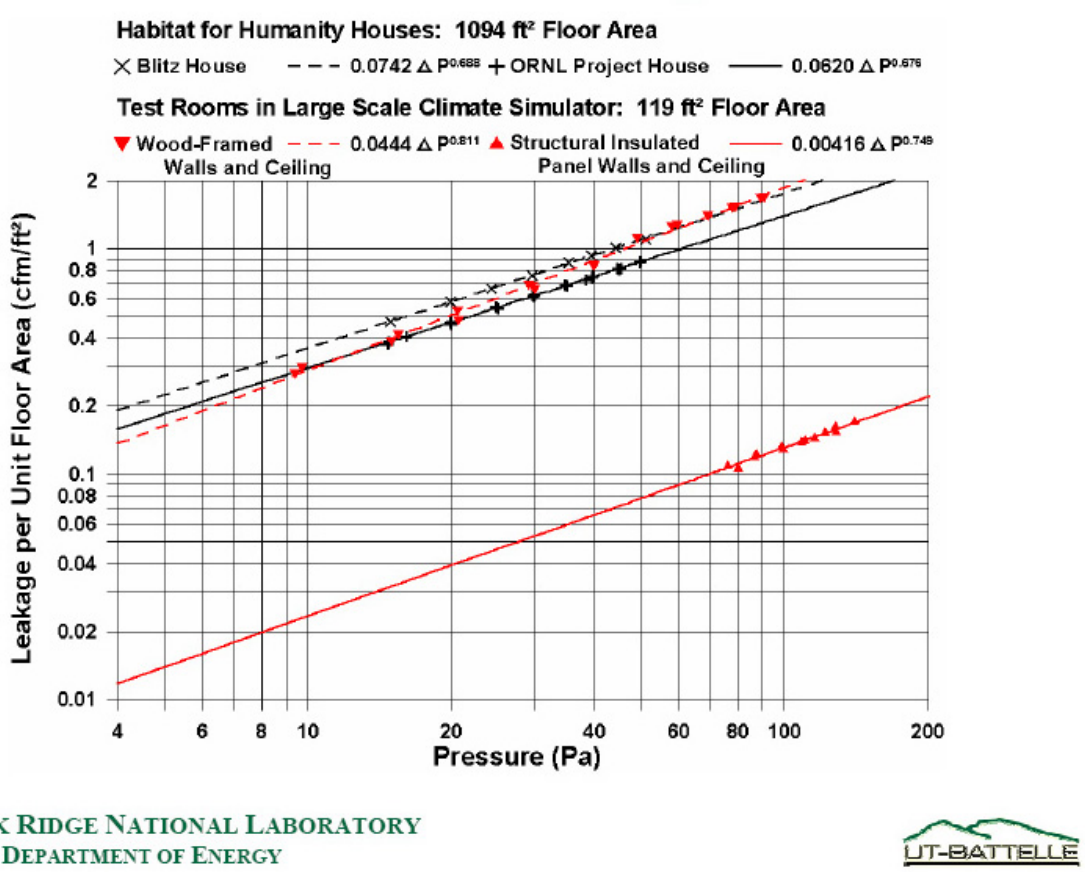

Figure 2.4: Air infiltration of SIPS construction compared to that of common frame construction

The ducting of the HVAC system is located in the insulated envelope of the house to reduce the thermal losses. The supply air discharges into the spaces high on the wall. The return air intake is close to floor level and near the center of the house to allow even air movement through the house and minimize uncomfortable temperature gradients.

The HVAC system itself was enhanced to minimize energy consumption through the use of advanced direct digital controls (DDC). The DDC system employs a series of self-tuning control sequences that control every powered system component. With temperature, humidity, and occupancy sensors feeding real-time data, the DDC building controller operates only those components required to maintain the required space conditions. For example, during periods of cooler weather, the supply fan speed reduces to match the reduced cooling load. There is a possibility of making the system even more efficient for the house by

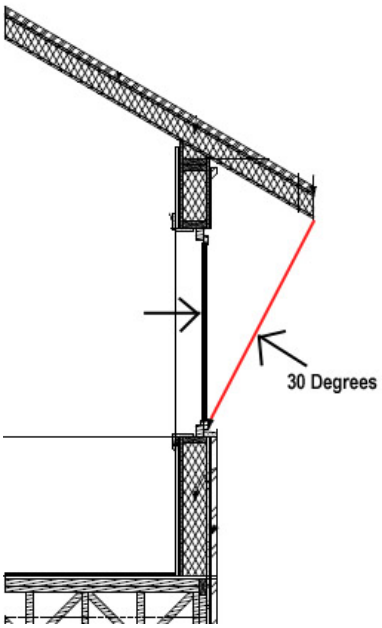

Figure 2.5: Overhang design: shows design consideration for overhangs specific to Tallahassee's latitude

retrofitting all of the motors to operate on direct current (DC), thus allowing for inversion losses to be avoided.

Lighting is another large consumer of electricity in a house. In order to address the efficiency of the lighting system, light emitting diodes (LEDs) were chosen as the primary light source. These lights are extremely efficient and produce more lumens per watt than incandescent bulbs.Day lighting will also be used to minimize the amount of false light required during daylight hours. The "cracker style" allows sun to come in the top windows and shine through the glass that makes up the top five feet of the interior walls. This light will also assist in the mood of the occupants of the building as it has been shown that sunlight positively affects peoples mood and aides in healthy living .

Water heaters are one of the largest energy consumers that generate heat. There are several solutions that, when used in combination, can bring the energy consumption for water heating to a minimum. One solution is the addition of a roof integrated solar thermal system. The chosen system has a 120 square foot thermal collector and a 250 gallon storage tank, which is located under the house. This system pipes the water up to the roof and through a panel that allows the water to absorb the heat before piping it back to the 250

gallon tank. The 120 square feet of collector absorbs 102,000 BTU of heat per day. Since, there are times when the solar thermal system is unable to produce the water temperature that the occupant desires, an on-demand gas water heater has been added to raise the temperature of the water to the occupants desired temperature. With the energy storage system using hydrogen as the medium, the on-demand gas hot water heater was retrofitted to burn hydrogen. This retrofit was preformed on all appliances that burn gas, such as the range, water heater and outdoor grill. The combustion of gas is more efficient at generating heat than using electric resistance, especially when there are no negative byproducts as is the case with hydrogen.

CHAPTER 3

HYDROGEN APPLIANCES

3.1 Introduction

To develop a replacement for hydrocarbon fuels, such as propane and natural gas, it is best to understand how they are formed and used. These fuels are a form of energy storage with an extremely long lifecycle. Millions of years ago plants used water, energy from the sun and CO_2 to form sugars and grow as carbon-based structures. When they died, there were no organisms to break them down, so they were buried and over time they became what we currently know as fossil fuels, which are then processed to become hydrocarbon fuels. The energy stored in these fuels can be used to produce electricity, power cars and create heat.

The solution discussed here supplants the hydrocarbon energy system with a much shorter life cycle through the use of photovoltaic (PV) panels. PV panels convert energy from the sun directly into electricity, replacing; the plants needed to convert energy into sugars, the thousands of years needed to convert those sugars into fossil fuels and the process that converts those fossil fuels into electricity. This direct conversion of energy can be used to power applications that use electricity. Excess electricity can be stored in the form of hydrogen through the use of a water electrolysis device, hereafter referred to as an electrolyzer, by splitting hydrogen from water molecules. Hydrogen is an energy storage medium because it does not naturally occur and when it is exposed to oxygen in an oxidation process, it wants to bond with oxygen, releasing energy. If this process is prevented by storing compressed hydrogen in tanks, the stored energy is not released. The energy stored as hydrogen can then be converted back to electricity in a fuel cell at times when the sun is unavailable and it can be combusted to power vehicles or for heating or cooling demands.

Currently, the predominant method of hydrogen production is steam reformation of hydrocarbon fuels, with only 4% of hydrogen being produced by water electrolysis[13].

Table 3.1: Flame Temperature and Fuel Energy Content[14]

Fuel	Heat of Combustion(MJ/kg)	Binary Diffusion Coefficient	Radiant Emission(kW/m^2)	Spark Energy(mJ)
Hydrogen	121	0.7975	0.3	0.02
Natural Gas	50	0.5	1.1	0.48
Propane	46	0.11	4.26	0.39

Equation 3.1 represents the process of breaking the bonds of the water molecule during electrolysis. It should be noted that no greenhouse gases are produced in this process. The reverse of this process occurs in a fuel cell to generate energy in the form of electricity.

$$2H_2O(liquid) + 474kJ \Longleftrightarrow 2H_2 + O_2 \tag{3.1}$$

This research focuses on understanding the properties of hydrogen combustion and applying these properties to appliances that generate heat. As shown in Table 3.1, hydrogen burns hotter, has a lower spark energy and has a higher energy content per unit mass than propane or natural gas. With this greater energy content, less hydrogen is required to obtain the same thermal output as propane or natural gas. This table also illustrates the higher diffusion coefficient and lower radiant emission of hydrogen, which will be discussed later.

The following equations illustrate the chemical processes that occur during the combustion of hydrogen and hydrocarbon fuels. The hydrogen molecules combine with oxygen to create water vapor. Propane (C_3H_8) and natural gas (CH_4) are combinations of hydrogen and carbon and, in the presence of oxygen, will combust to create water vapor, as well as carbon dioxide. Aside from being a greenhouse gas, CO_2 can also cause serious health issues if not vented properly.[14]

$$2H_2 + O_2 \Longleftrightarrow 2H_2O + heat$$
$$CH_4 + 2O_2 \Longleftrightarrow CO_2 + 2H_2O + heat$$
$$C_3H_8 + 5O_2 \Longleftrightarrow 3CO_2 + 4H_2O + heat$$

To better understand hydrogen combustion, one must be aware of the two types of combustion that exist; premixed flames and non-premixed, or diffusion, flames. In a

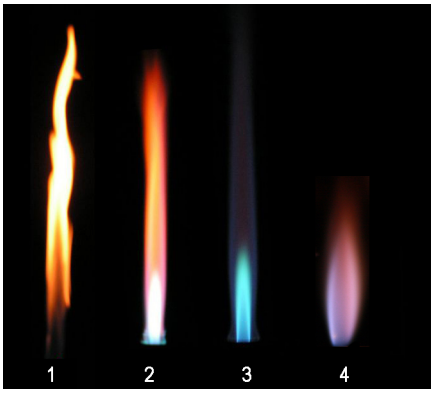

Figure 3.1: Illustration of various types of premixing:1)Hydrocarbon, no premixing, 2) Hydrocarbon, 50% premixing, 3) Hydrocarbon, 100% premixing, 4)Hydrogen no premixing

premixed flame the fuel and the oxidizer are mixed on an atomic level prior to combustion, thus allowing combustion to occur at multiple locations simultaneously. Internal combustion engines are an example of a premixed flame where the fuel and the air are mixed and then ignited. In a diffusion flame the air and the fuel are mixed at the site of combustion causing the flame to spread in a wave type manner. A candle is a good example of a diffusion flame, where the fuel and the air mix at the point of the wick and combust[14]. Most devices have a combination of both flames during combustion.

Premixing allows the molecules of the fuel to have better contact with the oxygen in the air, providing more efficient combustion. To better understand the effects of premixing it is useful to study it at different levels. Bunsen burners provide a good example of this as they allow the effects to be observed for a set amount of premixing. As shown in Figure 3.1, the more premixing that occurs the more efficient the flame, as indicated by the bluer color. With a higher diffusion coefficient than the other hydrocarbon fuels, hydrogen operates as a diffusion flame with the same efficiency as a premixed hydrocarbon flame. Therefore, the design of an efficient hydrogen burner can be accomplished without the need for a premixing apparatus.

One of the biggest drawbacks to hydrogen combustion is the negative public perception regarding its safety. Since the 1937 crash of the Hindenburg, hydrogen has had one of the most negative public images of all fuels. After 20 successful transatlantic flights during the preceding year, the Hindenburg, which was inflated with hydrogen, crashed during landing

on May 6, 1937. For 60 years, hydrogen was blamed for the death of 35 of the 97 people that were on the Hindenburg that day. It has since been hypothesized that the coating used on the Hindenburg, having the same chemical composition as thermite, was to blame for this epic tragedy[15]. The footage of the crash shows violent flames resembling that of thermite combustion, while hydrogen burns primarily outside the visible spectrum and is, at best, light blue. Even though hydrogen had no positive effect on the crash of the Hindenburg, it is unlikely that it was to blame for this disaster.

The safety of hydrogen gas goes far beyond the lack of harmful byproducts to that of molecule size. The hydrogen molecule, being significantly smaller than that of propane or natural gas, is the lightest of all gases, even lighter than air. This allows the hydrogen to rise up and away from people, while propane and natural gas sink, displacing the air and possibly resulting in the suffocation of the residents. The small molecular size of hydrogen causes it to have a high diffusion coefficient, as shown in Table 3.1, allowing it to rapidly diffuse in air rather than displacing it. Propane and natural gas, with their larger molecular size and smaller diffusion coefficient, displace air and build up into a cloud of gas, which flares up when ignited. Additionally, hydrogen's size allows it to escape through the smallest of gaps and naturally occurring spaces; gaps that propane and natural gas would be unable to pass through.

In order to use hydrogen gas as a safe and efficient fuel for residential combustion several properties must first be understood. The first, and most important, is the ability to prevent combustion of hydrogen that has yet to exit the burner orifice. The process of combustion following the gas into the burner and back to the source is referred to as "flashback" and can be prevented by knowing the quenching diameter of the gas. If the diameter of the orifice is smaller than the quenching diameter, then the flame will not pass through the orifice.

The determined quenching diameters were found to vary due to the differing properties of each of the gases. The published literature has primarily focused on hydrocarbon gases, with no reference given to the quenching diameter of hydrogen. However, the quenching distance of hydrogen was found to be 0.6 mm ($\sim$ 0.024 in)[16]. Quenching distance was observed by increasing the distance between two parallel plates, which served as the orifice of combustion, until the flame flashed back. The final distance observed just prior to the flashback is considered the quenching distance. The quenching diameter has been observed to be approximately 1.4 times that of the quenching distance of each gas[17]. As such, the

quenching diameter for hydrogen can be approximated as 8.4 mm (0.33 in).

The properties of hydrogen combustion are the building blocks needed to design the optimal hydrogen burner for a specific application. Understanding these properties will allow the burner to harness the benefits of hydrogen and design around its limitations. The thermodynamics of the hydrogen flame must be analyzed to ensure the heat transfer of the flame is optimized for the specific application. Schefer[18] researched relationships between fuel of a flame and the irradiative properties of the flame and he provided a method to calculate the radiant fraction of a flame based on the fuel. Radiant fraction is the percent of energy emitted by the flame in the form of radiation. In certain applications, like on-demand heating, thermal transfer in the form of omnidirectional radiation is typically wasted heat. Hydrogen has the lowest radiant fraction making it the ideal gas for these particular applications. Another benefit of hydrogen is observed when one considers space heating and that more than half of all the thermal energy is transmitted in the form of convection; whether a propane, natural gas, or hydrogen flame. Because propane and natural gas require ventilation for health reasons, a significant portion of their heat is lost in this process. With water vapor as the only byproduct of hydrogen combustion, hydrogen can be burned in a closed environment, thus preventing losses due to ventilation.

3.2 Experimental Setup and Procedures

3.2.1 Introduction

The work discussed here focuses on the understanding of the properties of hydrogen combustion and their effects on the optimal design of thermal heating systems. As such, the research concentrated on the thermal transfer properties of hydrogen, specifically the analysis of the heat propagation depending on the flame orientation and size. The goal of this work is to characterize the hydrogen flame, using the observed properties to retrofit current combustion appliances to burn hydrogen. These properties were observed based on three-dimensional temperature profiles. This chapter contains a detailed description of the systems and procedures associated with the experiments to determine the bulk properties of the flame.

3.2.2 Thermal Gradient Apparatus

A thermal profile of the hydrogen flame was achieved by taking temperature readings in a three-dimensional grid around the flame while varying fuel pressure, orifice size, and flame orientation. Industrial grade hydrogen (99.5% pure) was supplied by a K-type cylinder. The hydrogen gas was regulated to 15 psig using a dual stage high pressure hydrogen regulator from Airgas, model Y12-244D. After exiting the regulator the hydrogen passed through a Harris flashback arrestor, model 88-5FBHFRL. This arrestor prevented the flame from propagating back to the tank in case of a malfunction in the experiment or catastrophic failure of the equipment. The 15 psig hydrogen gas was further reduced to between 0.25 and 1.25 psig, the required pressure for testing, by a type 700 hydrogen regulator from ControlAir, Inc. The hydrogen flow then passed through a small stagnation chamber that allowed for the pressure to be measured by an Omega PX40G15V pressure transducer before passing to the burner for combustion.

Base Plate

The base plate provided the structure to hold 44 thermocouples and the burner and set the spacing between the thermocouples and the burner. There were four thermocouples directly to the right of the burner, five rows of five thermocouples above the burner and three rows of five thermocouples below. The farthest thermocouple to the left of each of the rows is directly in line with the burner. In each row the thermocouples were spaced 63.5 mm (2.5 in) apart and the rows were spaced 63.5 mm (2.5 in) from each other. The burner was held at a fixed distance of 76.2 mm (3 in) from the plate.

Four rectangles were cut through the base plate in an attempt to allow any convective and radiative heating to pass through the plate, thus preventing it from heating up. This allowed the setup to resemble traditional burner installations that lack side walls, while still allowing for thermocouples to be installed in a grid formation.

Burner

Two burners were constructed for these experiments. Each burner was constructed of 3.175 mm (0.125 in) stainless steel tube, sealed on one end with silver solder. The only difference between the burners was the size of the orifice, which was located 7.62 mm (0.3 in) from the sealed end. The two orifice diameters were 0.396 and 0.61 mm (0.0156 and

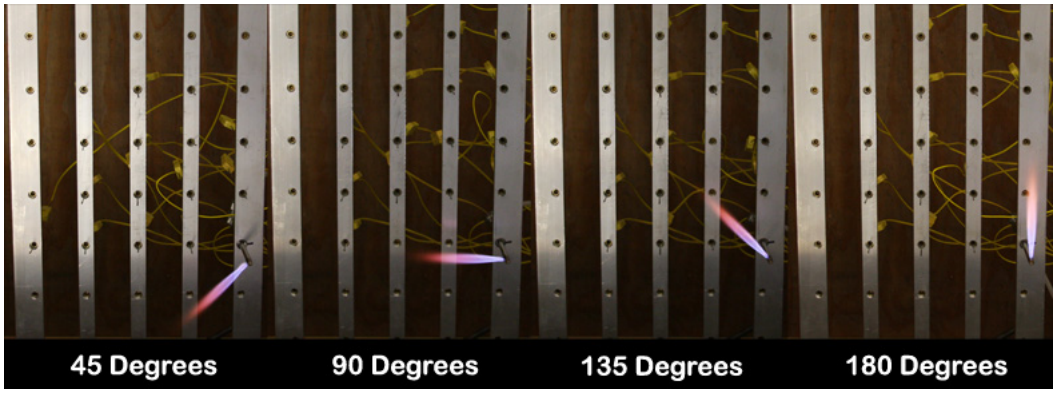

Figure 3.2: Variation of the flame angle from 45 to 180 degrees

0.024 in). The flame distance was set at 76.2 mm (3 in) from the plate and the angle of the flame was varied from 45 degrees to 180 degrees, as shown in Figure 3.2.

Thermocouples

In order to cover the anticipated temperature range, K-type thermocouple probes were used for these tests. These thermocouples have a range of -200 to 1250 degrees Celsius (-328-2282 deg F) and a standard error of 0.75%. The thermocouples were 152.4 mm (6 in) long and had an exposed bead, which had a diameter of 1.016 mm (0.04 in). A thermocouple holder was used that allowed the thermocouple distance from the flame to be varied for each of the different tests but maintained throughout each individual test.

Burner Housing

A box was constructed to surround the burner and test setup on all four sides to prevent any adverse effects from drafts created by opening doors or air conditioning vents. This box was constructed such that its dimensions were 109.22 mm (43 in) high by 688.5 mm (27.5 in) deep by 1016 mm (40 in) wide. The left, right and back sides of the box were constructed using plywood. The front of the box was covered for the first 228.6 mm (9 in) from the bottom with plywood while the remainder of the front consisted of a thin layer of plexiglass hinged at the top to allow access for changes and for the apparatus to be viewed during testing.

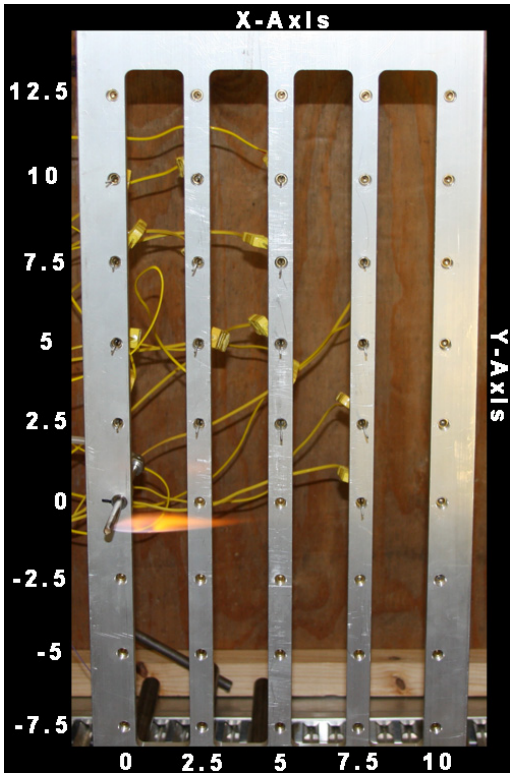

Figure 3.3: Base plate with axis values and orientations, z-axis is perpendicular to the xy plane

Data Acquisition

The thermocouples were read by a National Instruments (NI) PCI-MIO-16E-4 (PCI-6040E) card and a NI PCI-MIO-16E-1 (PCI-6070E) card, each reading 8 channels configured in differential mode. The cold junction compensation for the thermocouples was determined using an Analog Devices TMP37 thermistor. The thermistor and the PX40-15G5V pressure transducer were connected to a NI USB-6008 and all of the data was acquired using Labview software. The error in the data was ± 0.5 °C for the thermocouples, ± 0.1 °C for the thermistor and ± 0.0092 psi for the pressure transducer.

3.2.3 Thermal Gradient Procedure

For the thermal gradient experiments, the thermocouple base plate was oriented such that the long edge was vertical with the burner close to the bottom, as can be seen in

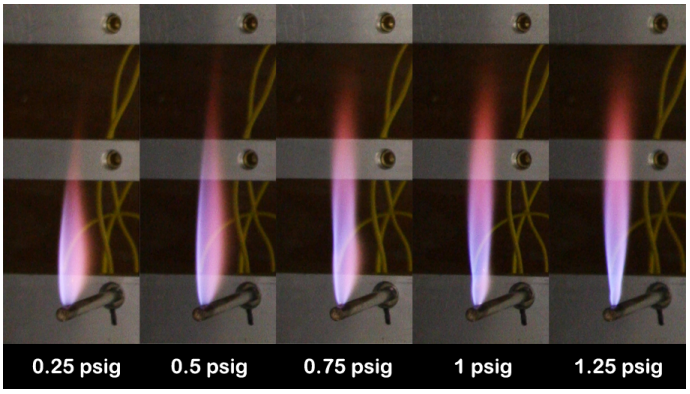

Figure 3.4: Effects of pressure on 0.396 mm burner: flame pressure varied from 0.25 psig to 1.25 psig in 0.25 psig increments

Figure 3.3. The burner was installed such that the flame would be 76.2 mm (3 in) from the surface. The thermocouples were initially installed such that the probe tip was 50.8 mm (2 in) from the base plate. The hydrogen fuel supply was then connected to the burner and the pressure was varied from 0.25 to 1.25 psig at 0.25 psig increments, the results of which can be seen in Figure 3.4. The pressure range was tested at various flame angles, from 45 to 180 degrees at 45 degree increments, where 180 degrees is oriented straight up, as shown in Figure 3.2. Due to the limitations of the data acquisition boards, only sixteen thermocouples were used during each test. This required that the thermocouples be moved to different locations for each pressure-angle combination. Each time the thermocouples were moved, three thermocouples were retained at the previous position in order to verify the repeatability of the tests. Temperatures were recorded for each pressure-angle combination at 50.8, 63.5 and 76.2 mm (2, 2.5 and 3 in) from the base plate. By compiling these temperatures, and assuming symmetry, a three-dimensional profile of each iteration of variables can be plotted.

For each run, the pressure, angle, and thermocouple distance were set and the burner was ignited. The flame was allowed to reach steady state before data was acquired. A LabView program was used to acquire the temperature data while monitoring the pressure and cold junction temperature. Temperature data from each thermocouple was acquired every 1.5 seconds for 100 seconds and compiled into a data file. Three runs were recorded for each set of variables. These runs were compared to verify the repeatability of the tests by reviewing variations in the temperatures. Upon verification of repeatability the runs were averaged

to give a temperature for each thermocouple at each set of variables. This data was then compiled using "TecPlot" to provide 3D contour plots of the flame temperature.

3.2.4 Thermal Gradient Analysis

Data from the experiments were compiled and converted into two-dimensional and three-dimensional temperature contour plots. The contour plots provided a visual representation of the temperature at each of the thermocouple locations in the grid. These visual representations were used to observe how the hydrogen flame developed and the heat transfered from the flame to the atmosphere. The axes were set, as seen in Figure 3.3, where the y-axis is the the vertical orientation, the x-axis is in the horizontal orientation and the z-axis is perpendicular to the plane of the page. In the plot the orifice of the flame was oriented at x=0, y=0 and z=0. These contour plots were then broken down into several different views of the flame to illustrate different aspects of the flame development. The separate views are two-dimensional cross sections of the three-dimensional plot to give a better view of the flame development and heat production.

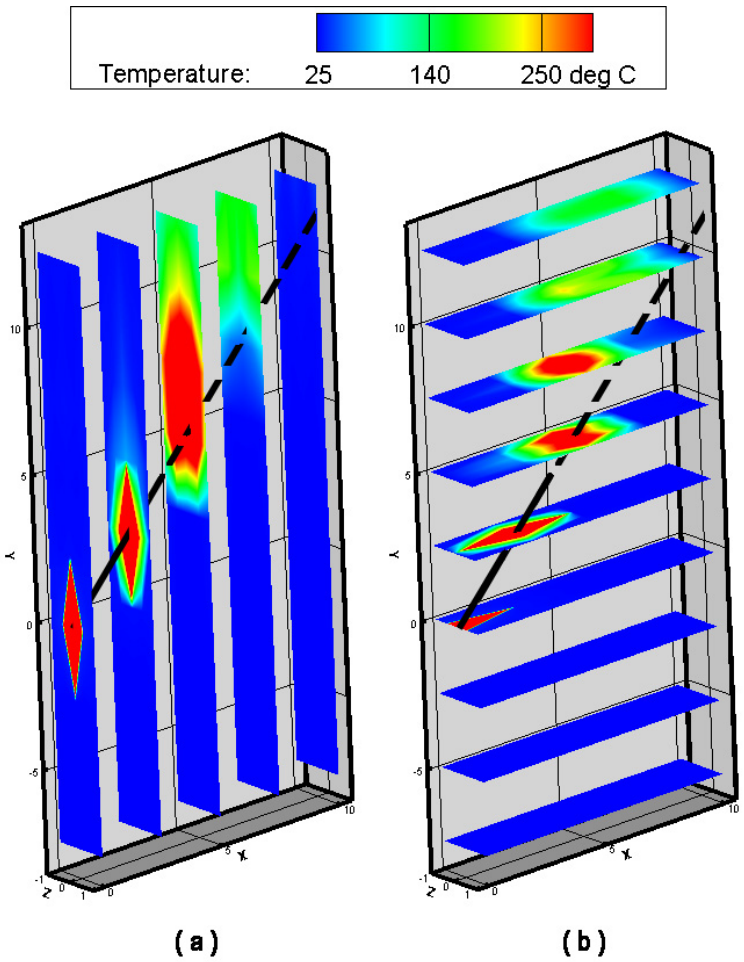

Figure 3.5: Three-dimensional temperature gradient: two-dimensional cross sections at constant X and Y values of the 1.25 psig flame at 135 degrees

The first images rendered from the contour plot were linear progressions along the horizontal (x axis) and vertical (y axis) axes of the flame. In these images a solid black line represents the flame and the dotted black line represents the the flames direction showing the heat does not follow the flame direction past the flame itself. The first image took two-dimensional contour plots at constant x-axis values while varying the y and z values, as seen in Figure 3.5(a). The second plot took two-dimensional contour plots by using constant values of y while varying x and z, shown in Figure 3.5(b). This plot would be useful in determining the distance of the flame from a cook-top to ensure certain temperatures were produced at the cooking surface. These plots allow the flame development to be observed to

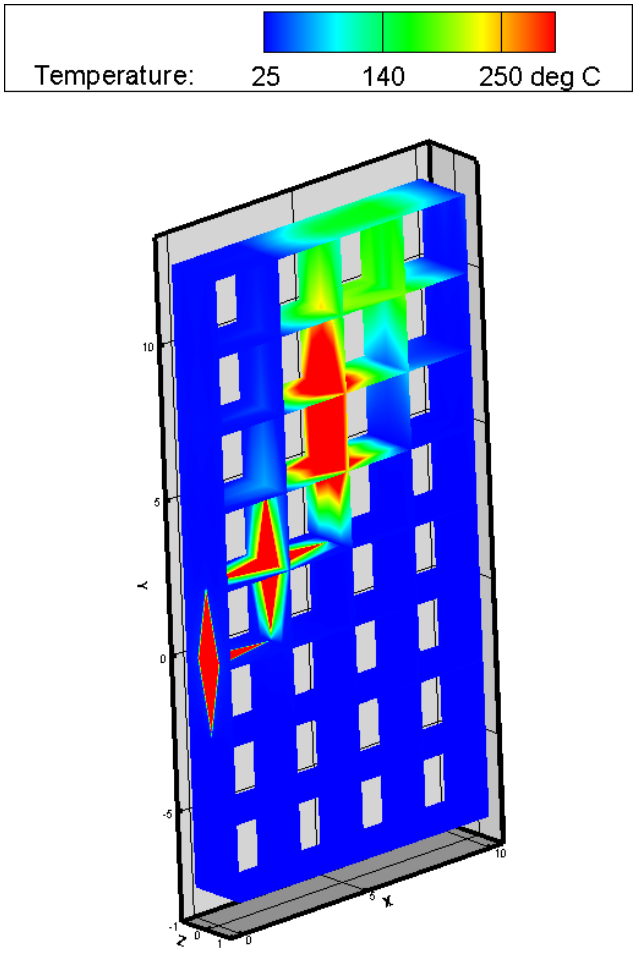

Figure 3.6: Three-dimensional temperature gradient: combination of the two-dimensional cross sections at constant X and Y values of the 1.25 psig flame at 135 degrees

determine the expansion of the flame.

The third image rendered from the contour plot is a combination of Figures 3.5(a) and (b). This plot shows a more complete representation of the heat transfer by compiling the cross sections to show a three-dimensional representation of the flame, as seen in Figure 3.6.

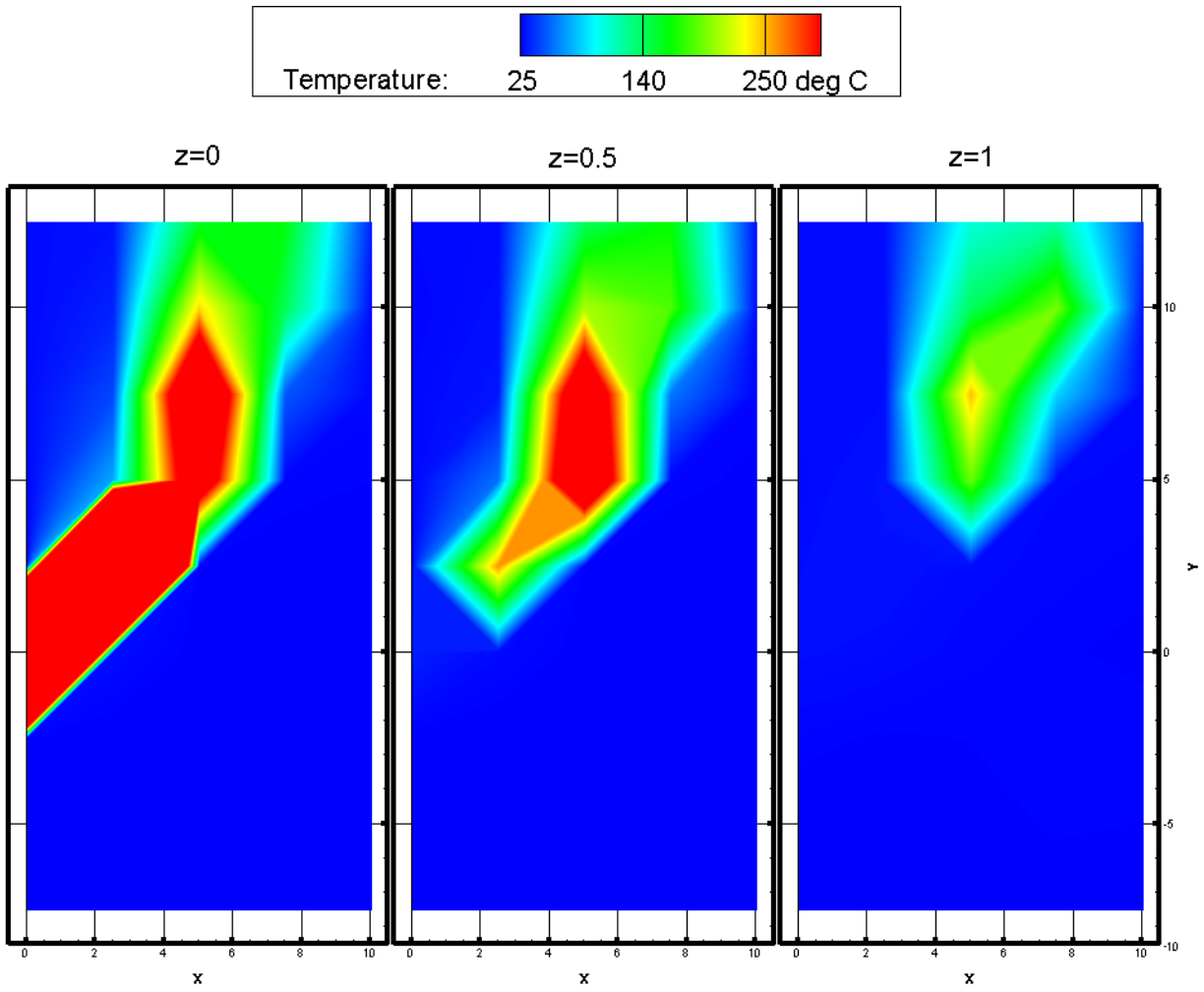

Figure 3.7: Two-dimensional temperature gradient: cross sections at constant Z values of the 1.25 psig flame at 135 degrees

The next three images rendered from the contour plot are cross sections taken at 50.8 mm (2 in), 63.5 mm (2.5 in) and 76.2 mm (3 in) from the base plate and corresponds to z equal 1, 0.5 and 0, respectively. These images are in-line with the flame and show the extreme heat in the flame and convective current emanating from the flame, shown in Figure 3.7.

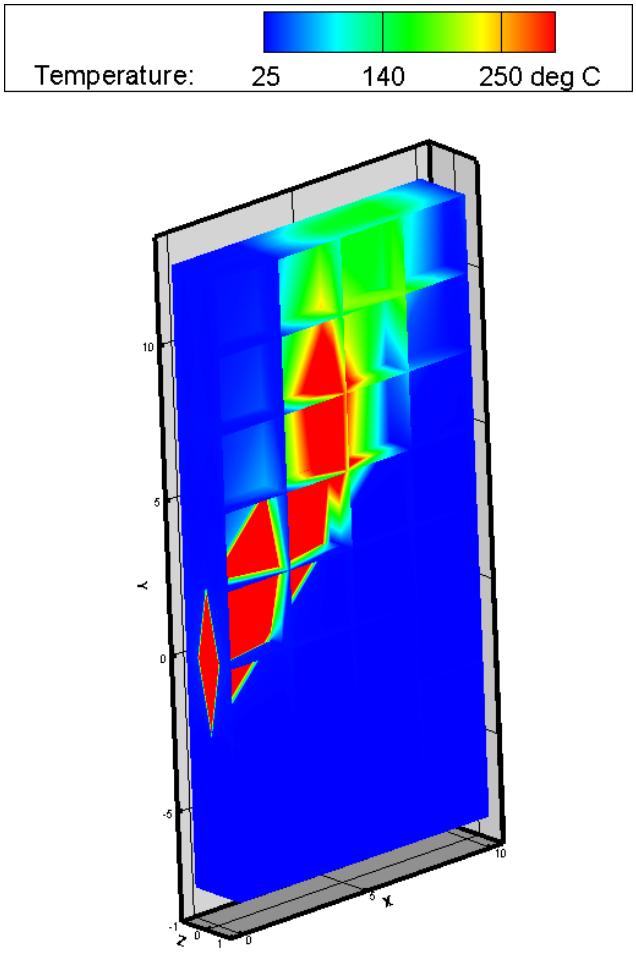

Figure 3.8: Three-dimensional temperature gradient: combination of two-dimensional cross sections at constant X and Y values and the two-dimensional temperature gradient at z=0 from the 1.25 psig flame at 135 degrees

The final image rendered from the contour plot is a combination of Figures 3.6 and the z=0 slice of Figure 3.7. This plot shows a more complete representation of the heat transfer by compiling the cross sections to show a three-dimensional representation of the flame, which can be seen in Figure 3.8. Contour plots for every iteration of the variables are in Appendix A.

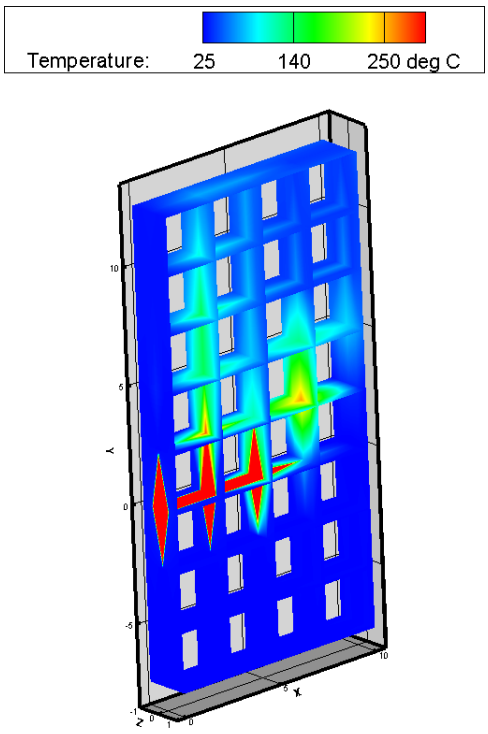

Figure 3.9: Three-dimensional temperature gradient: 0.61 mm orifice at 0.5 psig and oriented at 90 degrees

3.3 Results and Discussion

This section reviews the results from the temperature gradient experimentation. The observations of the tests will be discussed, as well as their application to the retrofit process.

3.3.1 Results

The first trend noticed in the data was that the hydrogen flame radiated little to no heat to thermocouples that are outside the path of the convective currents, as illustrated by the lack of temperature change in the thermocouples in Figure 3.9. This lack of radiative heat transfer, observed for all of the conditions, was predicted by the low radiant fraction and makes hydrogen an ideal gas for directional combustion in close proximity to a heat sensitive apparatus. However, hydrogen would be insufficient for lighting applications and omni directional heating.

It was noted that when the pressure was increased from 0.25 to 1.25 psig the flame

diameter and length increased as predicted through computation. The flame length was calculated to be between 85 and 86 mm for the 0.396 mm orifice and between 131 and 132 mm for the 0.61 mm orifice and the observed flame lengths were observed to be in this range. Temperature gradients can also be shifted in the x direction with the adjustment of pressure, as shown when comparing Figure 3.9 and 3.10. In Figure 3.9 there is an average temperature of 140°C for the entire x-axis while Figure 3.10 has an average temperature of 200°C that starts at x=5 and it is apparent it extends past the maximum distance. This shows that not only does increasing the pressure shift the heating region in the x direction but also that the average temperature of the region increases due to the increase in hydrogen. This allows the location of heating and temperature to be set for the optimal situation depending on the application. The burner can also be designed in a manner that prevents the heating of exterior walls, preventing thermal losses.

Similar to what had been observed, the average temperature and location of the flame's most even temperature distribution region were affected by adjusting the angle of the flame. Figure 3.11 shows that the 135 degree flame orientation has the most even temperature distribution at greater distances from the orifice, while the 90 degree flame provided the most even temperature profile closer to the orifice, as seen in Figure 3.9. This shows that 135 degrees is better for applications that require distributed heat at a large vertical distance in a confined area (water heater) while 90 degrees would be better for applications where the distribution must be closer and the surroundings are less affected by heat (grill). It was also noted that the distribution grew larger as the angle rotated from 180 to 45 degrees, thus causing the average temperature to decrease. The rotation of the flame had little to no affect, within the precision of measurement, on the flame length. It was noticed that rotating the flame past the 90 degree to the 45 degree orientation was inefficient at producing significant heating.

The final observation occurred when the different orifice sizes were analyzed. The flame lengths were non-dimensionalized and it was determined that the flame length corresponded to about 216 diameters. The thermal profiles were also non-dimensionalized in reference to the orifice size to determine if one could compare the orifice size to the heat distribution. Figures 3.12(a) and (b) suggest that thermal effects are non-dimensional, however, a much finer resolution is required to determine the specific relationship. Being able to non-dimensionalize the results allows burners to be designed for different variables without having

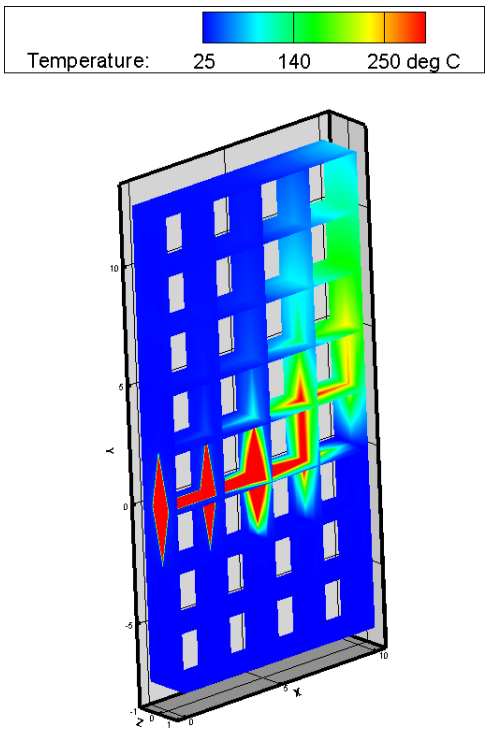

Figure 3.10: Three-dimensional temperature gradient: 0.61 mm orifice at 1.25 psig and oriented at 90 degrees

to specifically test them.

3.3.2 Discussion

The design of a burner is dependent on several variables and the optimal design requires an understanding of the defined limitations in which the combustion must occur. Water heaters, for example, require the flame to exist within a set volume and produce enough thermal output that will increase the temperature in a fluid to a desired temperature. The following formulae can be used to assist in designing for such limitations.

Equations 3.2 to 3.7 provide the velocity of the jet and the thermal output of the flame. These equations require the assumption of a fuel supply pressure (P_0), stagnation temperature (T_0) and an orifice size (in the form of area, A).

$$P_0 = \rho_0 \cdot R \cdot T_0 \tag{3.2}$$

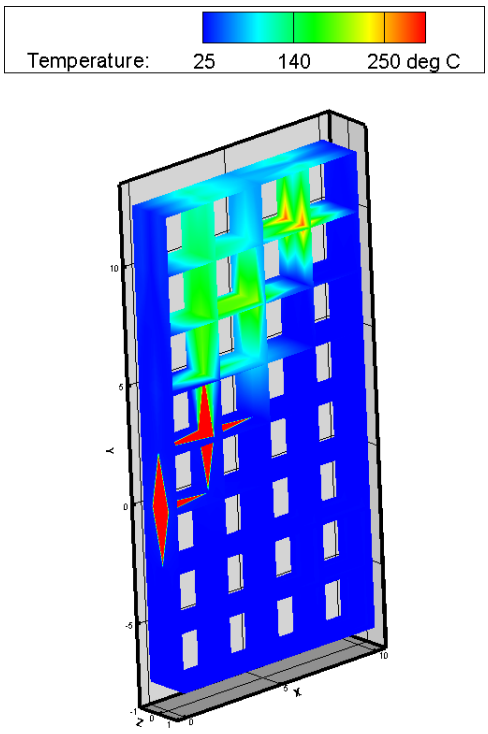

Figure 3.11: Three-dimensional temperature gradient: 0.61 mm orifice at 0.5 psig and oriented at 135 degrees

$$\frac{P_0}{P_{inf}} = (\frac{T_0}{T_j})^{\frac{\gamma}{\gamma-1}} = (\frac{\rho_0}{\rho_j})^{\gamma} \tag{3.3}$$

$$\frac{T_0}{T_j} = 1 + \frac{\gamma - 1}{2} \cdot M_j^2 \tag{3.4}$$

$$c_j = (\gamma \cdot R \cdot T_j)^{\frac{1}{2}} \tag{3.5}$$

$$U_j = M_j \cdot c_j \tag{3.6}$$

$$\dot{Q} = \Delta h_c \cdot \rho_j \cdot U_j \cdot A \tag{3.7}$$

The temperature of the jet (T_j), and density of the jet (P_j) can be calculated using

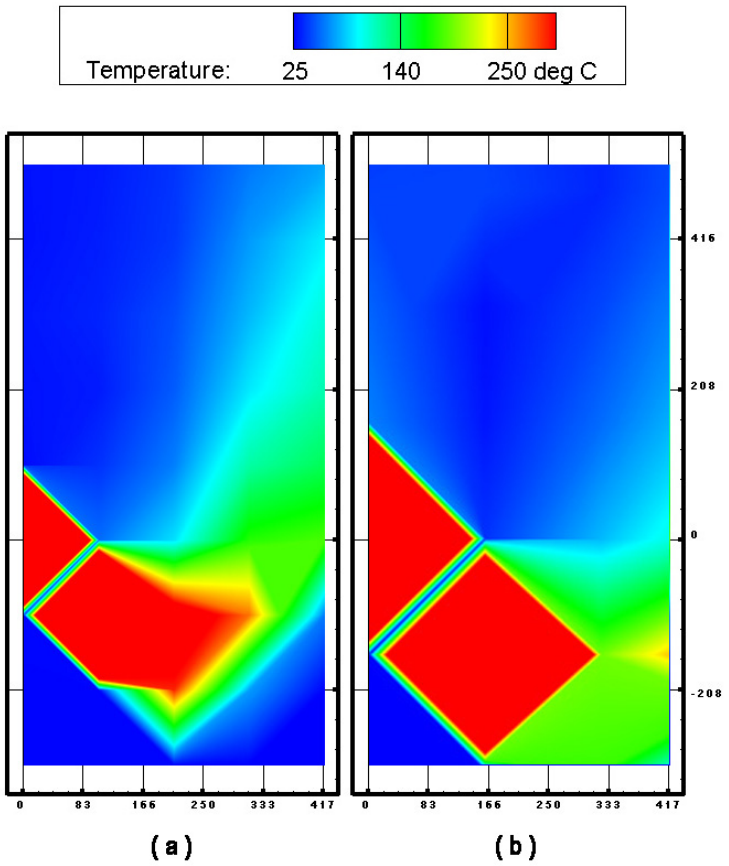

Figure 3.12: Non-dimensionalized temperature gradient:1.25 psig and oriented at 45 degrees with and orifice of (a)0.61 mm, (b)0.40 mm

Equation 3.2 and the specific heat ratio, γ, which is 1.41 for hydrogen gas. These values can then be used to determine the Mach number of the jet (M_j) using Equation 3.4. The Mach number and the speed of sound in the jet (c_j) can then be used to find the velocity of the jet (U_j) using Equation 3.6. The energy production of the flame ($\dot{Q}$) can then be calculated by using Equation 3.7 and the heat of combustion value for hydrogen (Δh_c), which also happens to be the lower heating value of hydrogen.

This procedure only provides the energy production for one flame and can be multiplied by the number of orifices to give the total energy production of the burner. It is also important to consider the total orifice area when determining the area of the lines supplying the hydrogen to the burner to make sure the flow is not limited.

Flame length is also an important issue when designing a burner in order to prevent direct contact between the flame and certain surfaces within the device. The length of the flame can be calculated using the following equations and the values calculated in the previous equations.

$$Fr = \frac{U_j \cdot f^{(\frac{3}{2})}}{((\frac{\rho_j}{1.1934})^{\frac{1}{4}} \cdot (\frac{T-T_0}{T_0} \cdot g \cdot d)^{\frac{1}{2}}} \tag{3.8}$$

$$L^* = \frac{13.5 \cdot Fr^{0.4}}{(1 + 0.07 \cdot Fr^2)^{1.5}} \tag{3.9}$$

$$D^* = d \cdot (\frac{\rho_j}{1.1614})^{1/2} \tag{3.10}$$

$$L = \frac{Lstar \cdot Dstar}{f} \tag{3.11}$$

The Froude Number, Fr, is the non-dimensional value that compares gravitational forces (g) with inertial forces. It is used to quantify the resistance of one fluid moving through another by using the mass fraction of the fuel (f), and the diameter of the jet (d). If the Froude Number is five or greater, the non-dimensional flame length (L^*) is equal to 23. However, when the Froude Number is less than five, then Equation 3.9 can be used to find L^*. The non-dimensional flame diameter (D^*) can be calculated using Equation 3.10 and then be used in Equation 3.11 to find the flame length, L.

Using these values, in combination with the temperature profiles acquired through experimentation, the design process can occur efficiently and effectively. Two burners were designed in this research, one for use in a grill and the other for use in an on-demand water heater. These appliances will be installed into the OGZEB upon completion for endurance testing.

3.4 Hydrogen Retrofit Design

3.4.1 Grill

The burner for the grill was designed to retrofit a Solaire Anywhere Portable Grill. To provide the optimal temperature distribution, the 90 degree orientation was chosen with the

Figure 3.13: Hydrogen retrofit burner for the Solaire grill

flames staggered and pointed at one another to allow the entire burner to ignite from a single point, as seen in Figure 3.13. The burner is made of two, 6.35 mm (0.25 in) stainless steel tubes with spaced 127 mm (5 in) apart. The total heating area of the hydrogen burner is equivalent to that of the factory burner. Orifices were drilled every 50.8 mm (2 in) starting at 6.35 mm (0.25 in) from the end of one burner and 31.75 mm (1.25 in) from the other. When the burner was assembled, the distance between flames was 25.4 mm, providing an even temperature profile.

3.4.2 Grill Testing

The testing of the grill burner involved observing the temperature at seven different locations at the cooking surface, as seen in Figure 3.14. These temperatures were recorded every second for 300 seconds, thus allowing; the average temperature, the temperature fluctuations and the temperature distribution of the burner to be observed. When the hydrogen burner was compared to the original Solaire burner it was noted that the average temperature was higher for the hydrogen burner and more importantly, the hydrogen burner produced more consistent temperatures. The Solaire burner had an average temperature difference of 140°C, as shown in Figure 3.15 while Figure 3.16 shows that the hydrogen burner had an average temperature difference of 110°C. The Solaire burner was designed to release the gaseous fuel in the middle of the burner and the momentum and location of this causes thermocouples one and four to be significantly hotter than the rest while the hydrogen burner had a more distributed gas delivery providing a more distributed temperature grid.

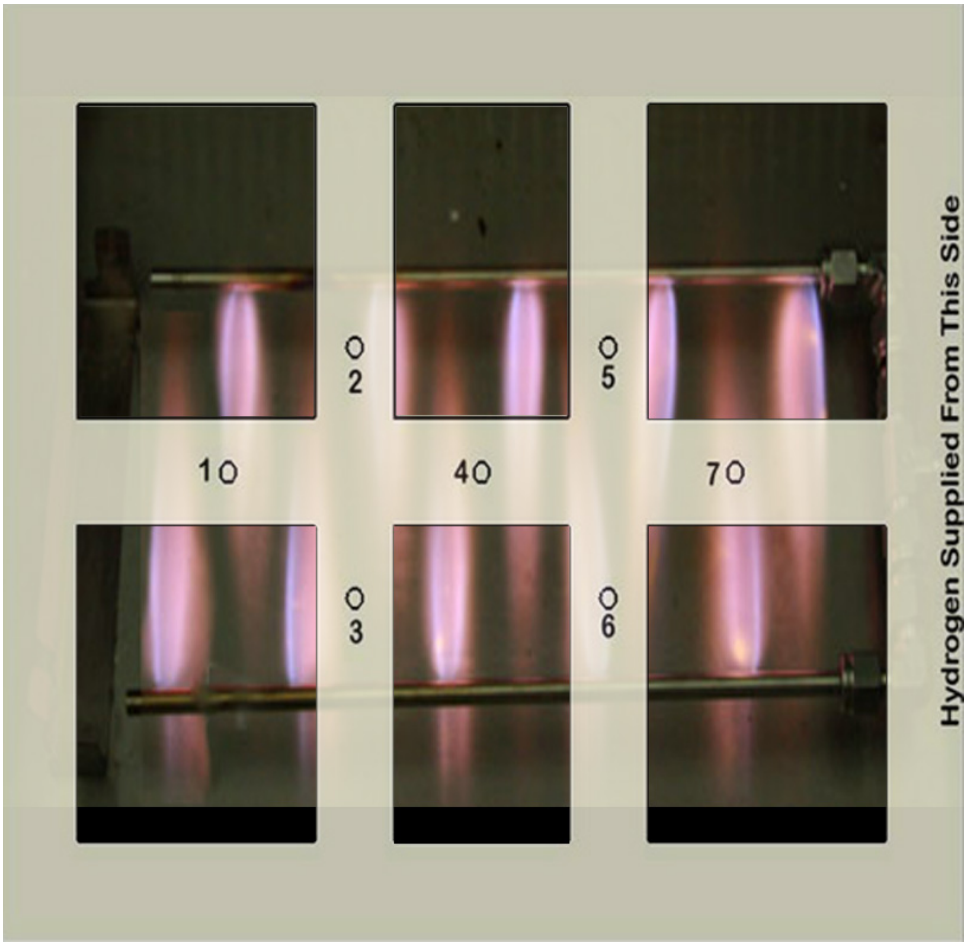

Figure 3.14: Illustration of thermocouple locations at the grill's cooking surface

This is very important for cooking to prevent hot and cold spots at the cooking surface. It was also noticed that the third thermocouple for the hydrogen burner was lower than the rest which was caused by fault in the burner construction. For most of the testing the orifice under thermocouple 3 was impeded slightly with flux introduced during assembly.

3.4.3 On Demand Water Heater

The burner for the on demand water heater was designed to retrofit a Rinnai C53 on demand water heater to combust hydrogen and heat water for the OGZEB. The OGZEB has a maximum hot water consumption of 7.57 lpm (2 gpm). The coldest water temperature is assumed to be 21°C with a desired hot water temperature of 41°C. These variables require

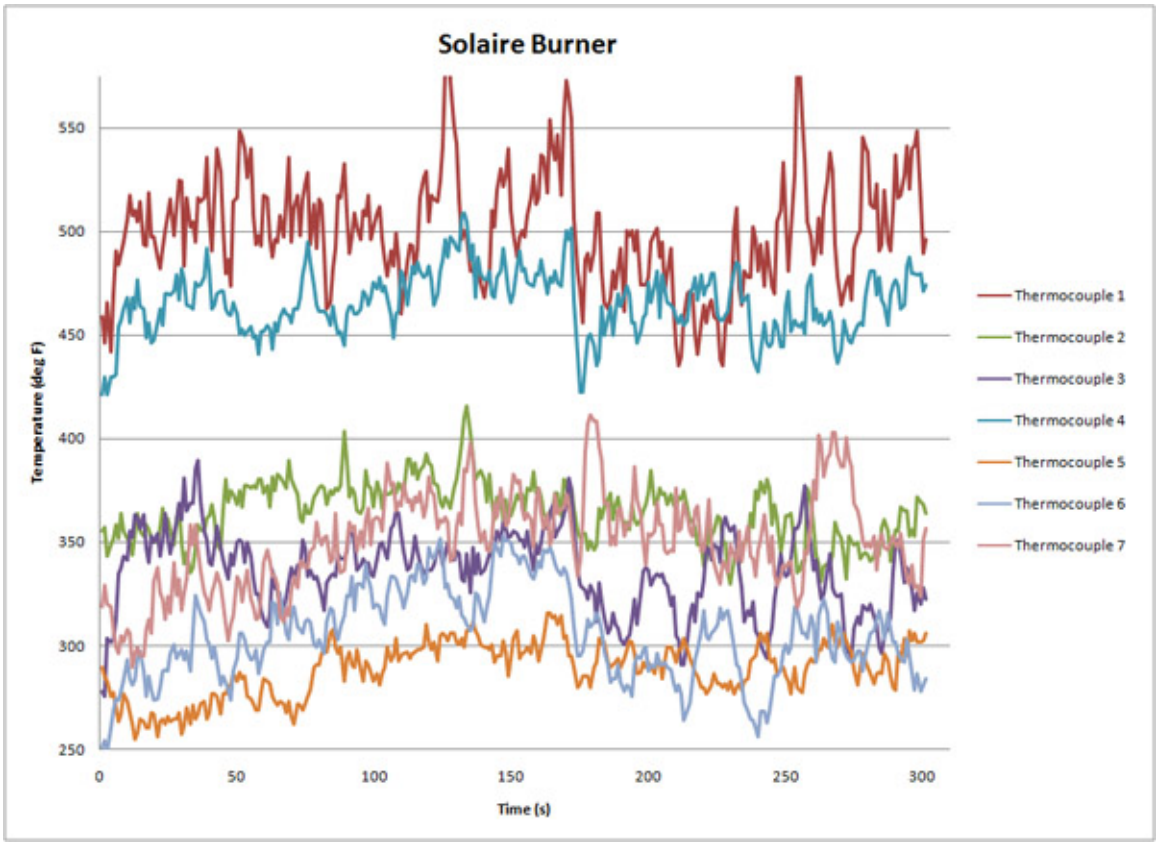

Figure 3.15: Solaire grill burner: temperatures at cooking plane

10.5 kJ/s of energy from the combustion of hydrogen. A hole size of 0.396 mm (0.0156 in) has a maximum flame length of 88.9 mm (3.5 in) which prevents the flame from contacting the heat exchangers, while providing a minimum of 0.25 kJ/s per orifice. A total of 52 holes are required to produce the total amount of energy for the system, assuming 80% efficiency. The burner is controlled by turning on and off four different sub burners that make up the complete burner. The sub burners were designed to be turned on and off in differing combinations to allow the energy output to be increased incrementally until all sub burners were on and producing 52 flames, as seen in Figure 3.17.

Each sub burner consists of 9.525 mm (0.375 in) stainless steel tubing with orifices drilled at even spacing. The first sub burner had four orifices that are aligned such that the flames are 45 degrees up from the tubes that make up sub burners three and four. Sub burner two has six orifices and the same 45 degree angle as sub burner one. Both sub burner one and two

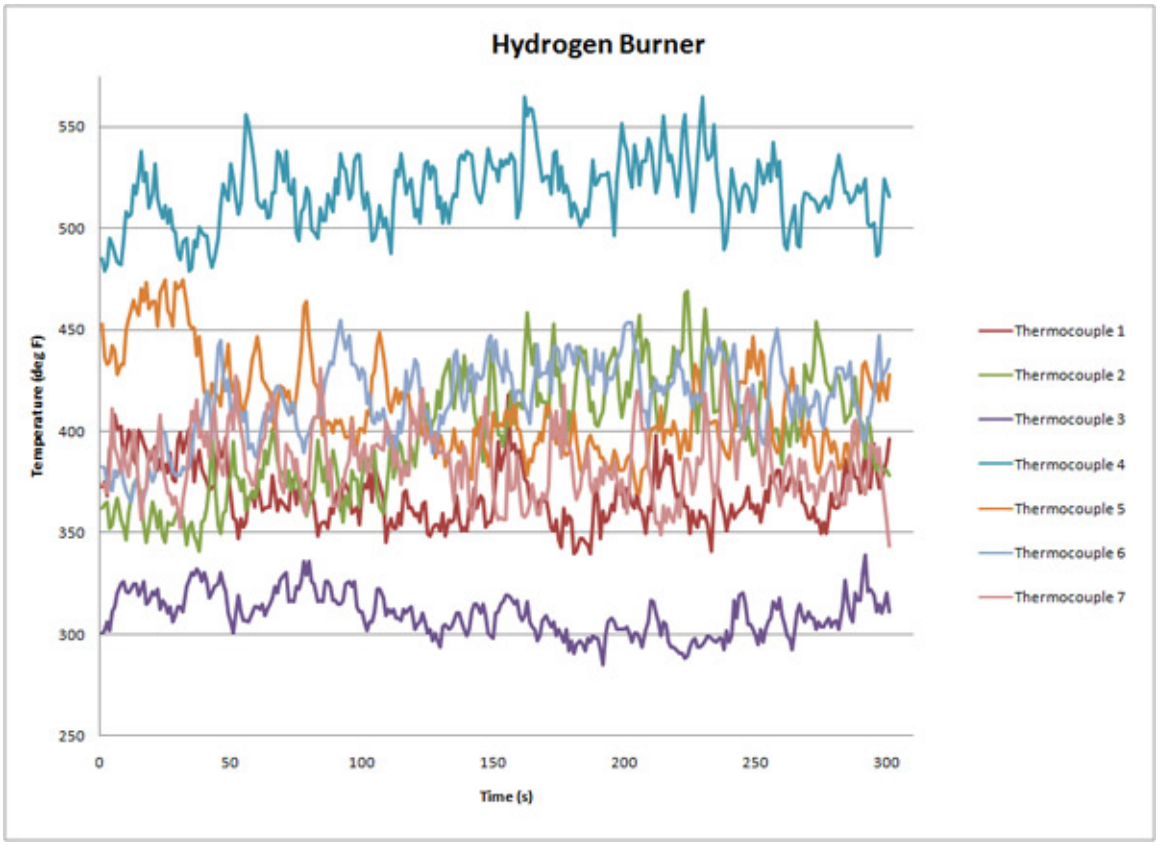

Figure 3.16: Hydrogen burner: temperatures at cooking plane

are pointed at the center of the burner. The 45 degree angle and orientation were chosen using Figure 3.18 due to the distributed nature of the heat gradient while not projecting heat further than 190 mm. Projecting heat past 190 mm would heat the wall of the burner cavity, causing thermal losses. The side burners also allow the entire burner to be lit from one location.

Sub burners three and four are fed by 12.7 mm (0.5 in) stainless steel tubing. Sub burner three has seven orifices on each 9.525 mm (0.375 in) tube while sub burner four has 14 orifices on each tube. Flames on sub burners three and four point straight up toward the heat exchangers. The design allows all sub burners to be lit simultaneously and only those not needed to be turned off. Appendix B contains design drawings of the burner.

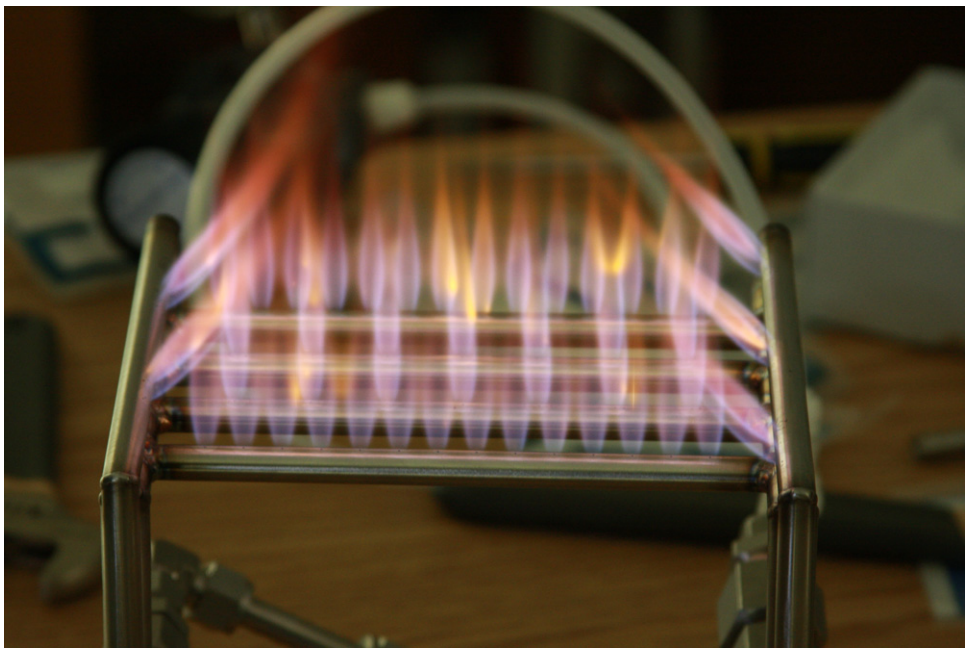

Figure 3.17: Hot water heater hydrogen burner

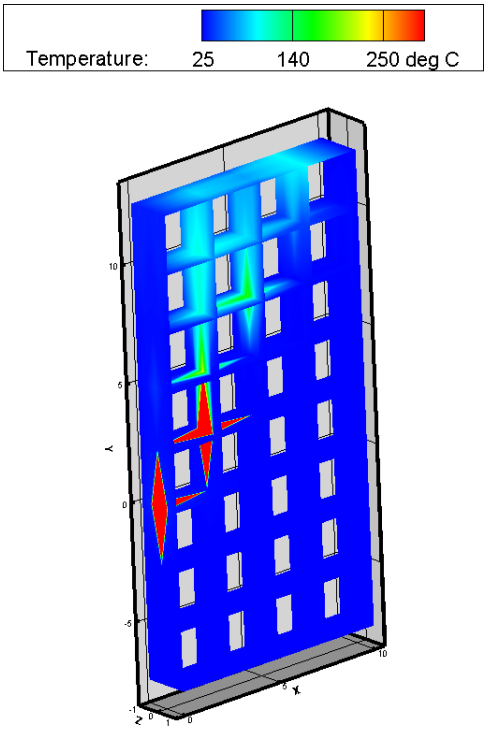

Figure 3.18: Three-dimensional thermal gradient: 0.396 mm orifice at 0.5 psig at 135 degrees

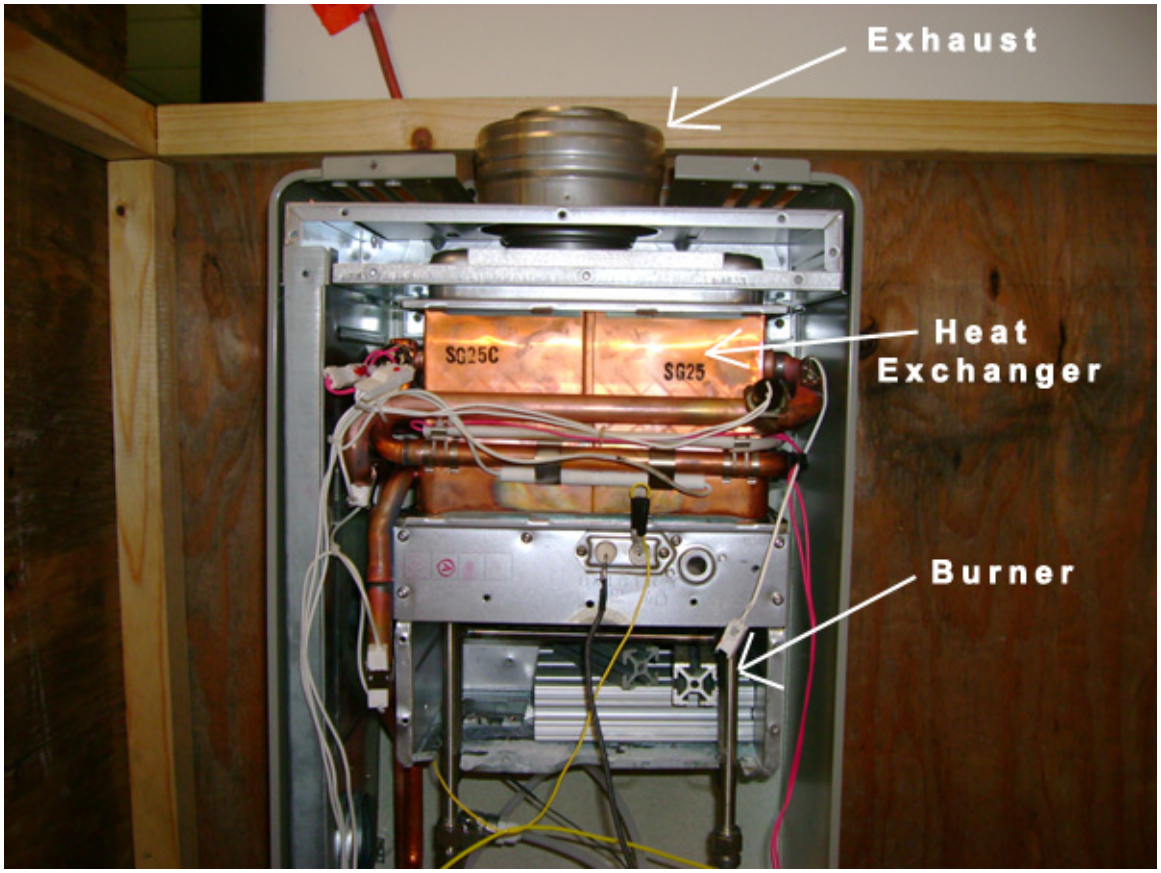

Figure 3.19: Rinnai water heater assembly

3.4.4 On Demand Water Heater Testing

To test the hydrogen burner in the Rinnai on demand water heater, the original burner, which was capable of using natural gas or propane, was removed along with the electronics, while leaving the heat exchanger in tact. The original burner was sealed with a defined air inlet supplied by a fan. The hydrogen burner was tested in three different formations. The first was an open system with the hydrogen burner installed in place of the propane burner under the heat exchangers with the front open, as seen in Figure 3.19. The second formation, shown in Figure 3.20, was with the front closed with no fan and the final formation was closed with a fan added and run at 25% and 100% power to observe effects on efficiency. Each formation was tested at 0.25 psig and 0.5 psig for water flow rates of 63.1 cc/s (1 gpm) and 126.2 cc/s (2 gpm).

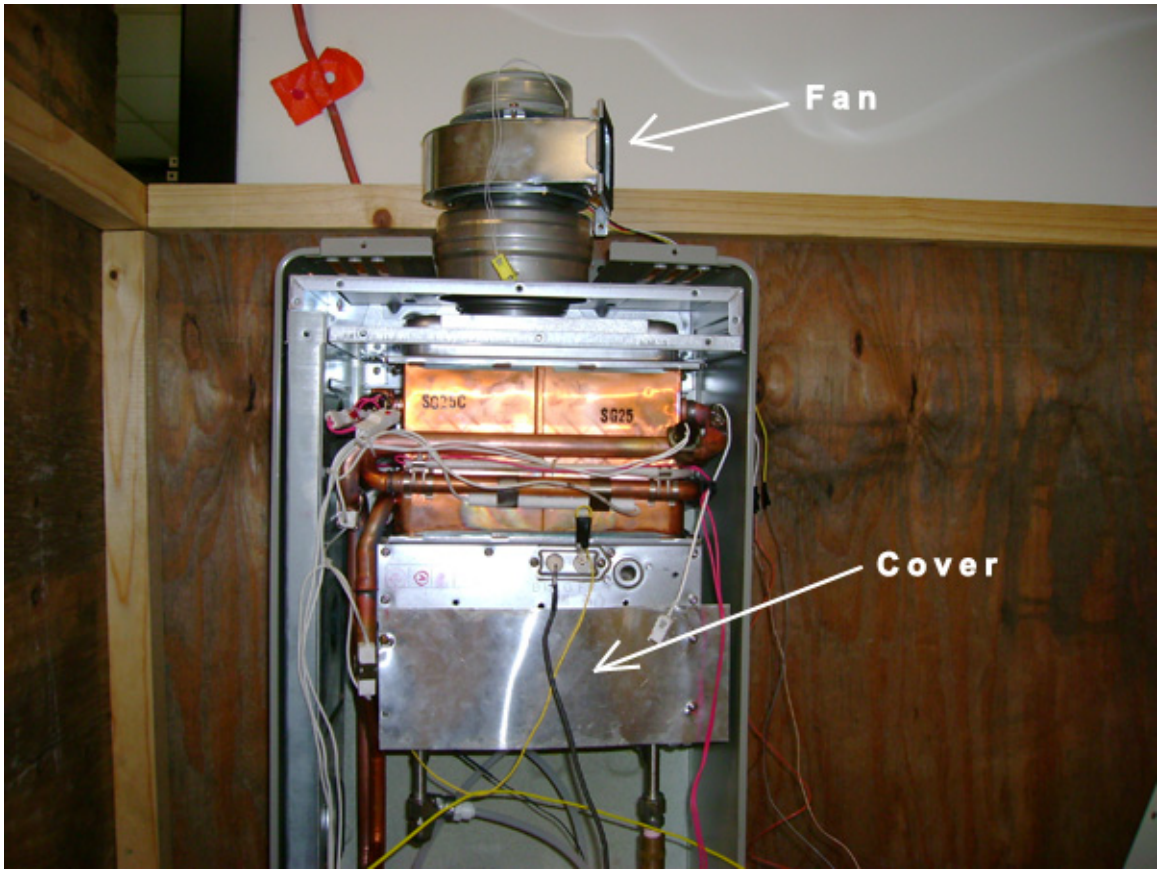

Figure 3.20: Rinnai water heater assembly with cover and fan

During the tests the burners were turned on and off stepping the number of burners from 4 flames to 52 flames. Results were similar for both water flow rates. At 0.25 psig the energy output of the burner ranged from 1 kW to 13 kW while the energy absorbed by the water ranged from 386 W to 3.41 kW as seen in Figure 3.21. At 0.5 psig and a water flow rate of 63.1 cc/s, the energy output of the burner ranged from 1.4 kW to 18.5 kW while the energy absorbed by the water ranged from 611 W to 5.5 kW as seen in Figure 3.22. These graphs include the energy content in the hydrogen gas leaving the burner (H2 Energy) for comparison to energy absorbed by the water. Figures 3.23 and 3.24 show the effects of modifying the burner housing by adding a cover and a fan. The graphs show negligible improvement in energy transfer with the addition of a cover and marked losses with the addition of a fan. However the fan did reduce the amount of condensation produced on the heat exchanger during testing. The addition of the fan at 100% power caused an average

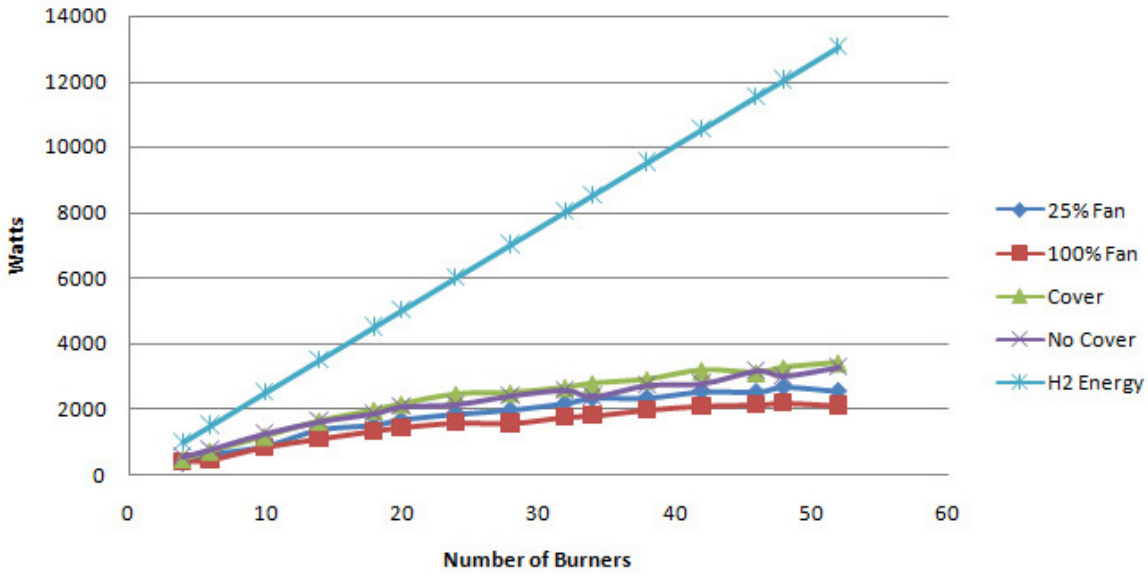

Figure 3.21: Energy absorbed by water at 0.25 psig and 63.1 cc/s

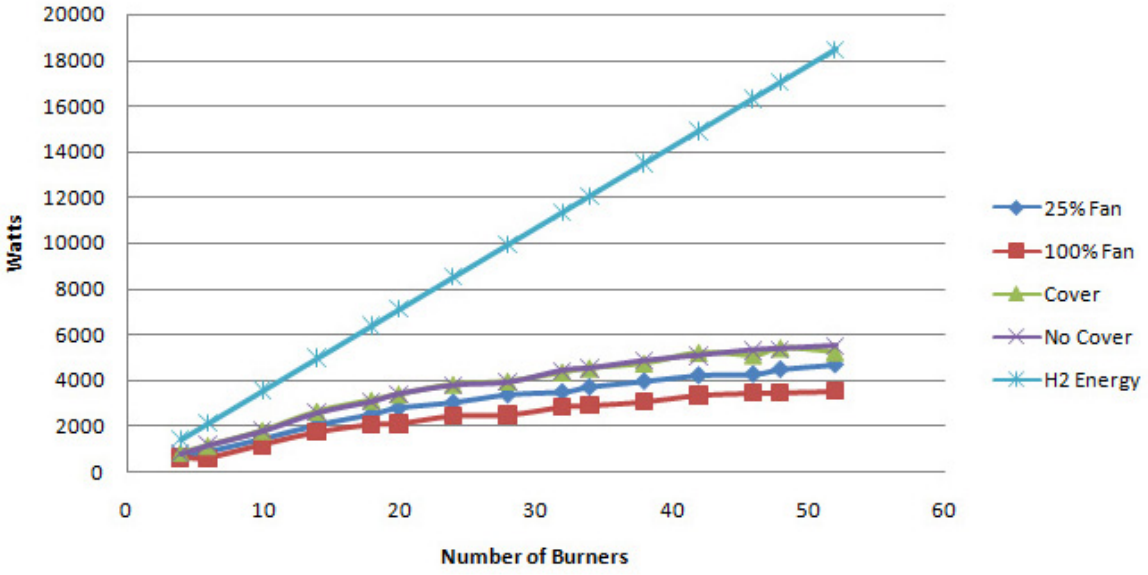

Figure 3.22: Energy absorbed by water at 0.5 psig and 63.1 cc/s

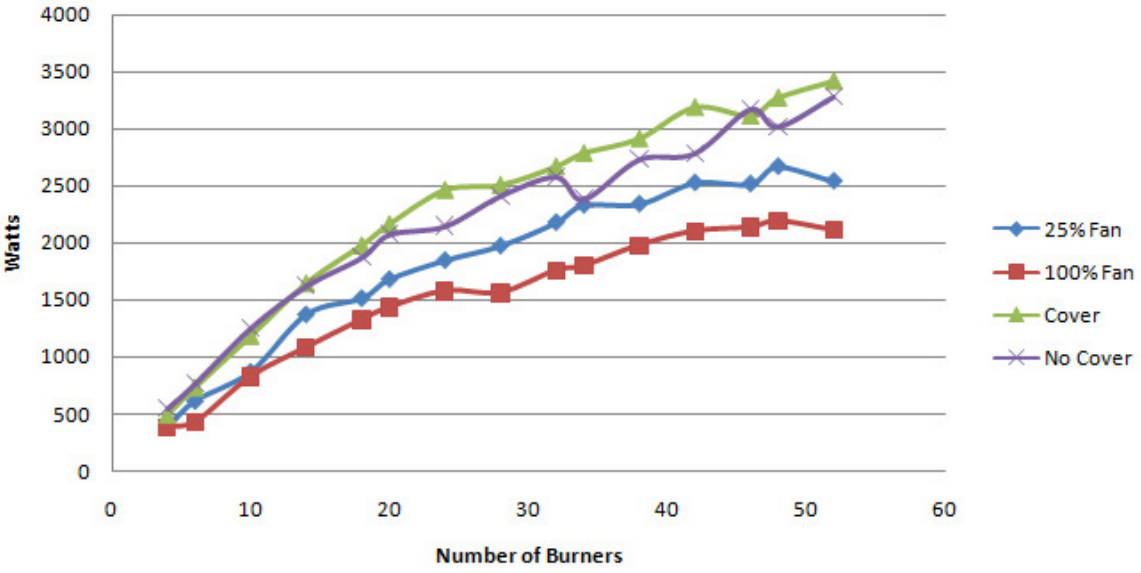

Figure 3.23: Energy absorbed by water at 0.25 psig and 63.1 cc/s

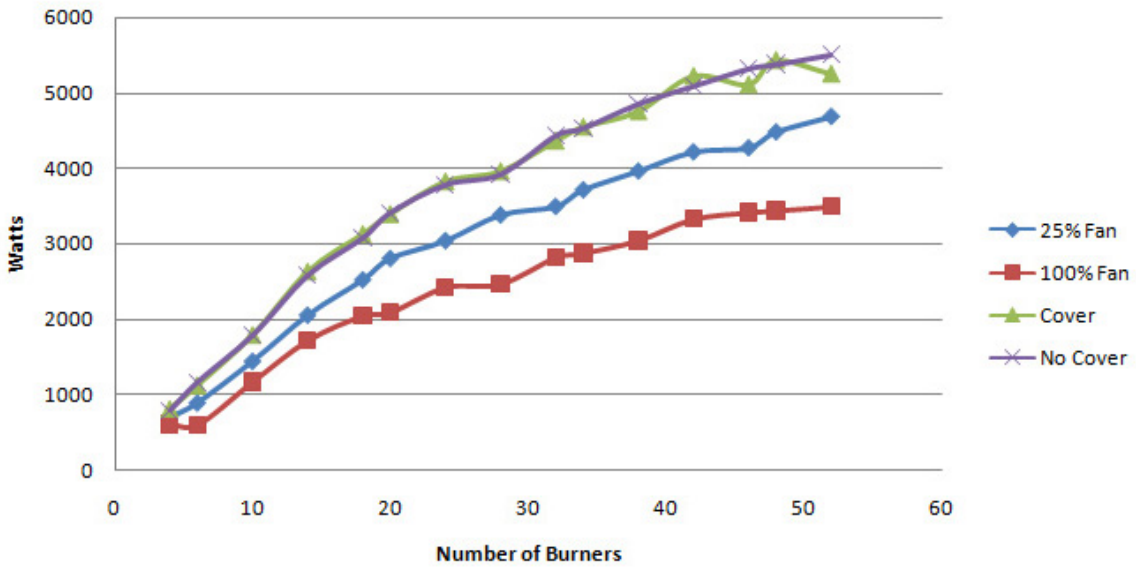

Figure 3.24: Energy absorbed by water at 0.5 psig and 63.1 cc/s

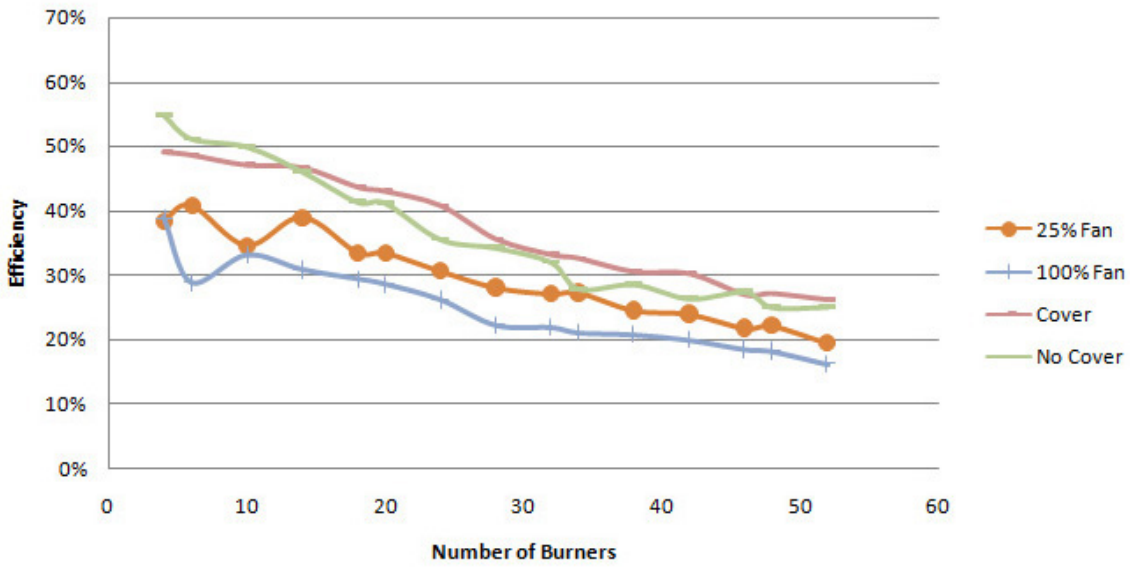

Figure 3.25: Efficiency of energy from the burner to energy absorbed by the burner at 0.25 psig and 63.1 cc/s

loss of 33% while the fan at 25% cause an average loss of 21%. It was surmised that these losses were caused by the fan increasing the rate at which the convective currents passed through the heat exchangers, thus reducing the time allowed for heat to be exchanged.

When the efficiency of the water heater was graphed in comparison to the number of burners, seen in Figures 3.25 and 3.26, it was noted that as orifices were added, the efficiency of the system decreased. The efficiency of the burner decreased at a fairly linear rate of 0.5% per burner.

Similar results were observed in the 126.2 cc/s tests as in the 63.1 cc/s test. All graphs for the water heater tests can be found in Appendix C.

With the higher efficiencies at 0.5 psig it is recommended the system be run at this case to reduce fuel consumption during operation.. It was also noted that it is ideal to run at the low flow rates of hydrogen but this application requires a certain number of flames in order to produce the required temperature change.

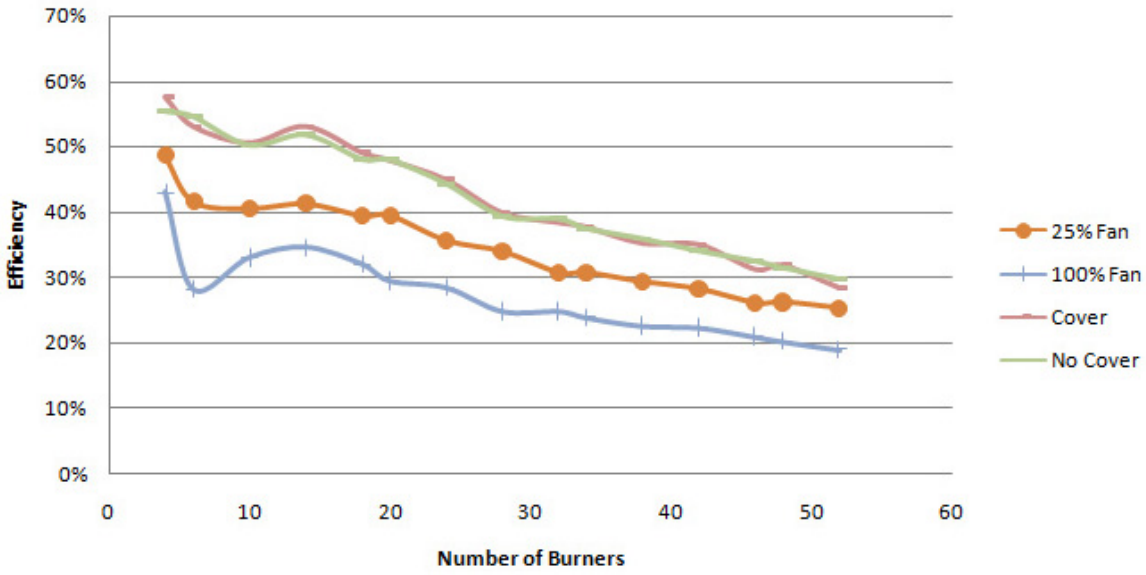

Figure 3.26: Efficiency of energy from the burner to energy absorbed by the burner at 0.5 psig and 63.1 cc/s

CHAPTER 4

CONCLUSIONS

The main objective of this work was to develop engineering solutions for sustainable building systems. The Off-Grid Zero Emissions Building (OGZEB) was designed and built using best practices as determined by the LEED certification process. Energy for the OGZEB is supplied by photovoltaic (PV) panels providing electricity, solar thermal for hot water and geothermal for air conditioning. Excess electricity produced by the PV panels will be stored using a hydrogen storage system.

The implementation of solar energy solutions combined with energy efficient design can lessen the burden of buildings on the energy sector, thus preventing the requirement of additional power plants. Hydrogen combustion is a better than electric resistive heating for heating applications, such as water heating and cooking. It is shown that direct combustion can be 26% more efficient than converting it into electricity and using resistive heating. A Solaire grill and a Rinnai water heater were retrofited to burn hydrogen and operate in the OGZEB. The grill retrofit provided a more uniform cooking temperature distribution than the factory burner. The water heater retrofit provided the proper water temperature for the OGZEB, accounting for varying flow rates and water inlet temperatures. While the efficiency of the hydrogen burner is less than originally anticipated, the design can be optimized to increase the efficiency. The information acquired during this research will also aide in the retrofit of a natural gas Viking range.

APPENDIX A

THREE DIMENSIONAL CONTOUR PLOTS

A.1 0.024 in Diameter Burner

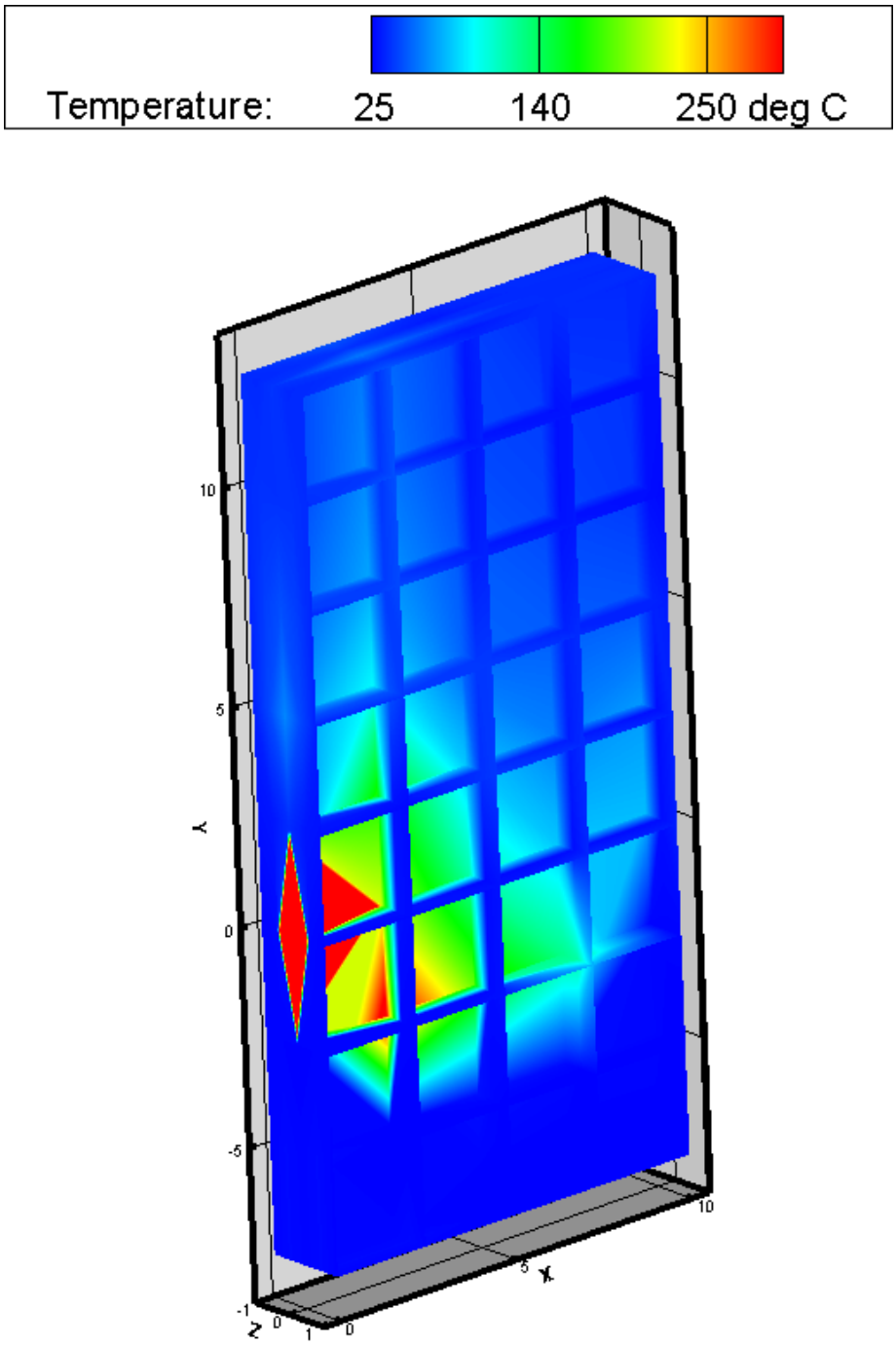

Figure A.1: Three-dimensional temperature gradient: combination of the two-dimensional cross sections of the 0.25 psig flame at 45 degrees

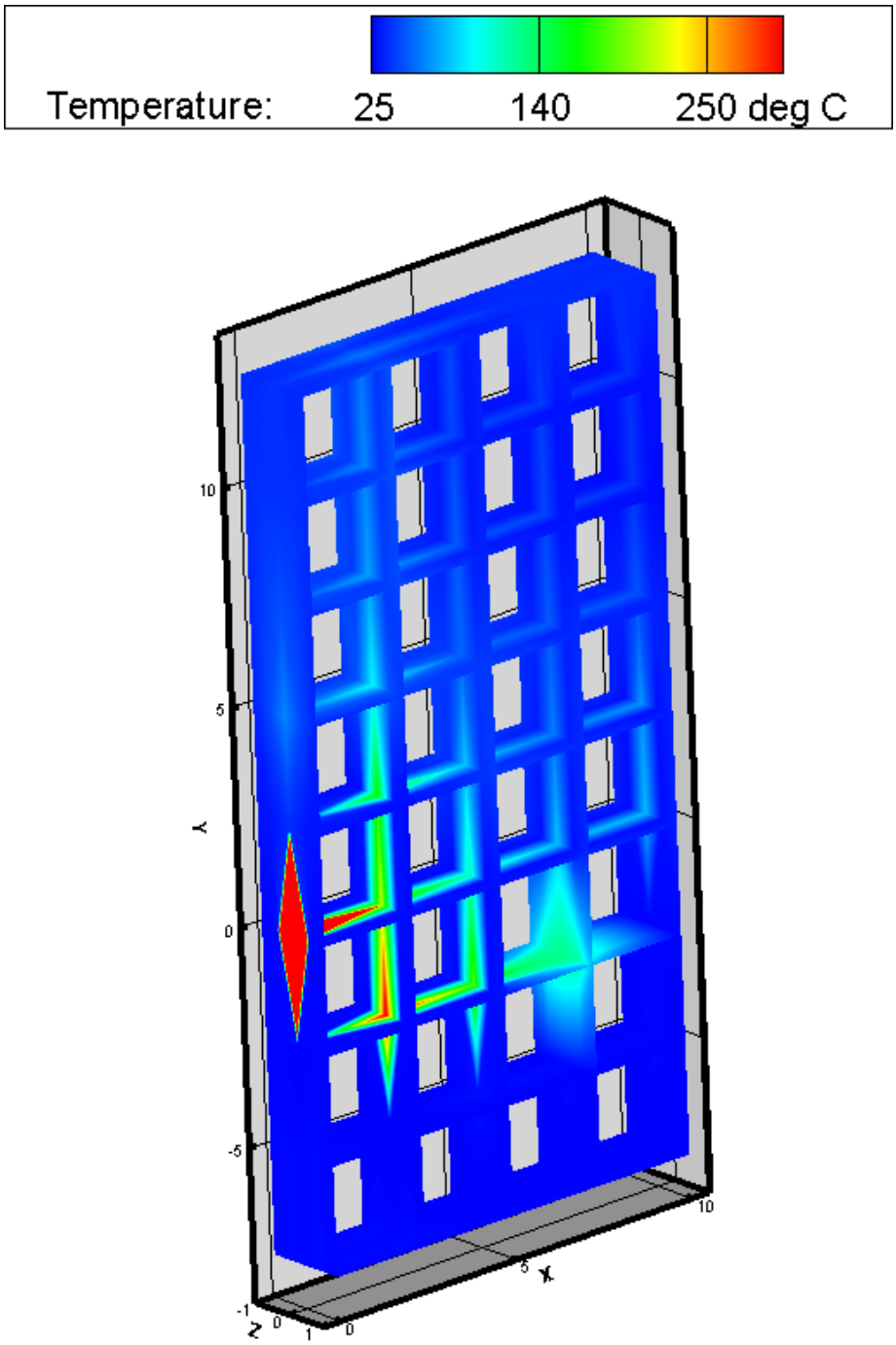

Figure A.2: Three-dimensional temperature gradient: combination of the two-dimensional cross sections of the 0.25 psig flame at 45 degrees

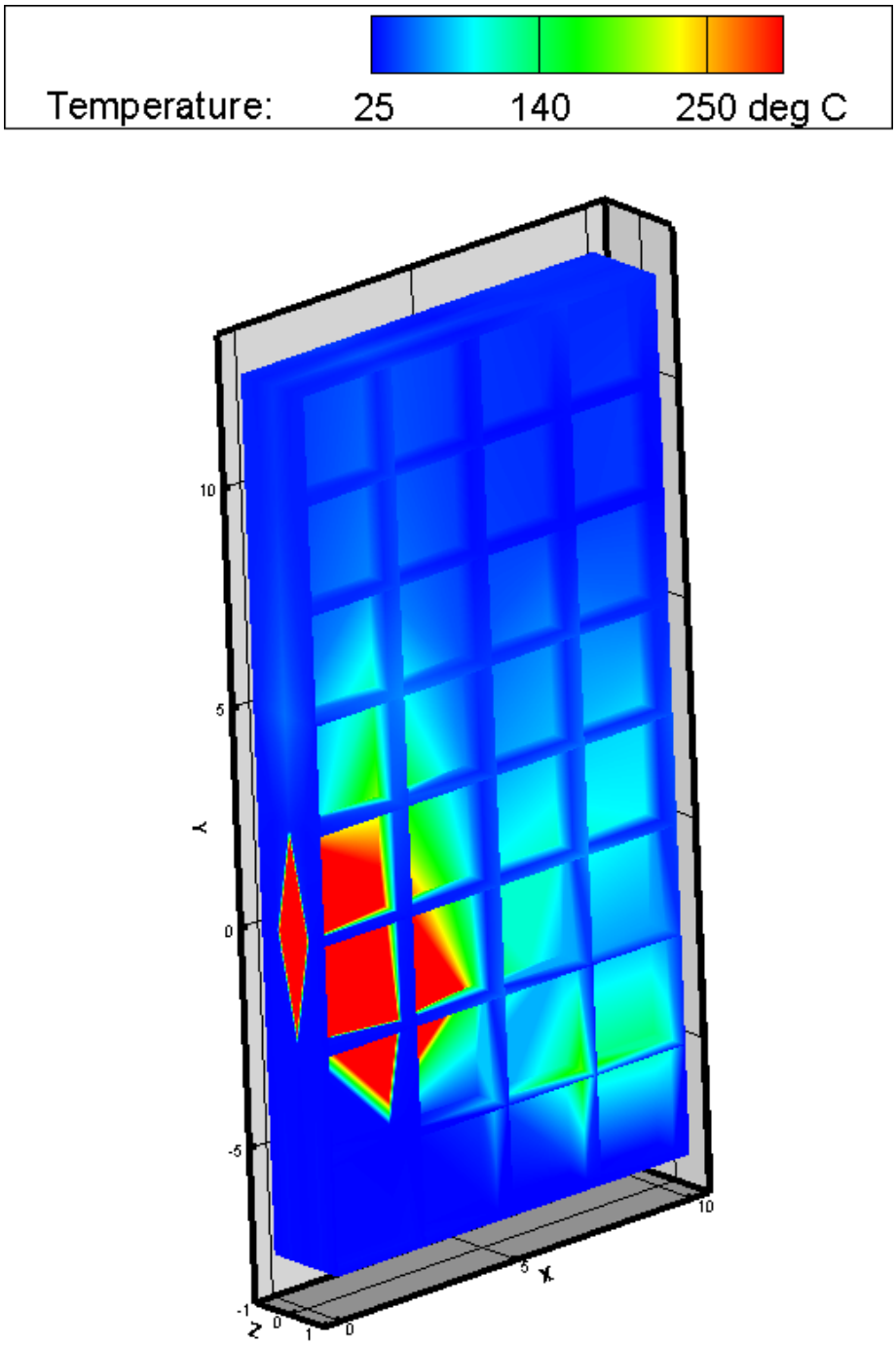

Figure A.3: Three-dimensional temperature gradient: combination of the two-dimensional cross sections of the 0.5 psig flame at 45 degrees

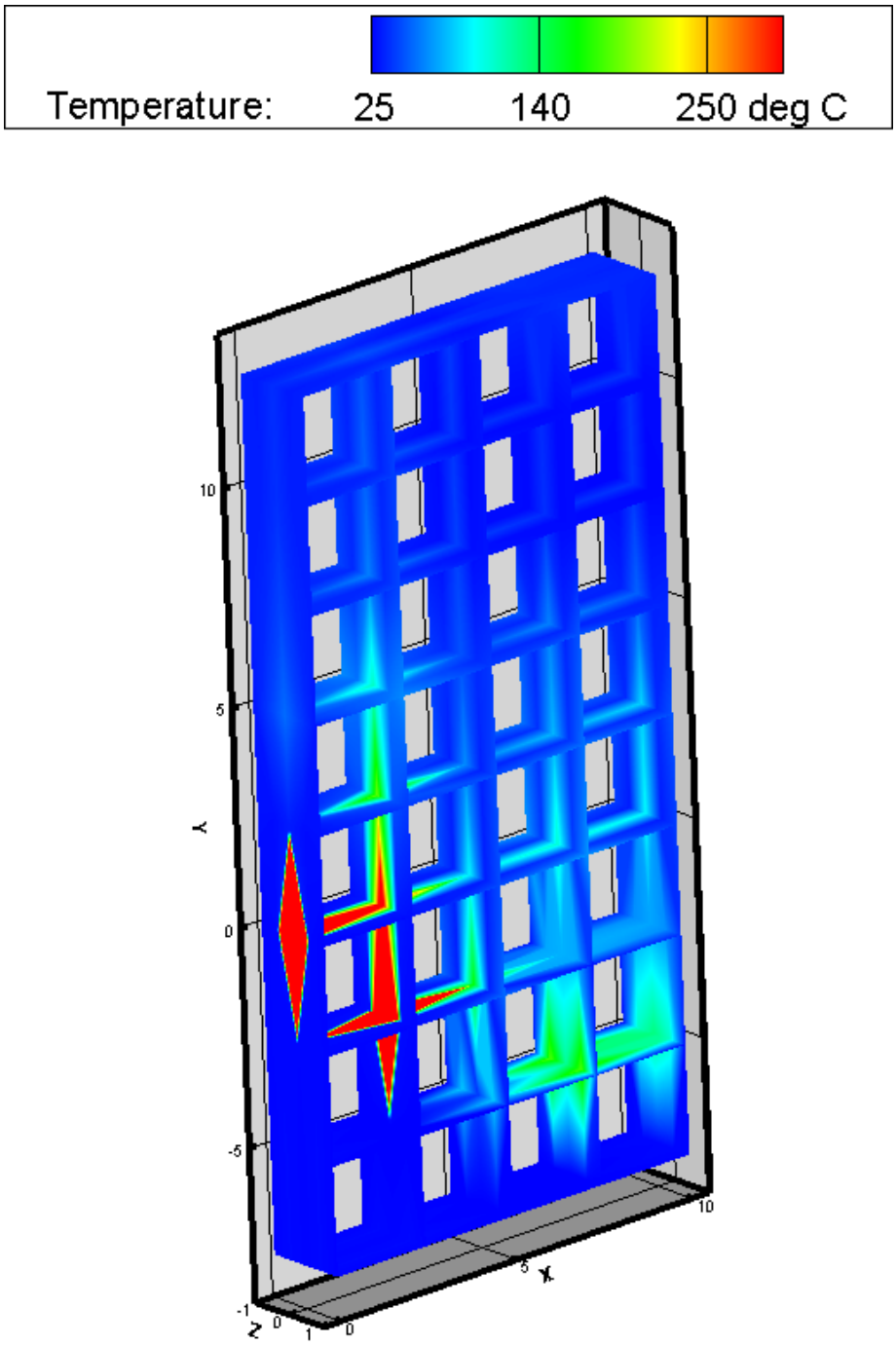

Figure A.4: Three-dimensional temperature gradient: combination of the two-dimensional cross sections of the 0.5 psig flame at 45 degrees

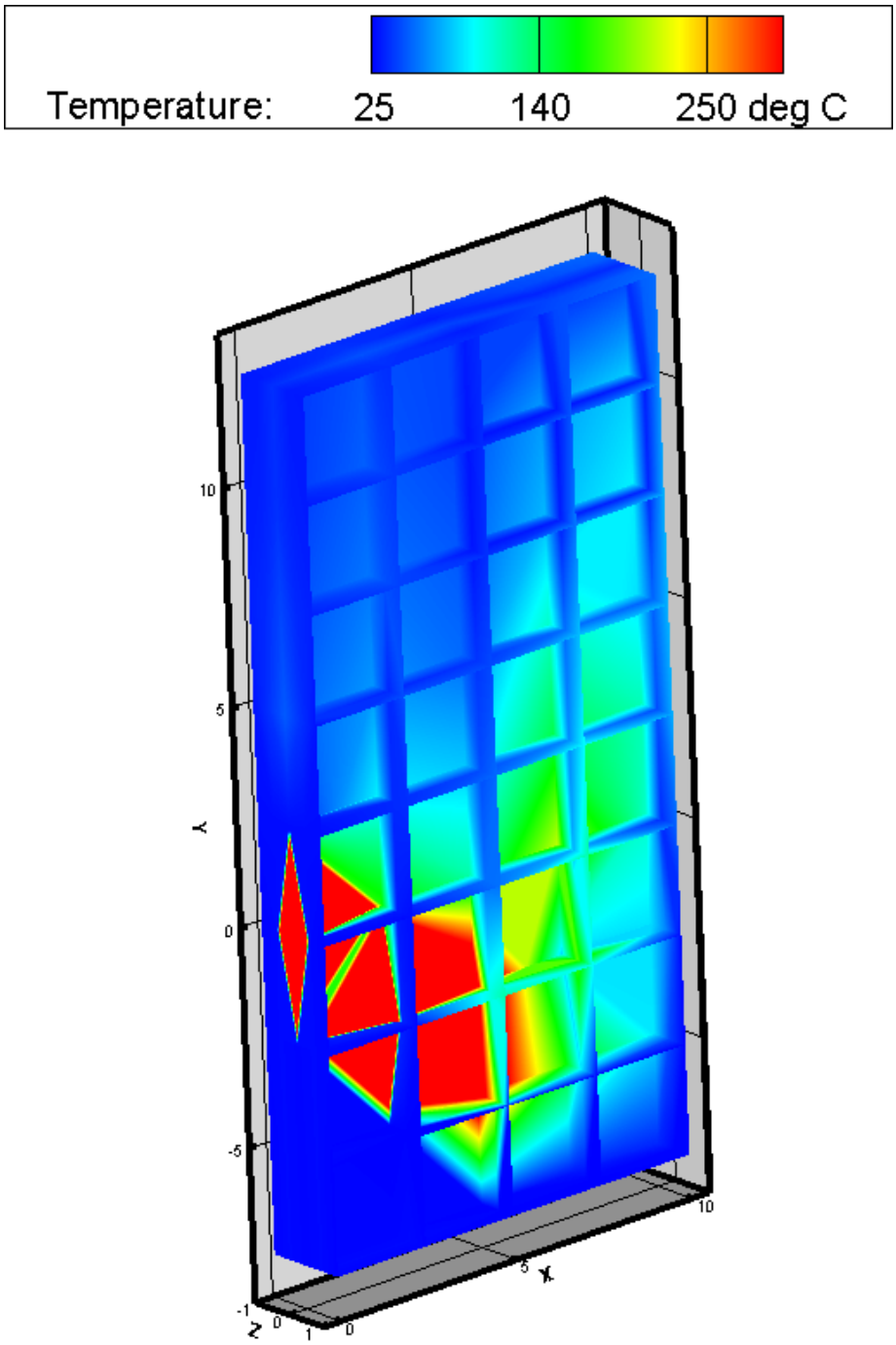

Figure A.5: Three-dimensional temperature gradient: combination of the two-dimensional cross sections of the 0.75 psig flame at 45 degrees

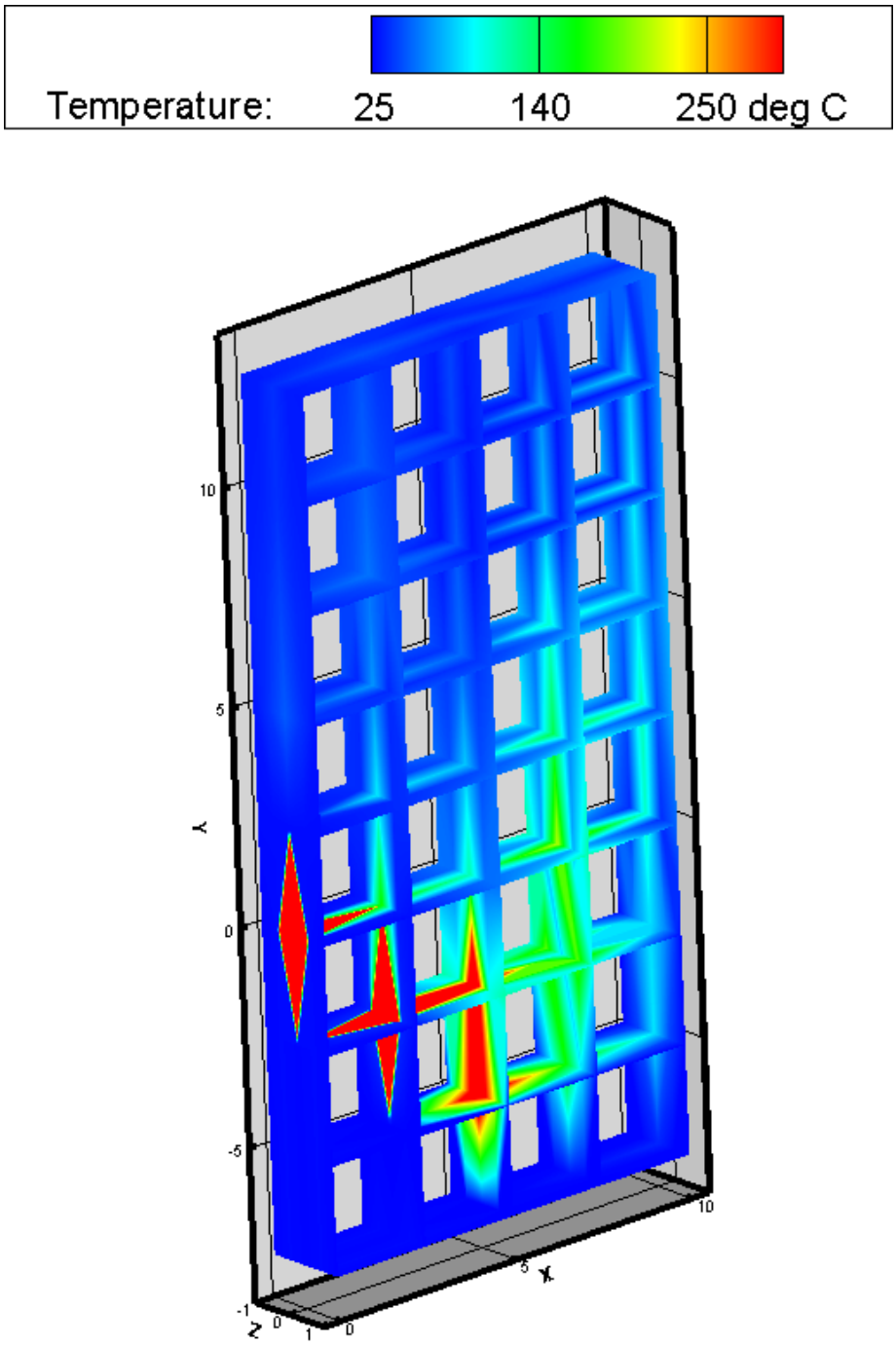

Figure A.6: Three-dimensional temperature gradient: combination of the two-dimensional cross sections of the 0.75 psig flame at 45 degrees

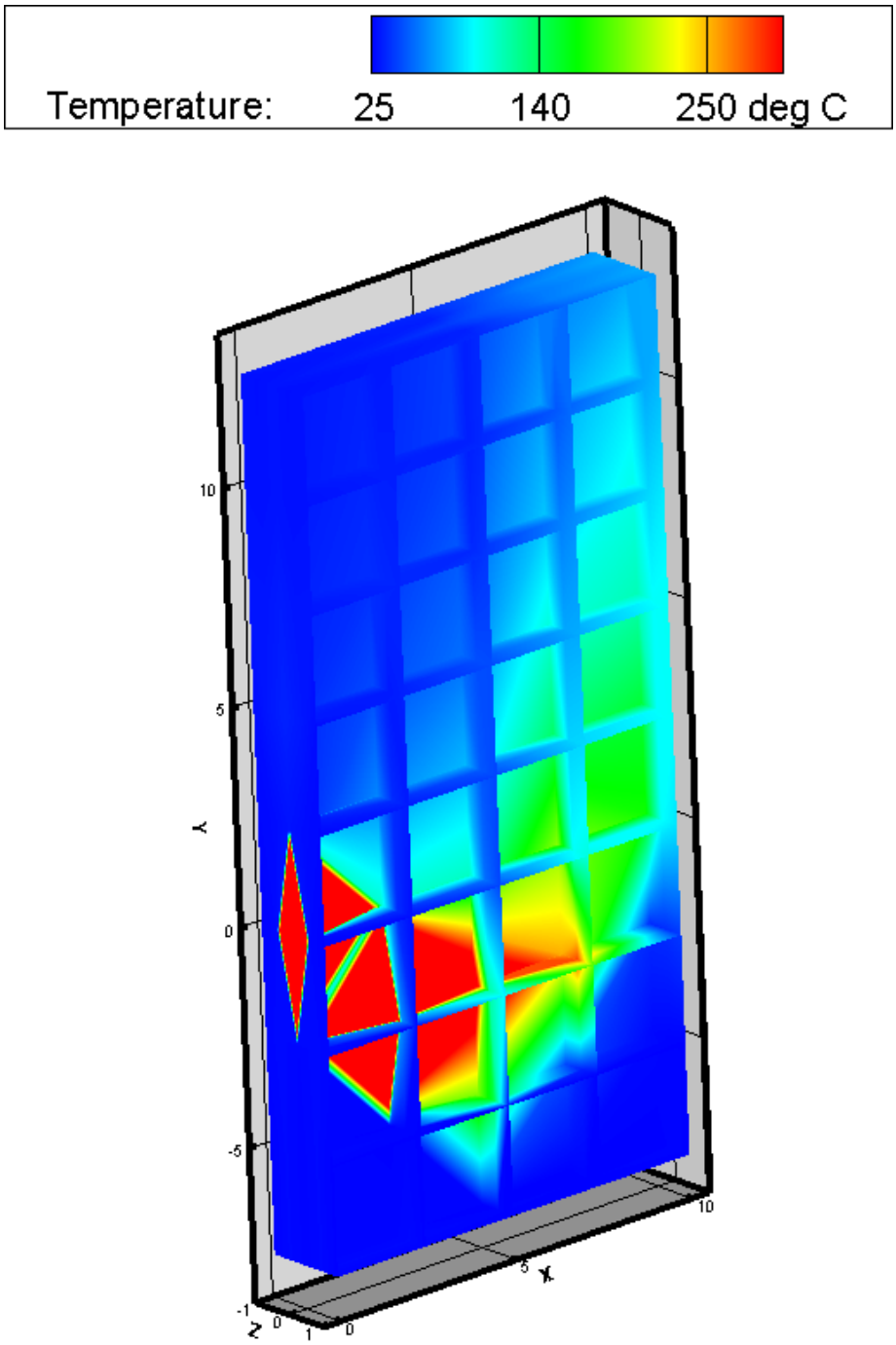

Figure A.7: Three-dimensional temperature gradient: combination of the two-dimensional cross sections of the 1.0 psig flame at 45 degrees

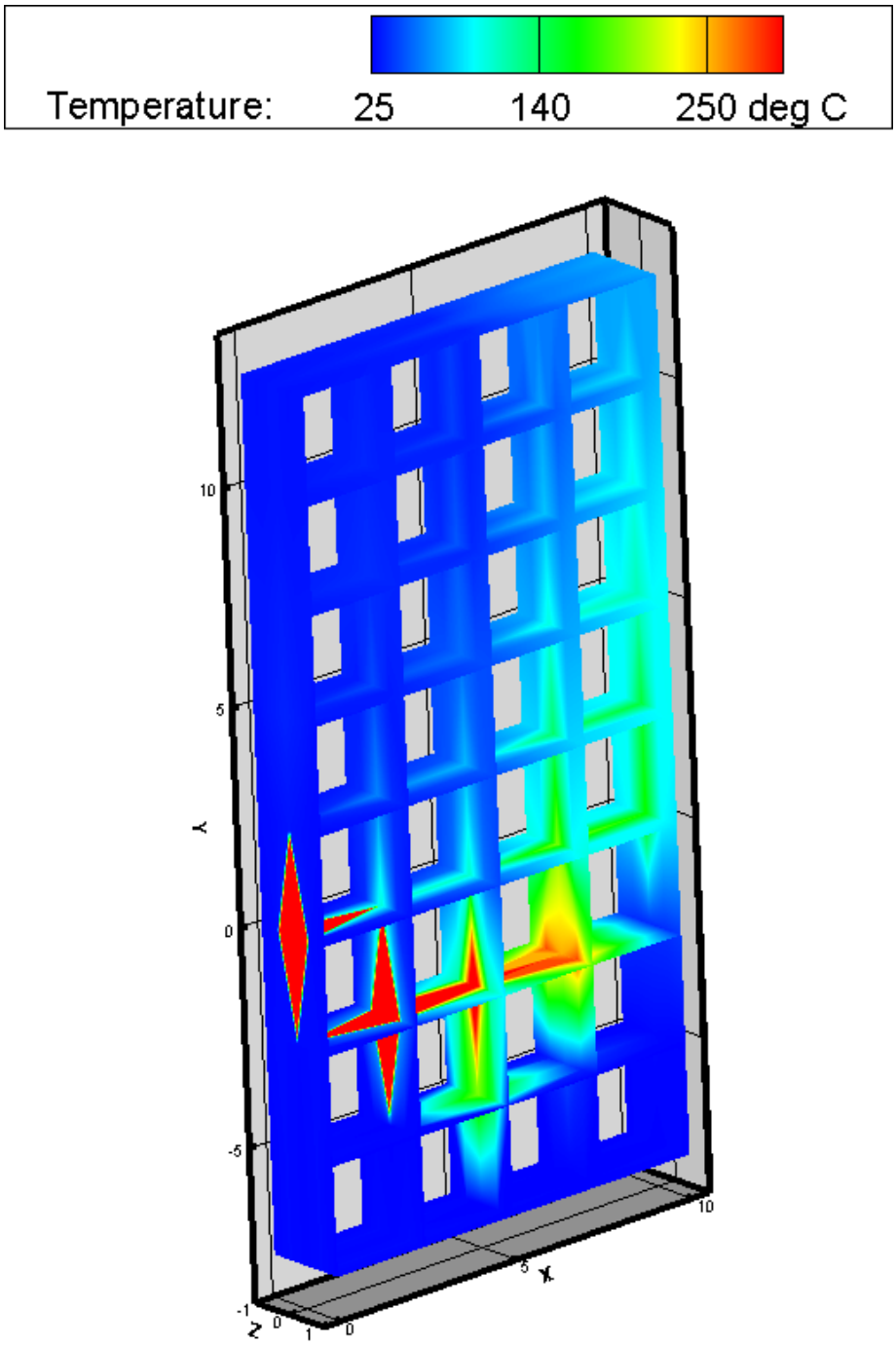

Figure A.8: Three-dimensional temperature gradient: combination of the two-dimensional cross sections of the 1.0 psig flame at 45 degrees

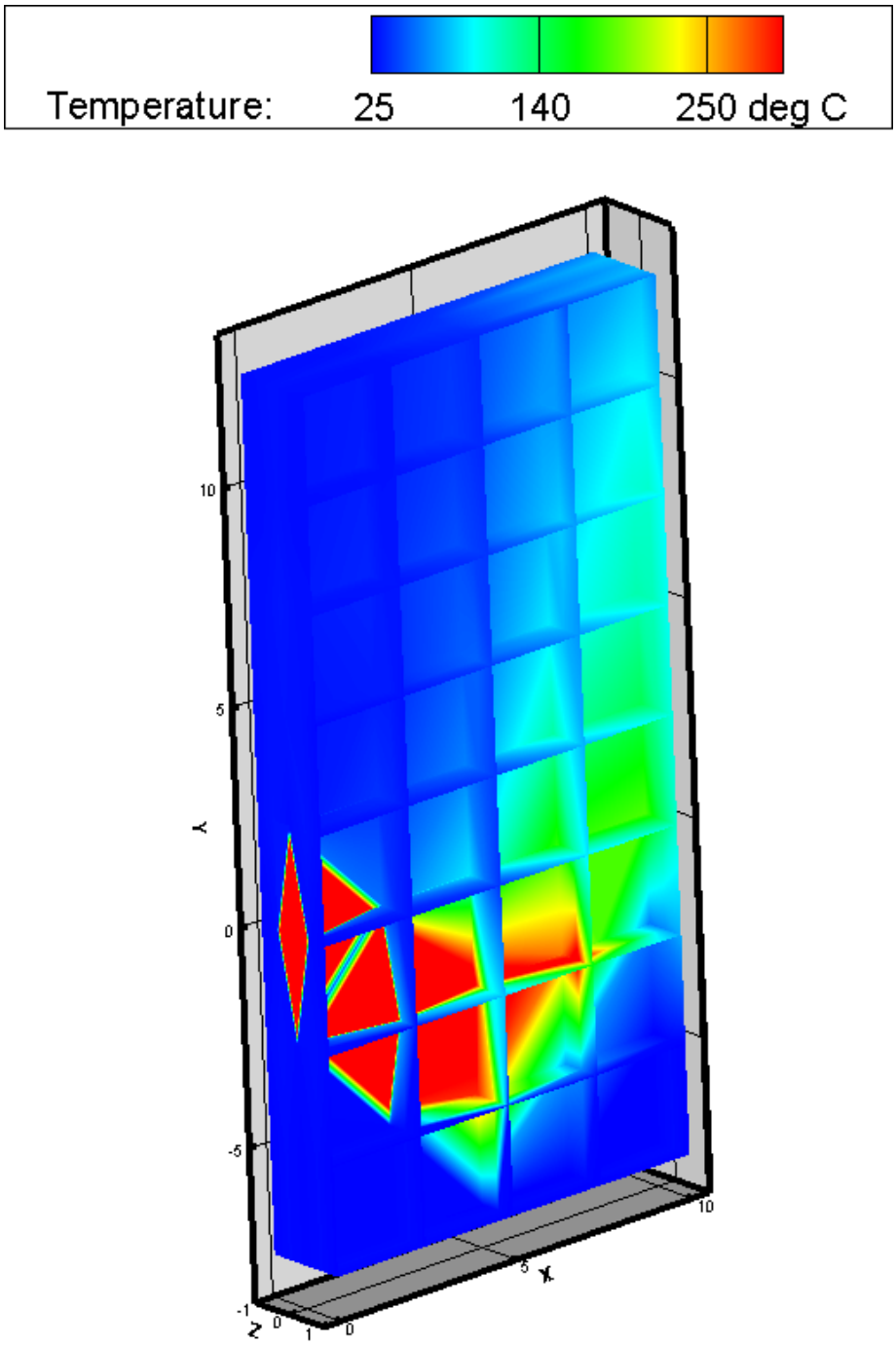

Figure A.9: Three-dimensional temperature gradient: combination of the two-dimensional cross sections of the 1.25 psig flame at 45 degrees

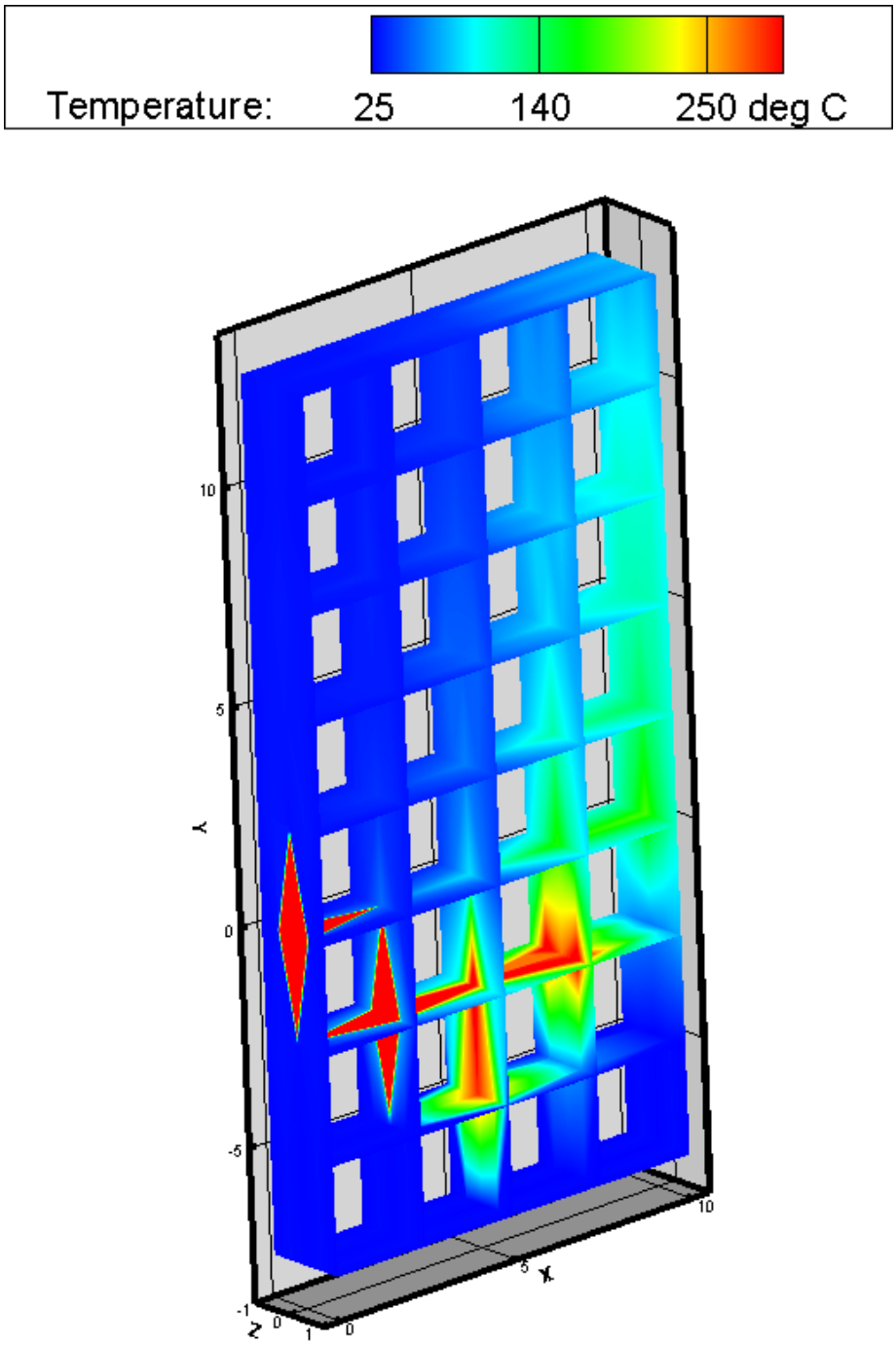

Figure A.10: Three-dimensional temperature gradient: combination of the two-dimensional cross sections of the 1.25 psig flame at 45 degrees

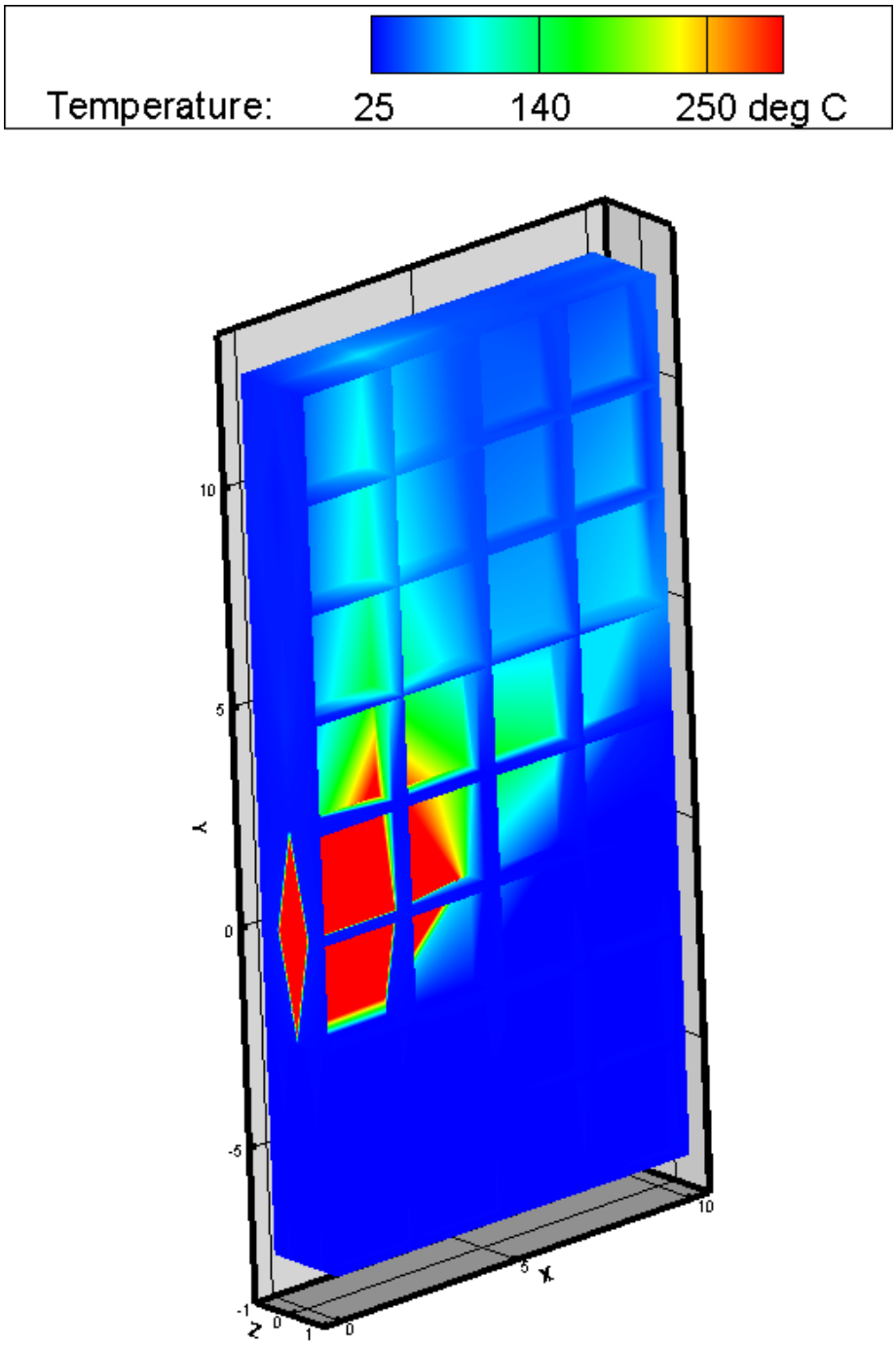

Figure A.11: Three-dimensional temperature gradient: combination of the two-dimensional cross sections of the 0.25 psig flame at 90 degrees

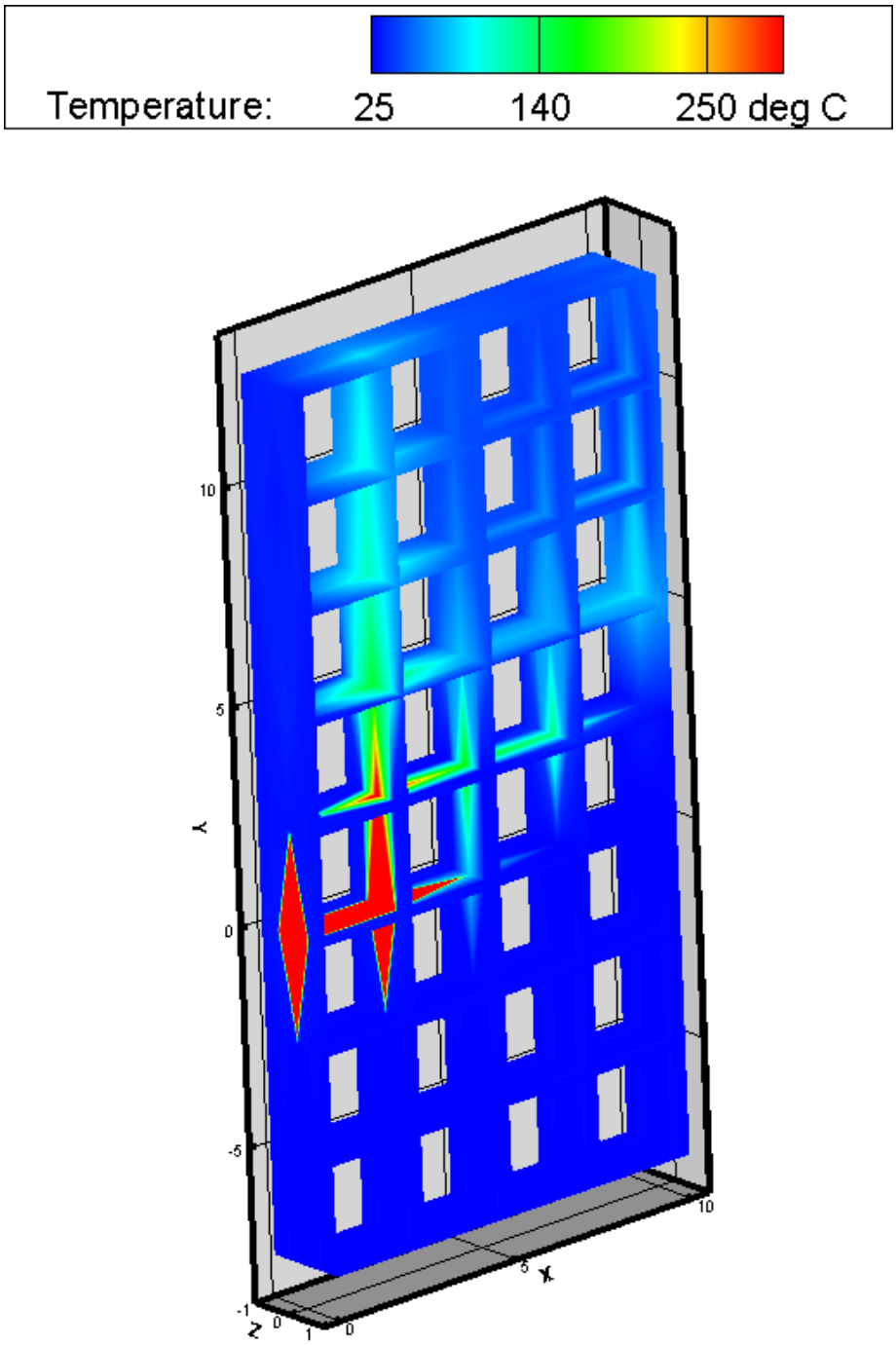

Figure A.12: Three-dimensional temperature gradient: combination of the two-dimensional cross sections of the 0.25 psig flame at 90 degrees

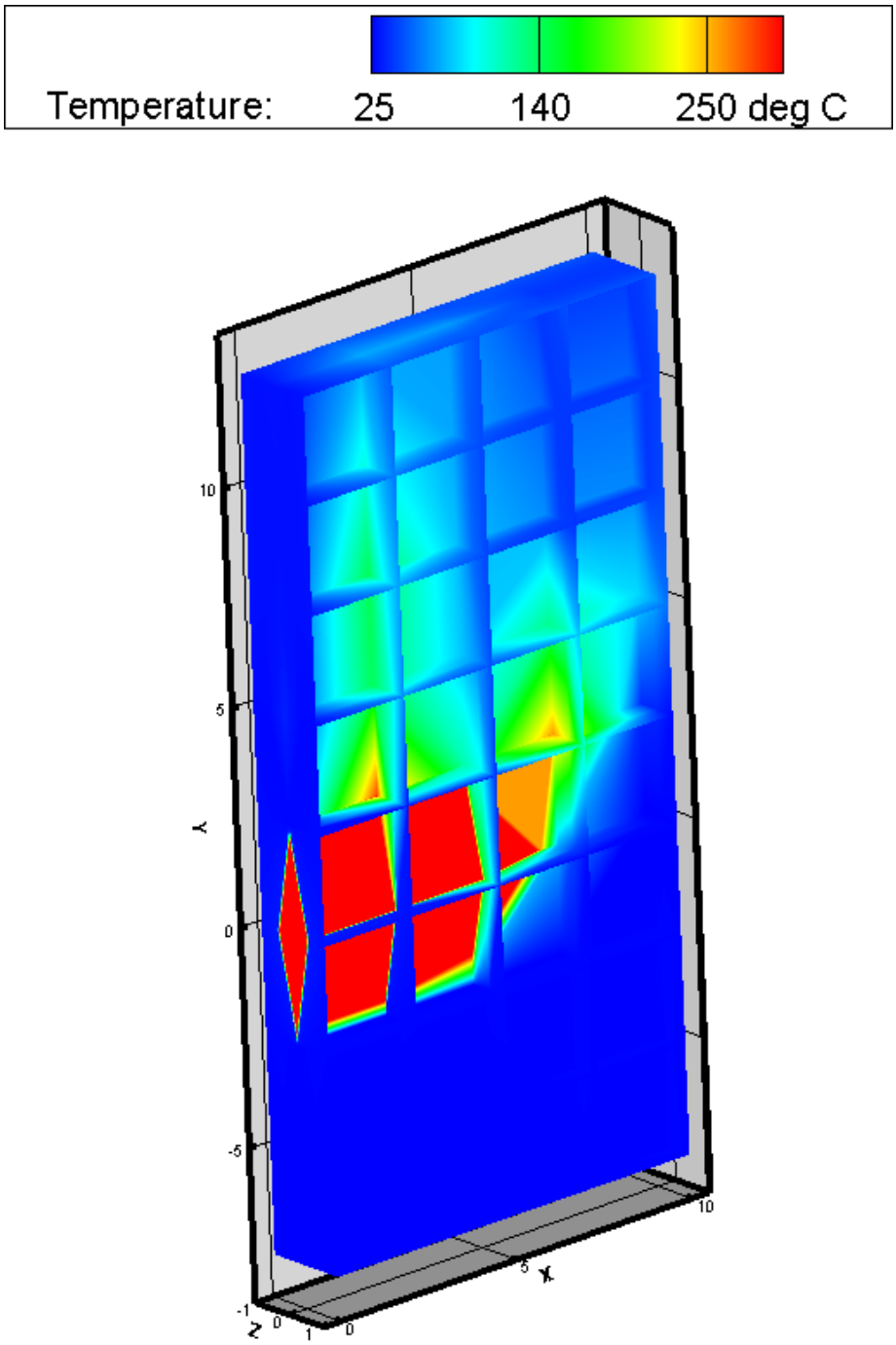

Figure A.13: Three-dimensional temperature gradient: combination of the two-dimensional cross sections of the 0.5 psig flame at 90 degrees

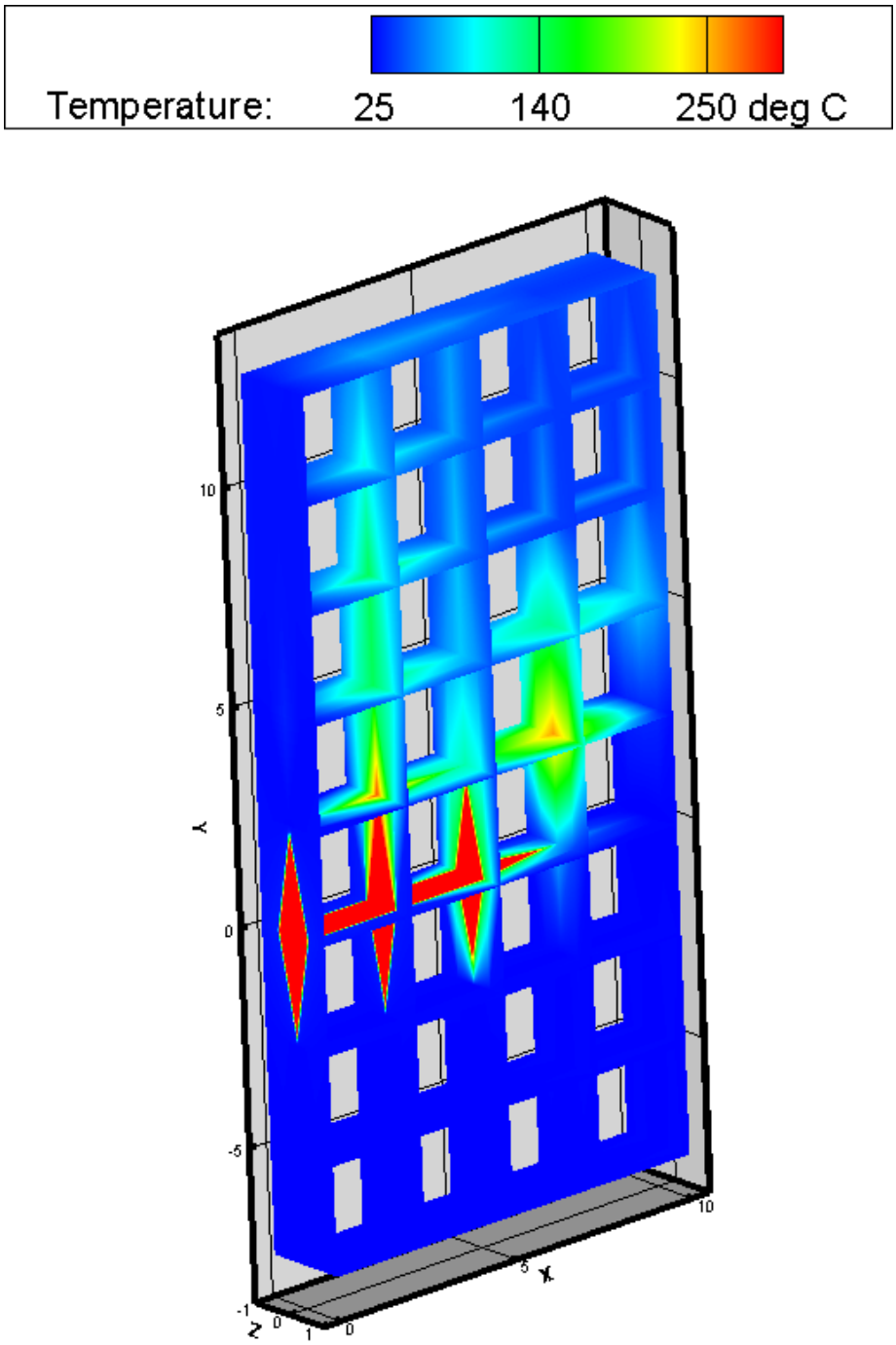

Figure A.14: Three-dimensional temperature gradient: combination of the two-dimensional cross sections of the 0.5 psig flame at 90 degrees

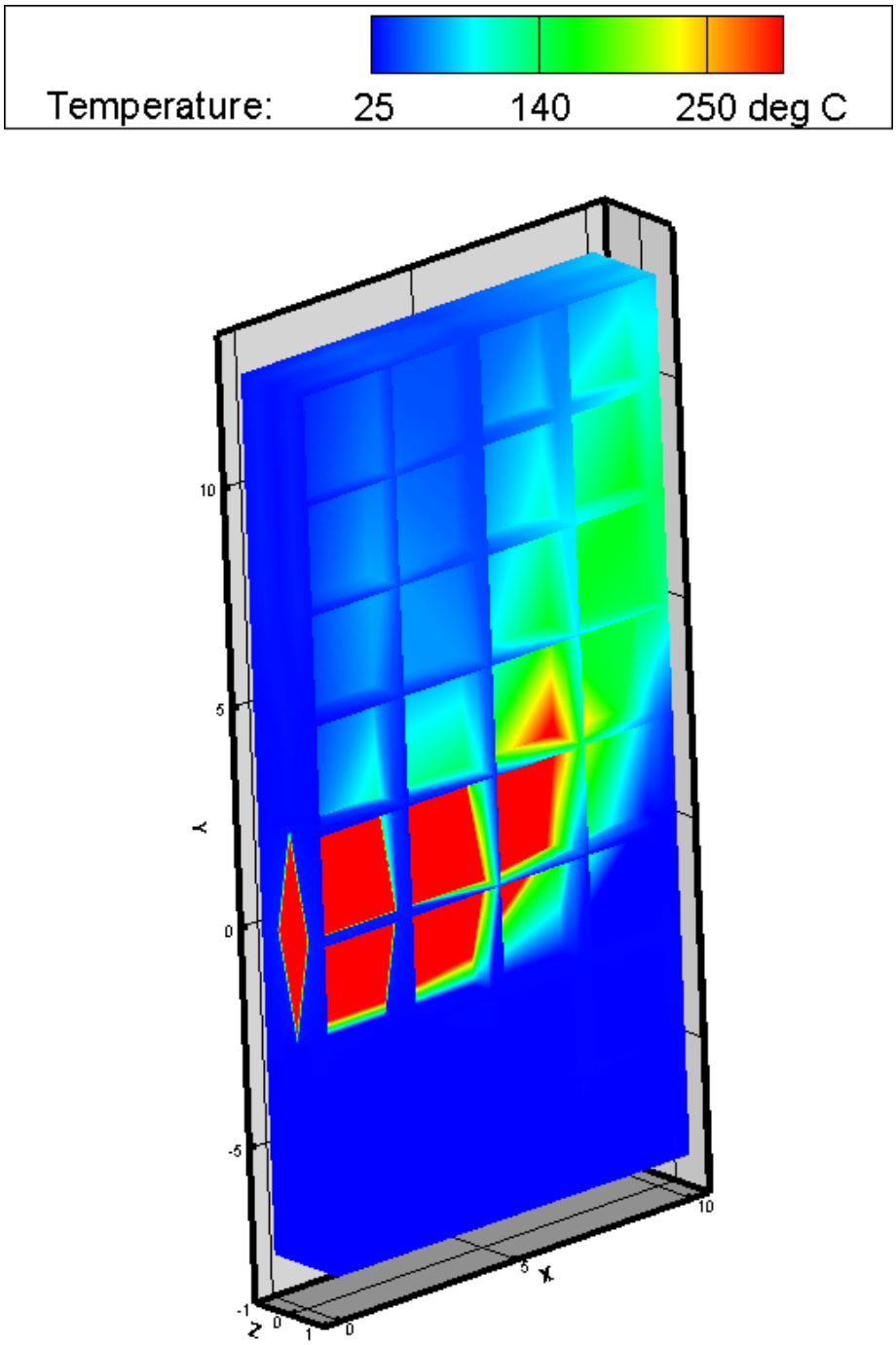

Figure A.15: Three-dimensional temperature gradient: combination of the two-dimensional cross sections of the 0.75 psig flame at 90 degrees

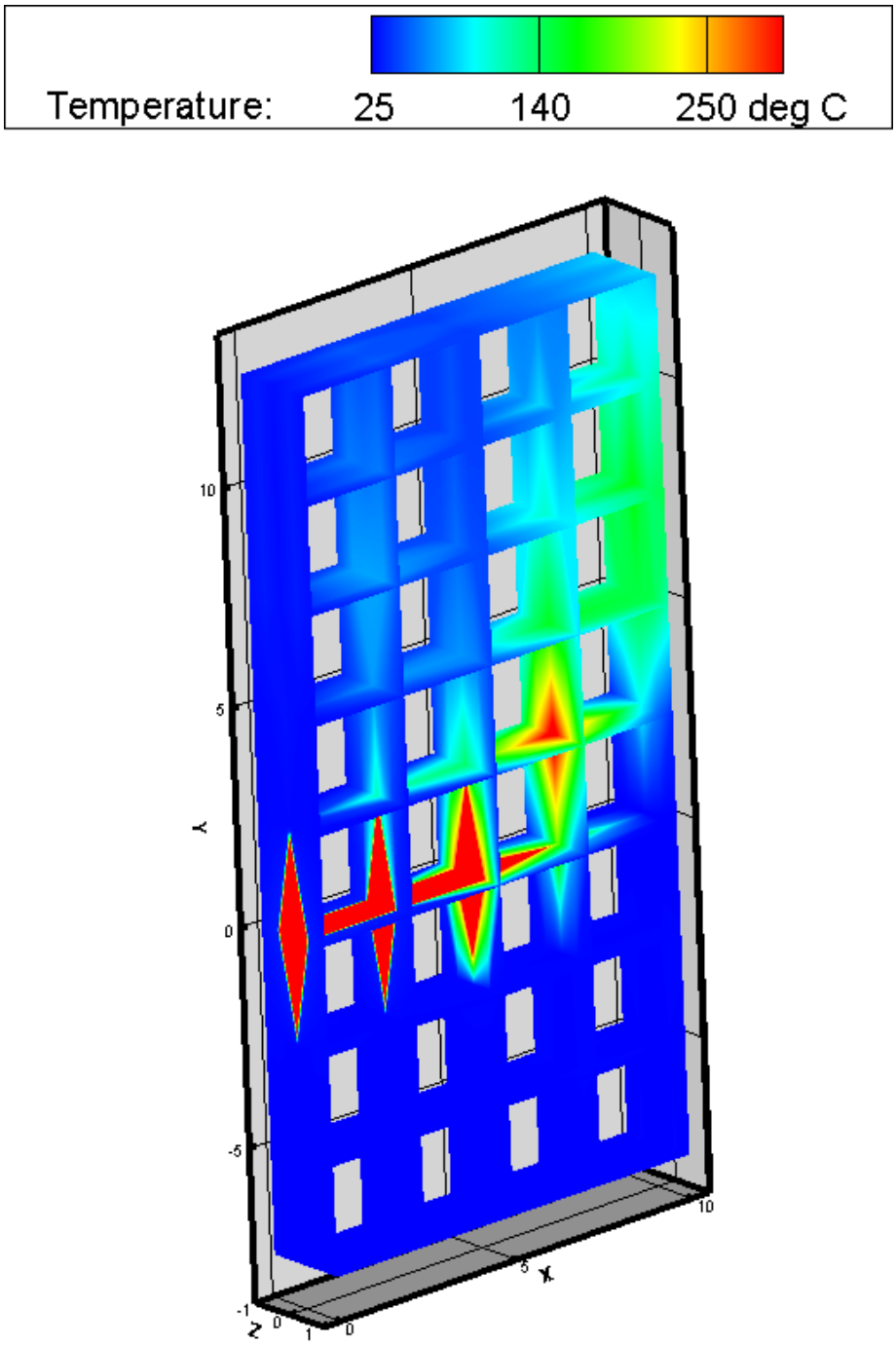

Figure A.16: Three-dimensional temperature gradient: combination of the two-dimensional cross sections of the 0.75 psig flame at 90 degrees

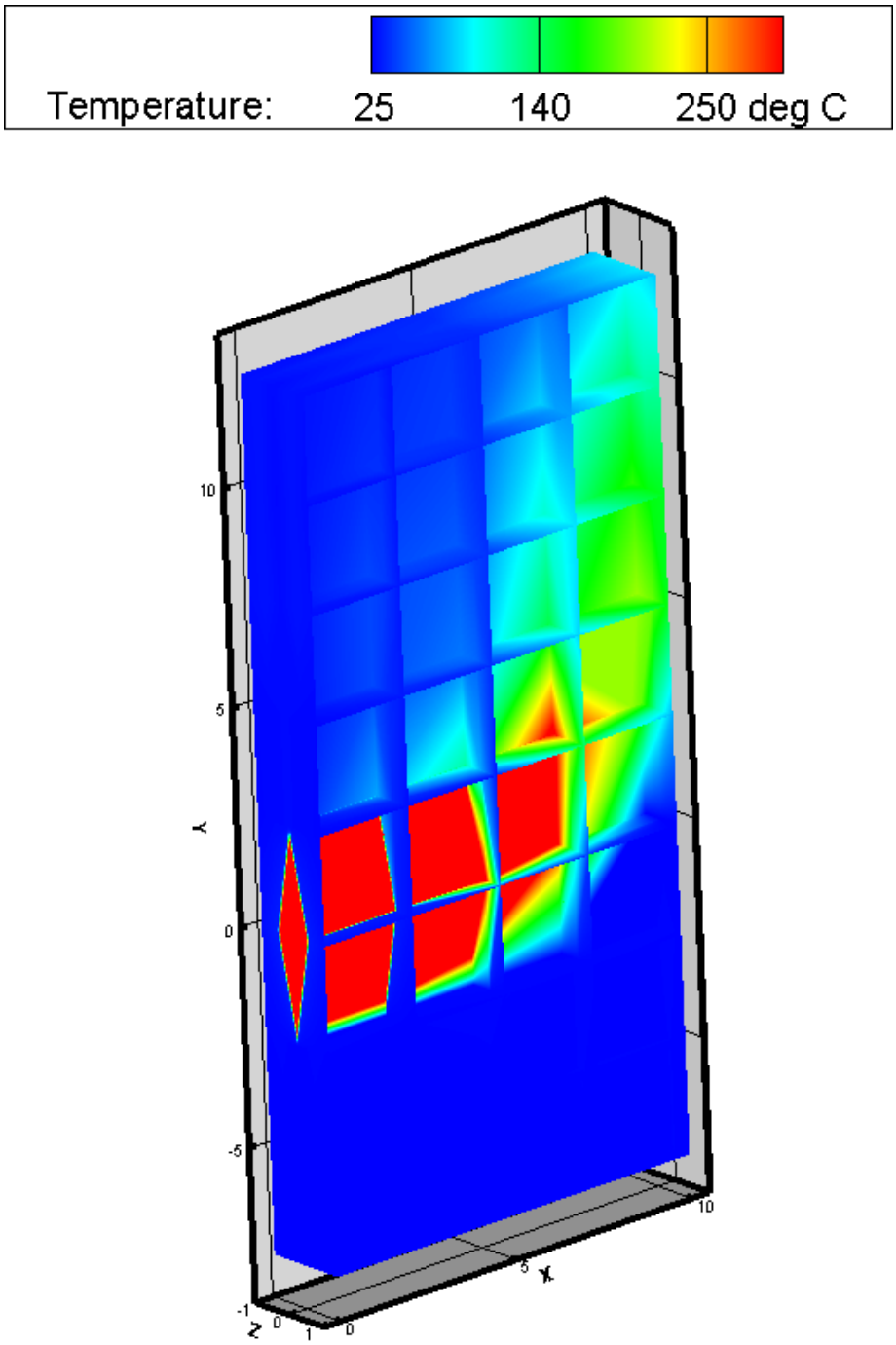

Figure A.17: Three-dimensional temperature gradient: combination of the two-dimensional cross sections of the 1.0 psig flame at 90 degrees

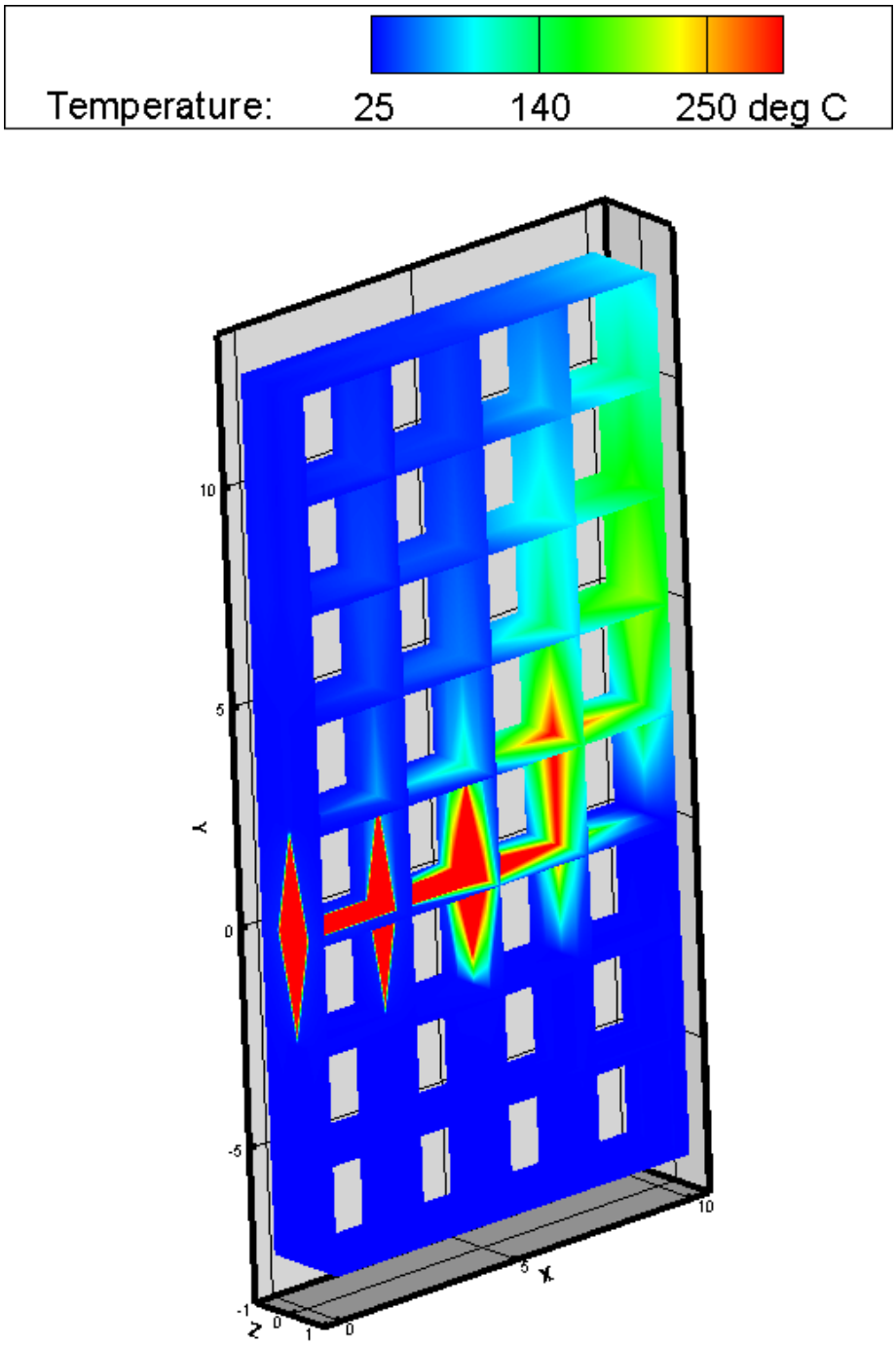

Figure A.18: Three-dimensional temperature gradient: combination of the two-dimensional cross sections of the 1.0 psig flame at 90 degrees

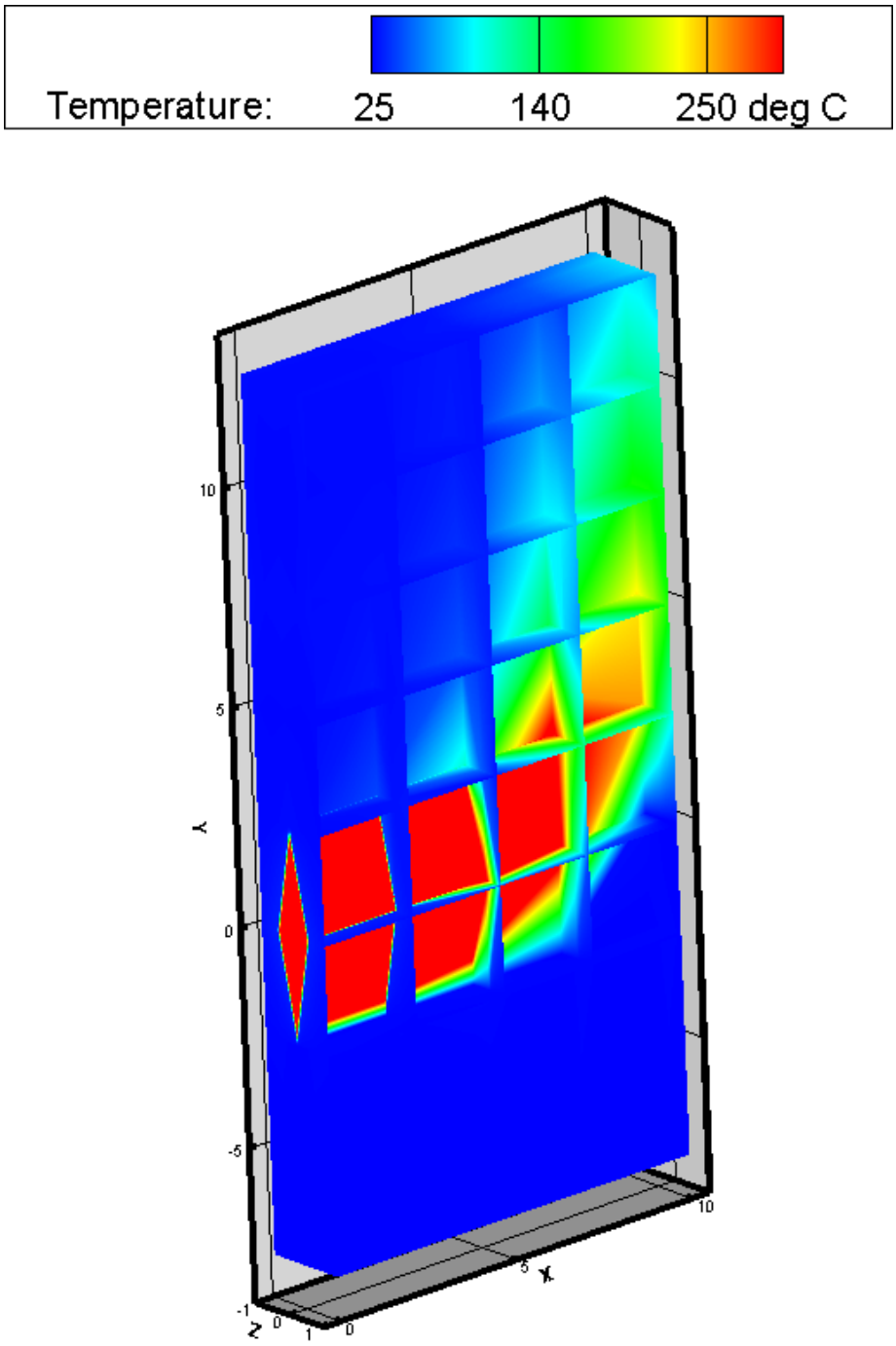

Figure A.19: Three-dimensional temperature gradient: combination of the two-dimensional cross sections of the 1.25 psig flame at 90 degrees

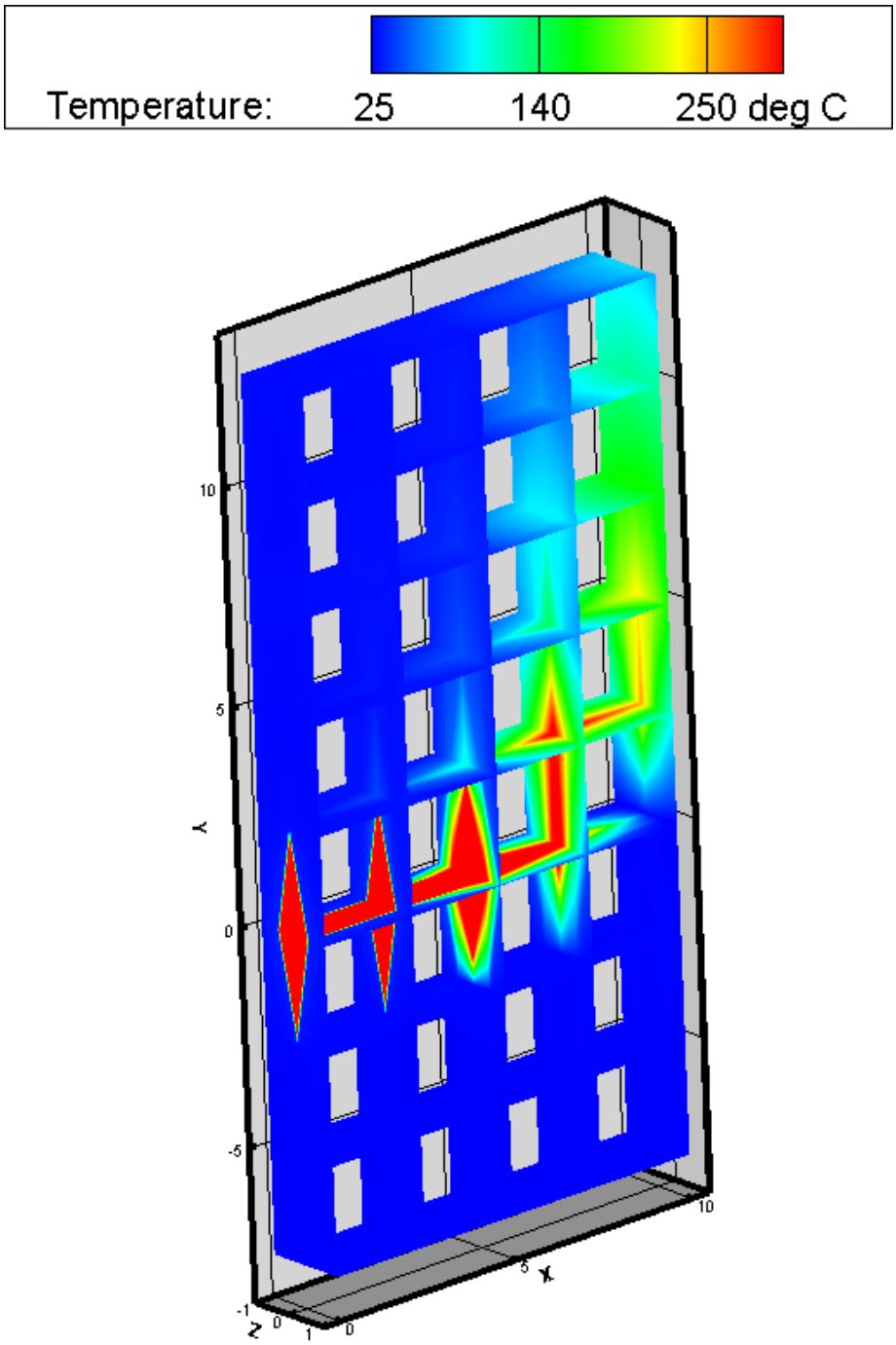

Figure A.20: Three-dimensional temperature gradient: combination of the two-dimensional cross sections of the 1.25 psig flame at 90 degrees

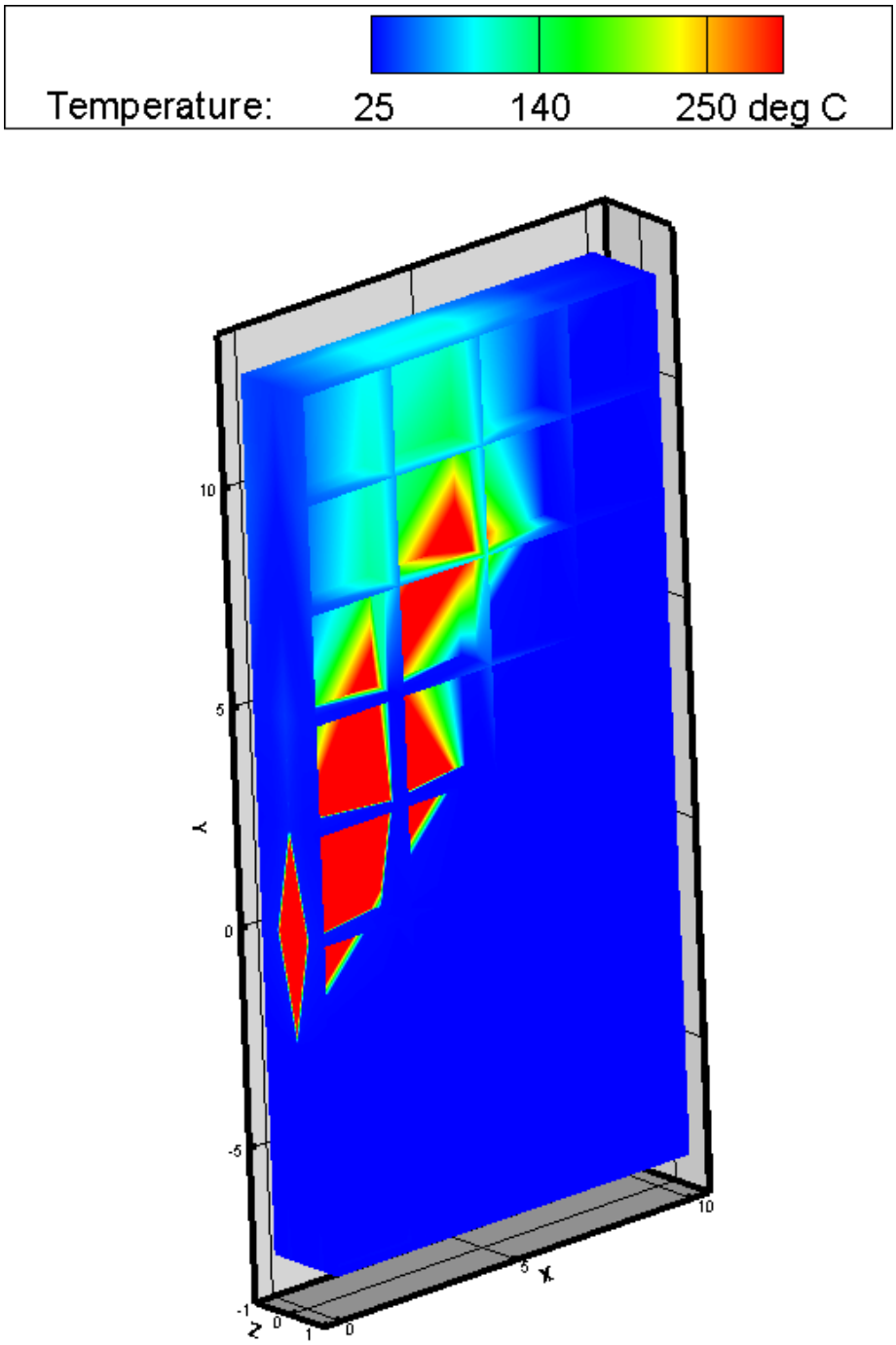

Figure A.21: Three-dimensional temperature gradient: combination of the two-dimensional cross sections of the 0.25 psig flame at 135 degrees

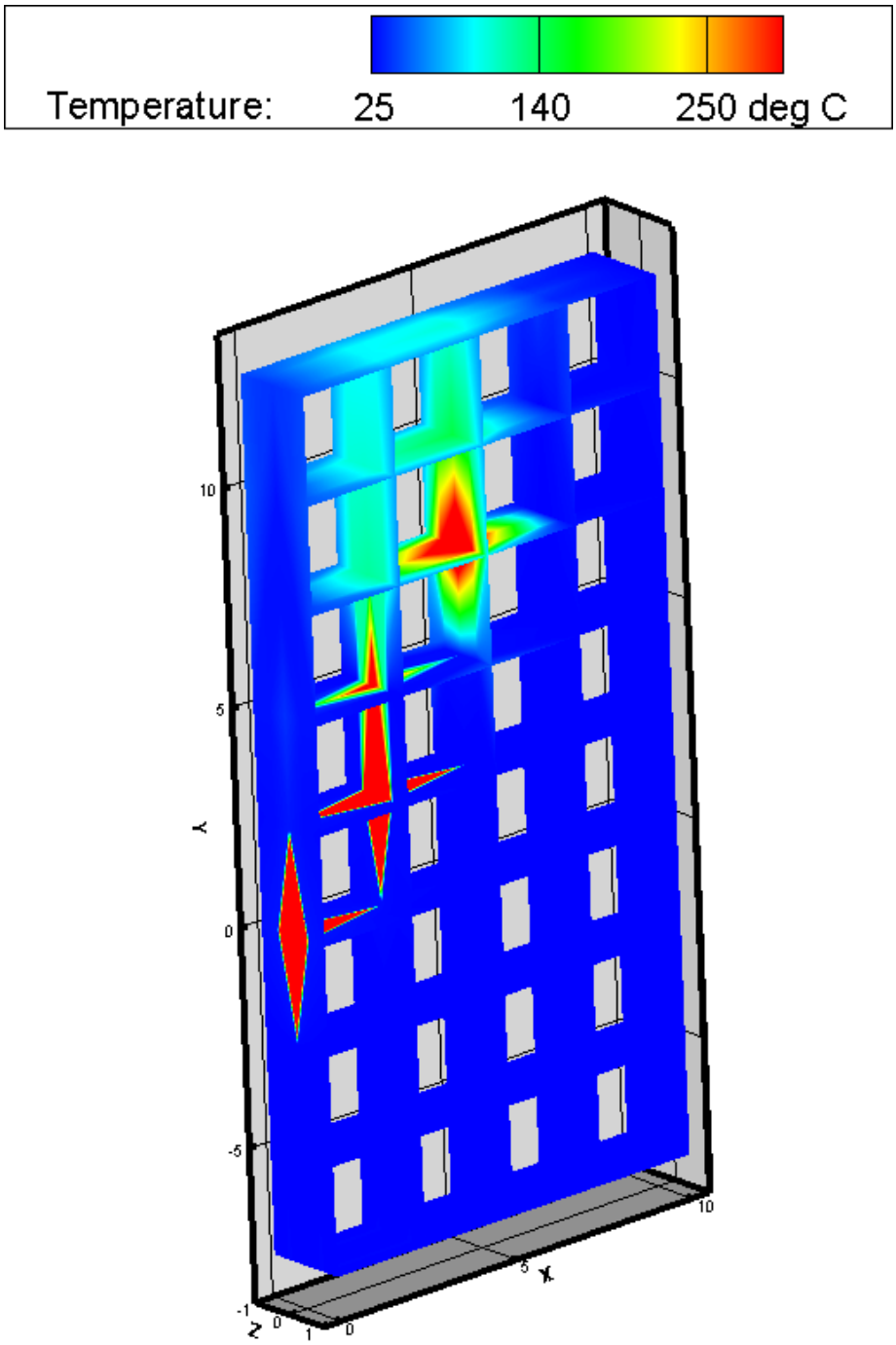

Figure A.22: Three-dimensional temperature gradient: combination of the two-dimensional cross sections of the 0.25 psig flame at 135 degrees

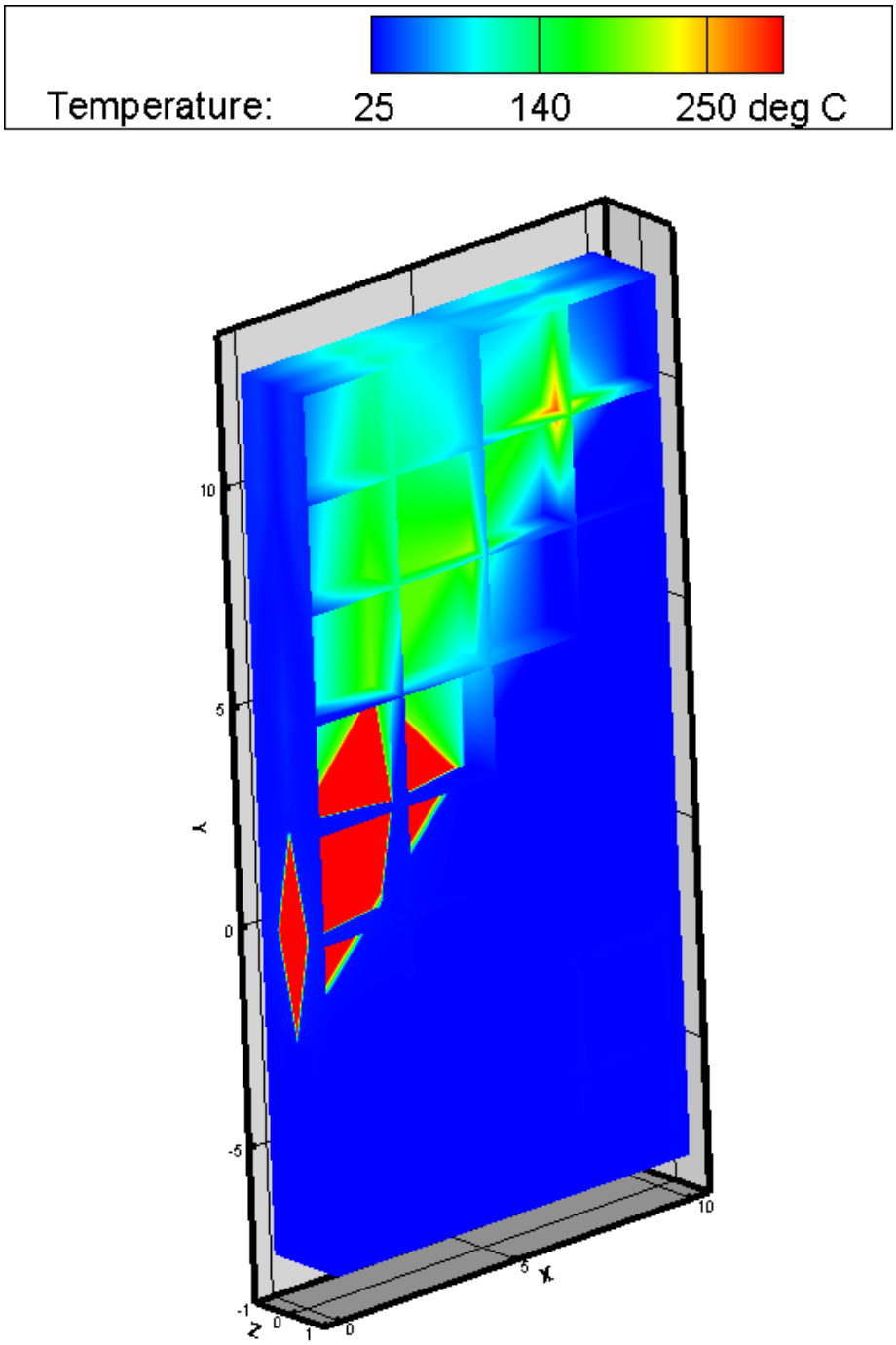

Figure A.23: Three-dimensional temperature gradient: combination of the two-dimensional cross sections of the 0.5 psig flame at 135 degrees

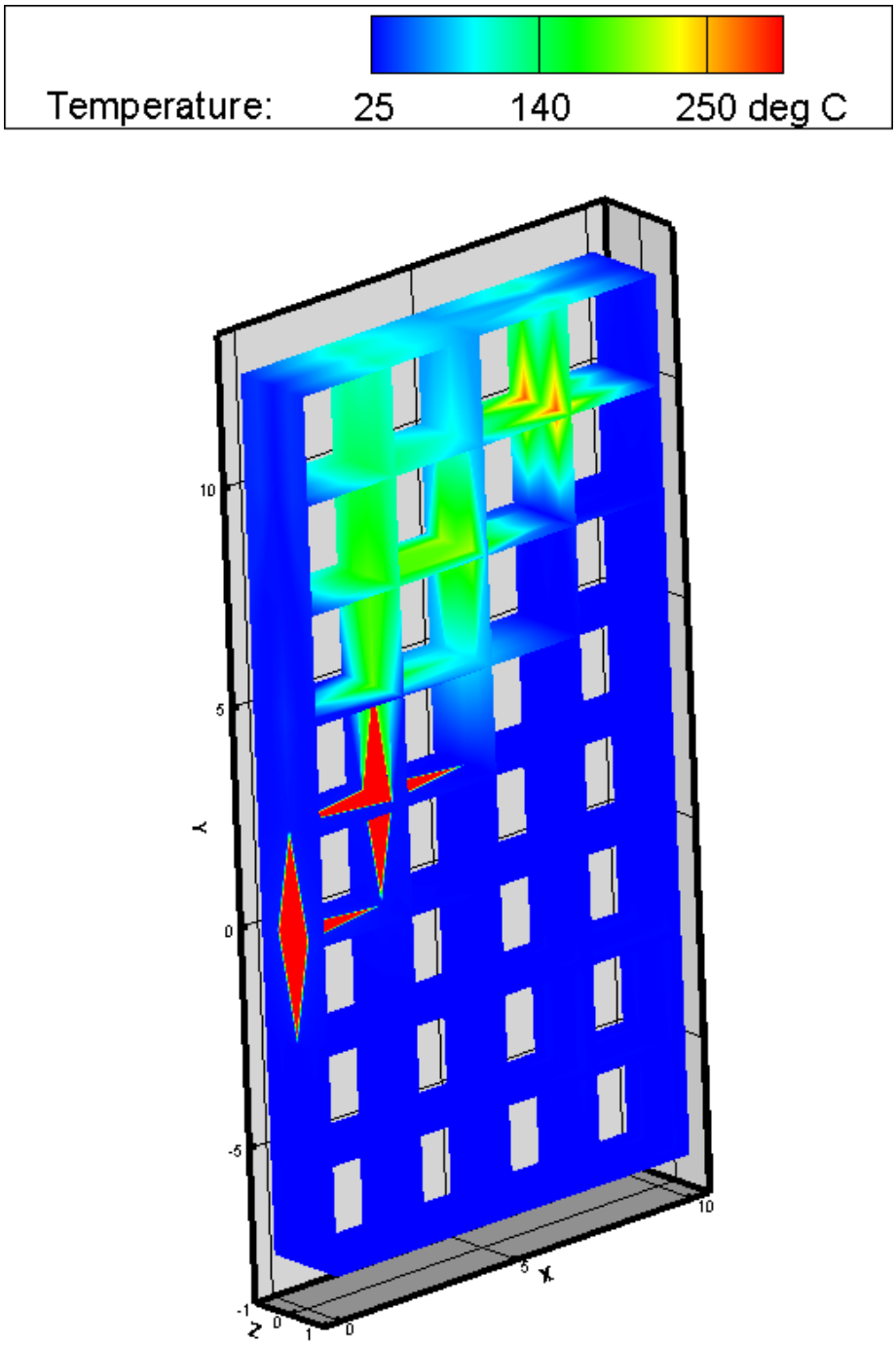

Figure A.24: Three-dimensional temperature gradient: combination of the two-dimensional cross sections of the 0.5 psig flame at 135 degrees

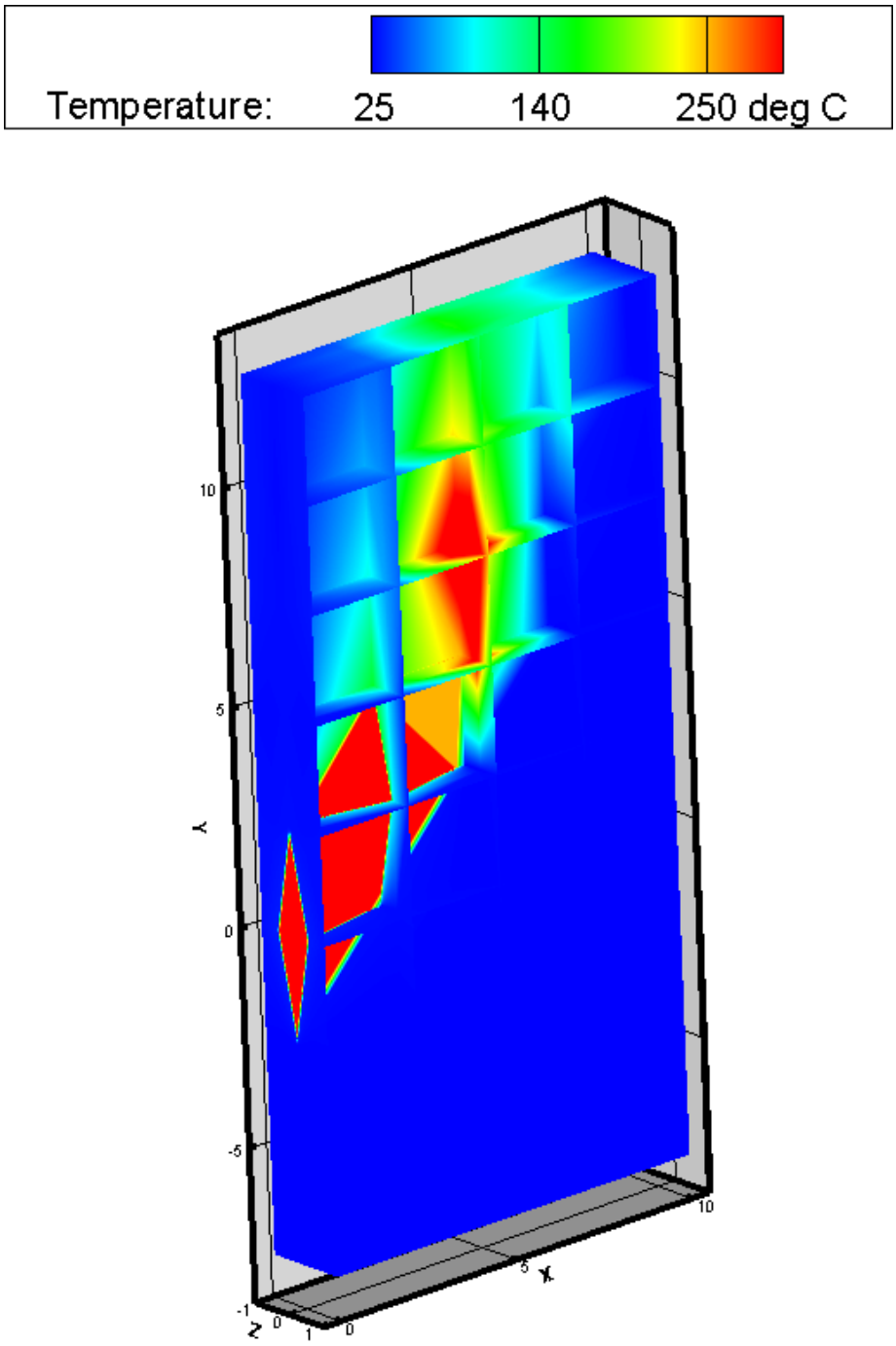

Figure A.25: Three-dimensional temperature gradient: combination of the two-dimensional cross sections of the 0.75 psig flame at 135 degrees

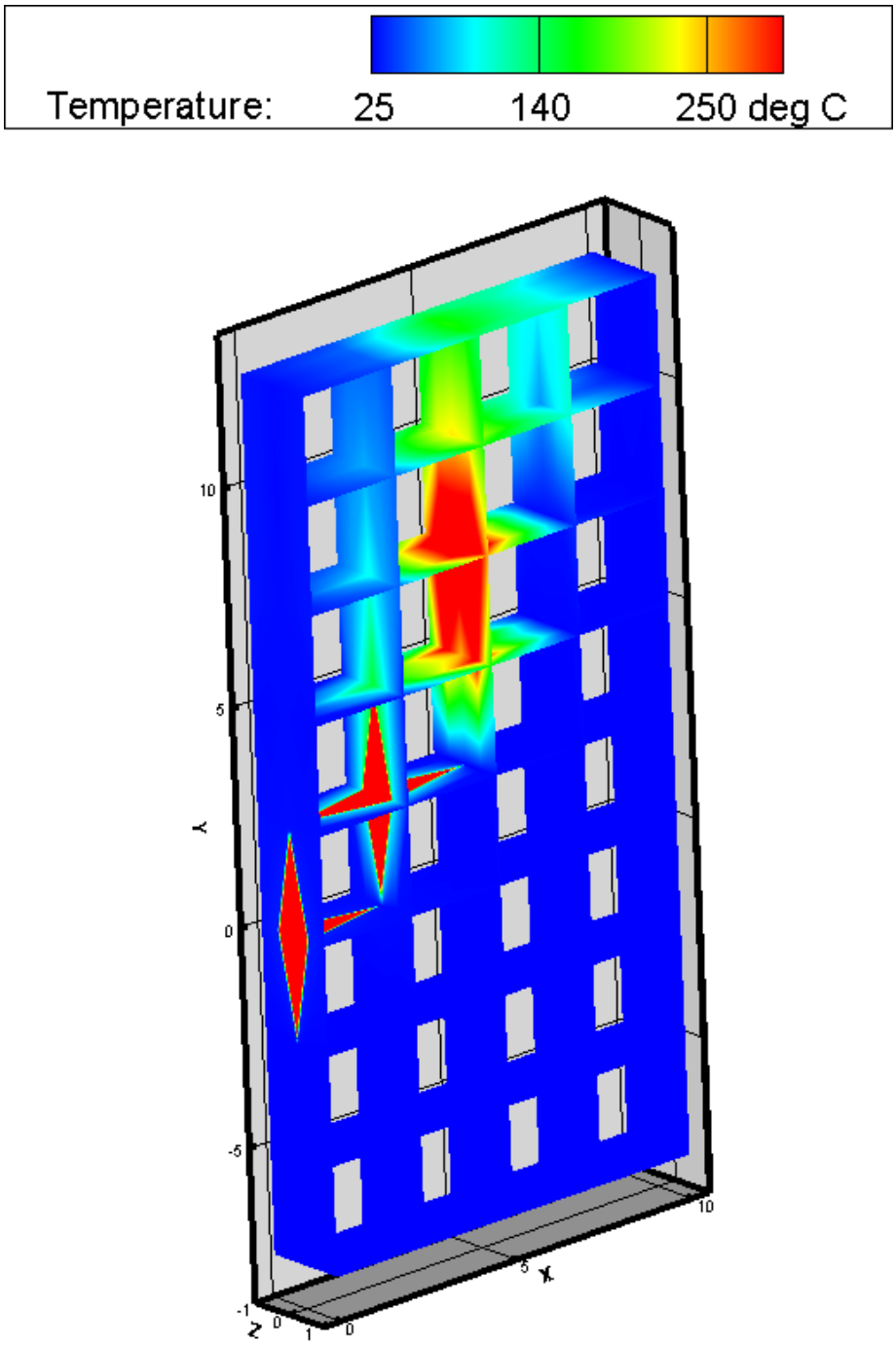

Figure A.26: Three-dimensional temperature gradient: combination of the two-dimensional cross sections of the 0.75 psig flame at 135 degrees

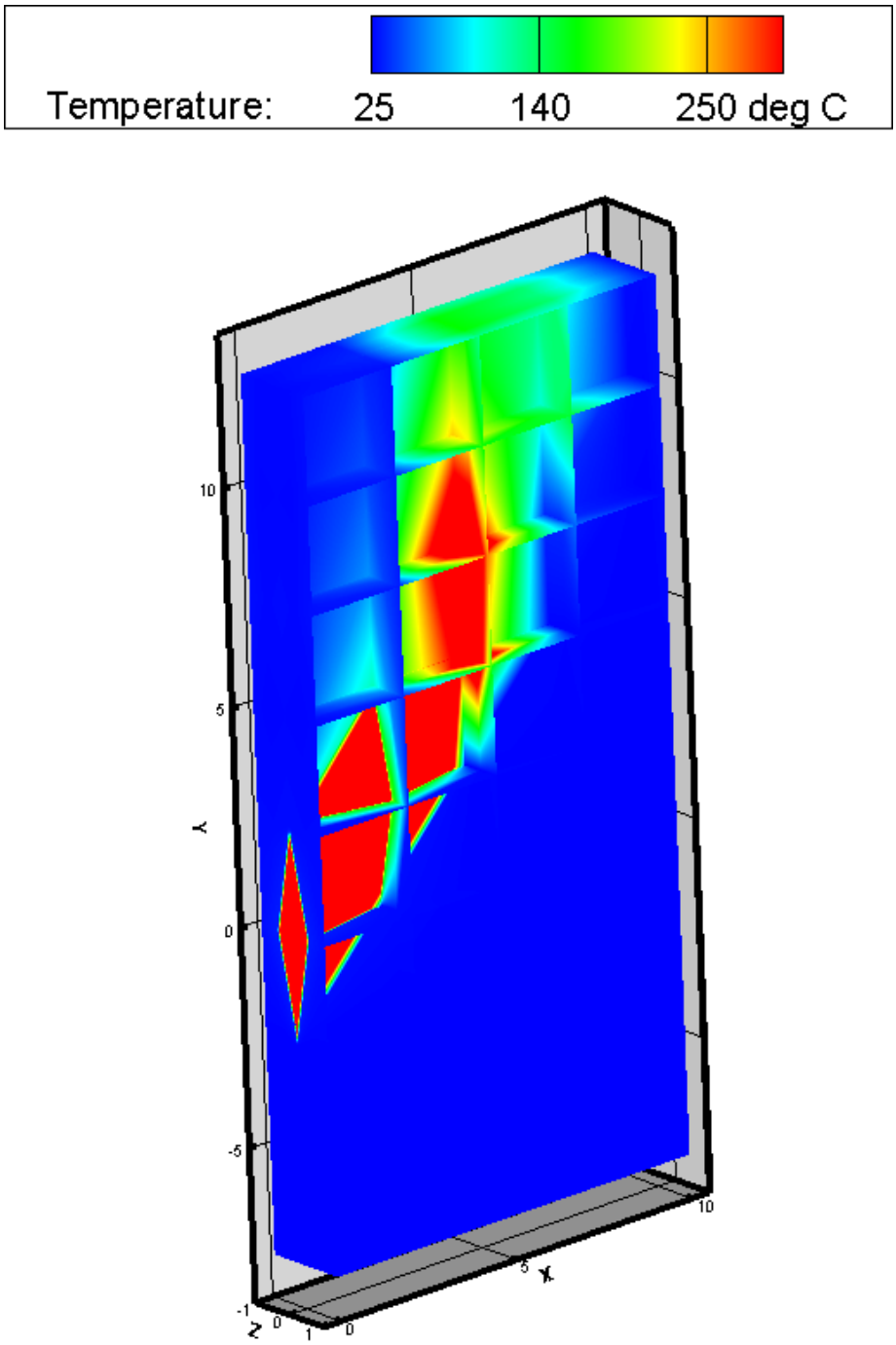

Figure A.27: Three-dimensional temperature gradient: combination of the two-dimensional cross sections of the 1.0 psig flame at 135 degrees

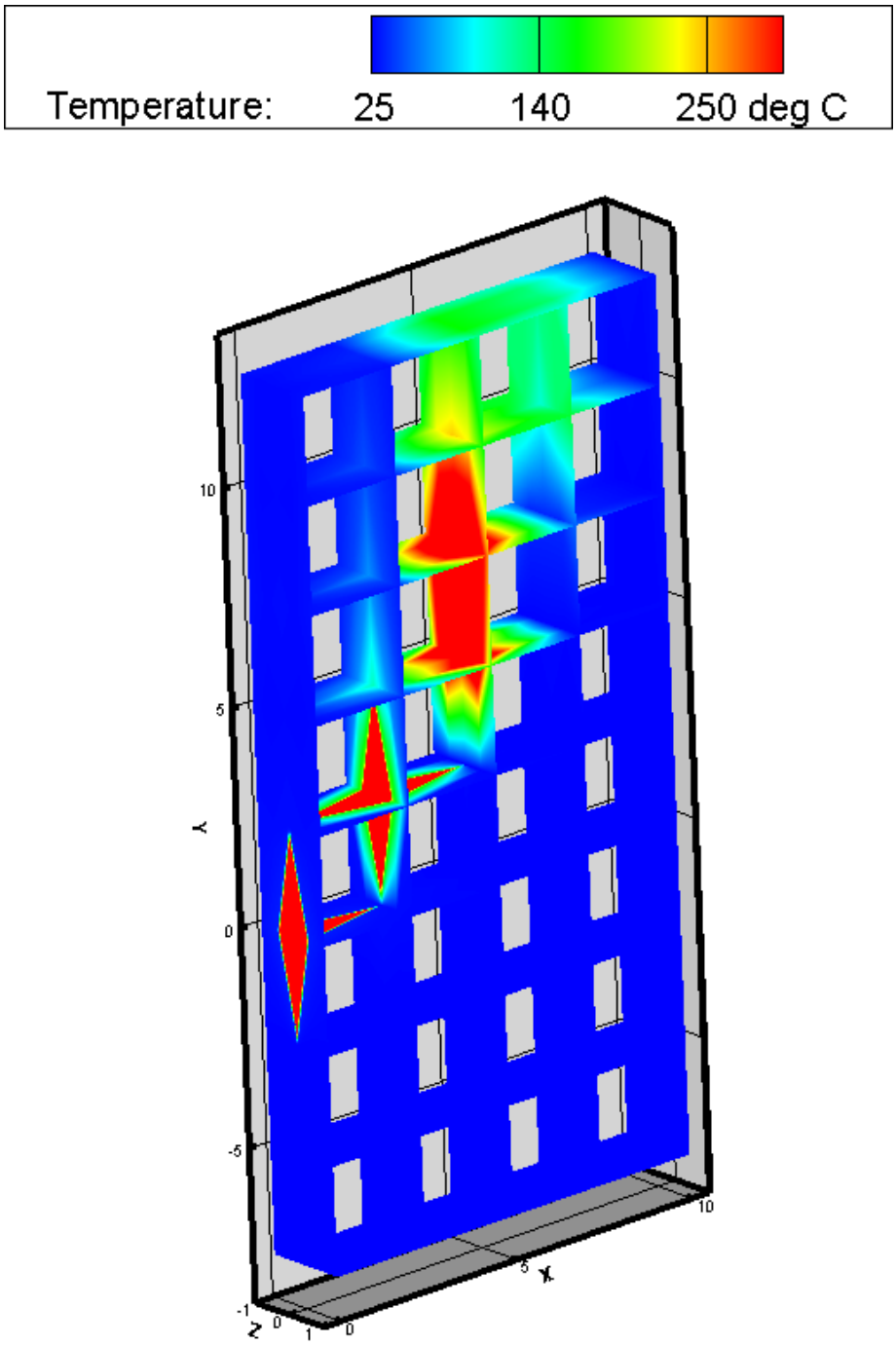

Figure A.28: Three-dimensional temperature gradient: combination of the two-dimensional cross sections of the 1.0 psig flame at 135 degrees

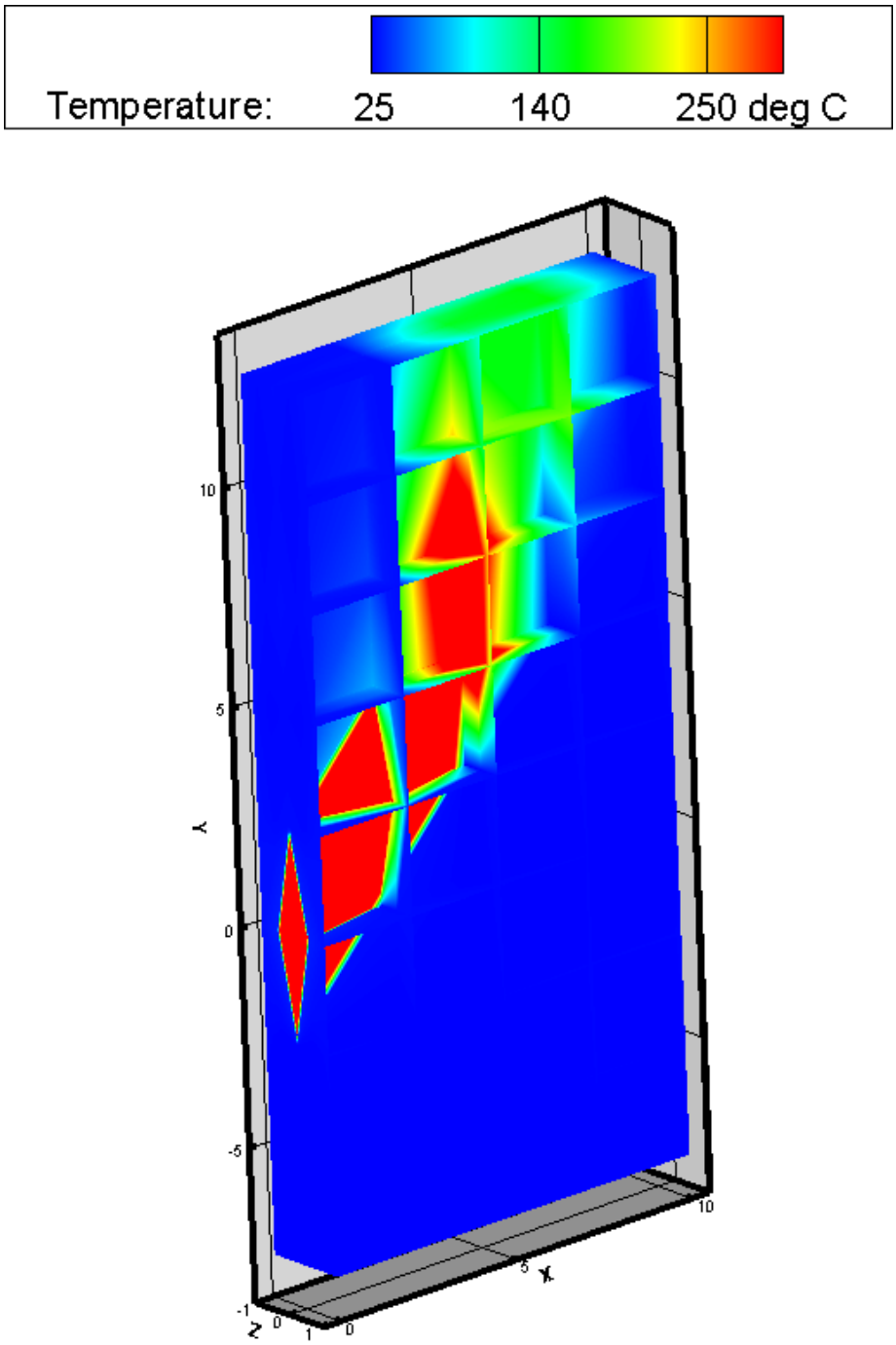

Figure A.29: Three-dimensional temperature gradient: combination of the two-dimensional cross sections of the 1.25 psig flame at 135 degrees

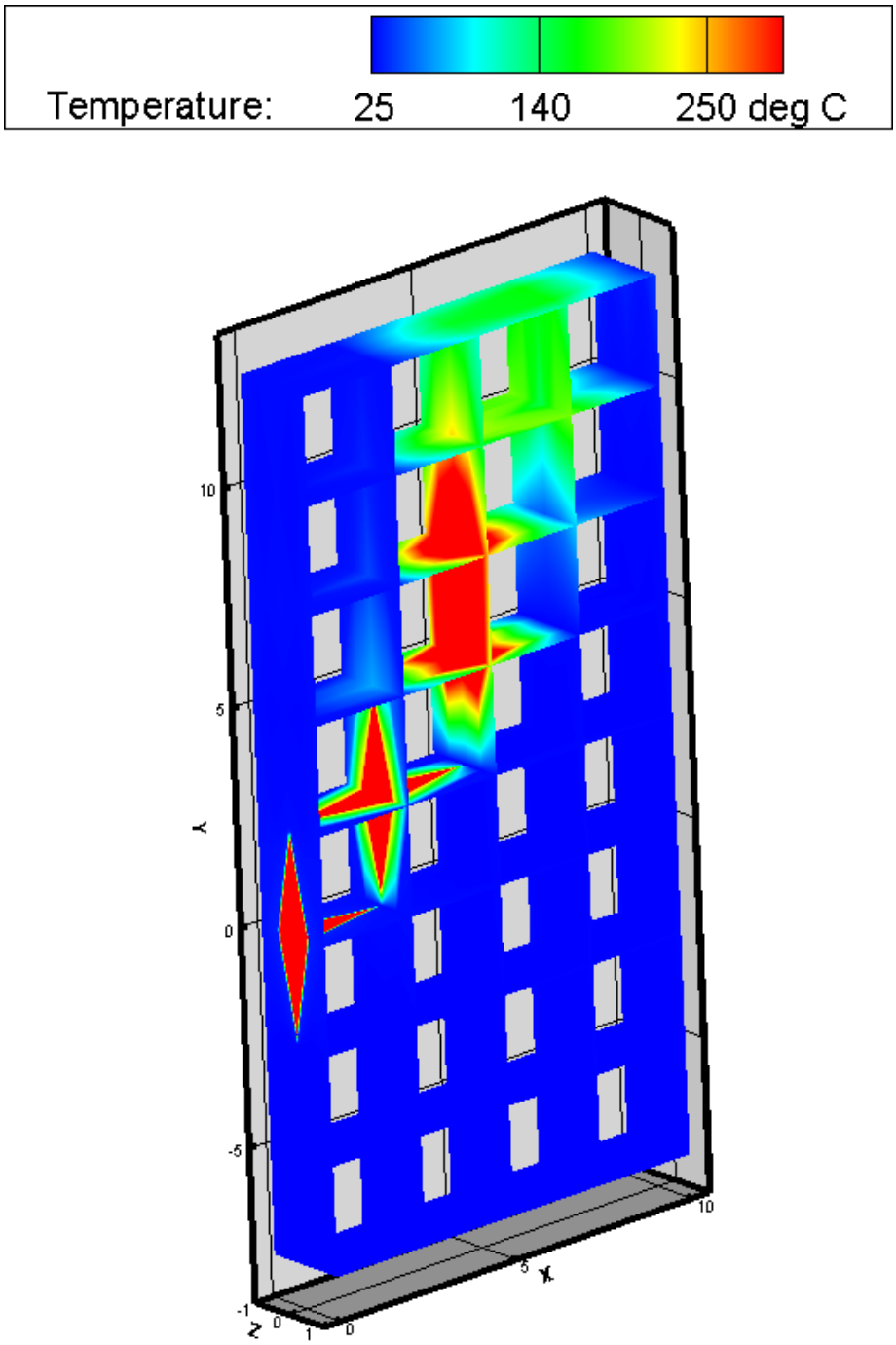

Figure A.30: Three-dimensional temperature gradient: combination of the two-dimensional cross sections of the 1.25 psig flame at 135 degrees

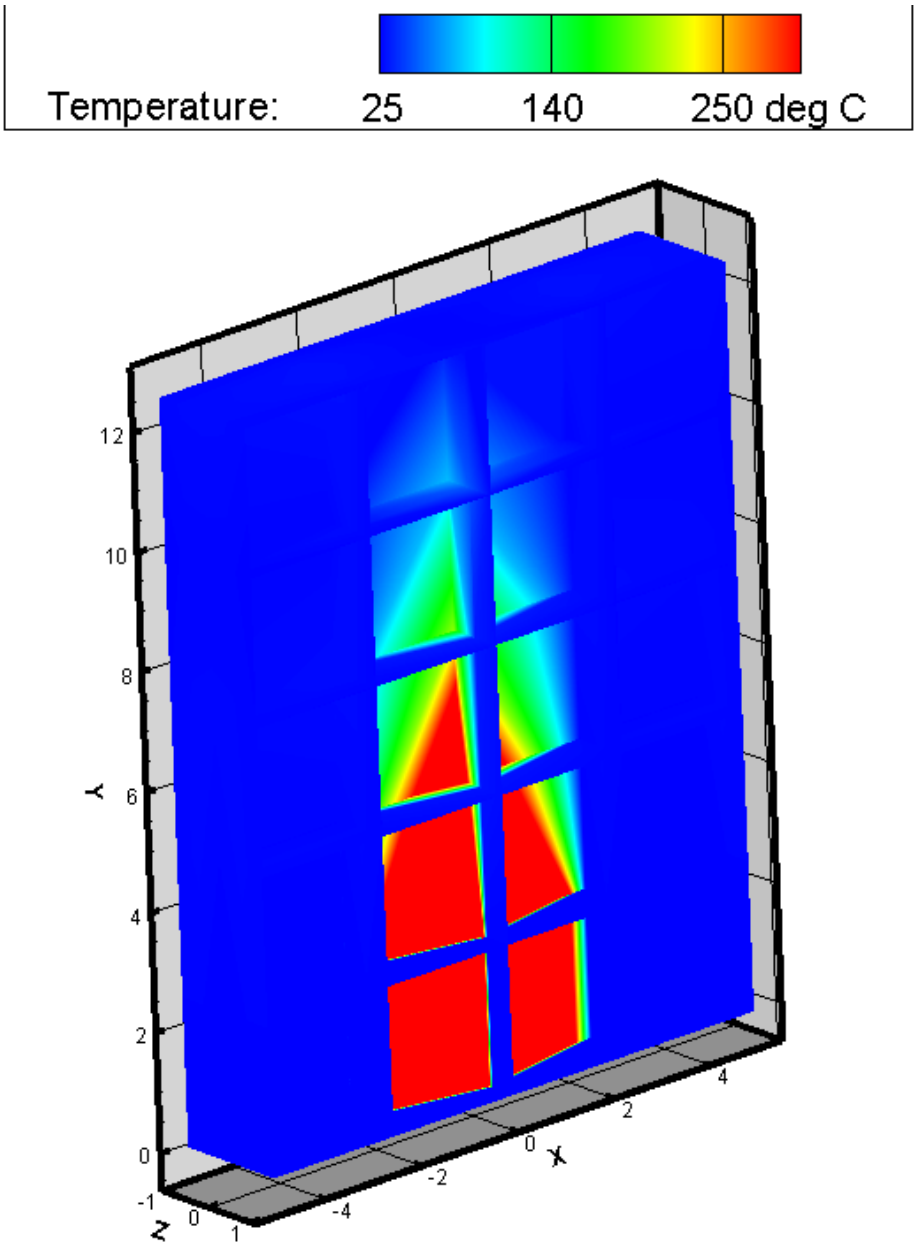

Figure A.31: Three-dimensional temperature gradient: combination of the two-dimensional cross sections of the 0.25 psig flame at 180 degrees

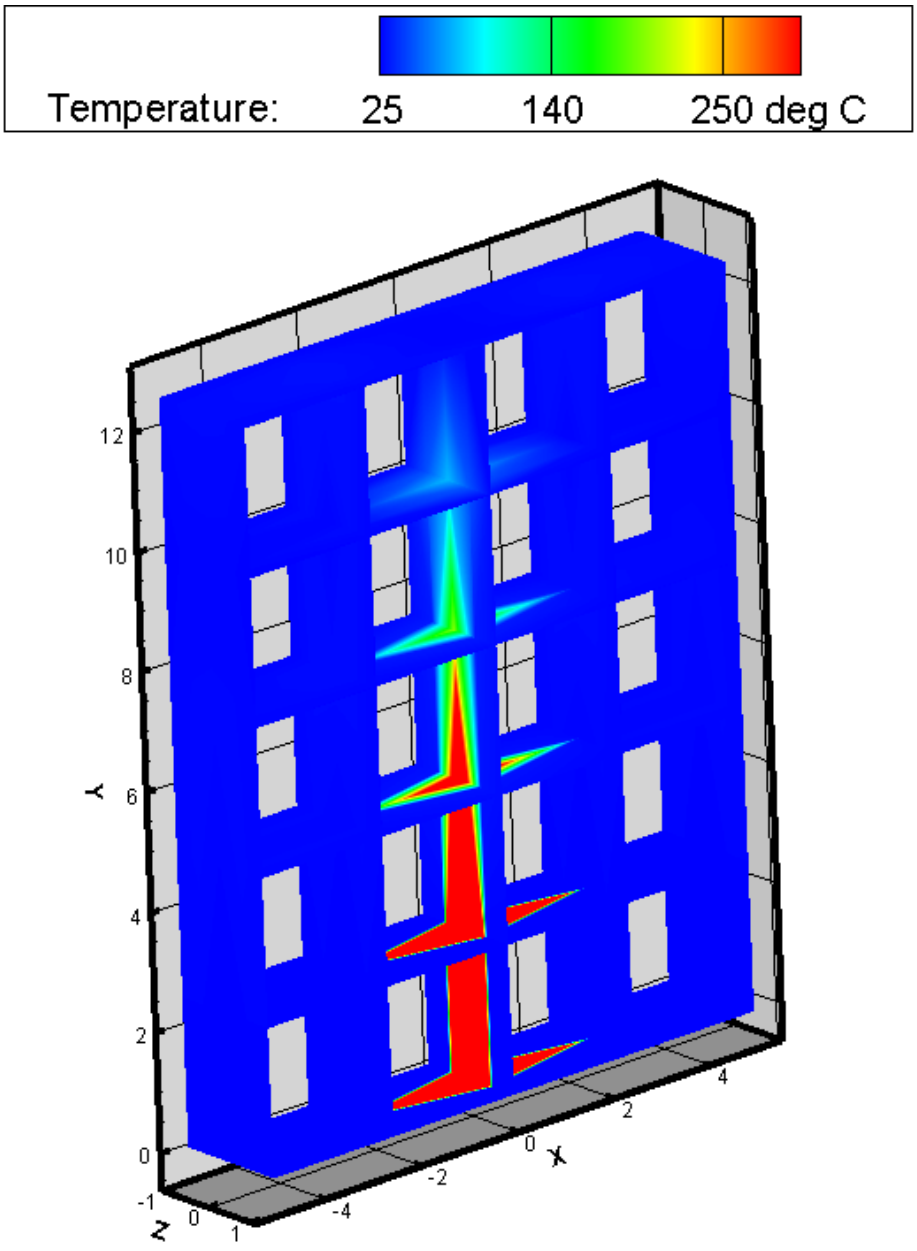

Figure A.32: Three-dimensional temperature gradient: combination of the two-dimensional cross sections of the 0.25 psig flame at 180 degrees

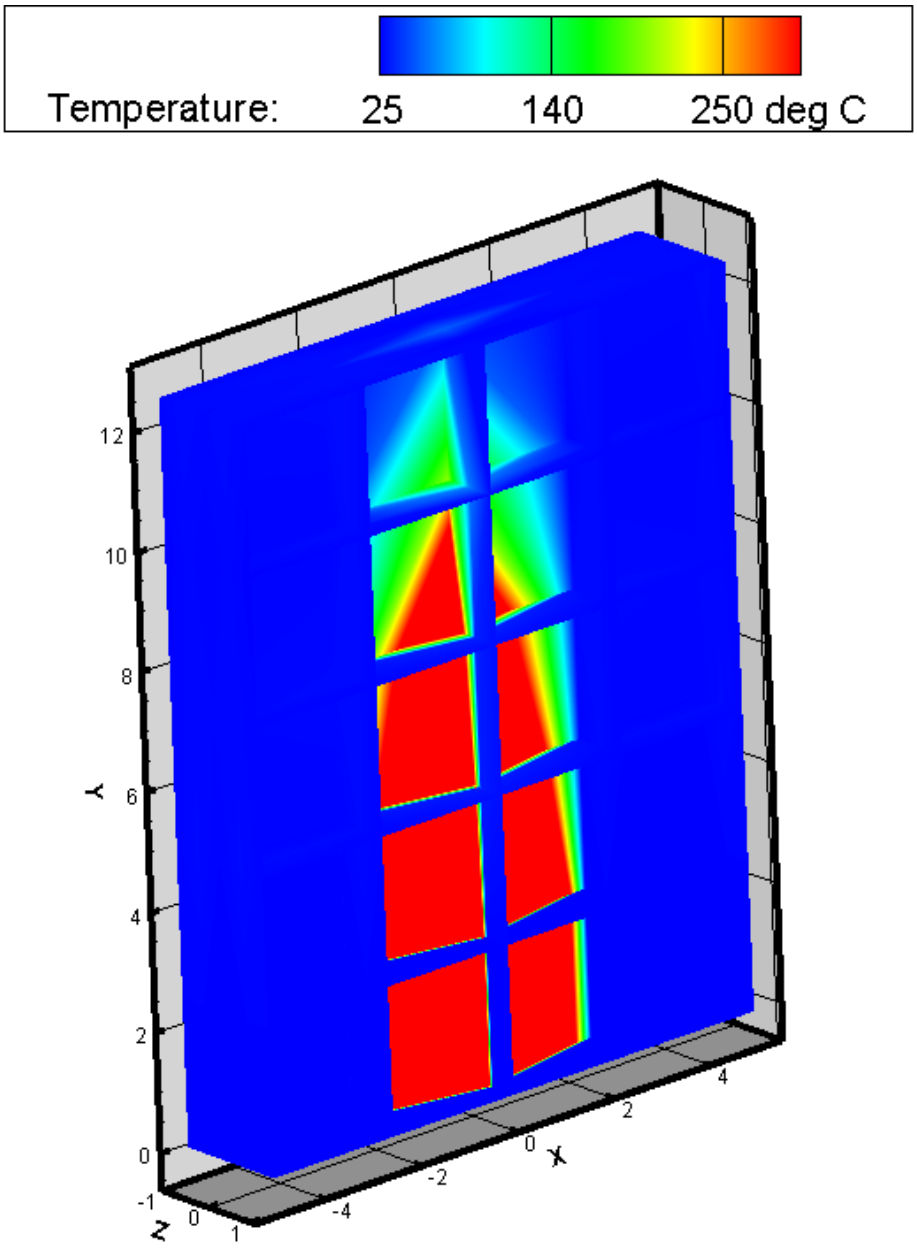

Figure A.33: Three-dimensional temperature gradient: combination of the two-dimensional cross sections of the 0.5 psig flame at 180 degrees

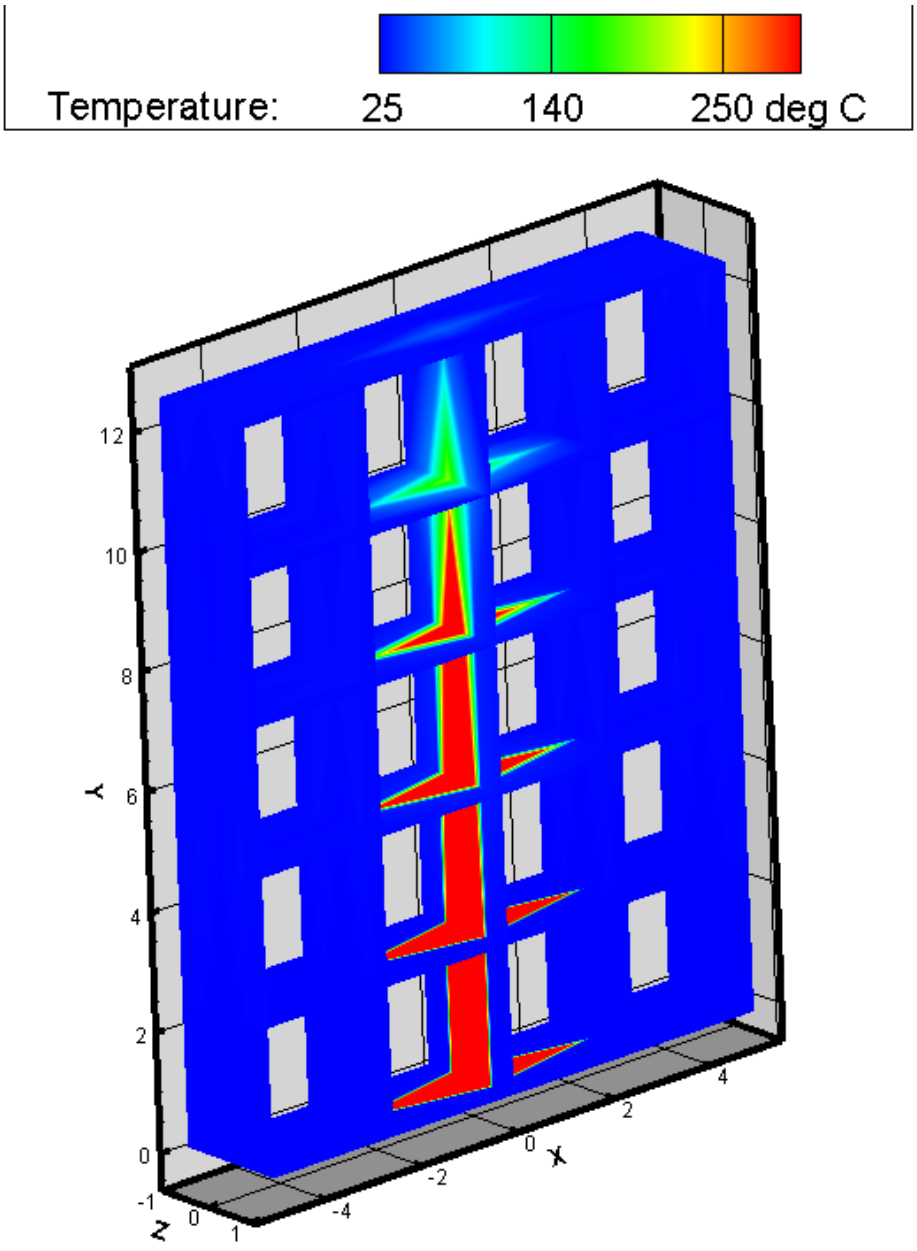

Figure A.34: Three-dimensional temperature gradient: combination of the two-dimensional cross sections of the 0.5 psig flame at 180 degrees

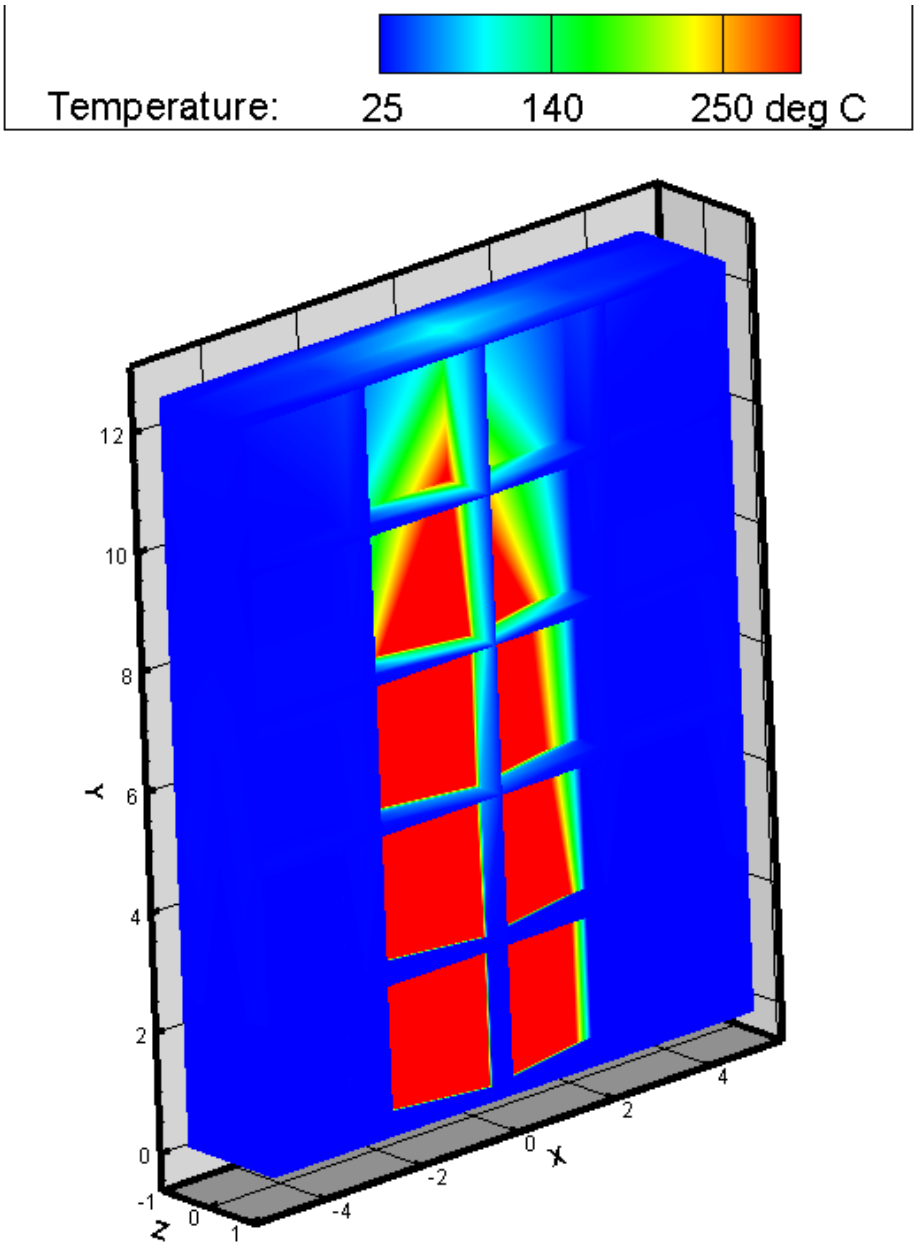

Figure A.35: Three-dimensional temperature gradient: combination of the two-dimensional cross sections of the 0.75 psig flame at 180 degrees

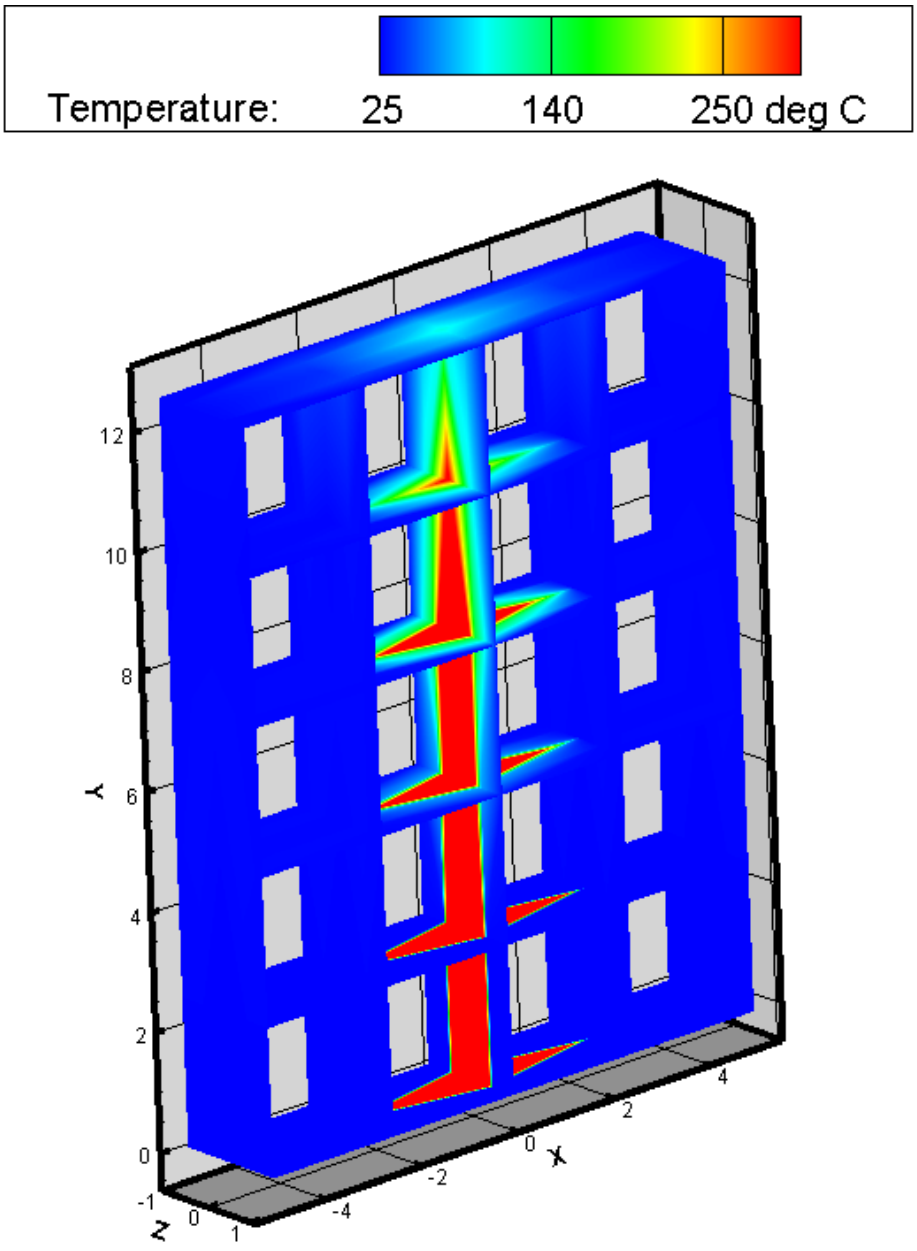

Figure A.36: Three-dimensional temperature gradient: combination of the two-dimensional cross sections of the 0.75 psig flame at 180 degrees

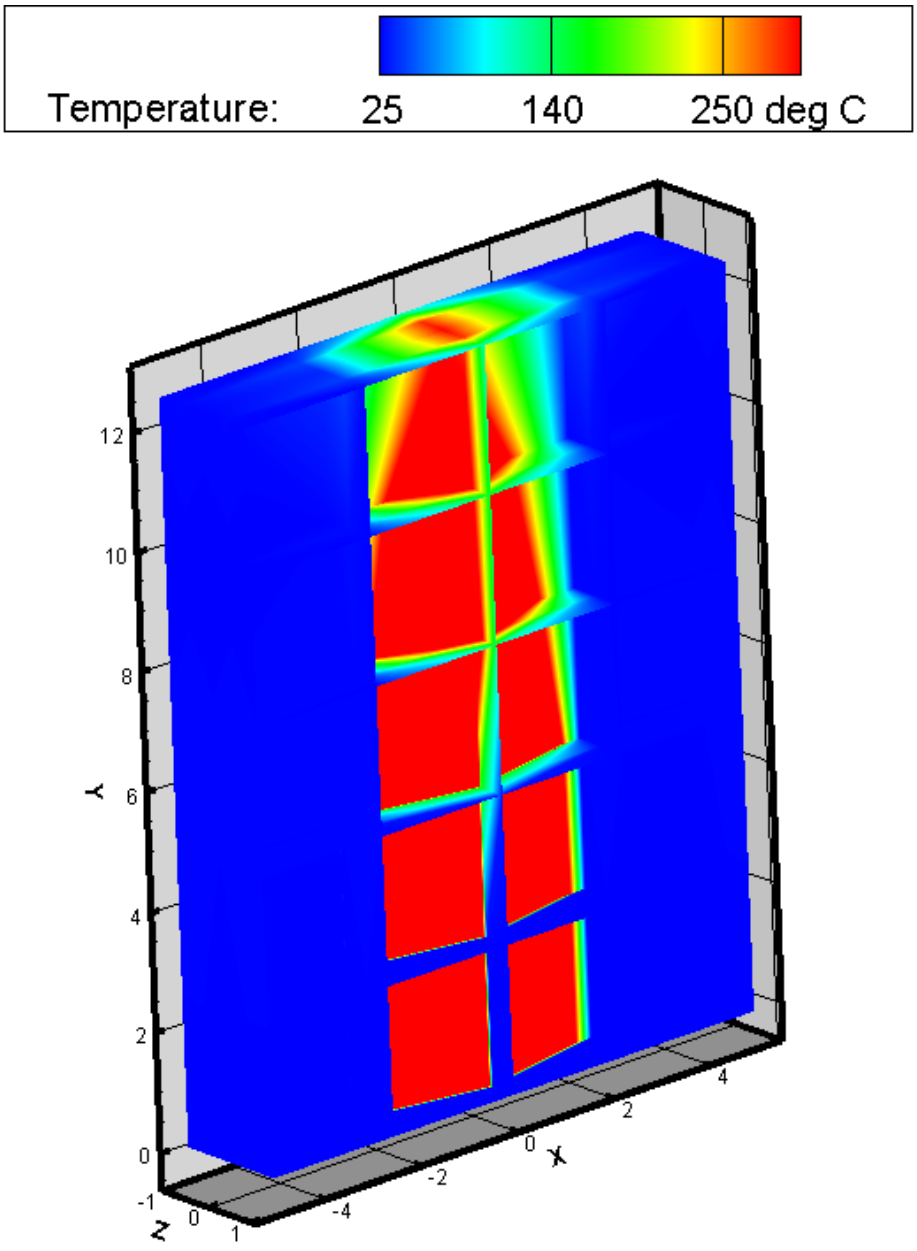

Figure A.37: Three-dimensional temperature gradient: combination of the two-dimensional cross sections of the 1.0 psig flame at 180 degrees

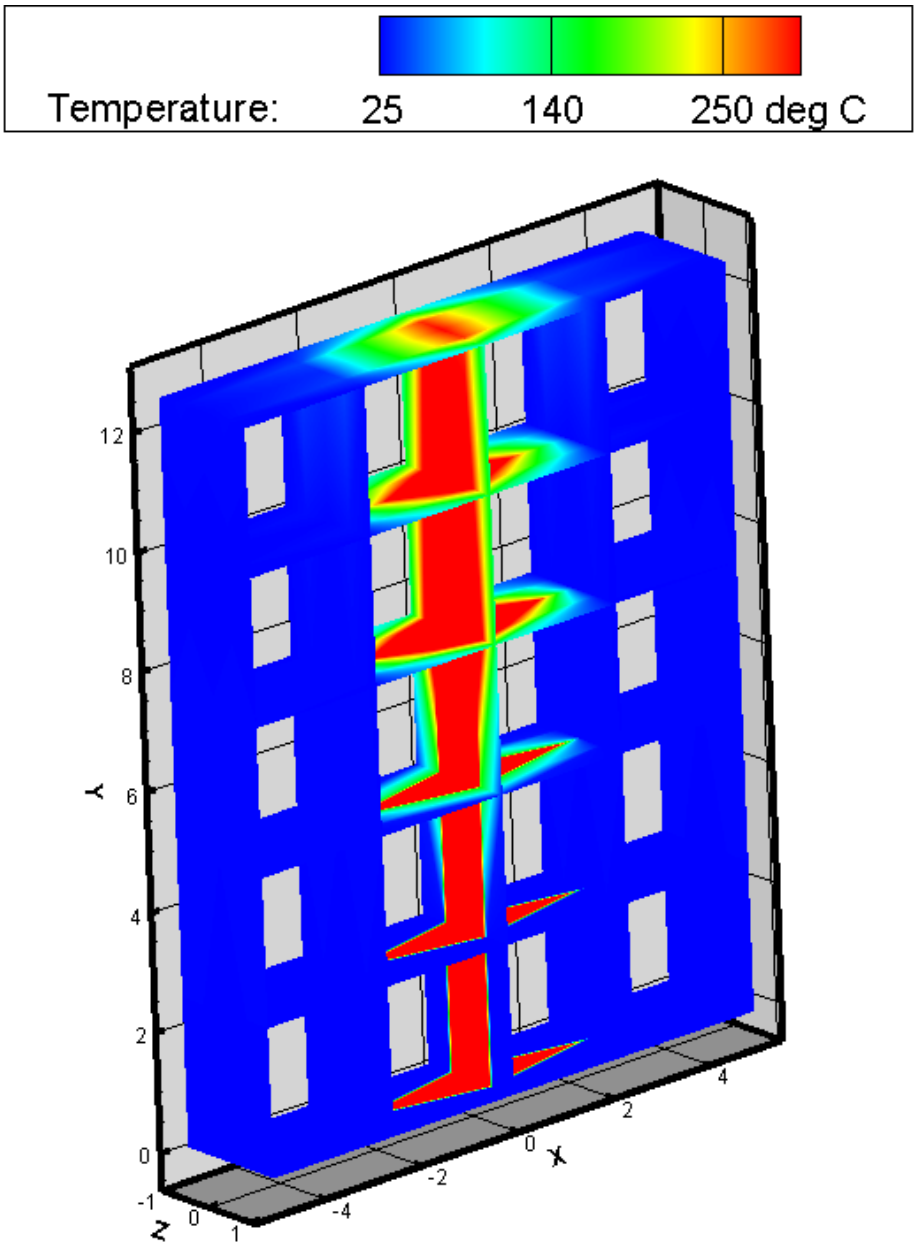

Figure A.38: Three-dimensional temperature gradient: combination of the two-dimensional cross sections of the 1.0 psig flame at 180 degrees

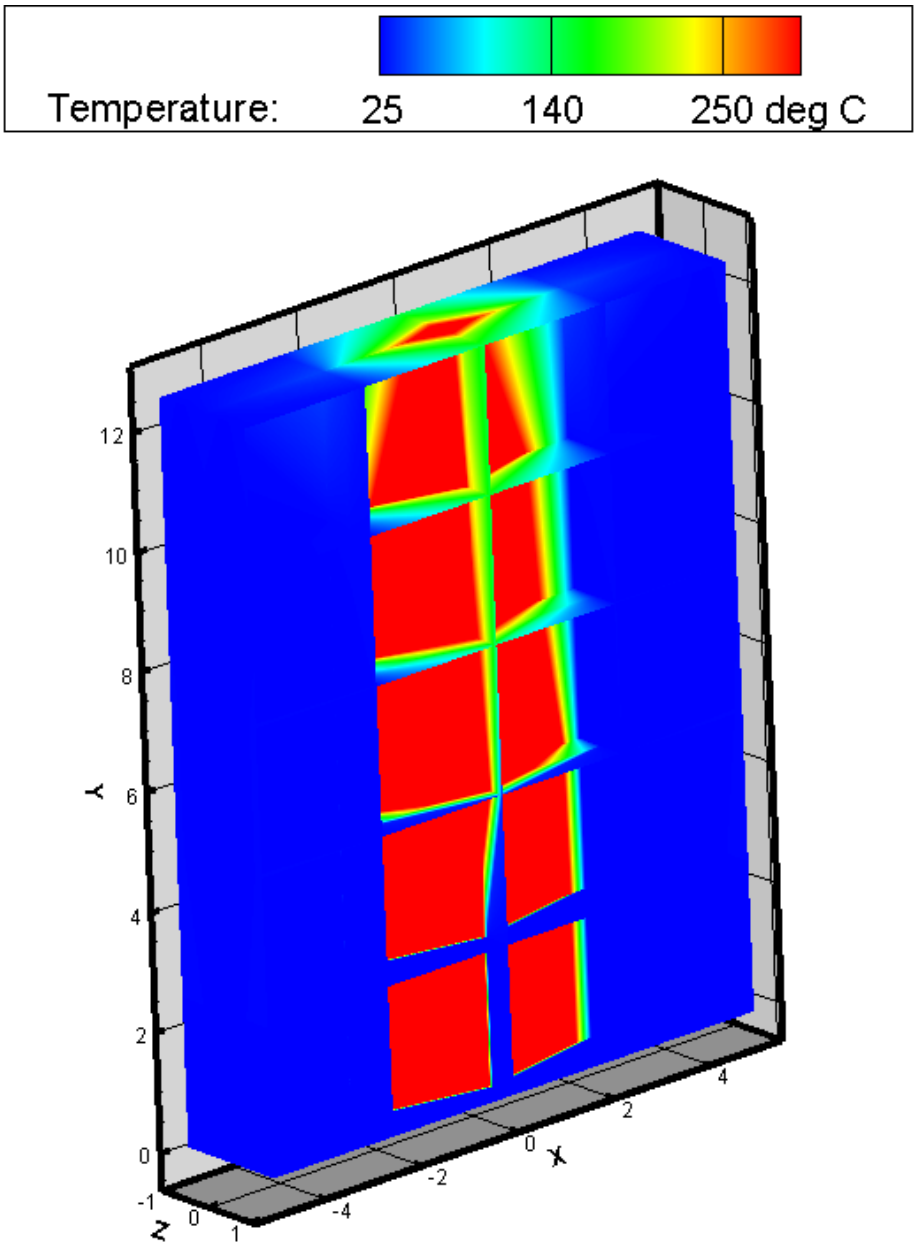

Figure A.39: Three-dimensional temperature gradient: combination of the two-dimensional cross sections of the 1.25 psig flame at 180 degrees

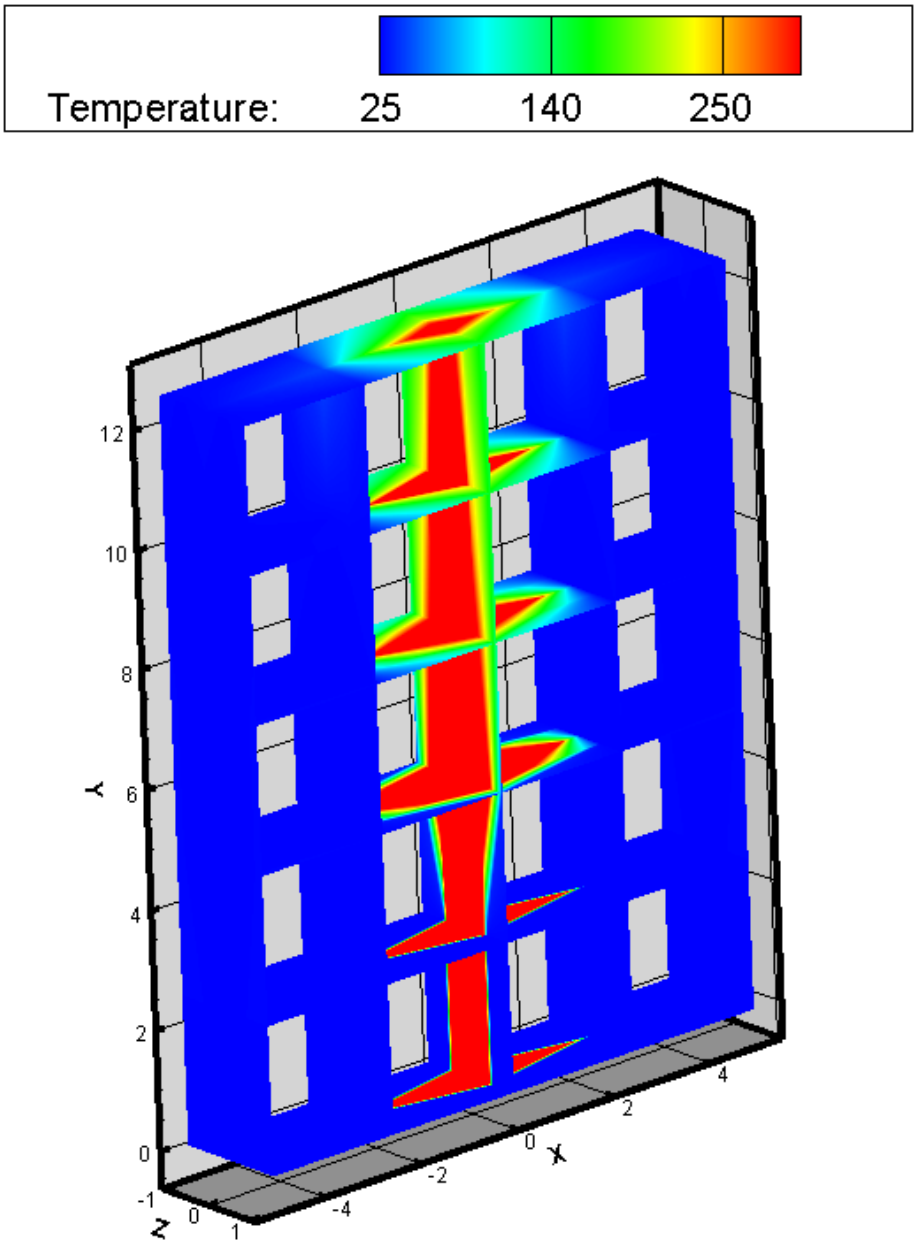

Figure A.40: Three-dimensional temperature gradient: combination of the two-dimensional cross sections of the 1.25 psig flame at 180 degrees

A.2 0.0156 in Diameter Burner

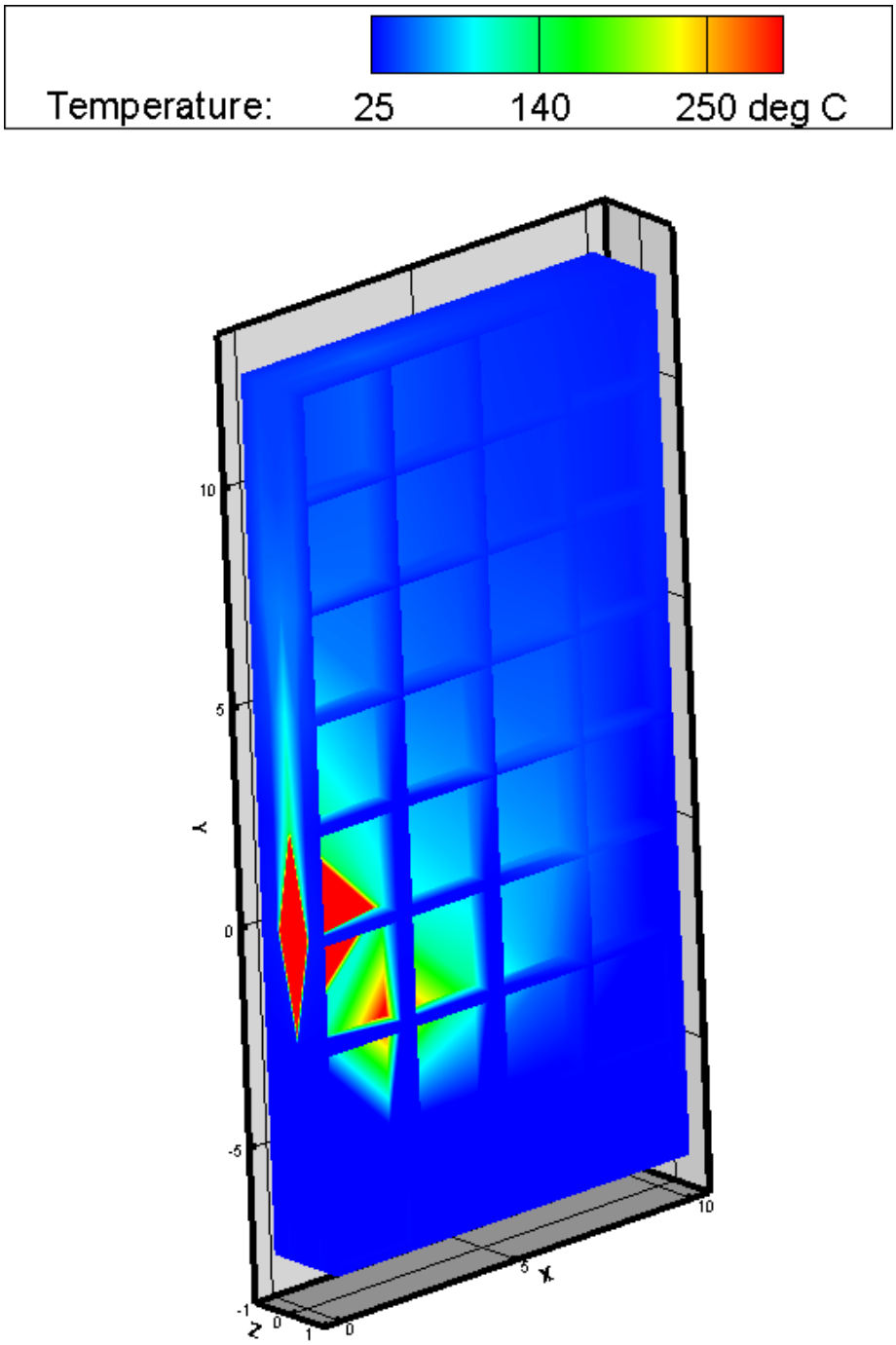

Figure A.41: Three-dimensional temperature gradient: combination of the two-dimensional cross sections of the 0.25 psig flame at 45 degrees

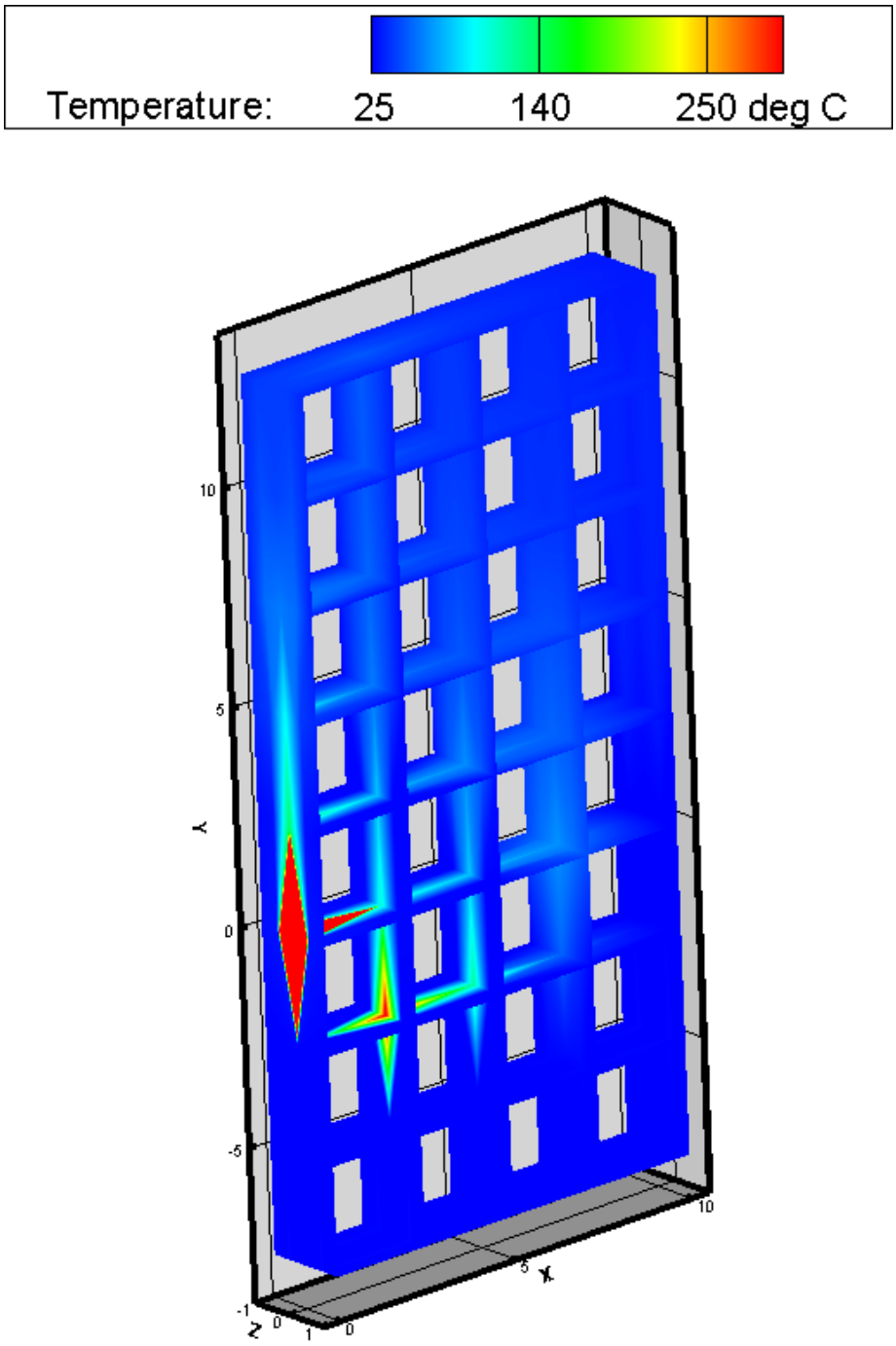

Figure A.42: Three-dimensional temperature gradient: combination of the two-dimensional cross sections of the 0.25 psig flame at 45 degrees

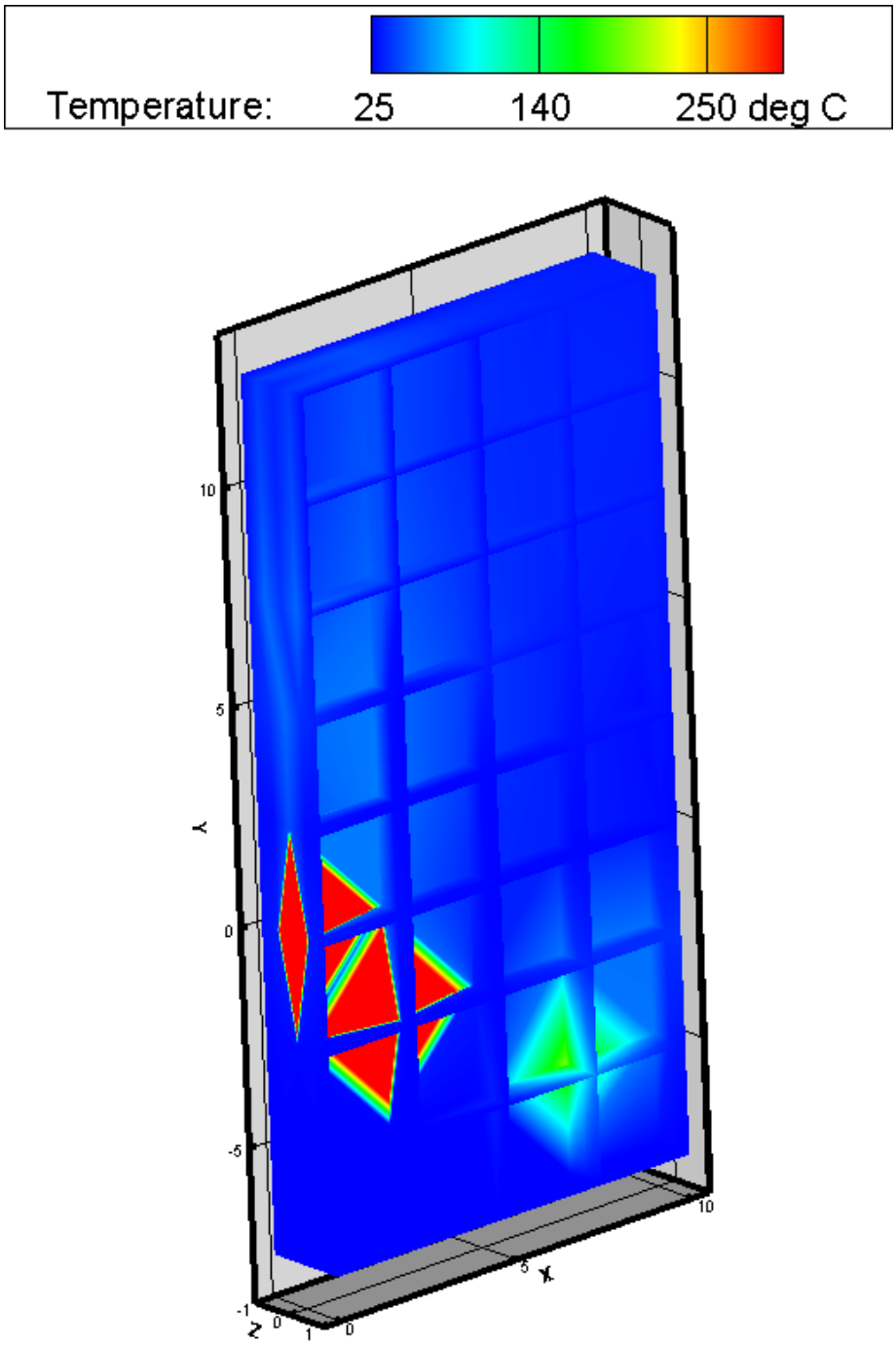

Figure A.43: Three-dimensional temperature gradient: combination of the two-dimensional cross sections of the 0.5 psig flame at 45 degrees

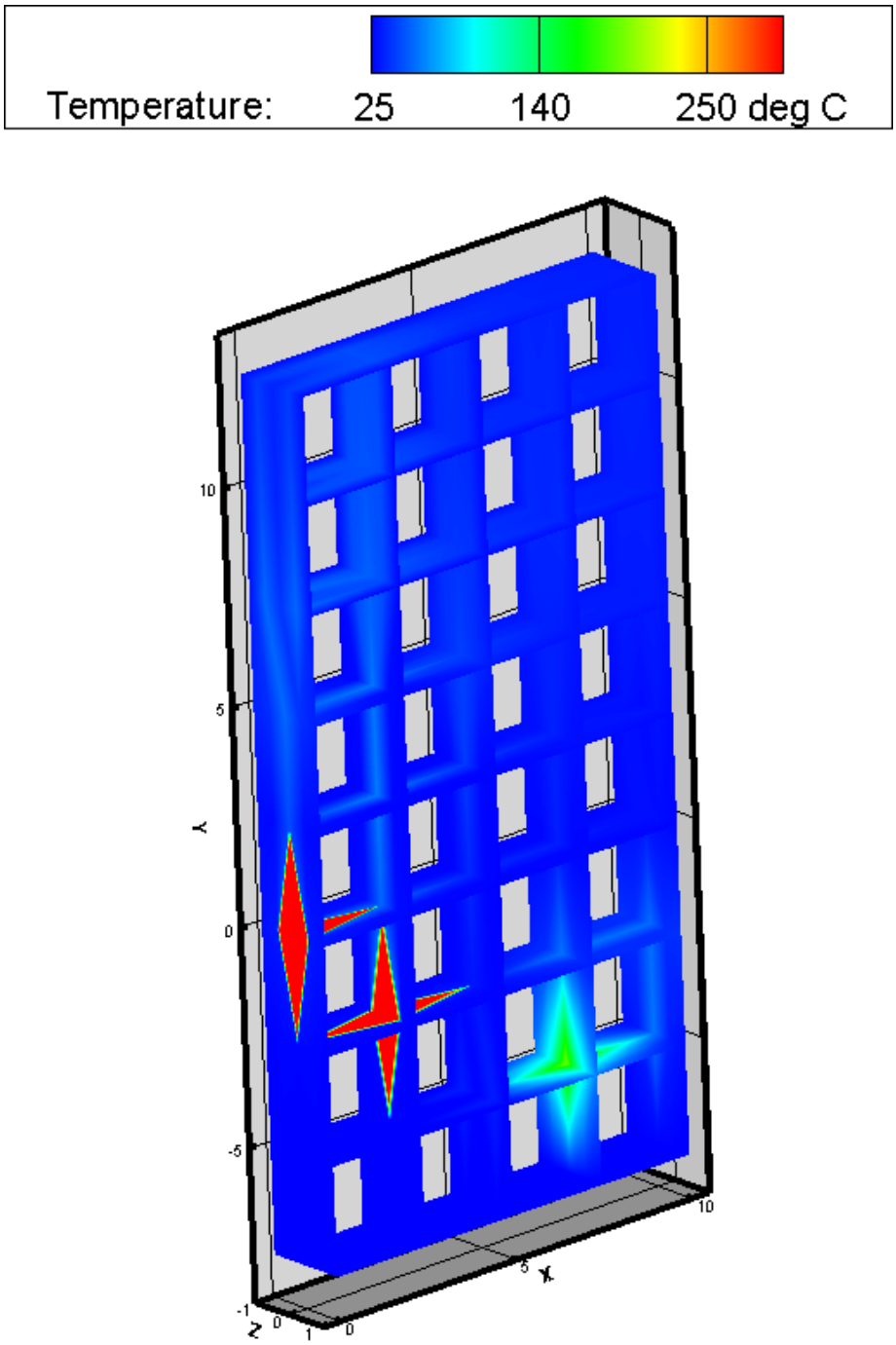

Figure A.44: Three-dimensional temperature gradient: combination of the two-dimensional cross sections of the 0.5 psig flame at 45 degrees

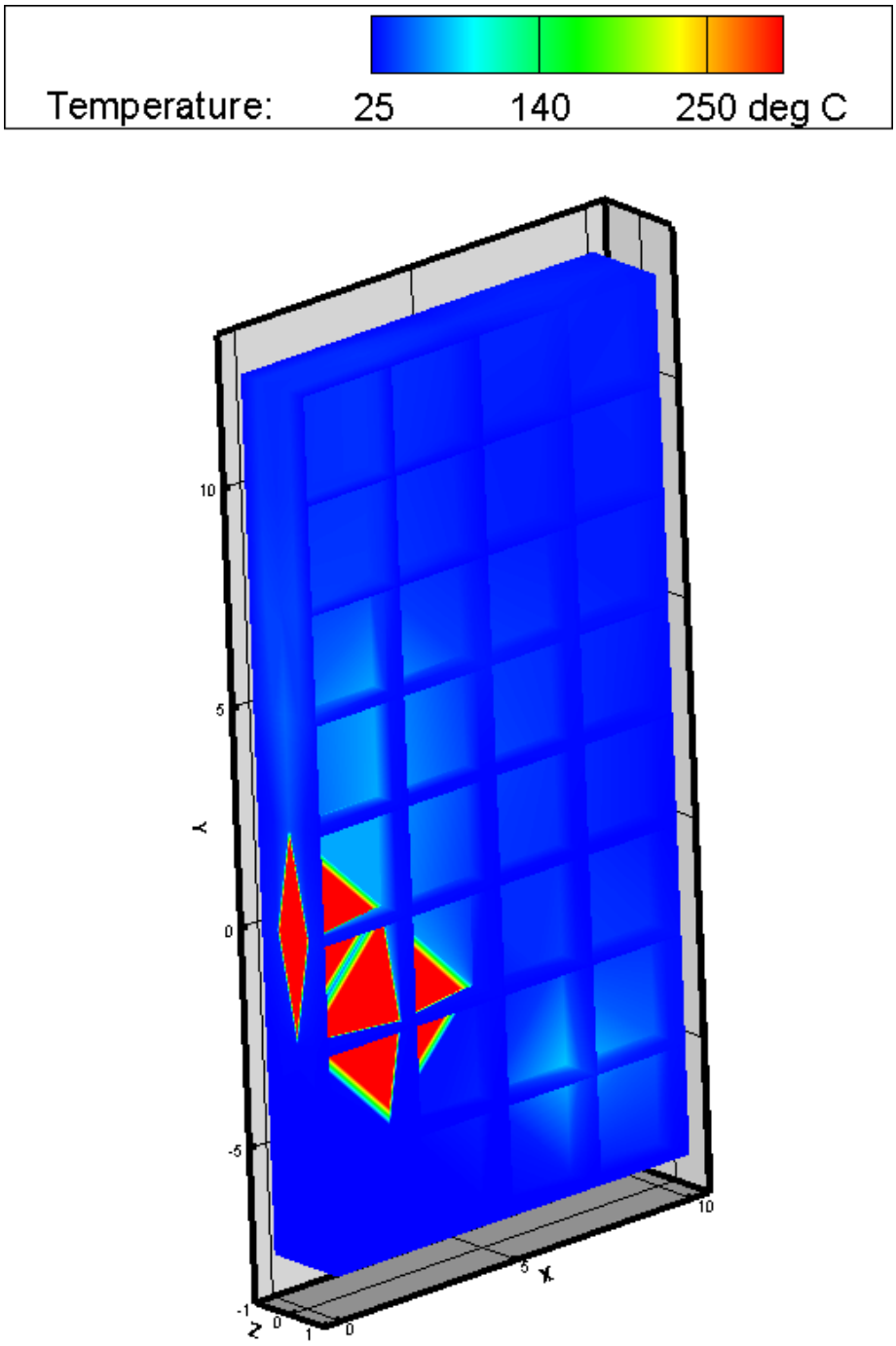

Figure A.45: Three-dimensional temperature gradient: combination of the two-dimensional cross sections of the 0.75 psig flame at 45 degrees

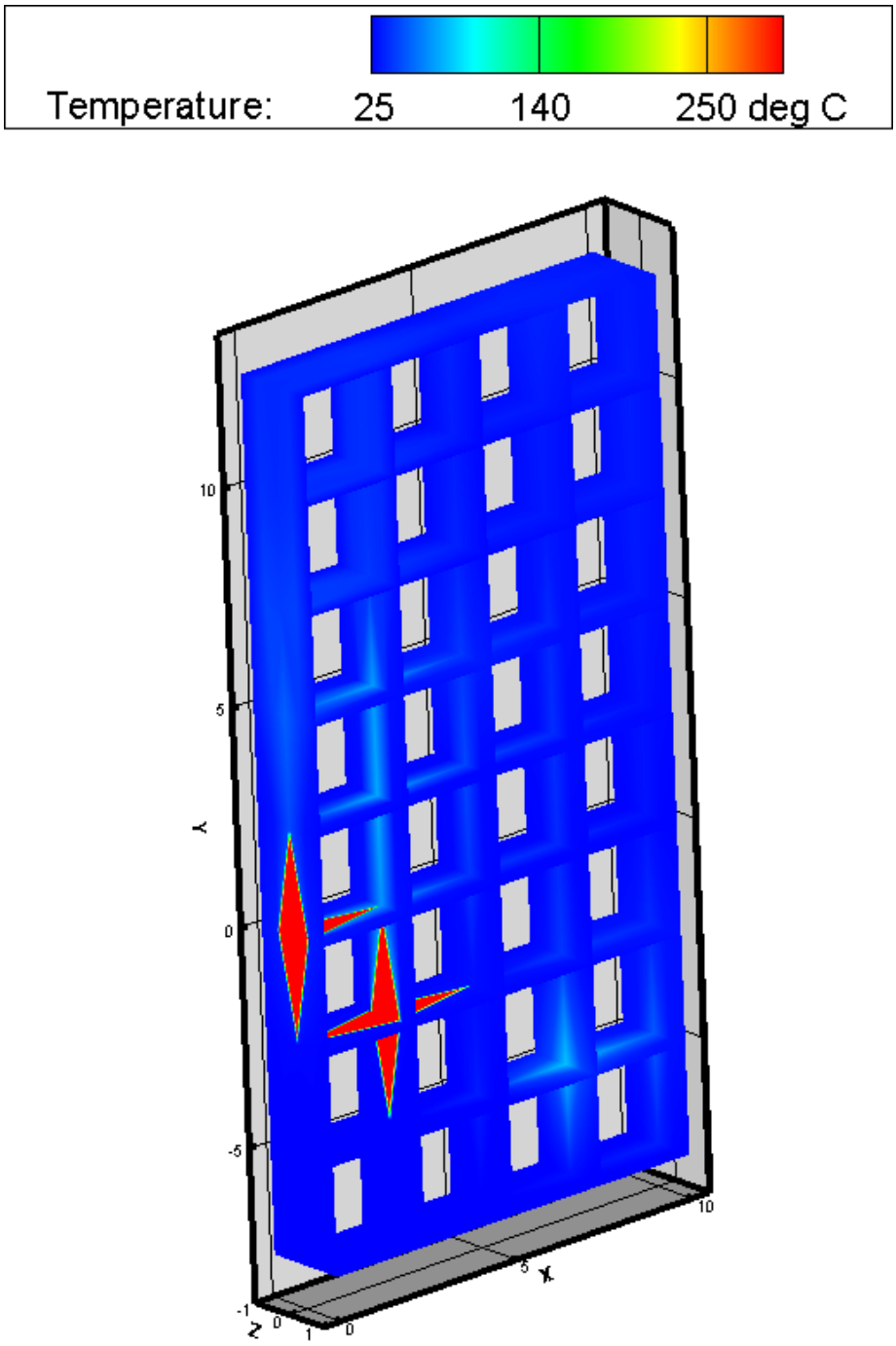

Figure A.46: Three-dimensional temperature gradient: combination of the two-dimensional cross sections of the 0.75 psig flame at 45 degrees

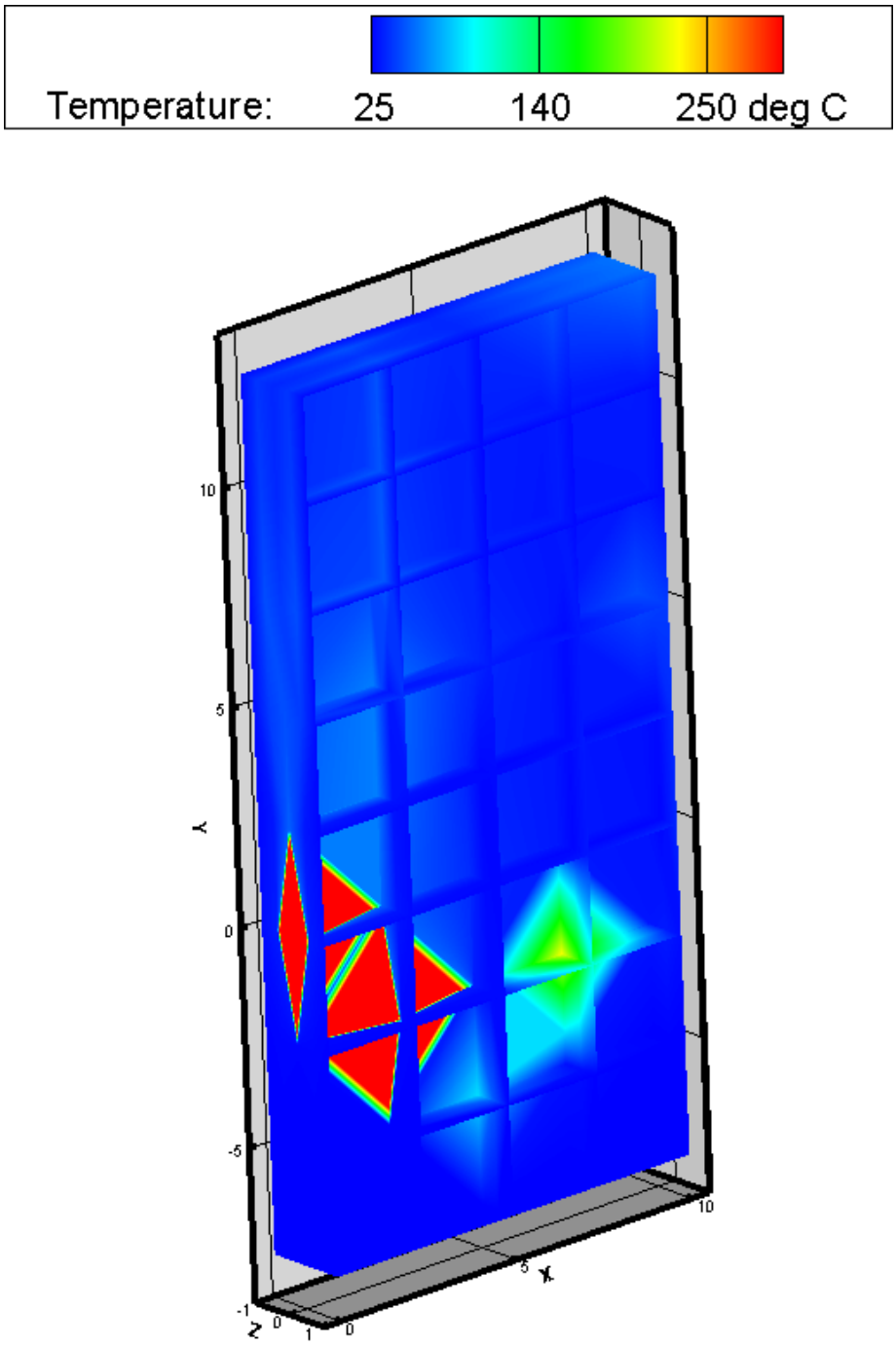

Figure A.47: Three-dimensional temperature gradient: combination of the two-dimensional cross sections of the 1.0 psig flame at 45 degrees

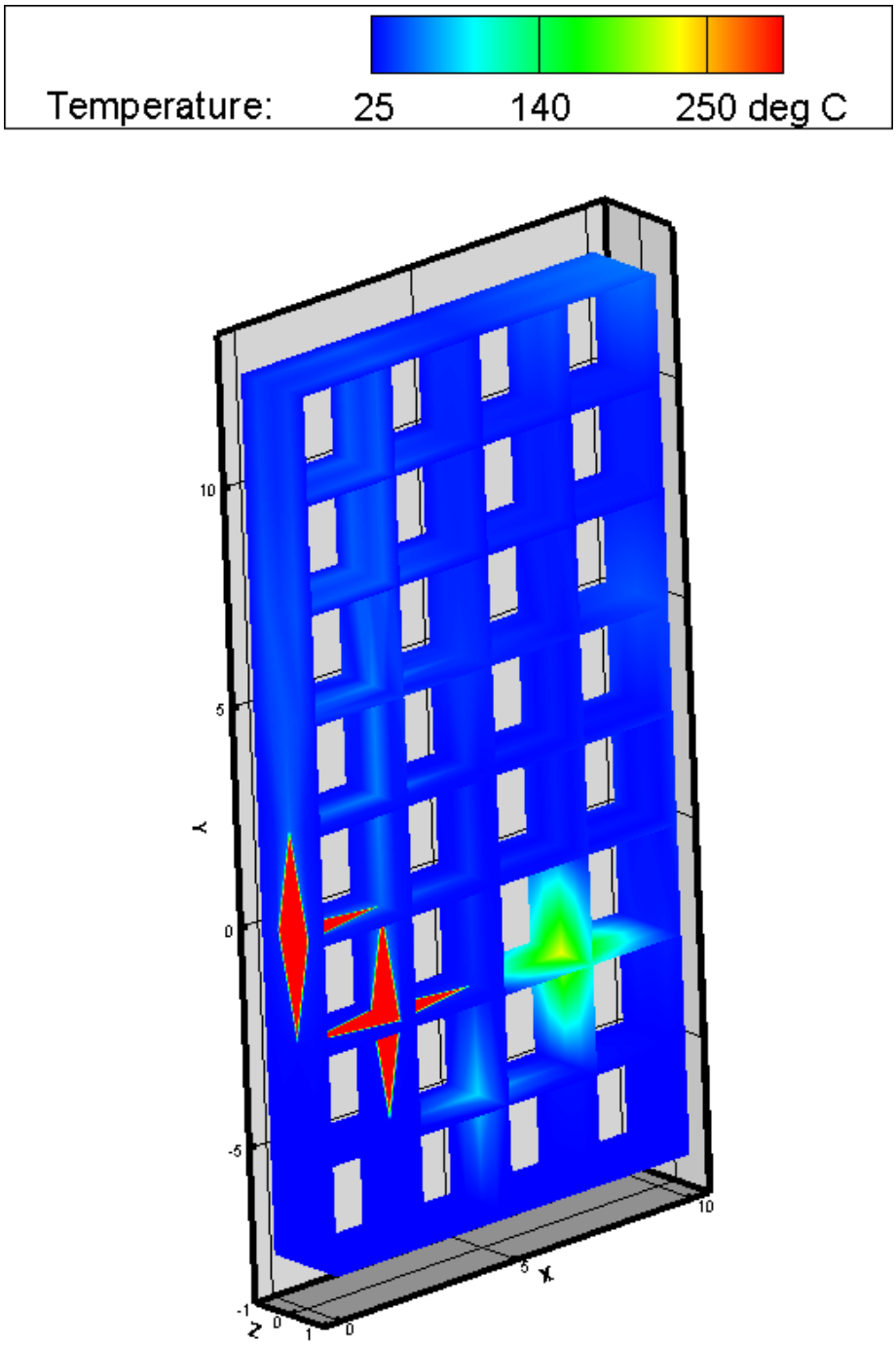

Figure A.48: Three-dimensional temperature gradient: combination of the two-dimensional cross sections of the 1.0 psig flame at 45 degrees

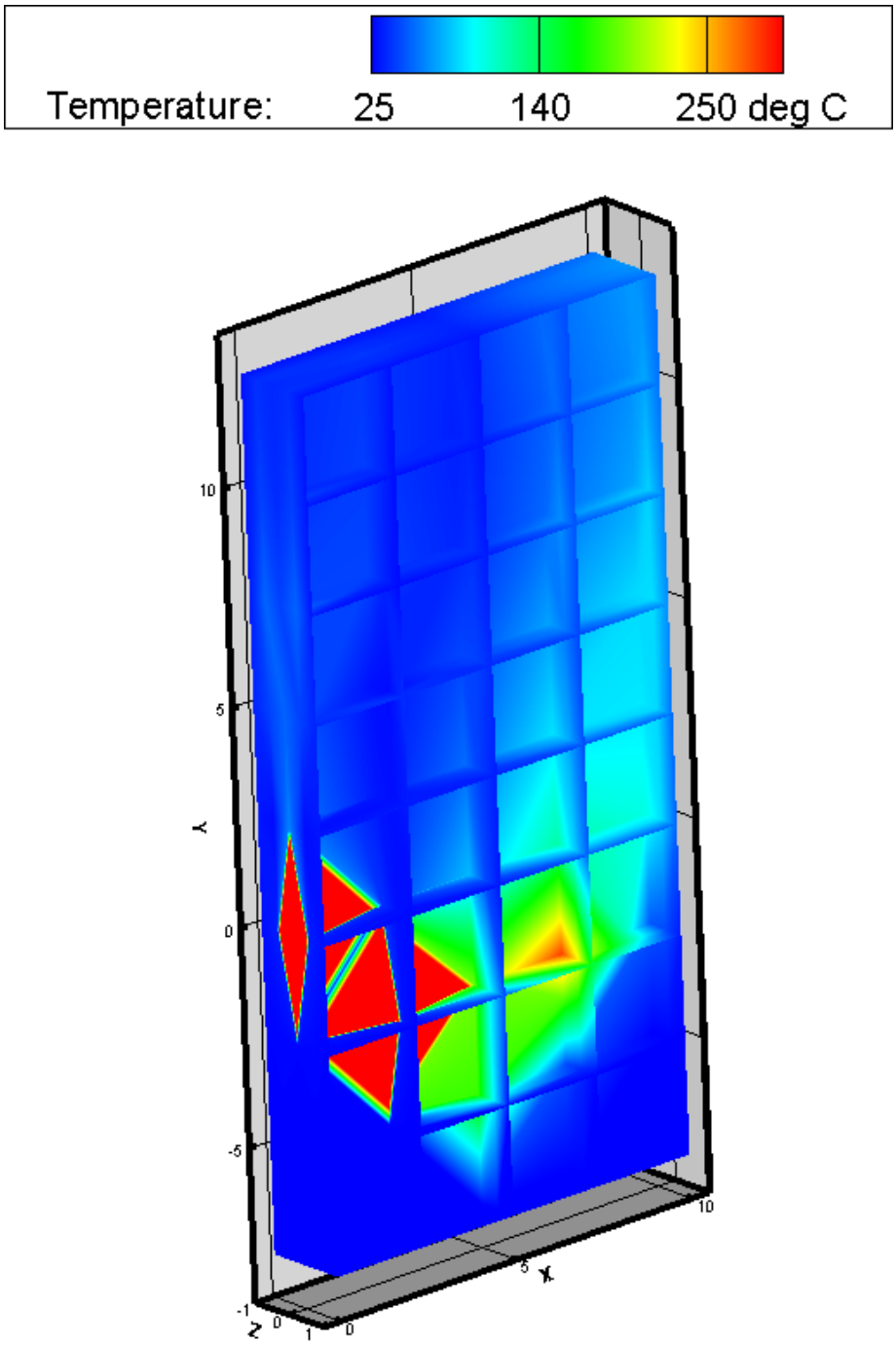

Figure A.49: Three-dimensional temperature gradient: combination of the two-dimensional cross sections of the 1.25 psig flame at 45 degrees

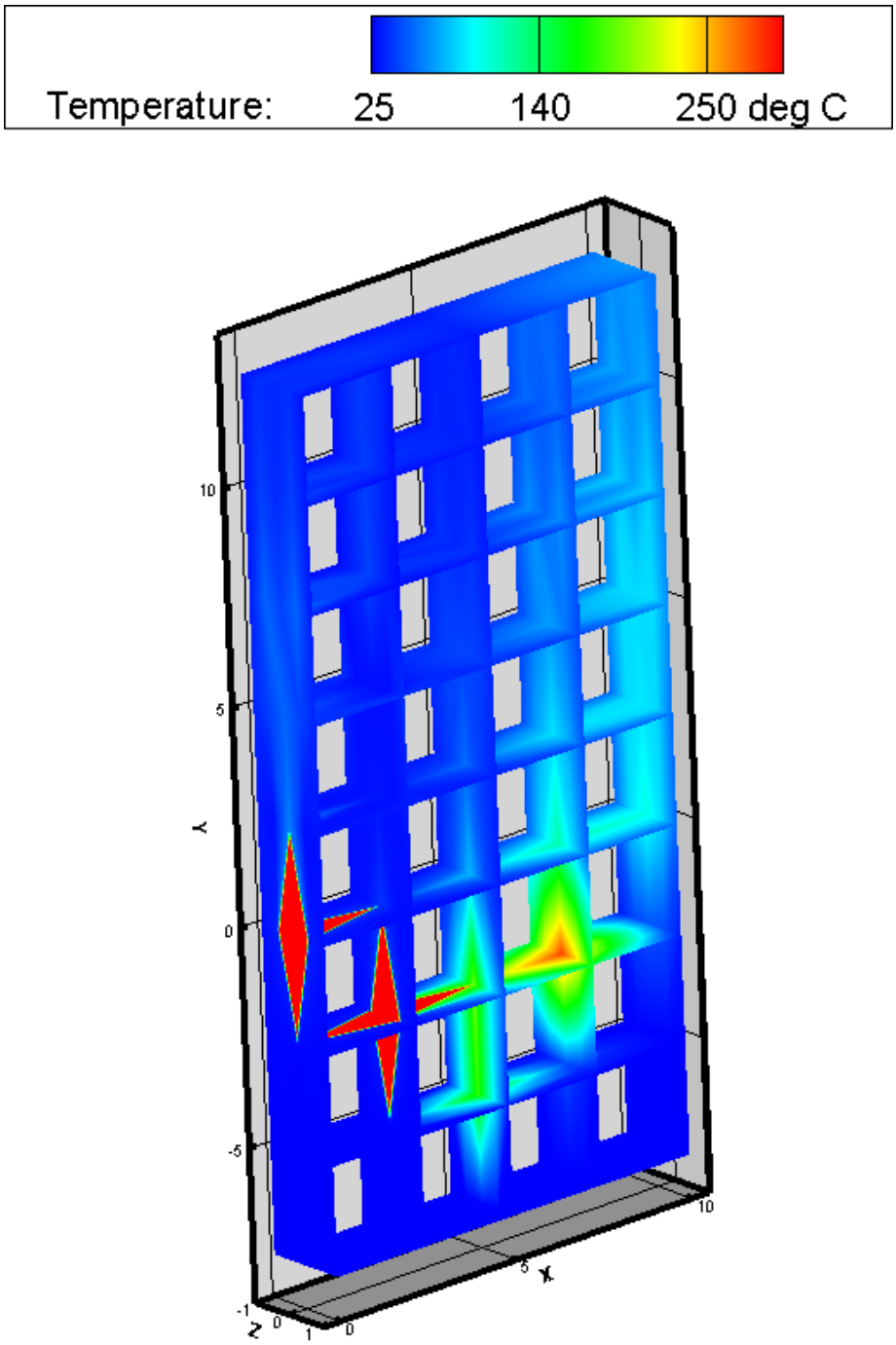

Figure A.50: Three-dimensional temperature gradient: combination of the two-dimensional cross sections of the 1.25 psig flame at 45 degrees

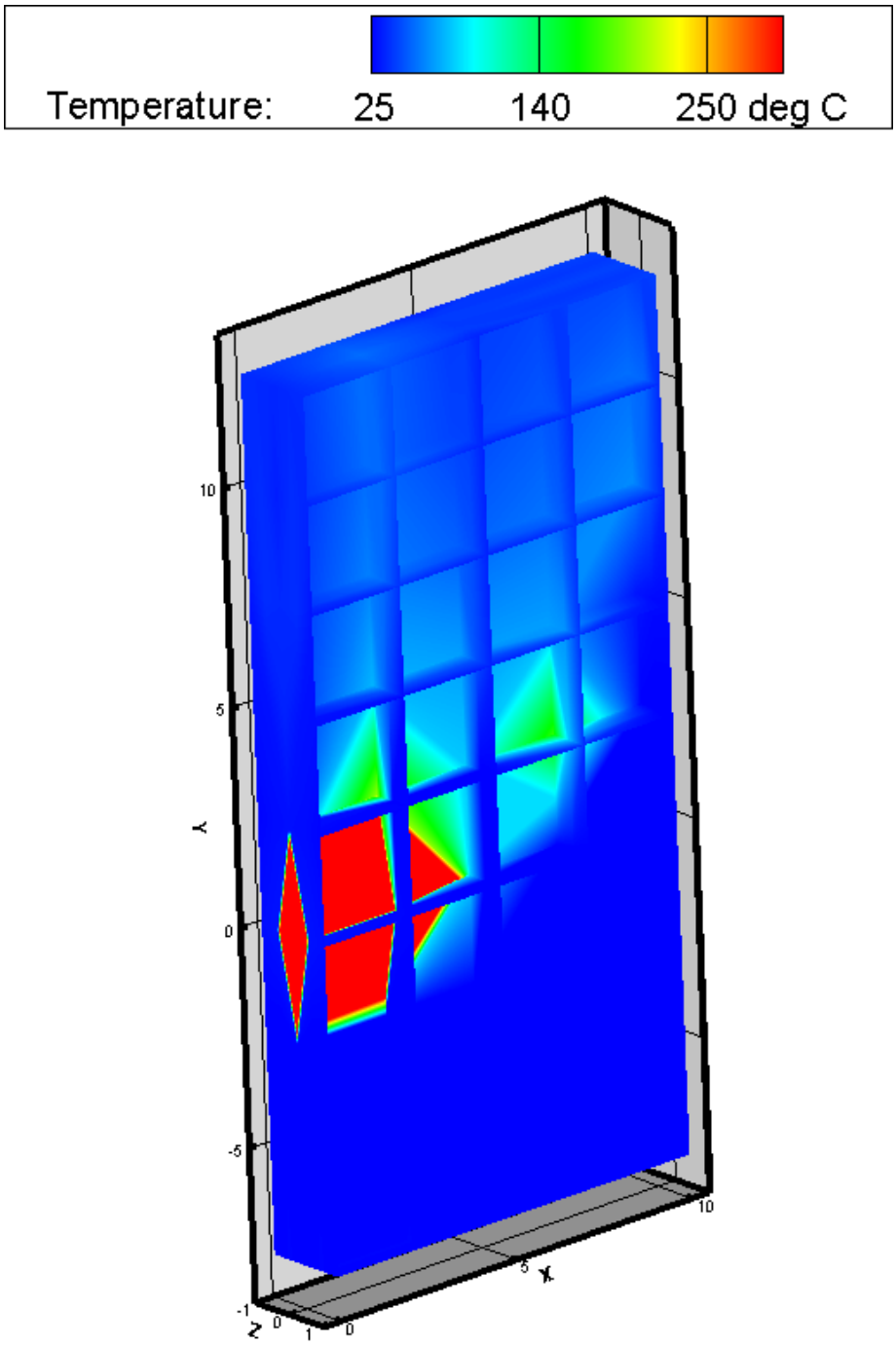

Figure A.51: Three-dimensional temperature gradient: combination of the two-dimensional cross sections of the 0.25 psig flame at 90 degrees

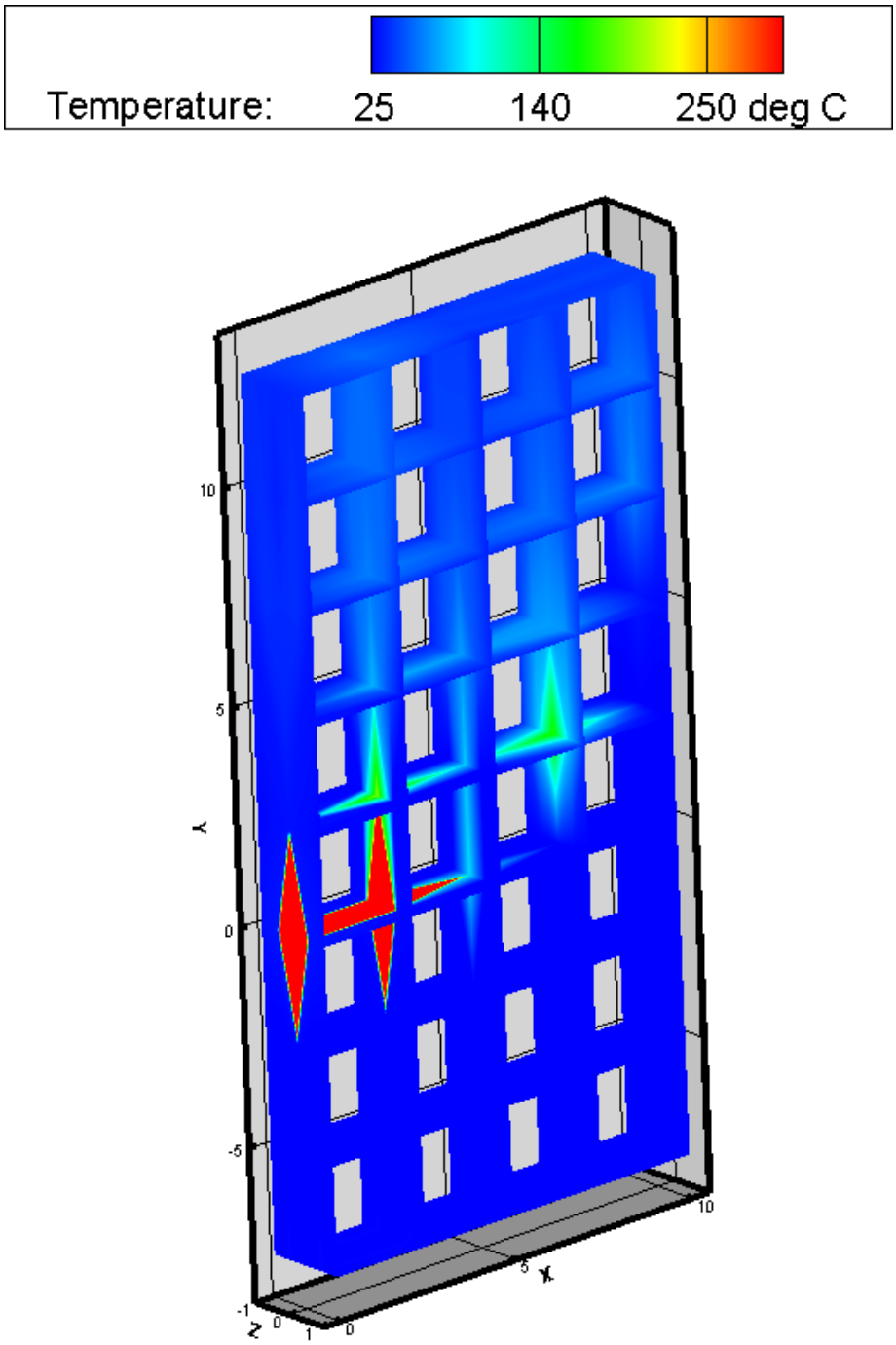

Figure A.52: Three-dimensional temperature gradient: combination of the two-dimensional cross sections of the 0.25 psig flame at 90 degrees

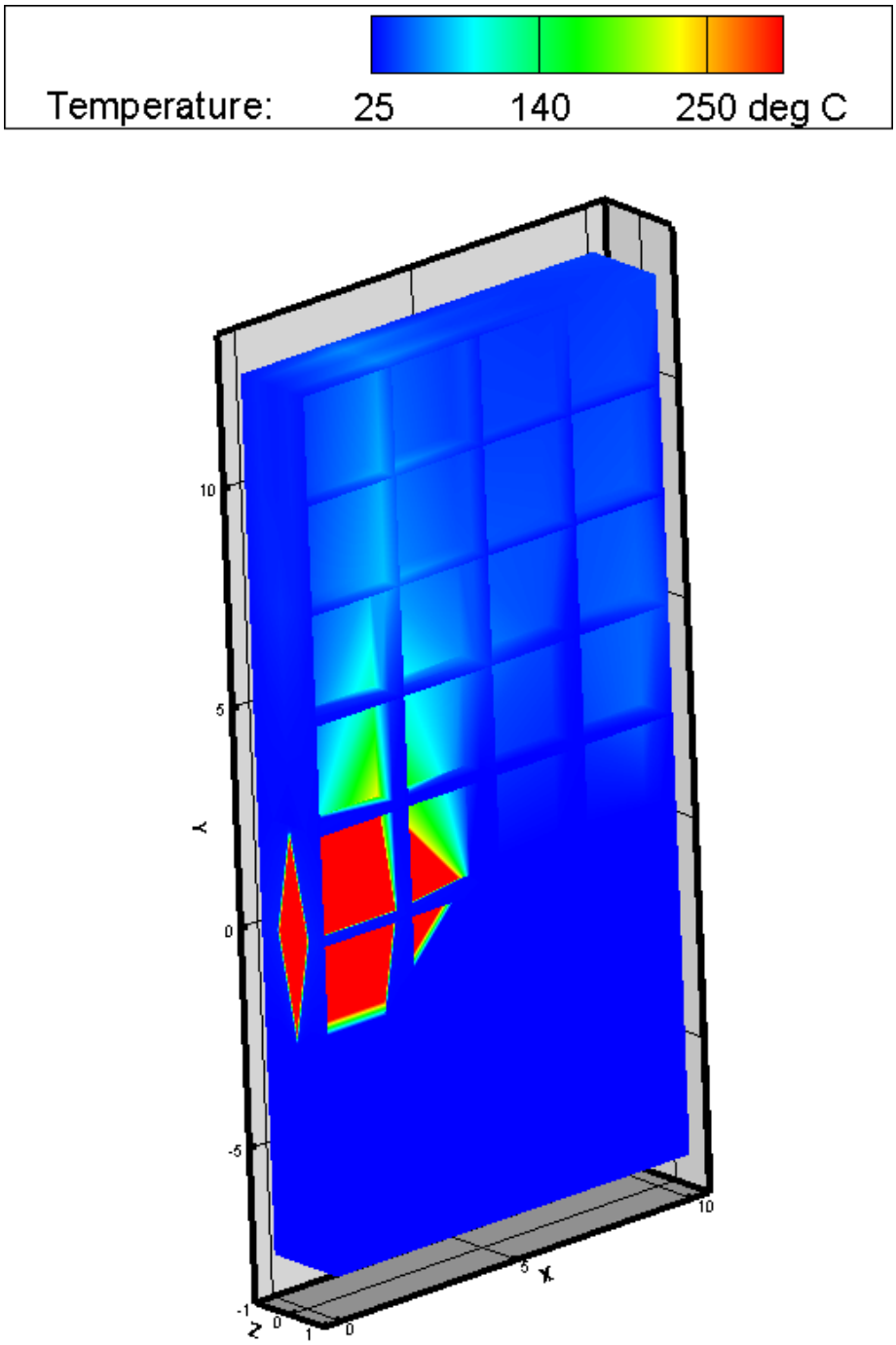

Figure A.53: Three-dimensional temperature gradient: combination of the two-dimensional cross sections of the 0.5 psig flame at 90 degrees

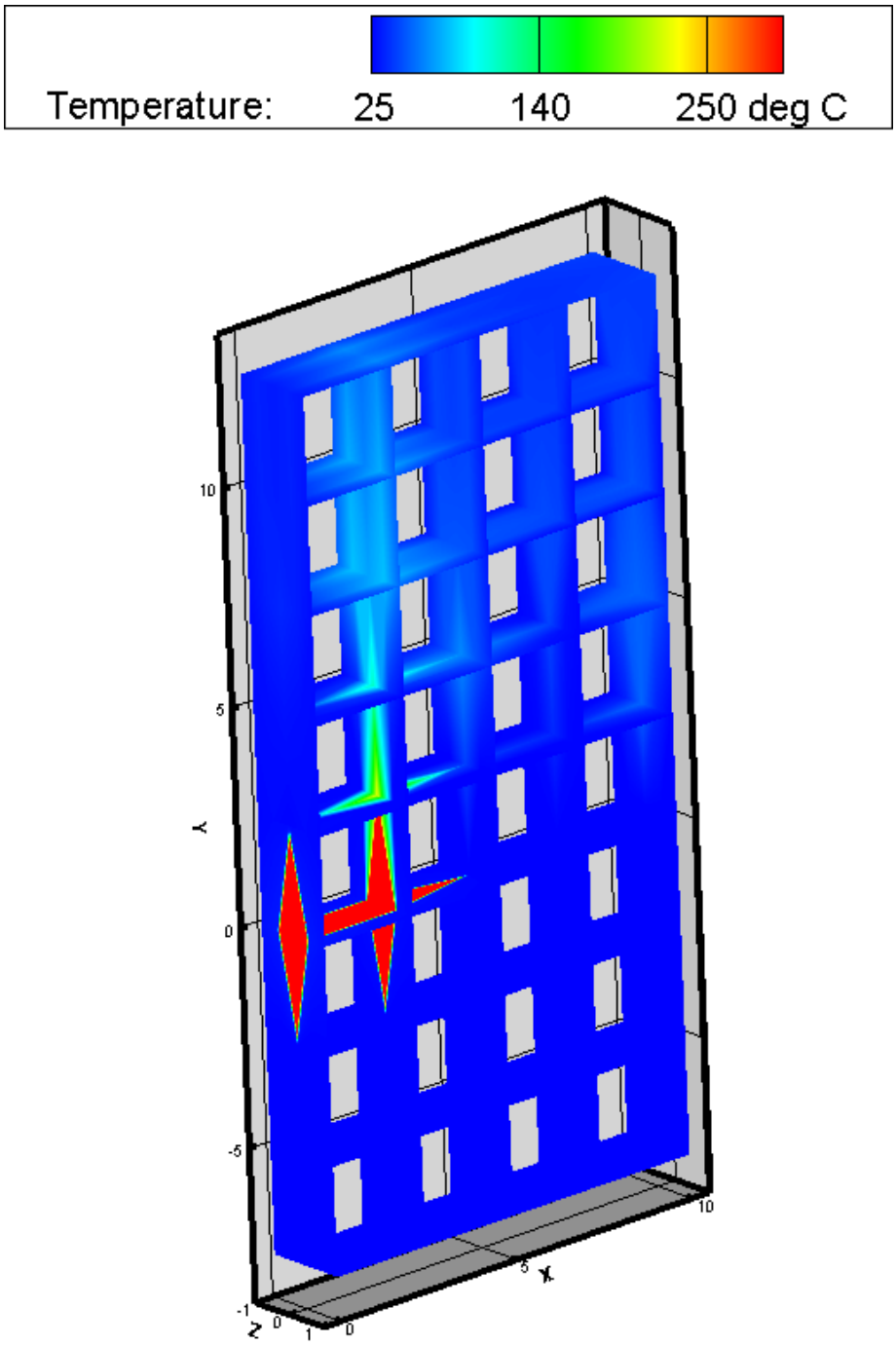

Figure A.54: Three-dimensional temperature gradient: combination of the two-dimensional cross sections of the 0.5 psig flame at 90 degrees

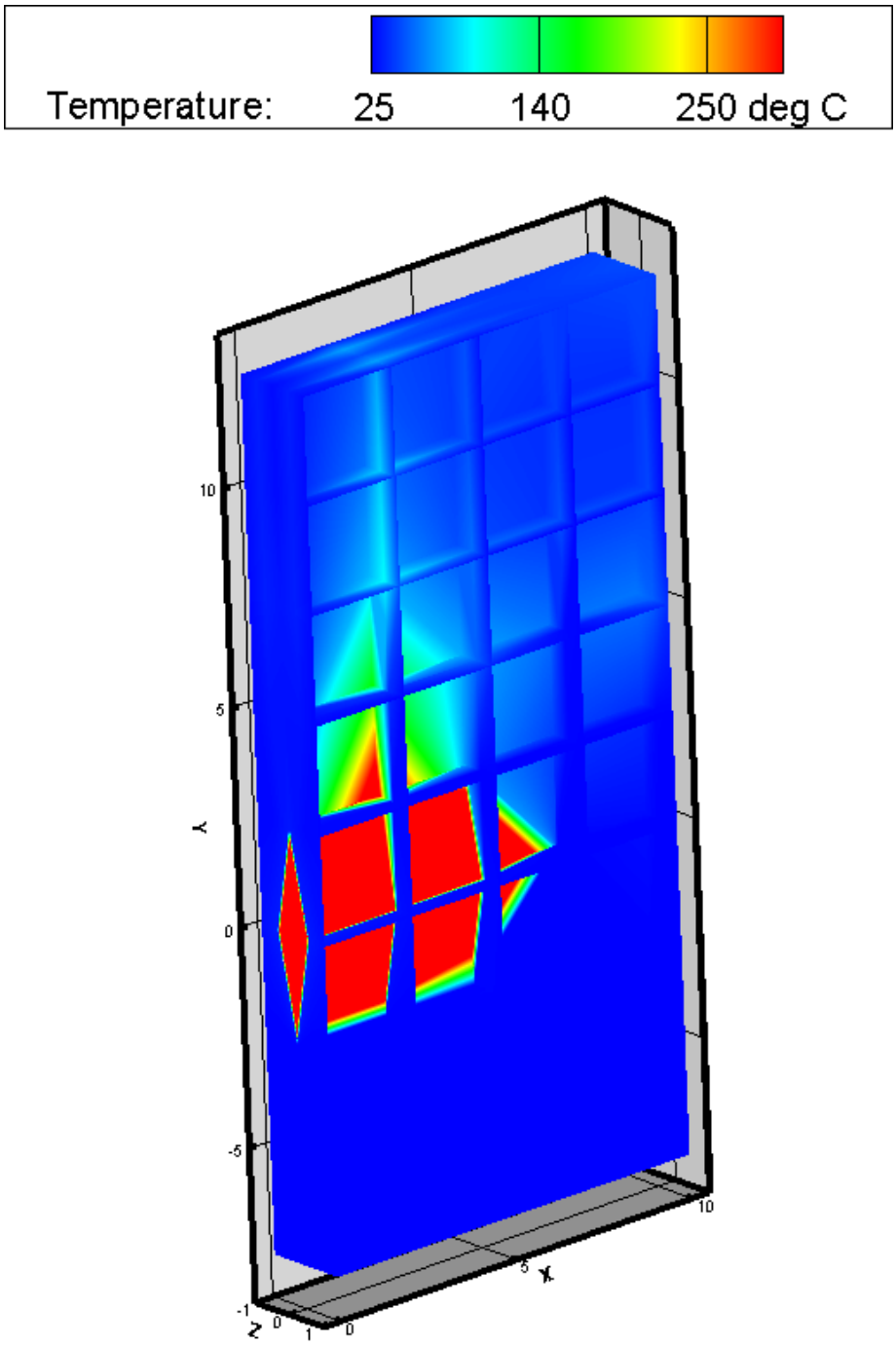

Figure A.55: Three-dimensional temperature gradient: combination of the two-dimensional cross sections of the 0.75 psig flame at 90 degrees

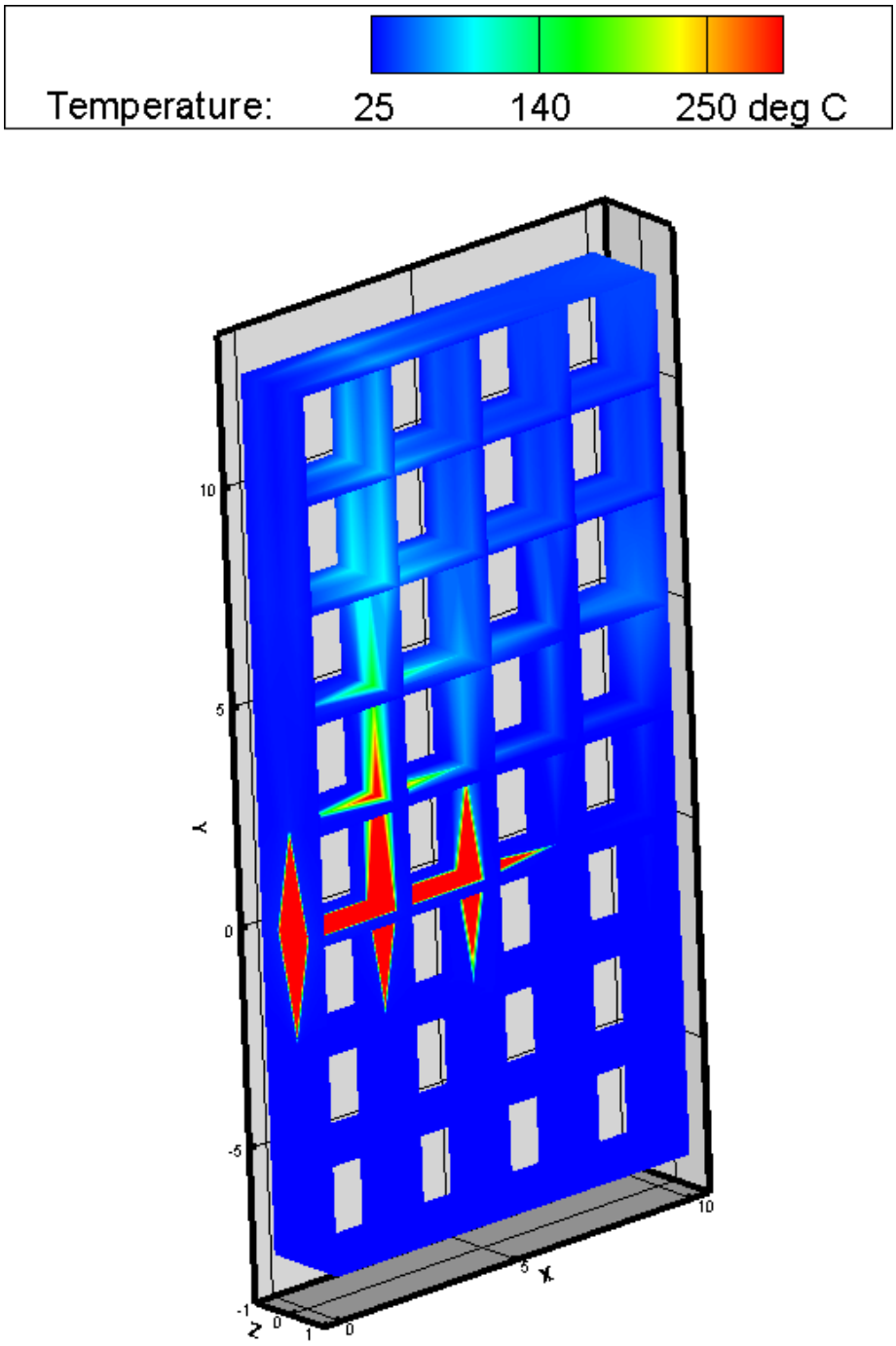

Figure A.56: Three-dimensional temperature gradient: combination of the two-dimensional cross sections of the 0.75 psig flame at 90 degrees

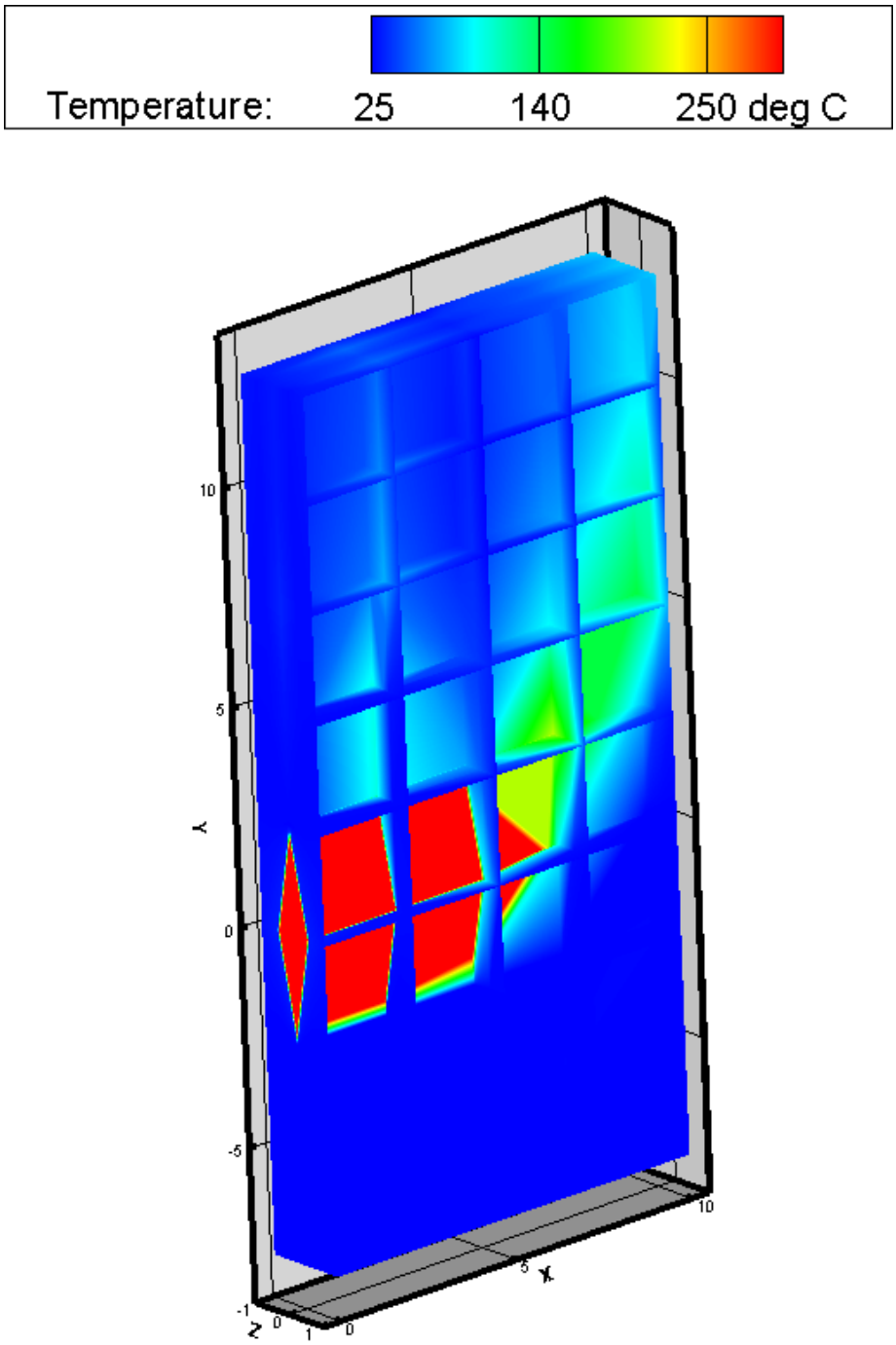

Figure A.57: Three-dimensional temperature gradient: combination of the two-dimensional cross sections of the 1.0 psig flame at 90 degrees

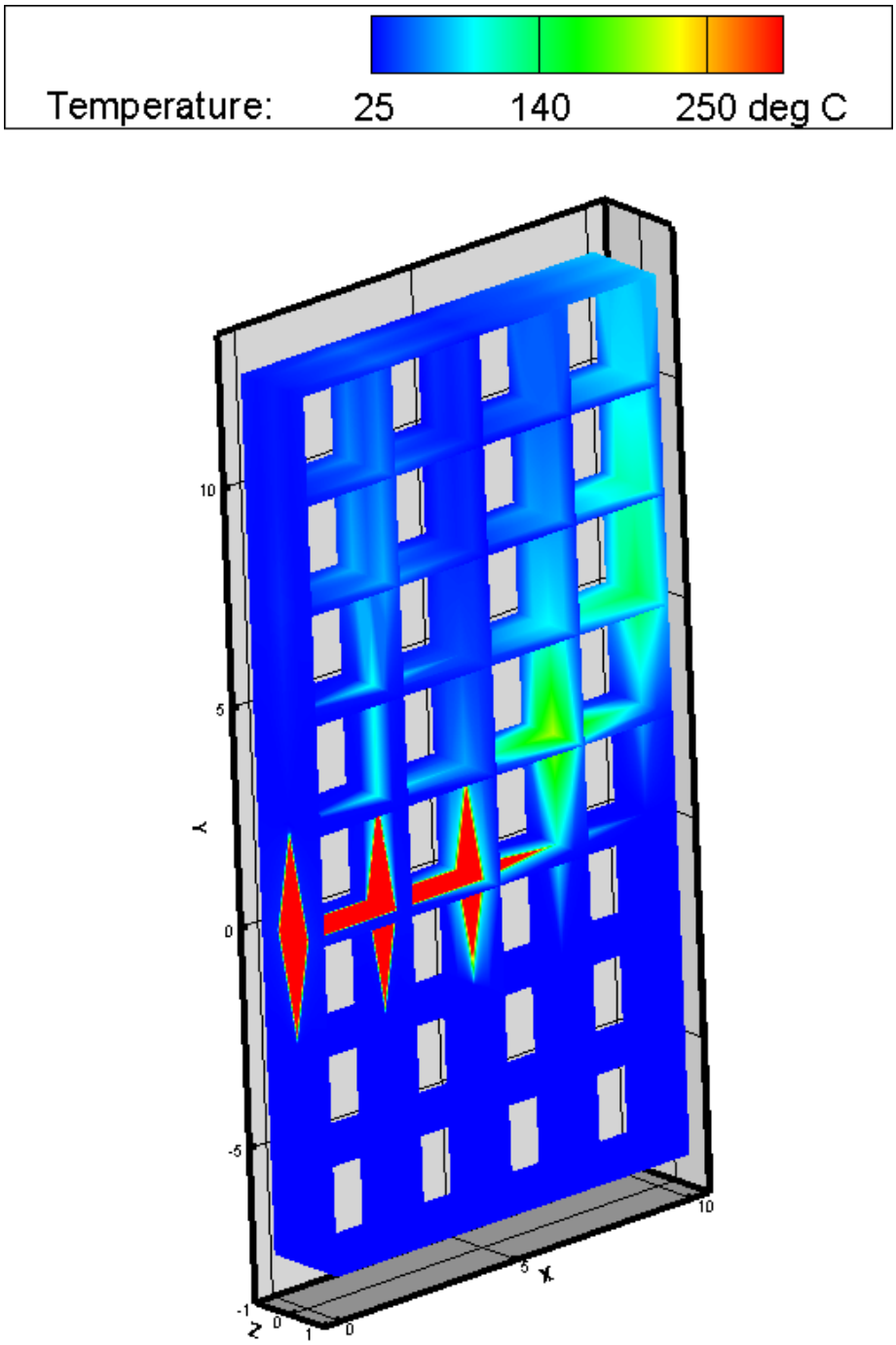

Figure A.58: Three-dimensional temperature gradient: combination of the two-dimensional cross sections of the 1.0 psig flame at 90 degrees

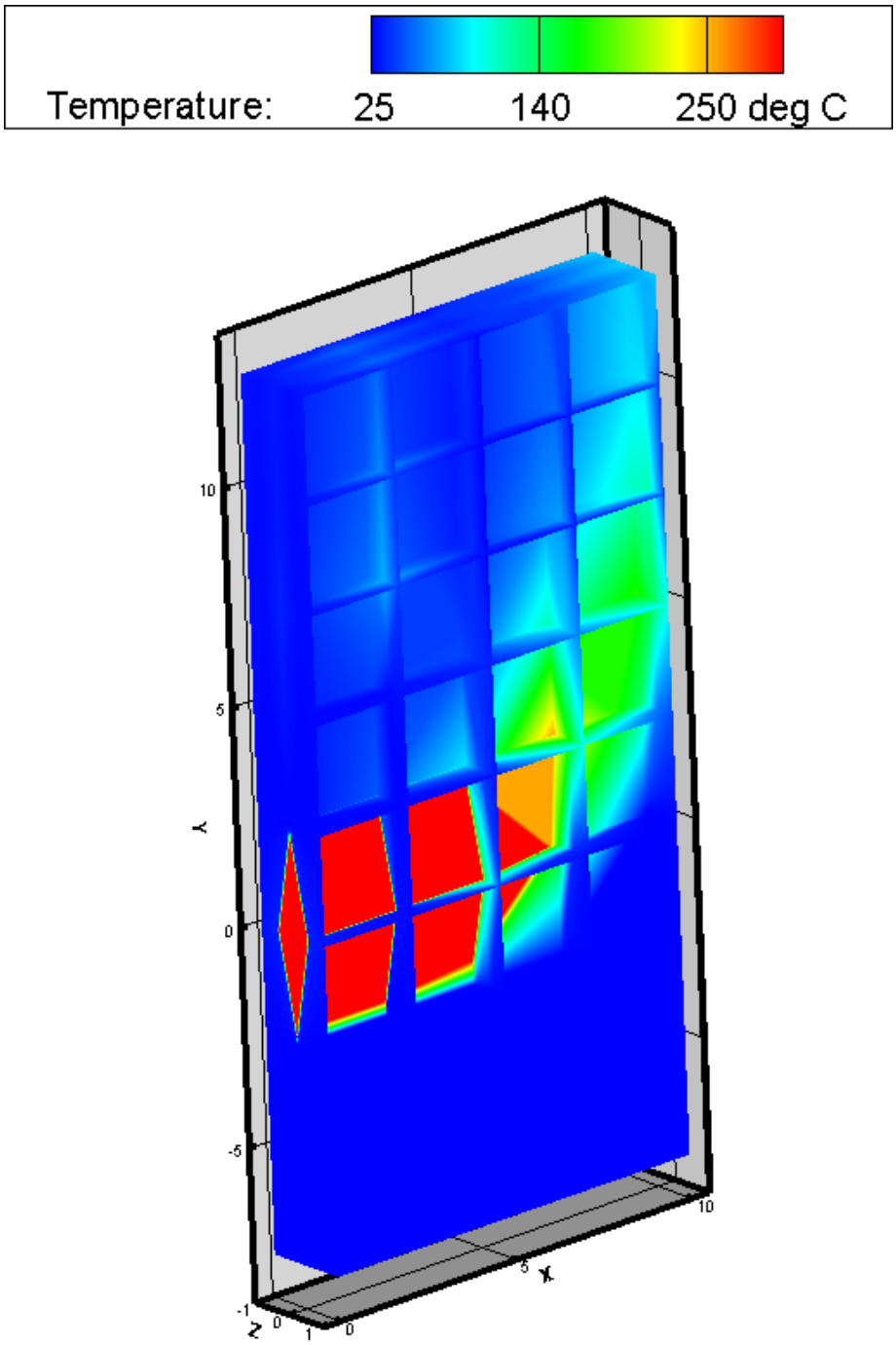

Figure A.59: Three-dimensional temperature gradient: combination of the two-dimensional cross sections of the 1.25 psig flame at 90 degrees

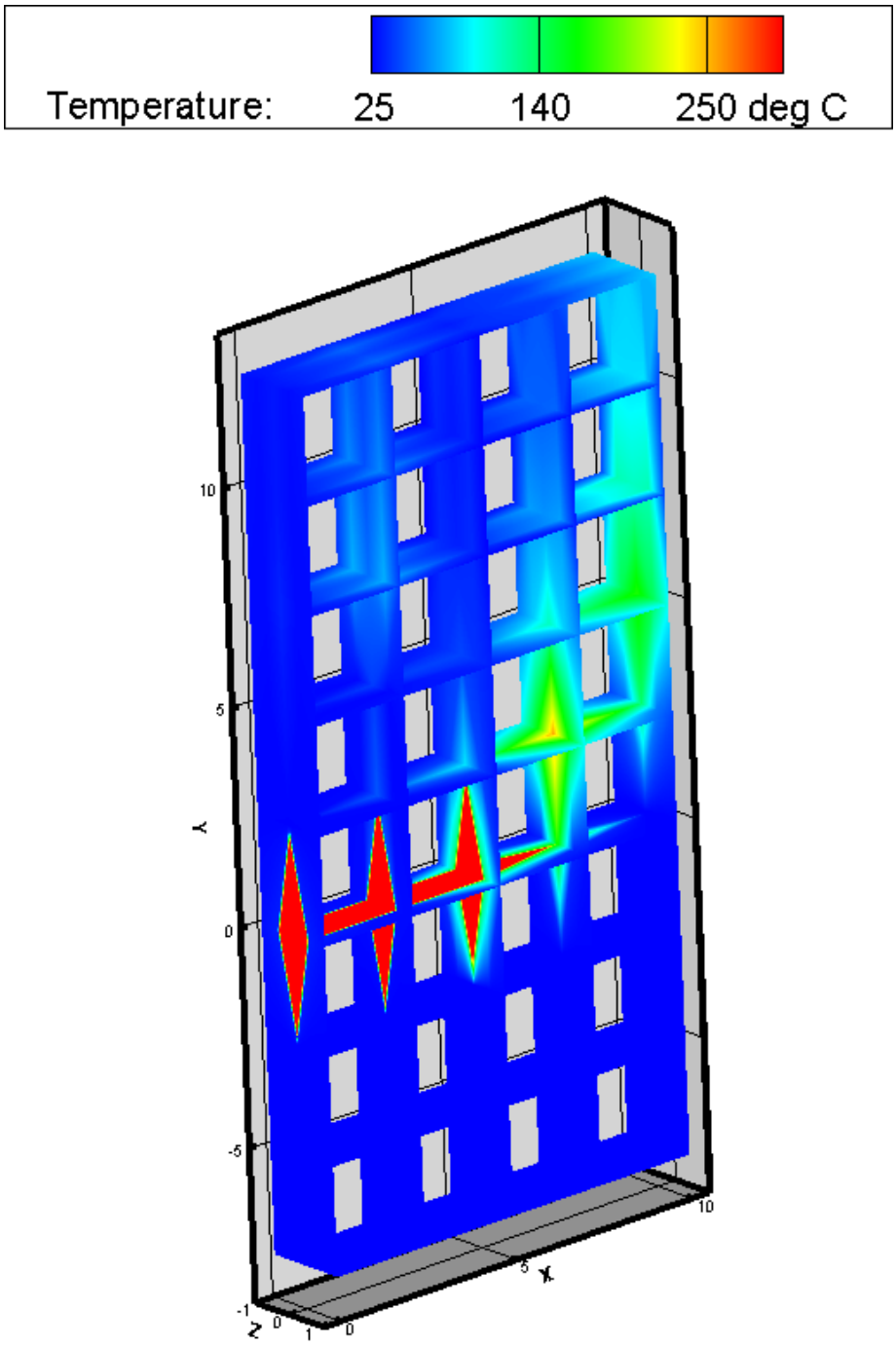

Figure A.60: Three-dimensional temperature gradient: combination of the two-dimensional cross sections of the 1.25 psig flame at 90 degrees

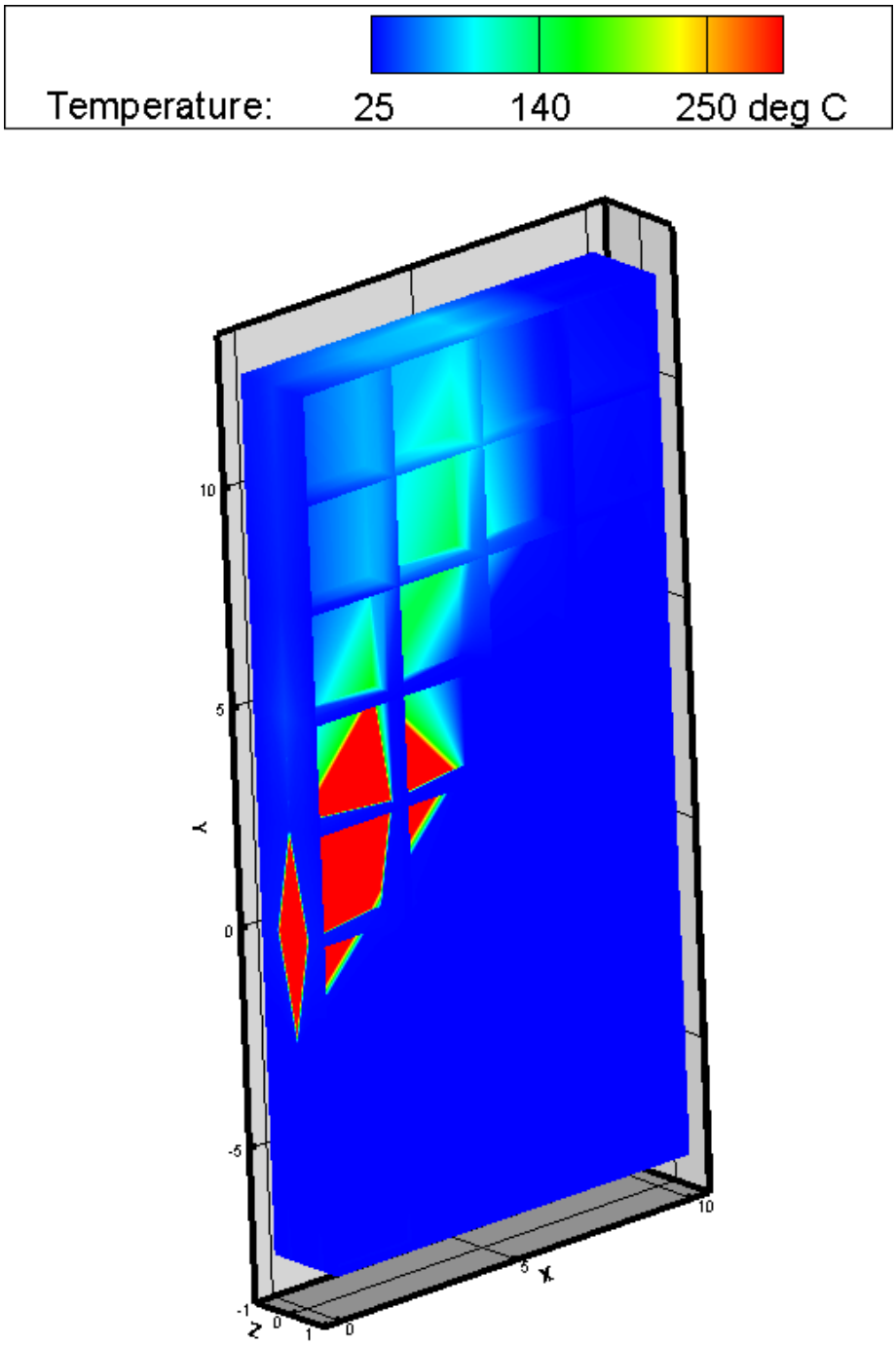

Figure A.61: Three-dimensional temperature gradient: combination of the two-dimensional cross sections of the 0.25 psig flame at 135 degrees

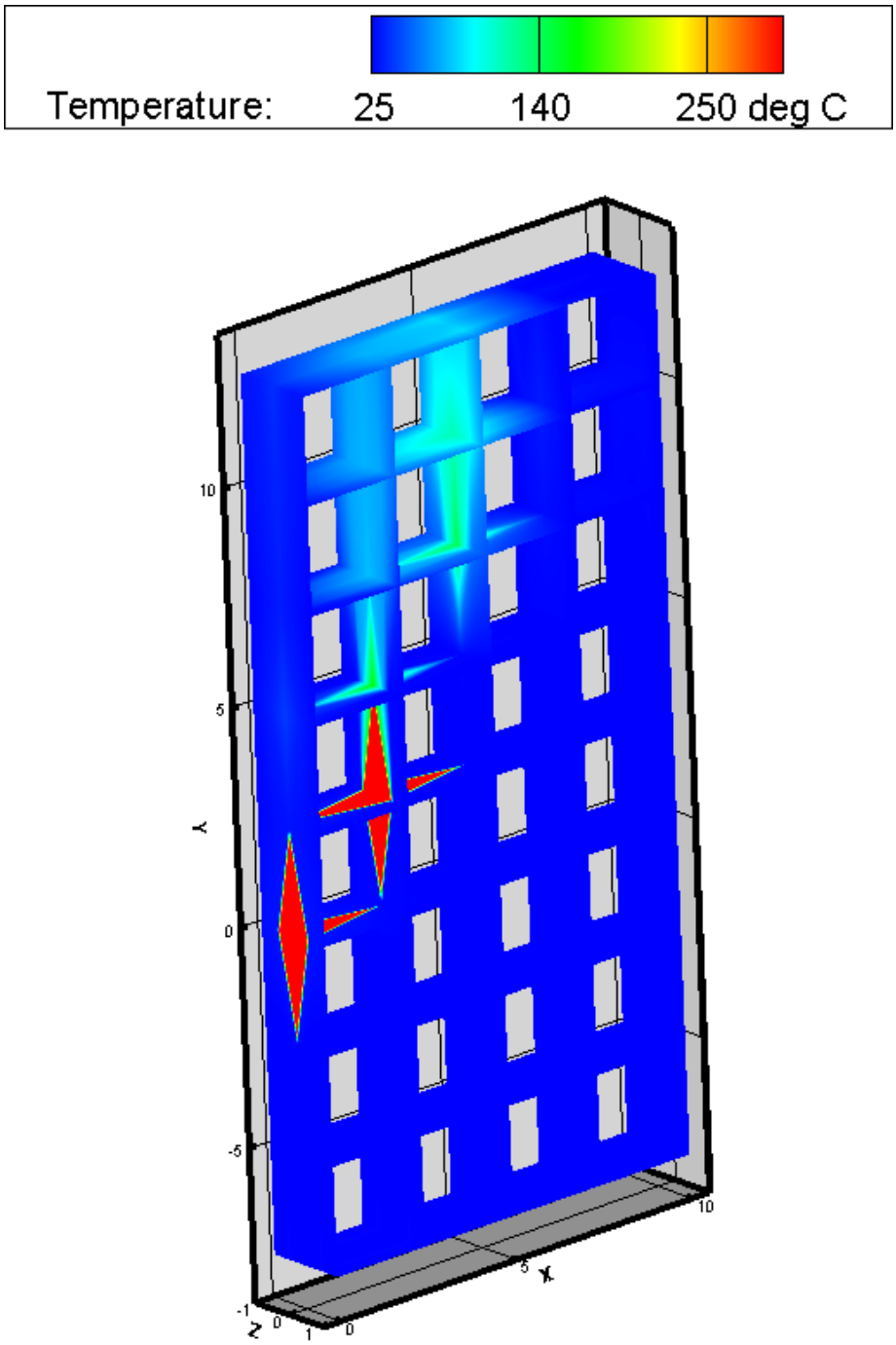

Figure A.62: Three-dimensional temperature gradient: combination of the two-dimensional cross sections of the 0.25 psig flame at 135 degrees

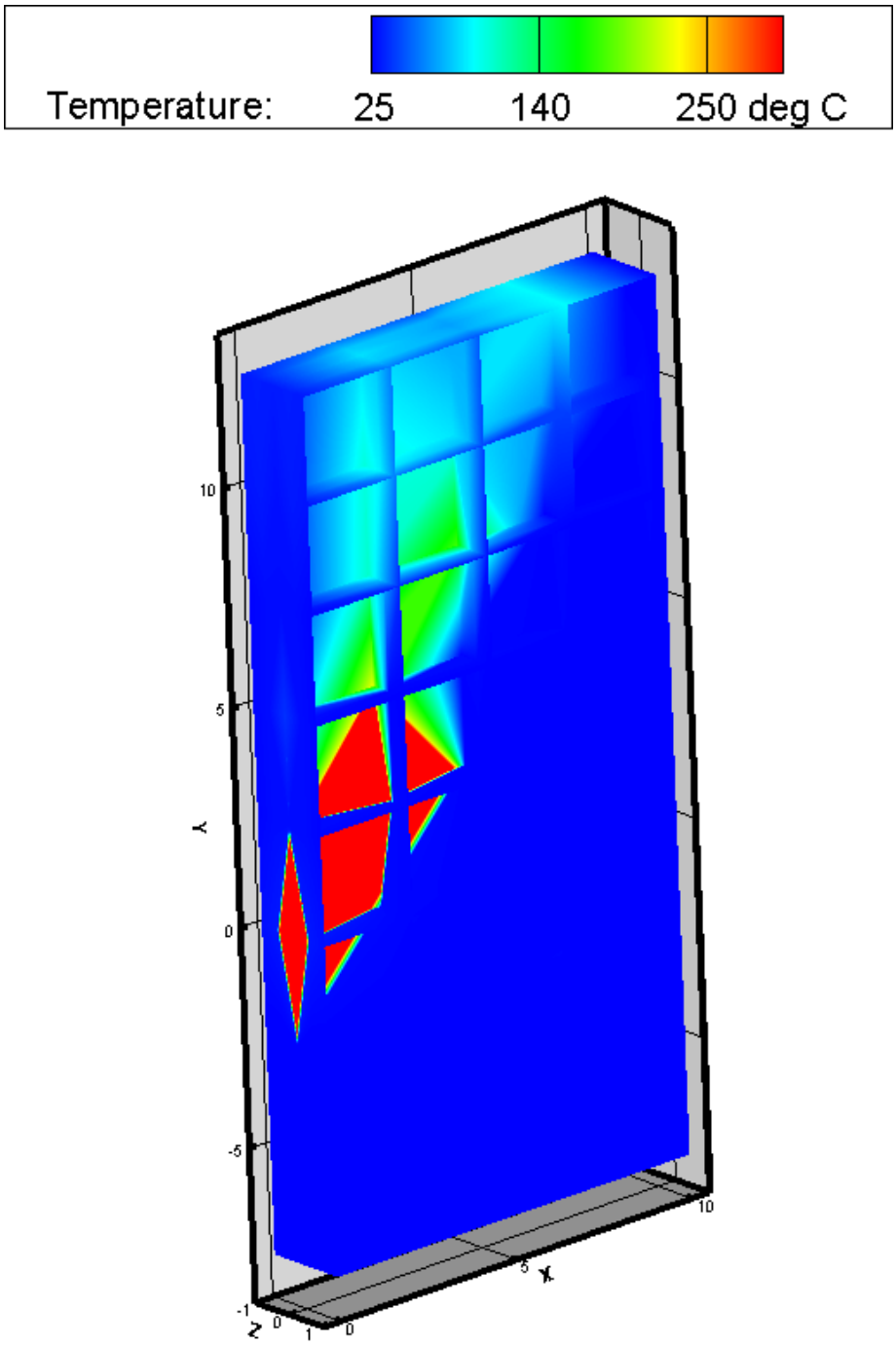

Figure A.63: Three-dimensional temperature gradient: combination of the two-dimensional cross sections of the 0.5 psig flame at 135 degrees

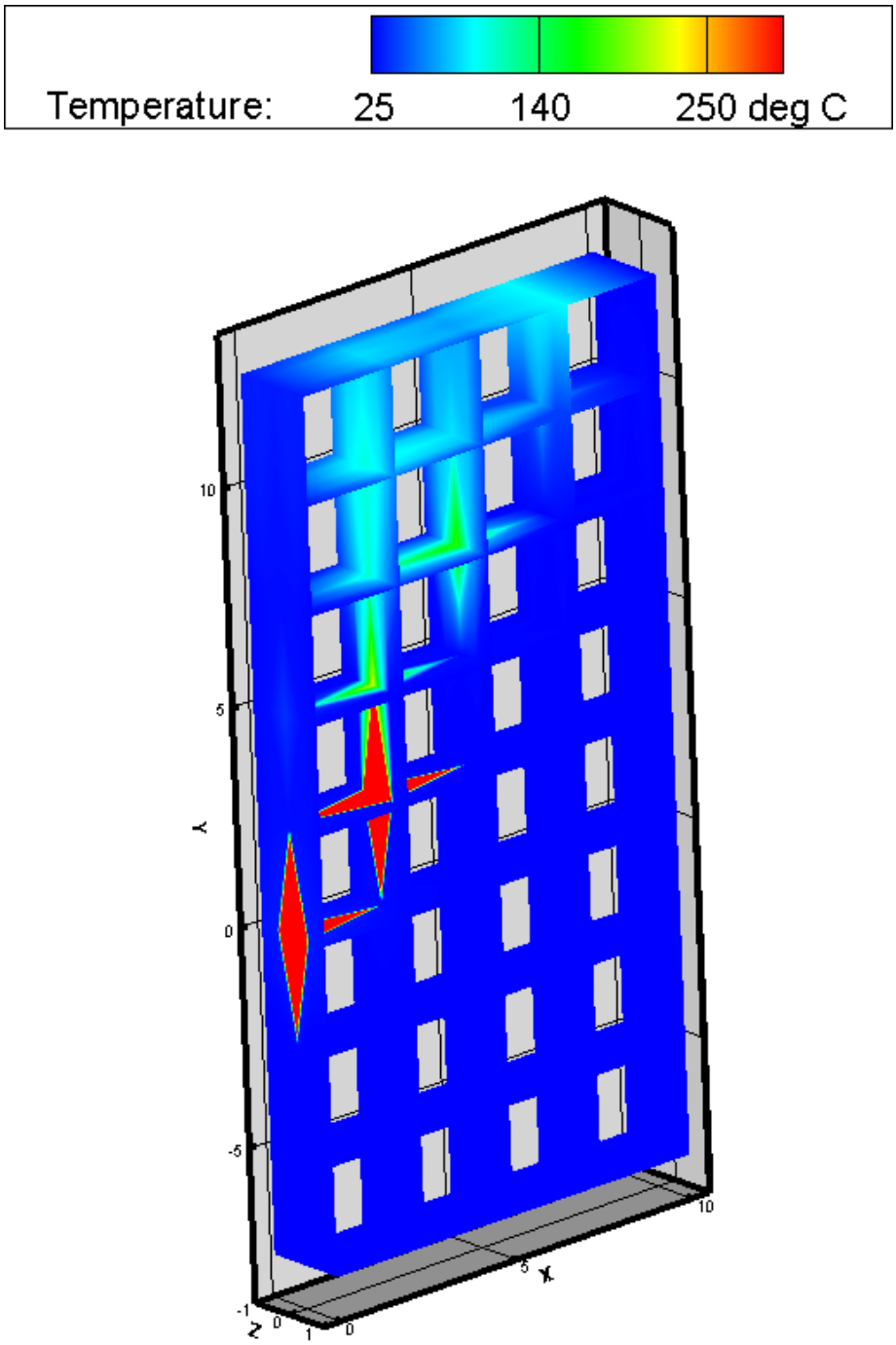

Figure A.64: Three-dimensional temperature gradient: combination of the two-dimensional cross sections of the 0.5 psig flame at 135 degrees

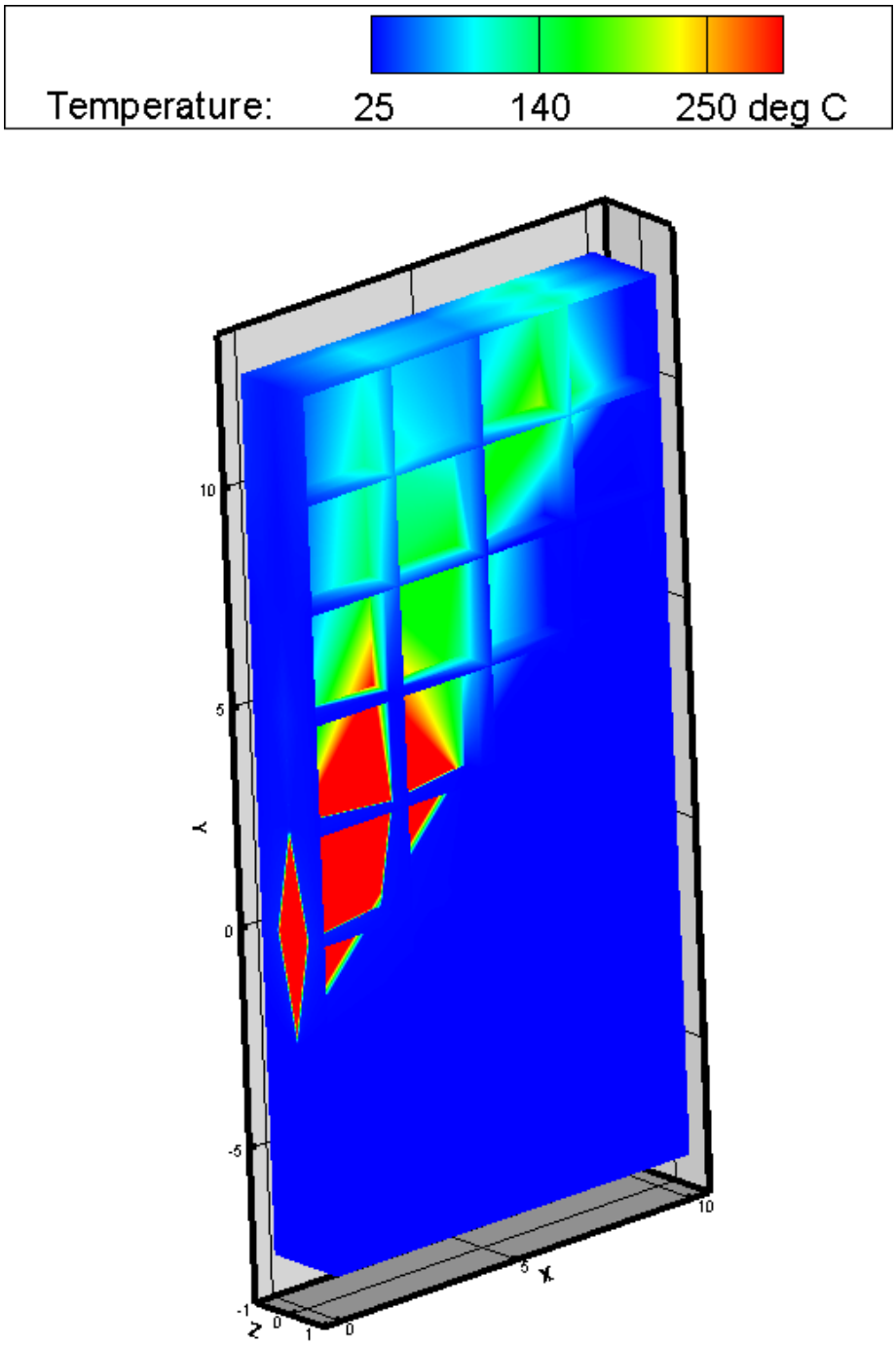

Figure A.65: Three-dimensional temperature gradient: combination of the two-dimensional cross sections of the 0.75 psig flame at 135 degrees

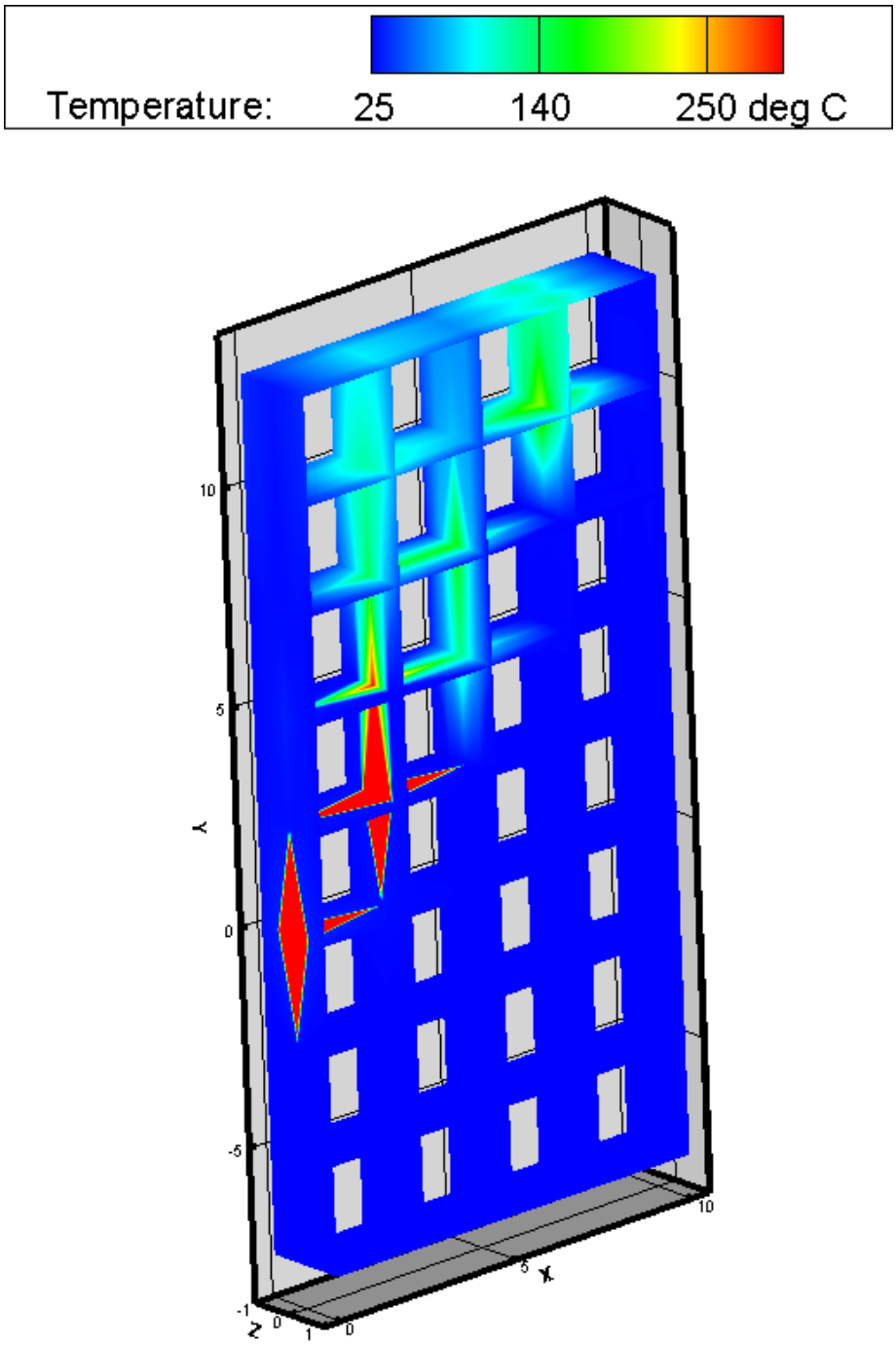

Figure A.66: Three-dimensional temperature gradient: combination of the two-dimensional cross sections of the 0.75 psig flame at 135 degrees

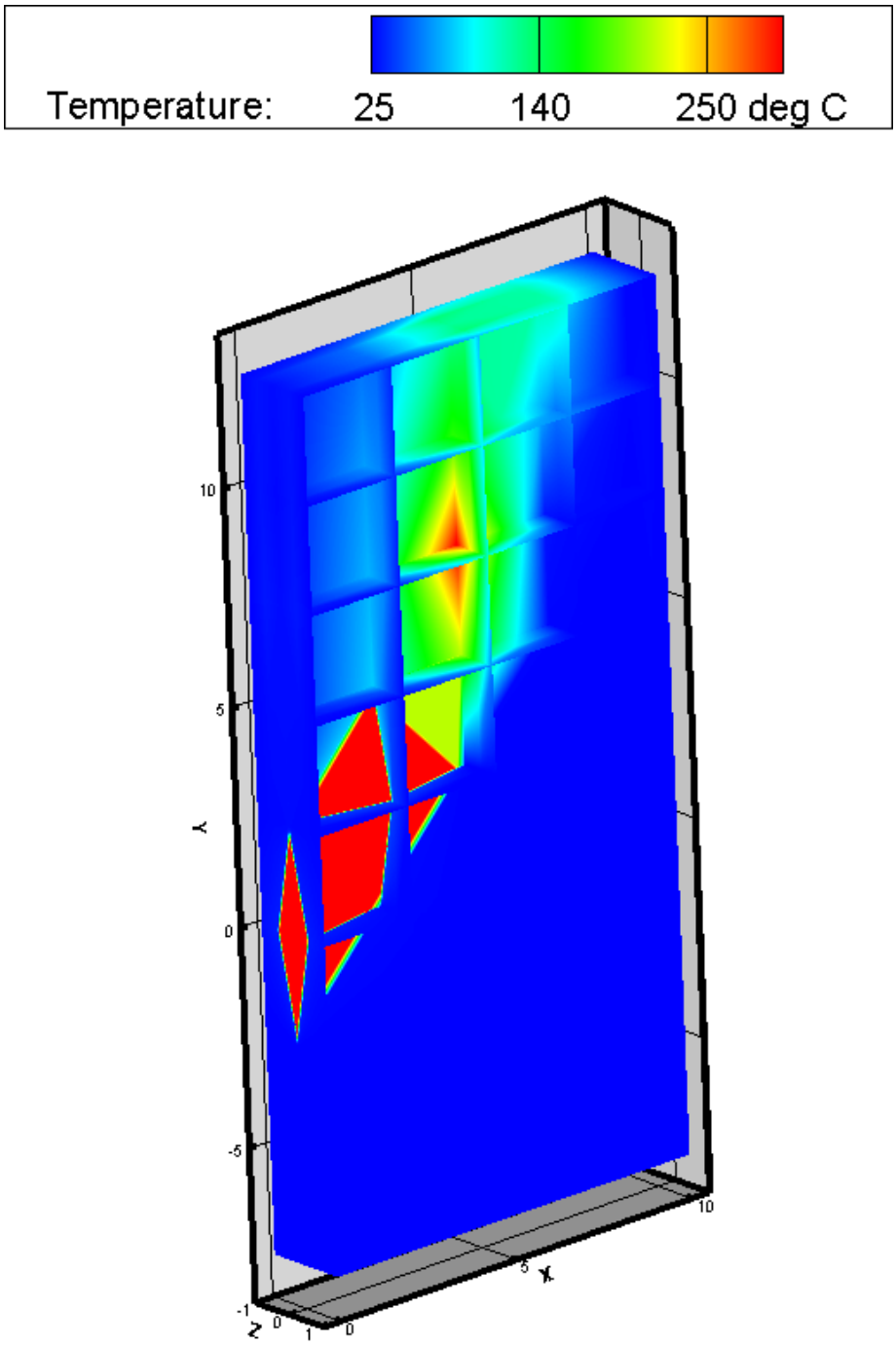

Figure A.67: Three-dimensional temperature gradient: combination of the two-dimensional cross sections of the 1.0 psig flame at 135 degrees

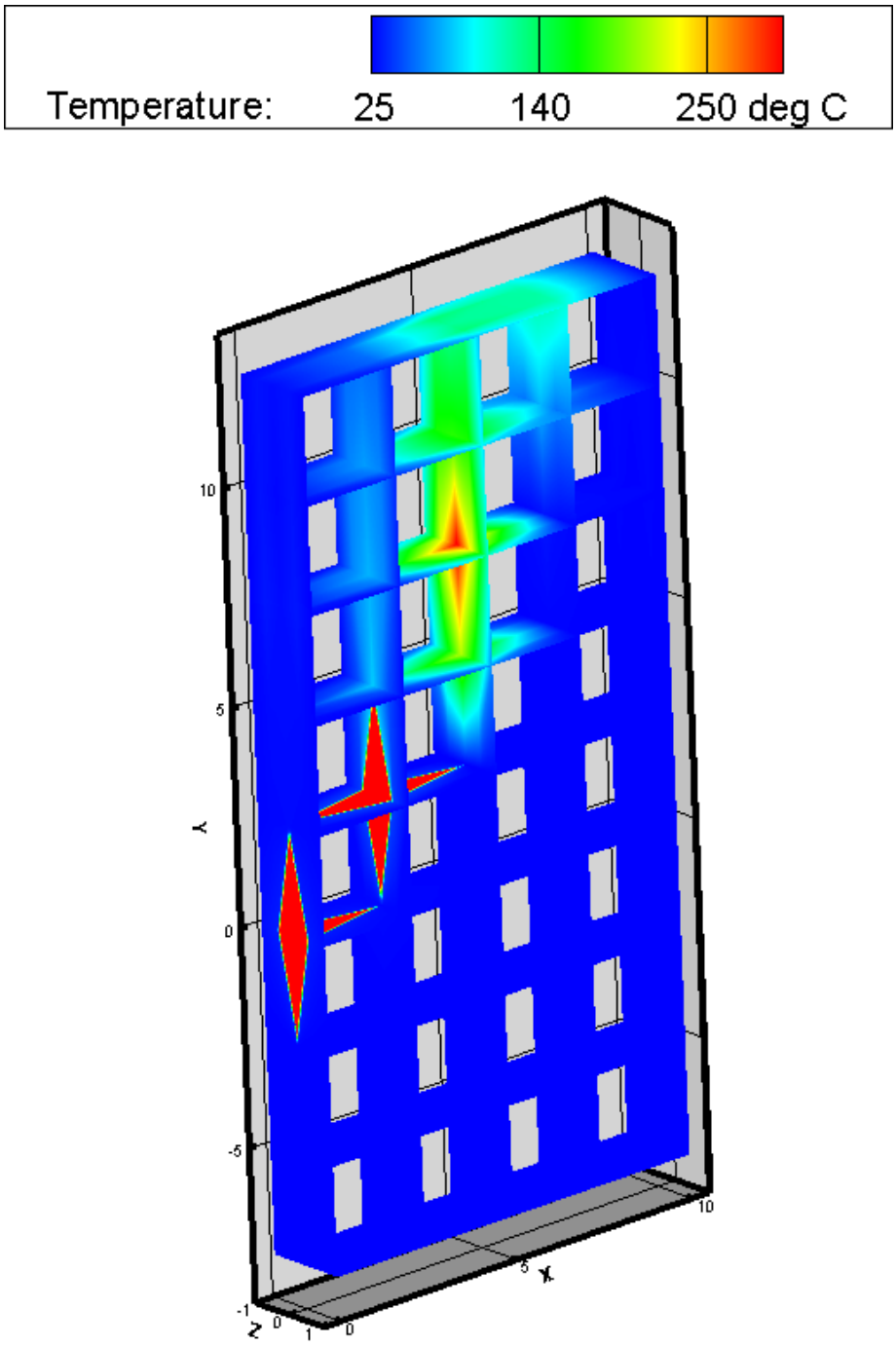

Figure A.68: Three-dimensional temperature gradient: combination of the two-dimensional cross sections of the 1.0 psig flame at 135 degrees

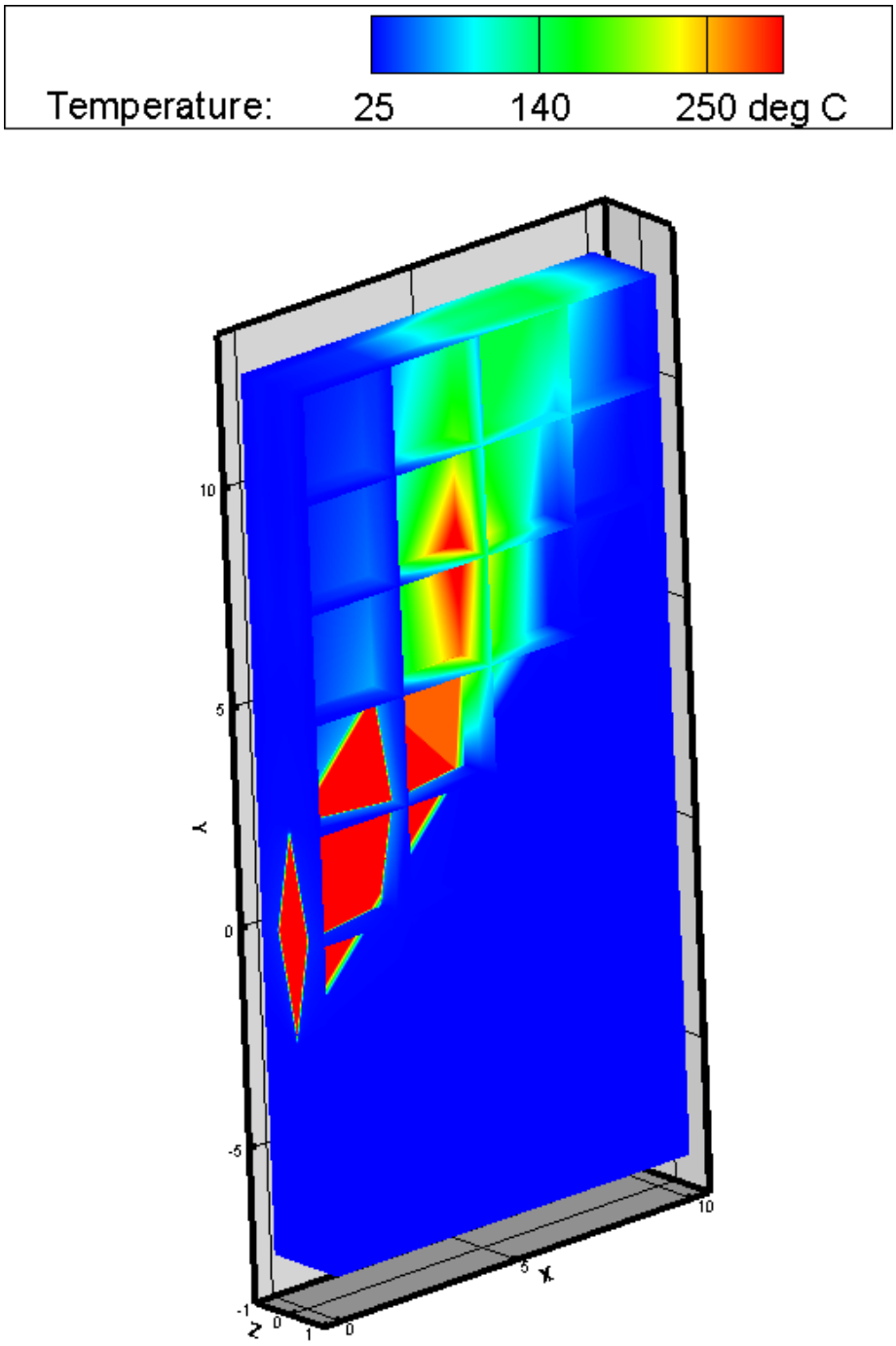

Figure A.69: Three-dimensional temperature gradient: combination of the two-dimensional cross sections of the 1.25 psig flame at 135 degrees

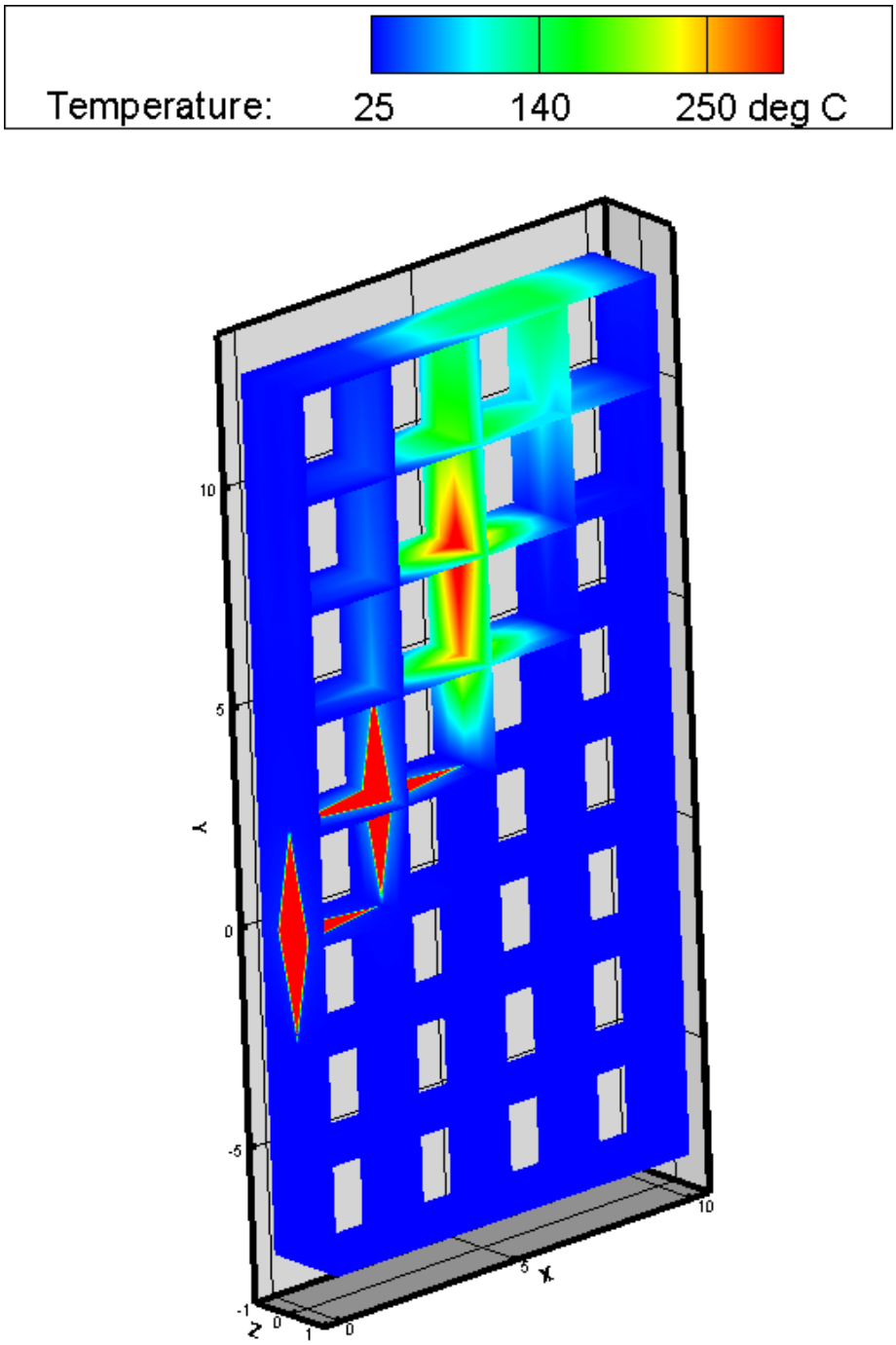

Figure A.70: Three-dimensional temperature gradient: combination of the two-dimensional cross sections of the 1.25 psig flame at 135 degrees

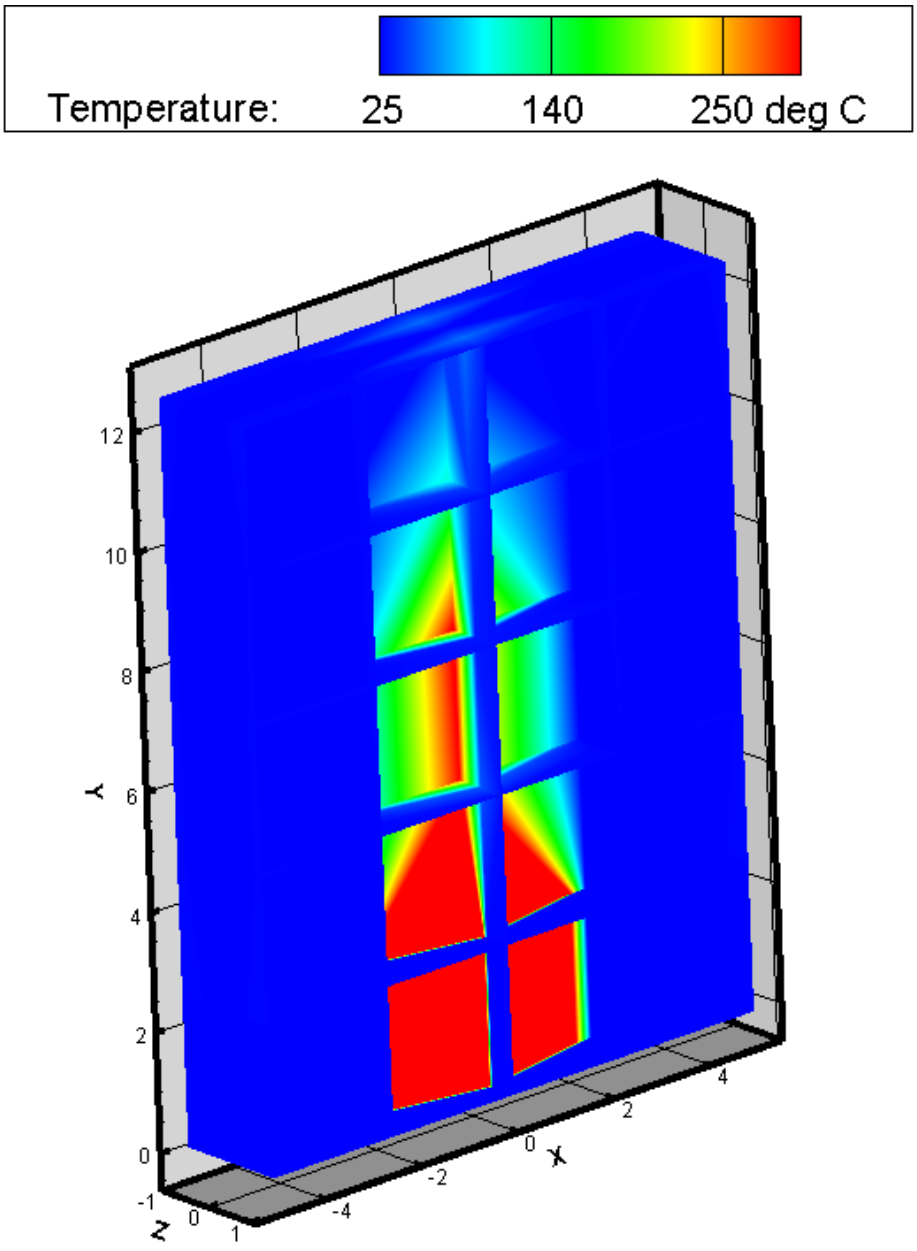

Figure A.71: Three-dimensional temperature gradient: combination of the two-dimensional cross sections of the 0.25 psig flame at 180 degrees

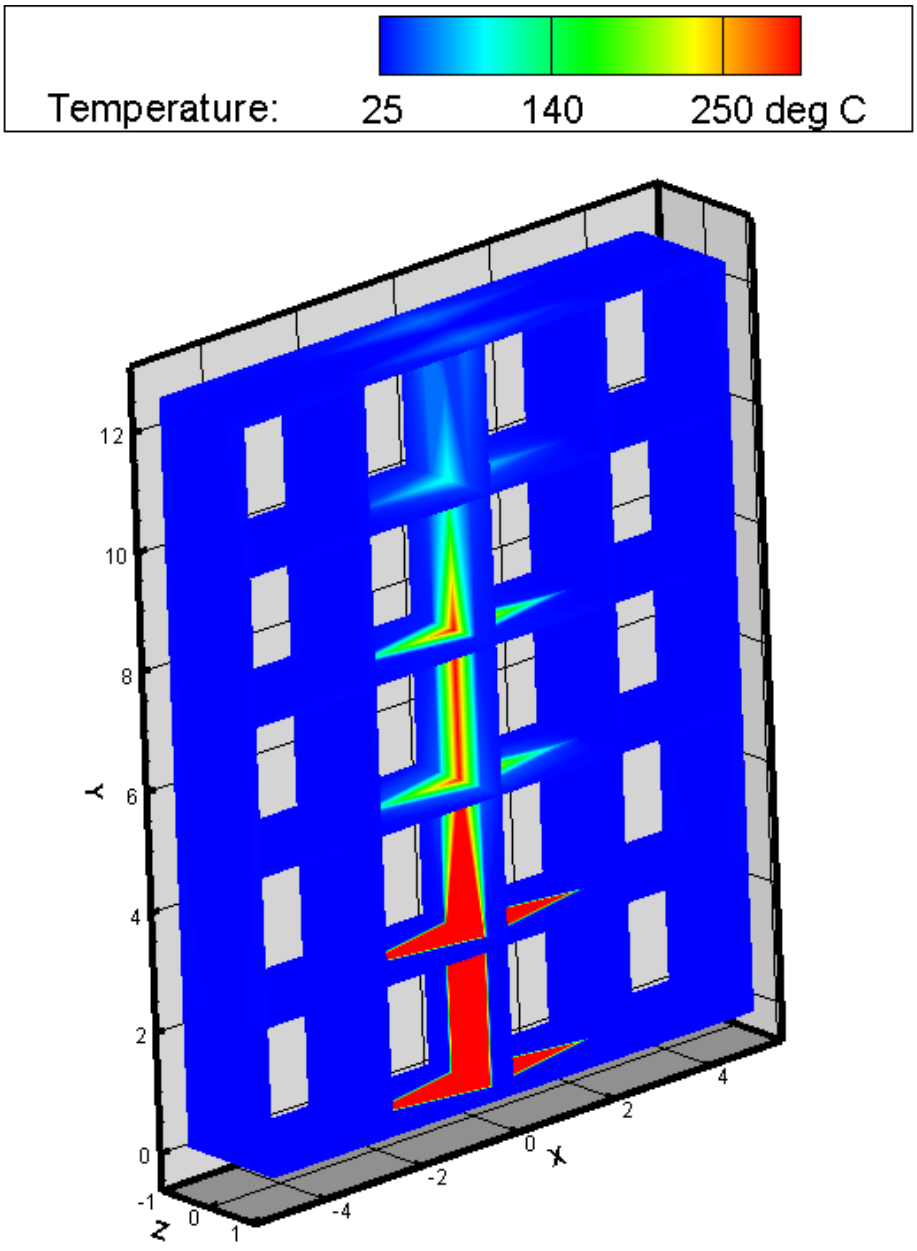

Figure A.72: Three-dimensional temperature gradient: combination of the two-dimensional cross sections of the 0.25 psig flame at 180 degrees

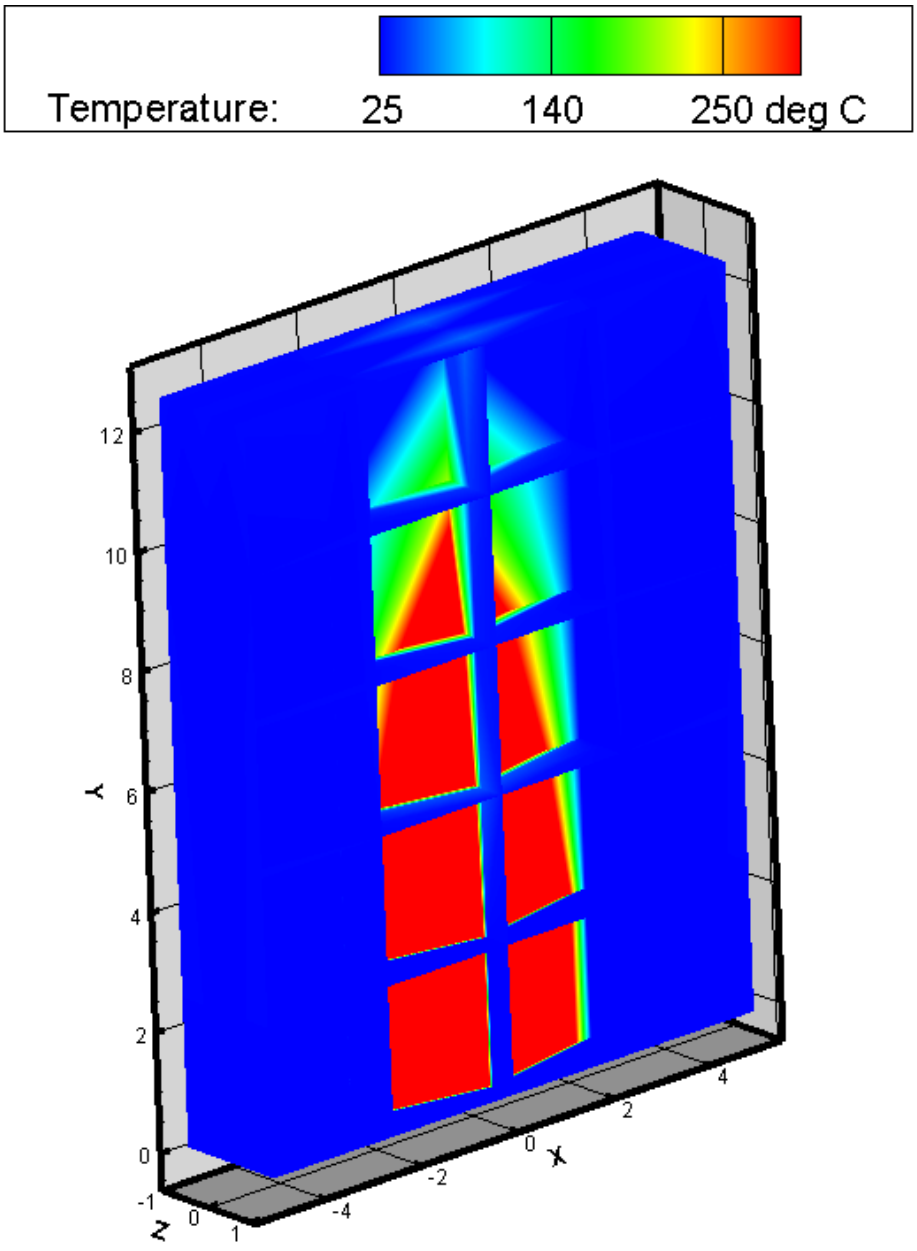

Figure A.73: Three-dimensional temperature gradient: combination of the two-dimensional cross sections of the 0.5 psig flame at 180 degrees

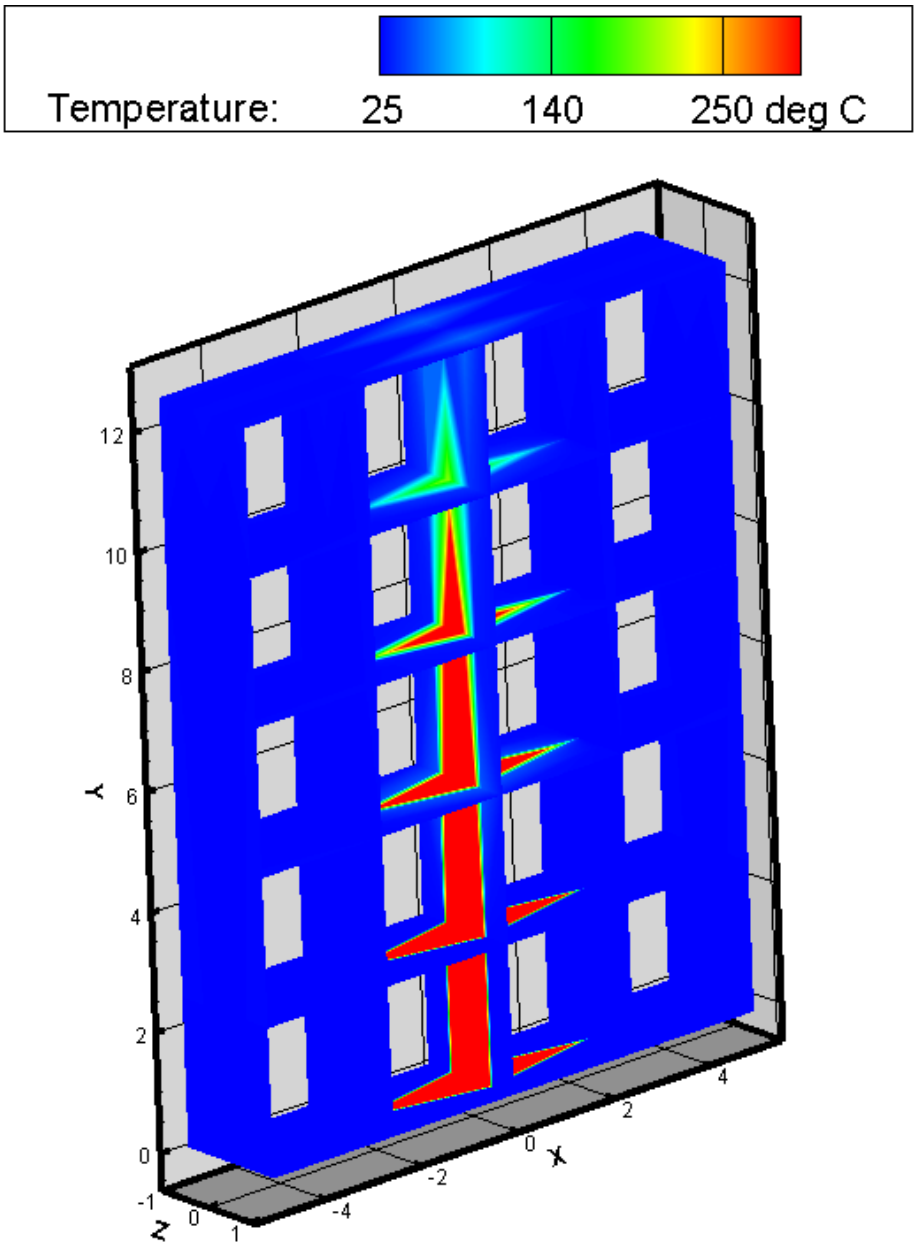

Figure A.74: Three-dimensional temperature gradient: combination of the two-dimensional cross sections of the 0.5 psig flame at 180 degrees

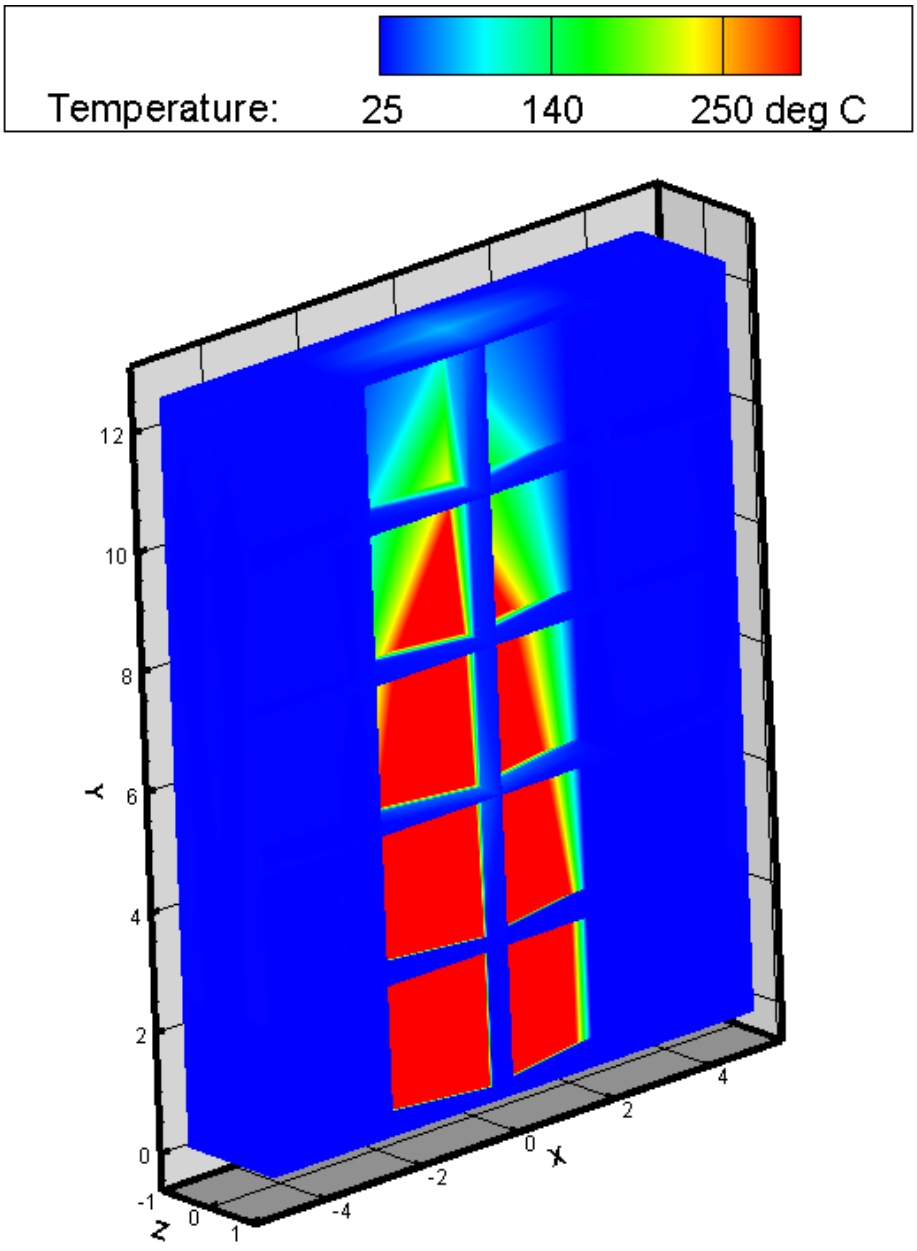

Figure A.75: Three-dimensional temperature gradient: combination of the two-dimensional cross sections of the 0.75 psig flame at 180 degrees

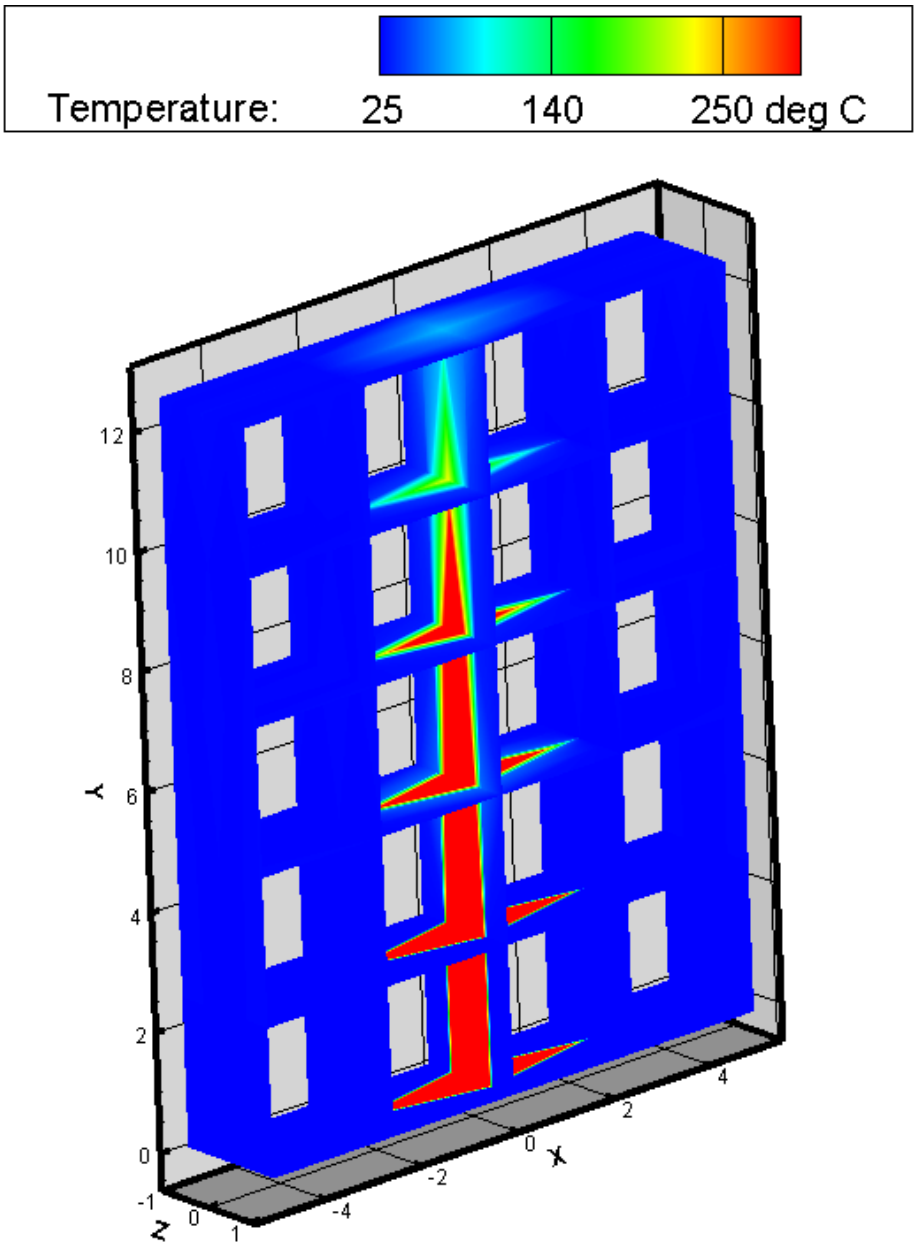

Figure A.76: Three-dimensional temperature gradient: combination of the two-dimensional cross sections of the 0.75 psig flame at 180 degrees

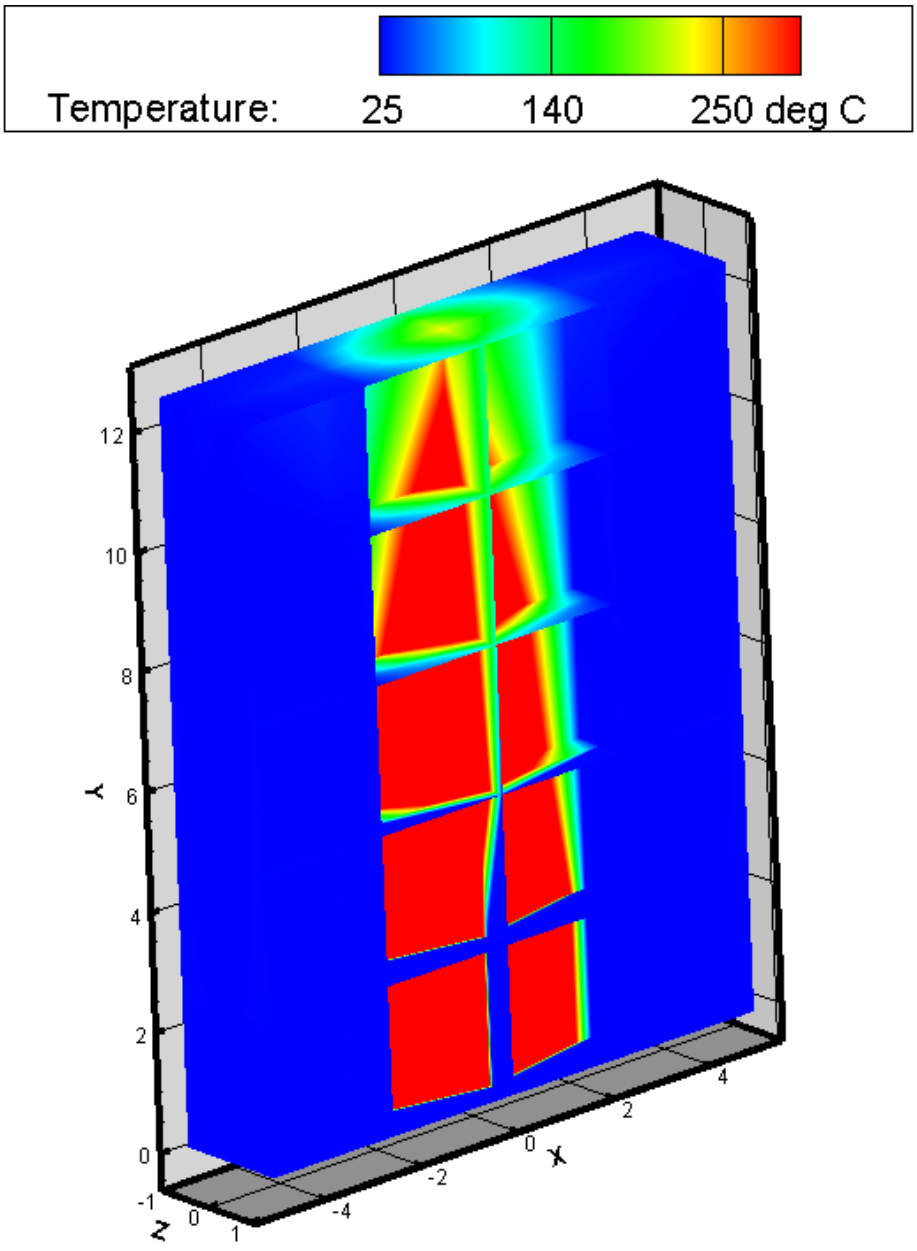

Figure A.77: Three-dimensional temperature gradient: combination of the two-dimensional cross sections of the 1.0 psig flame at 180 degrees

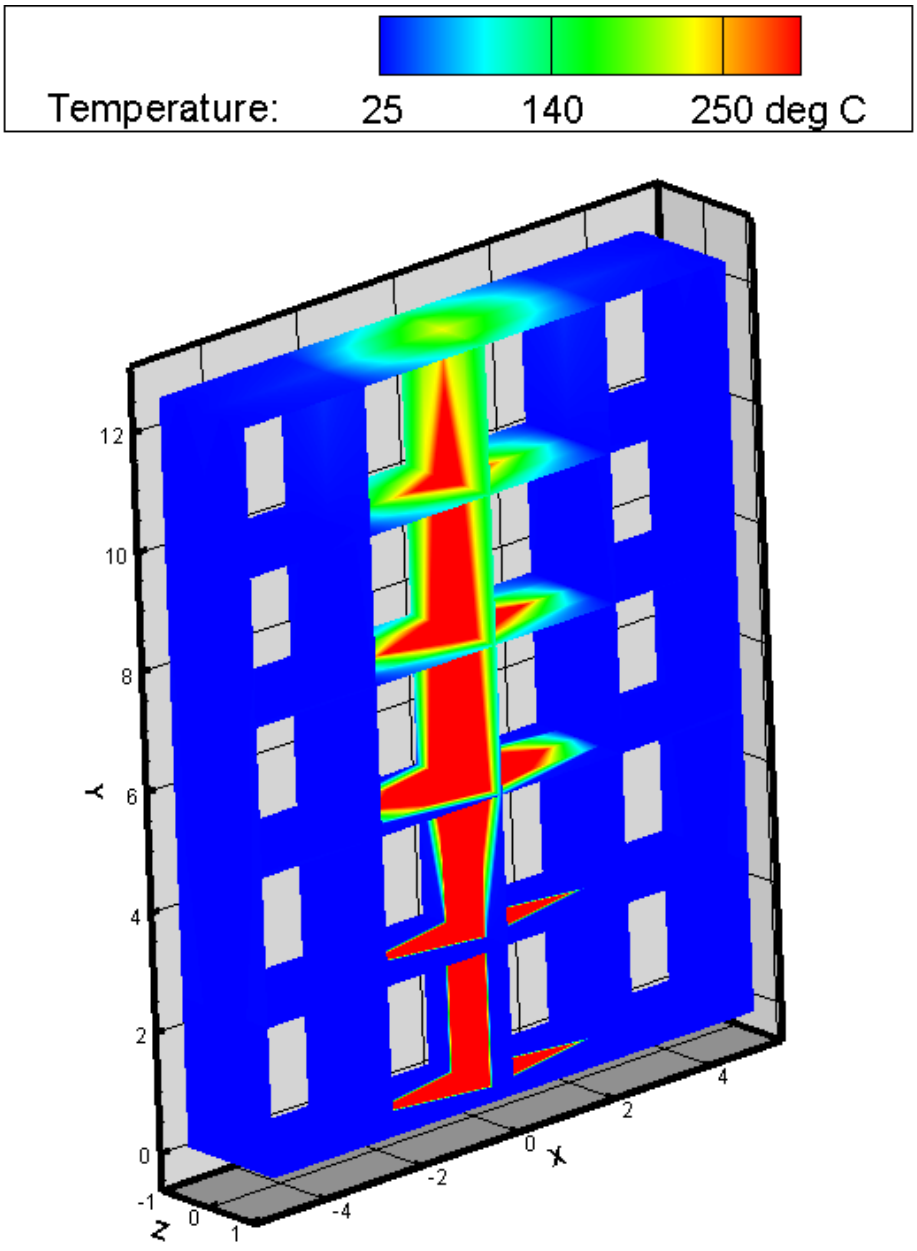

Figure A.78: Three-dimensional temperature gradient: combination of the two-dimensional cross sections of the 1.0 psig flame at 180 degrees

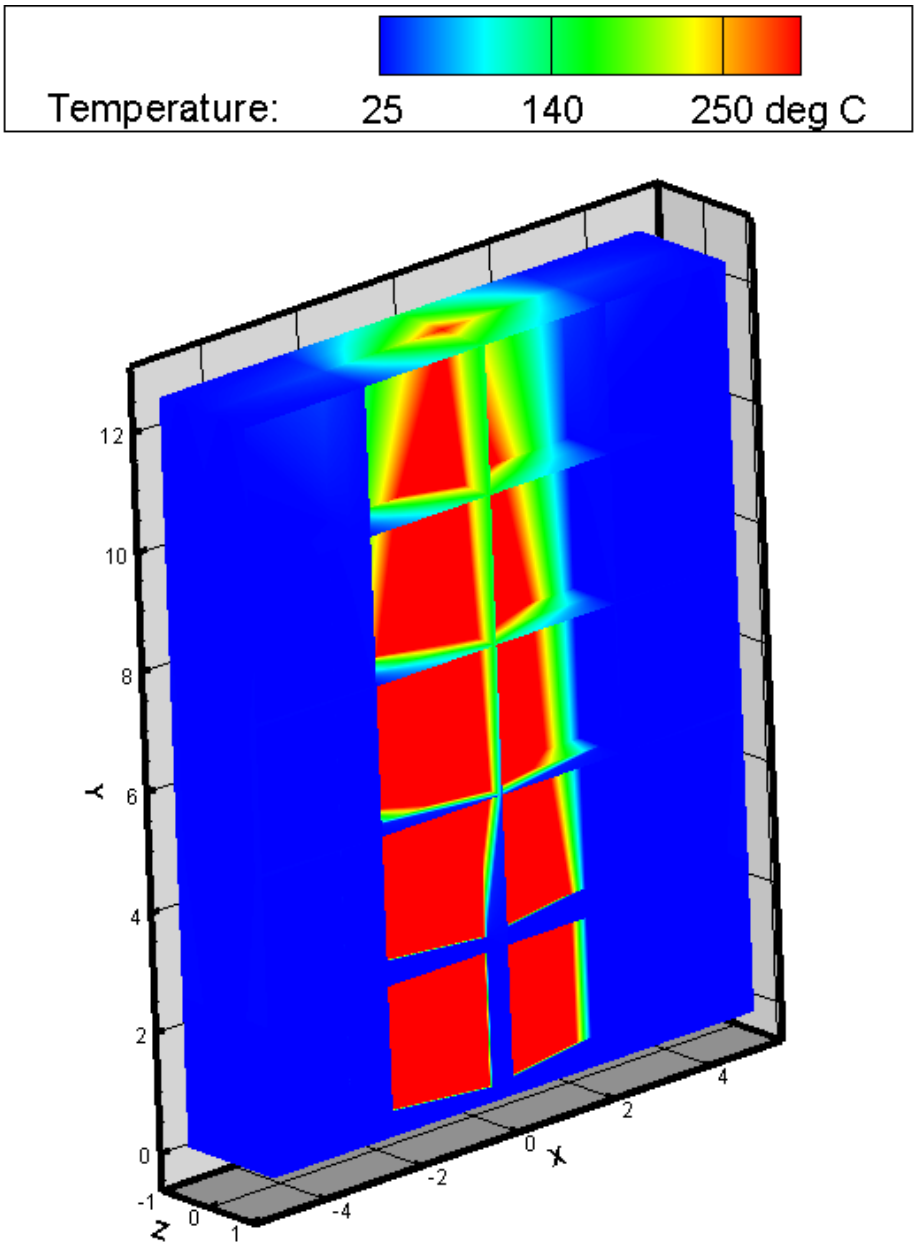

Figure A.79: Three-dimensional temperature gradient: combination of the two-dimensional cross sections of the 1.25 psig flame at 180 degrees

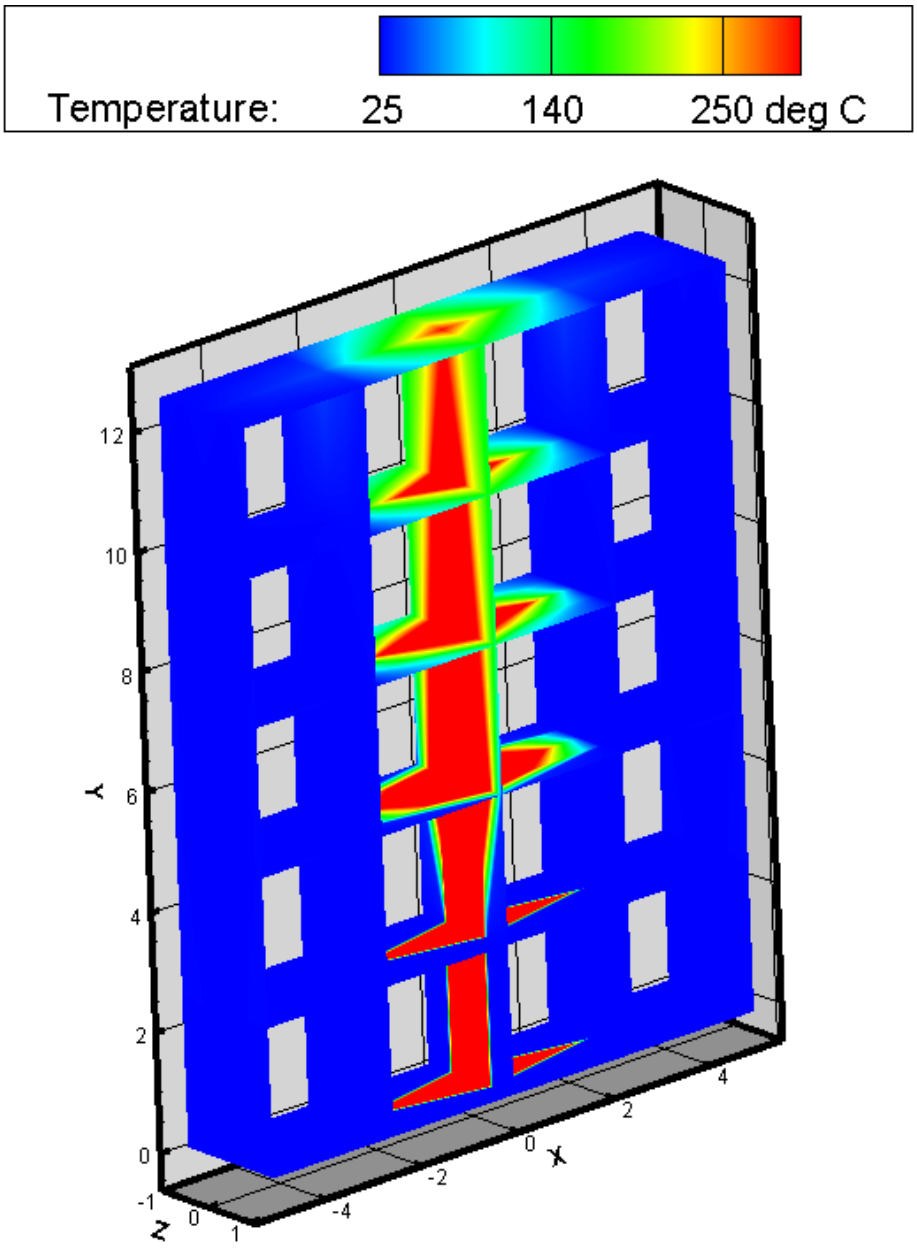

Figure A.80: Three-dimensional temperature gradient: combination of the two-dimensional cross sections of the 1.25 psig flame at 180 degrees

APPENDIX B

RINNAI BURNER DRAWINGS

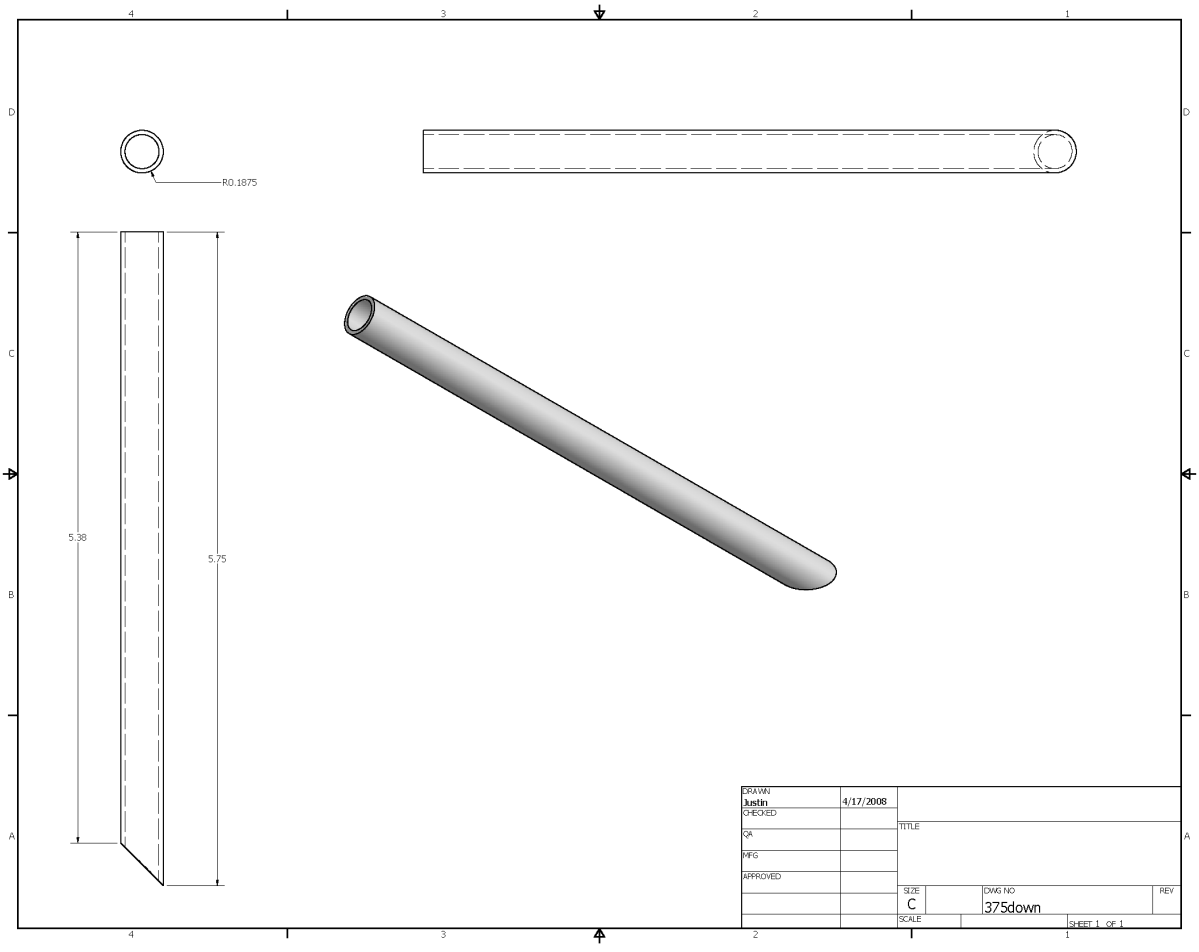

Figure B.1: Sub burners 1 and 2 fuel supply lines

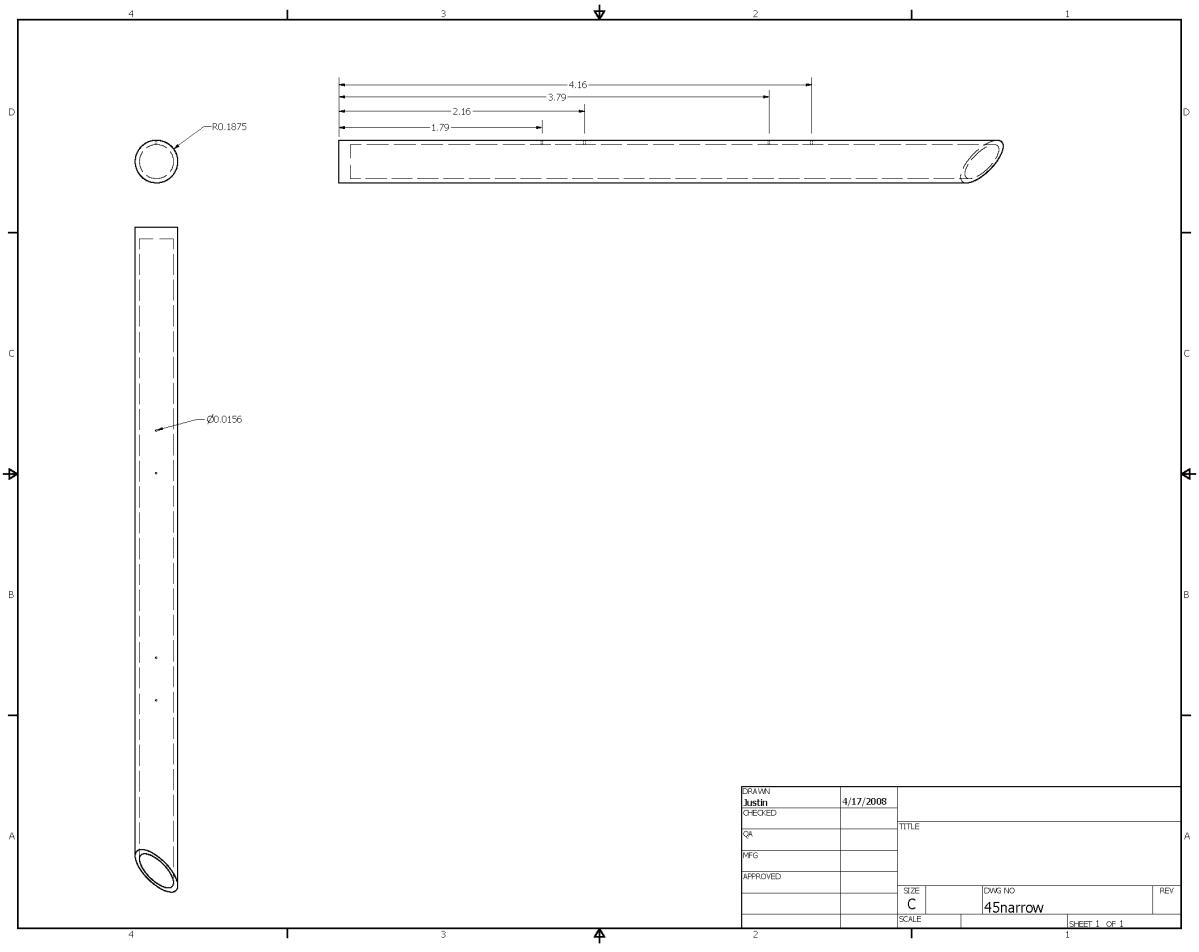

Figure B.2: Sub burner 1

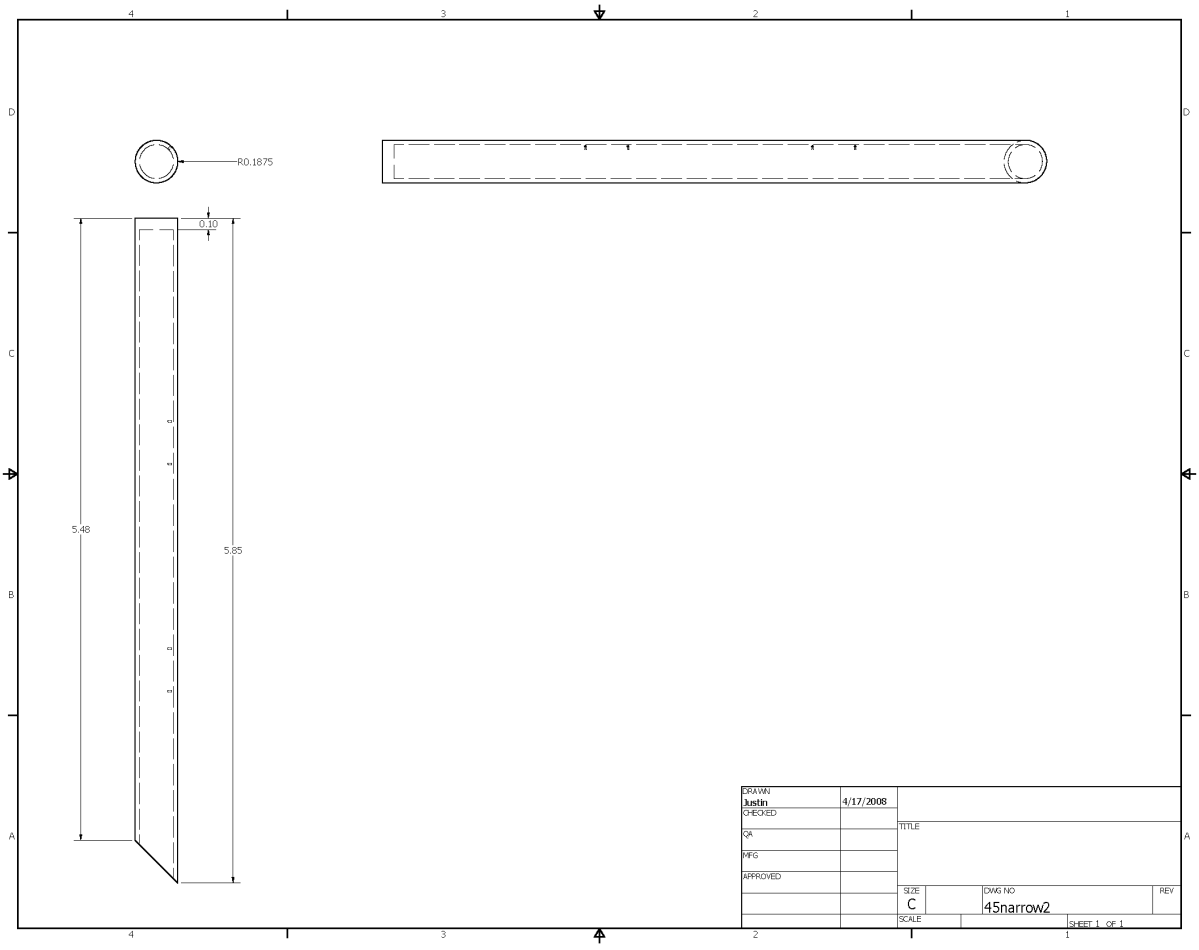

Figure B.3: Sub burner 1

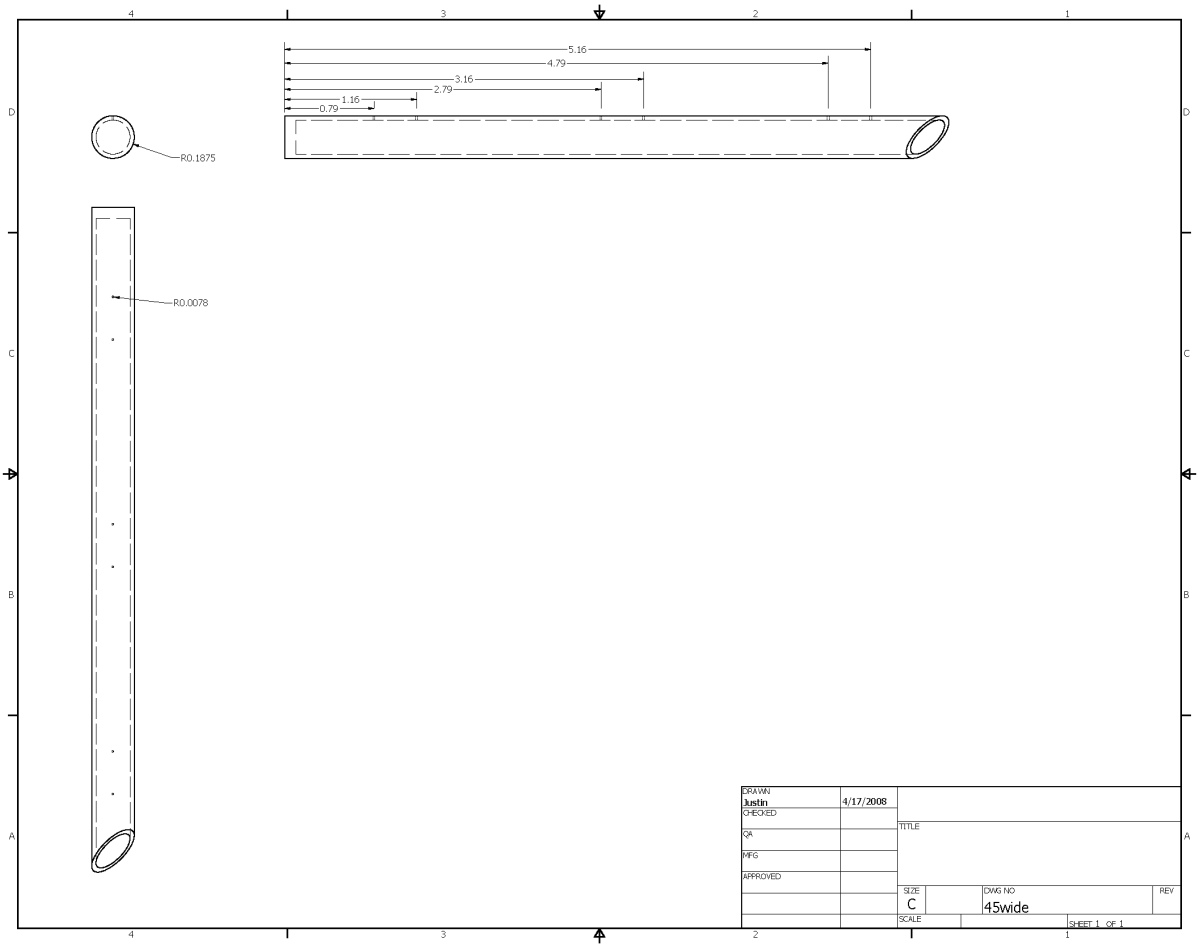

Figure B.4: Sub burner 2

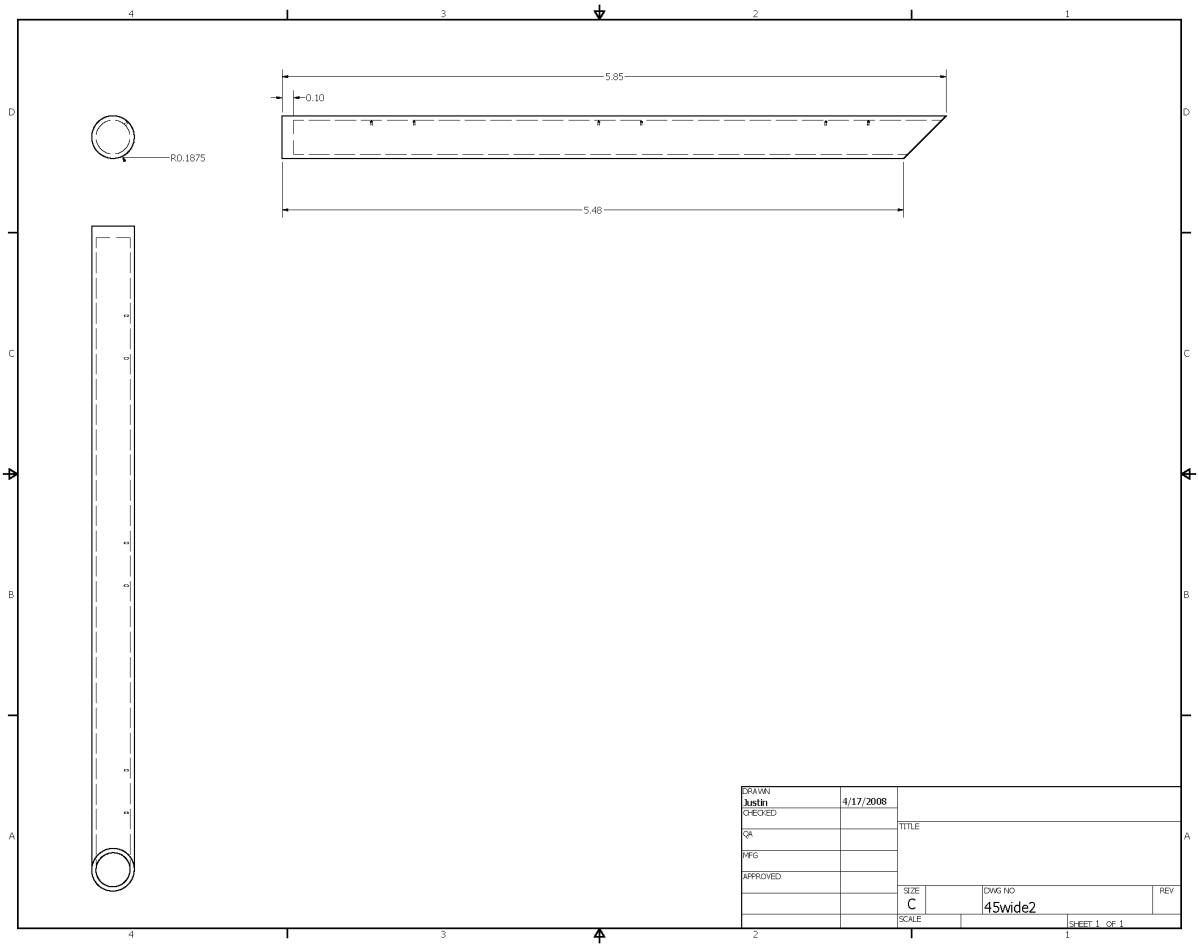

Figure B.5: Sub burner 2

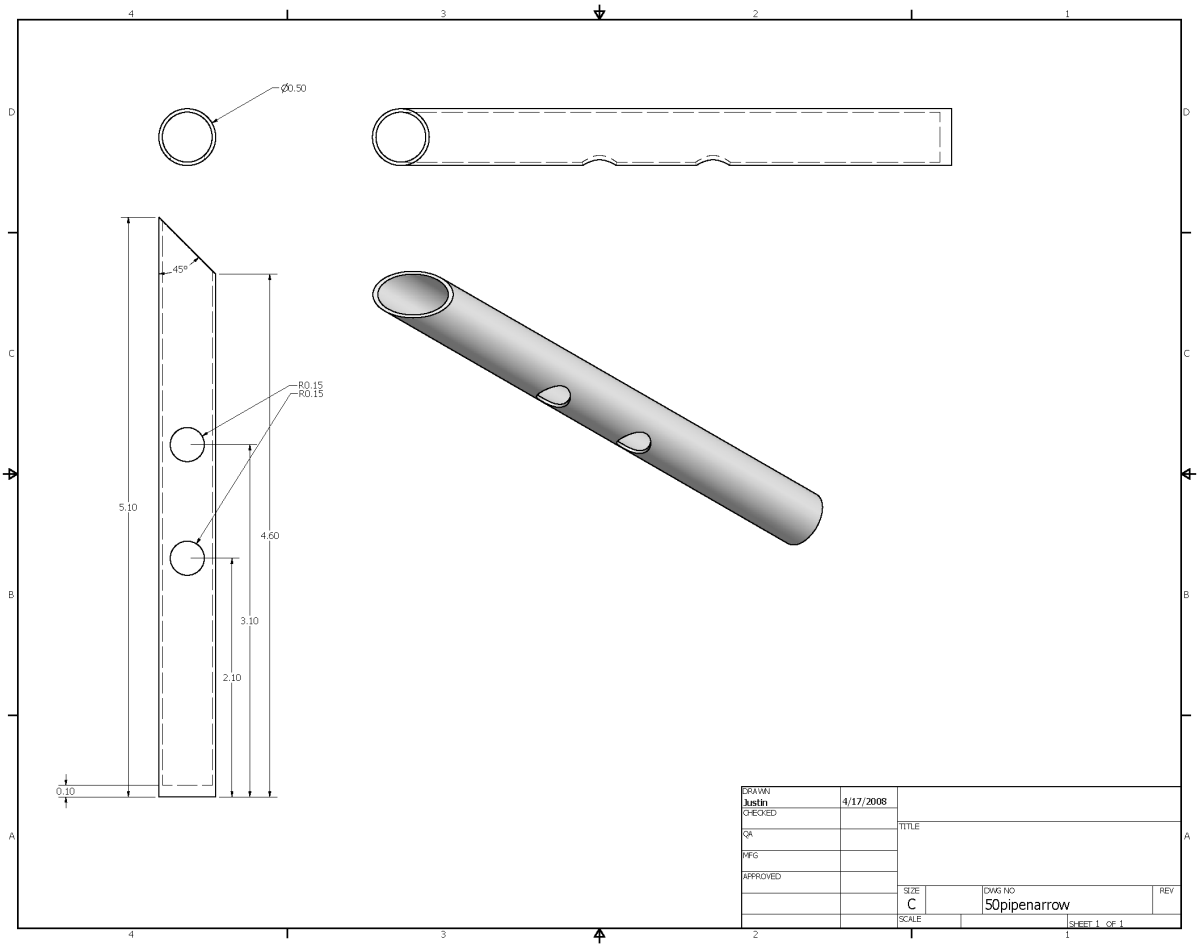

Figure B.6: Sub burner 3 fuel supply line

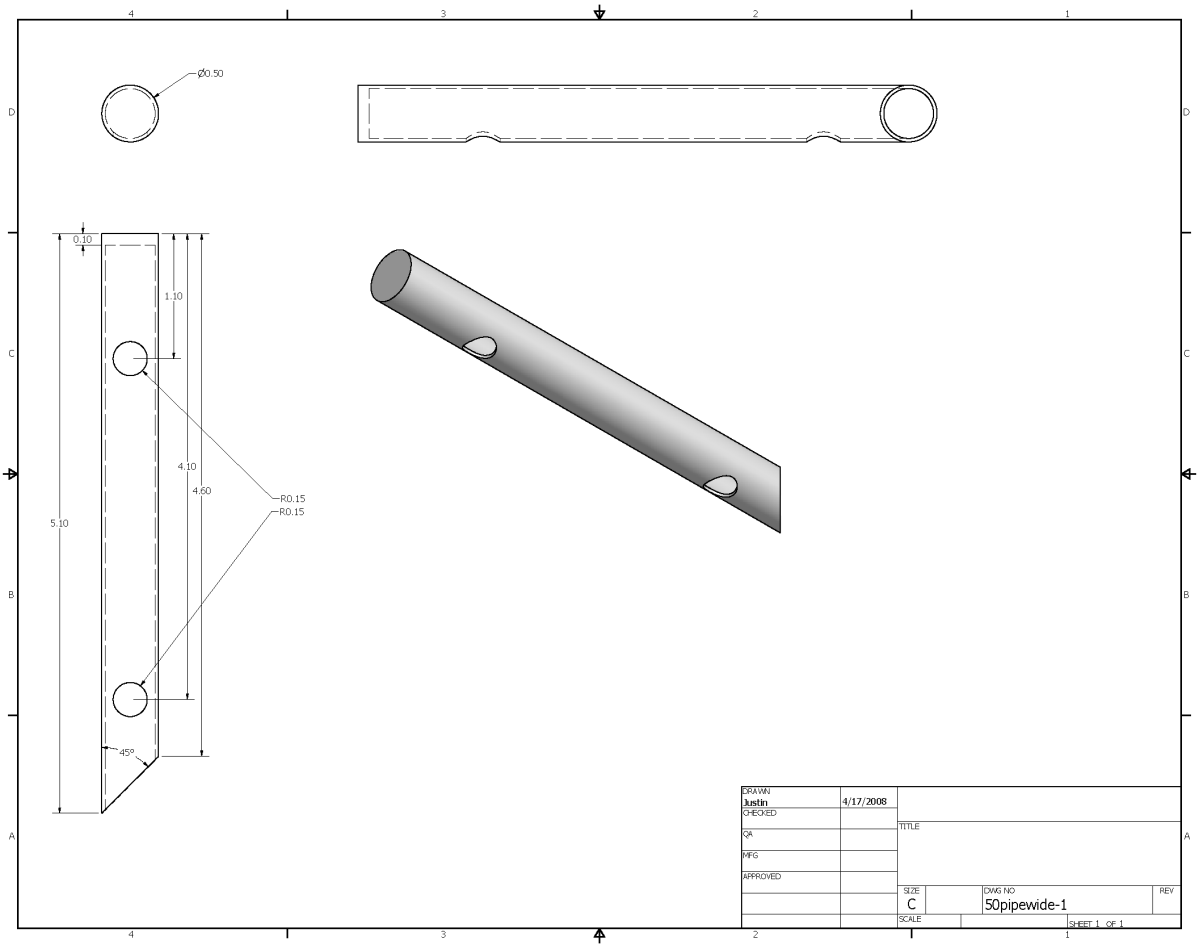

Figure B.7: Sub burner 4 fuel supply line

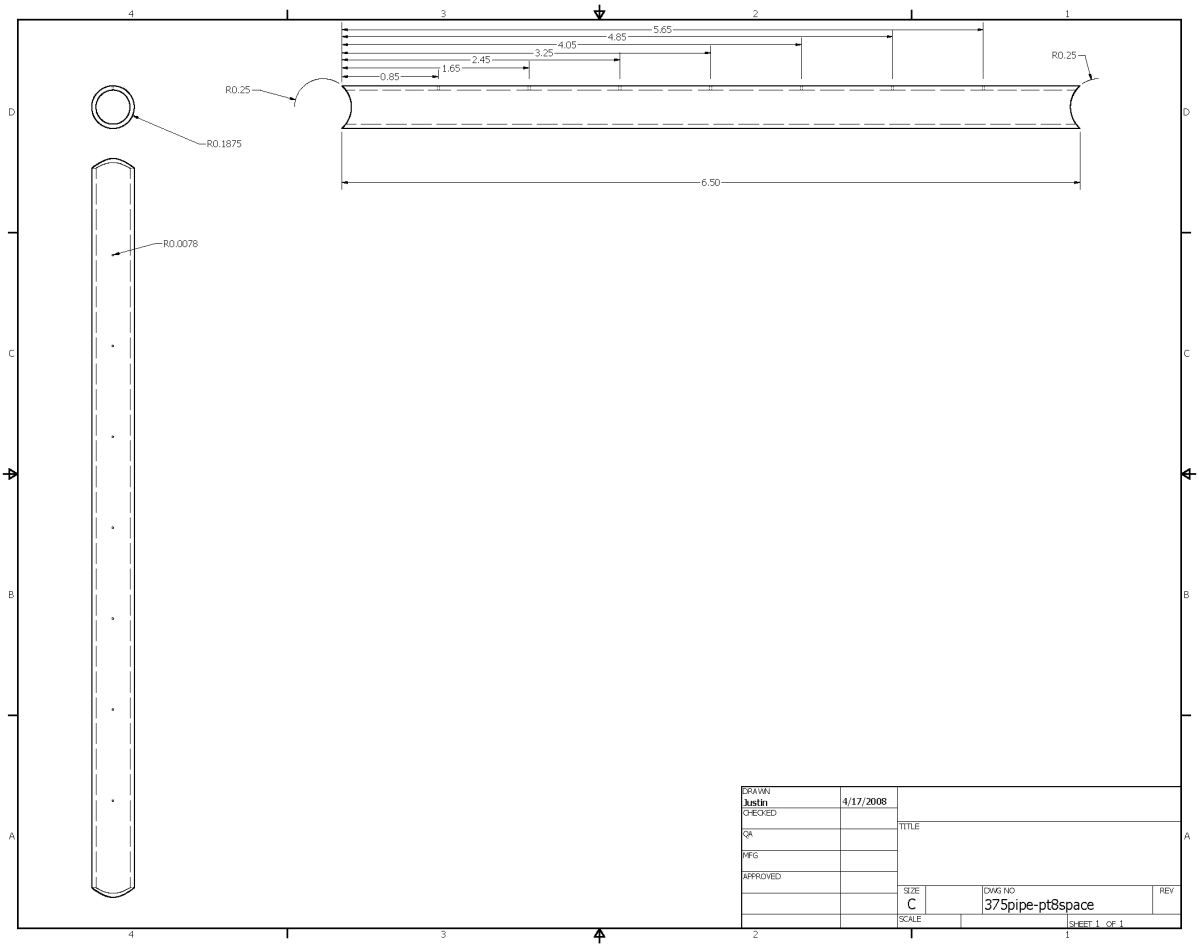

Figure B.8: One of the two orifice tubes of sub burner 3

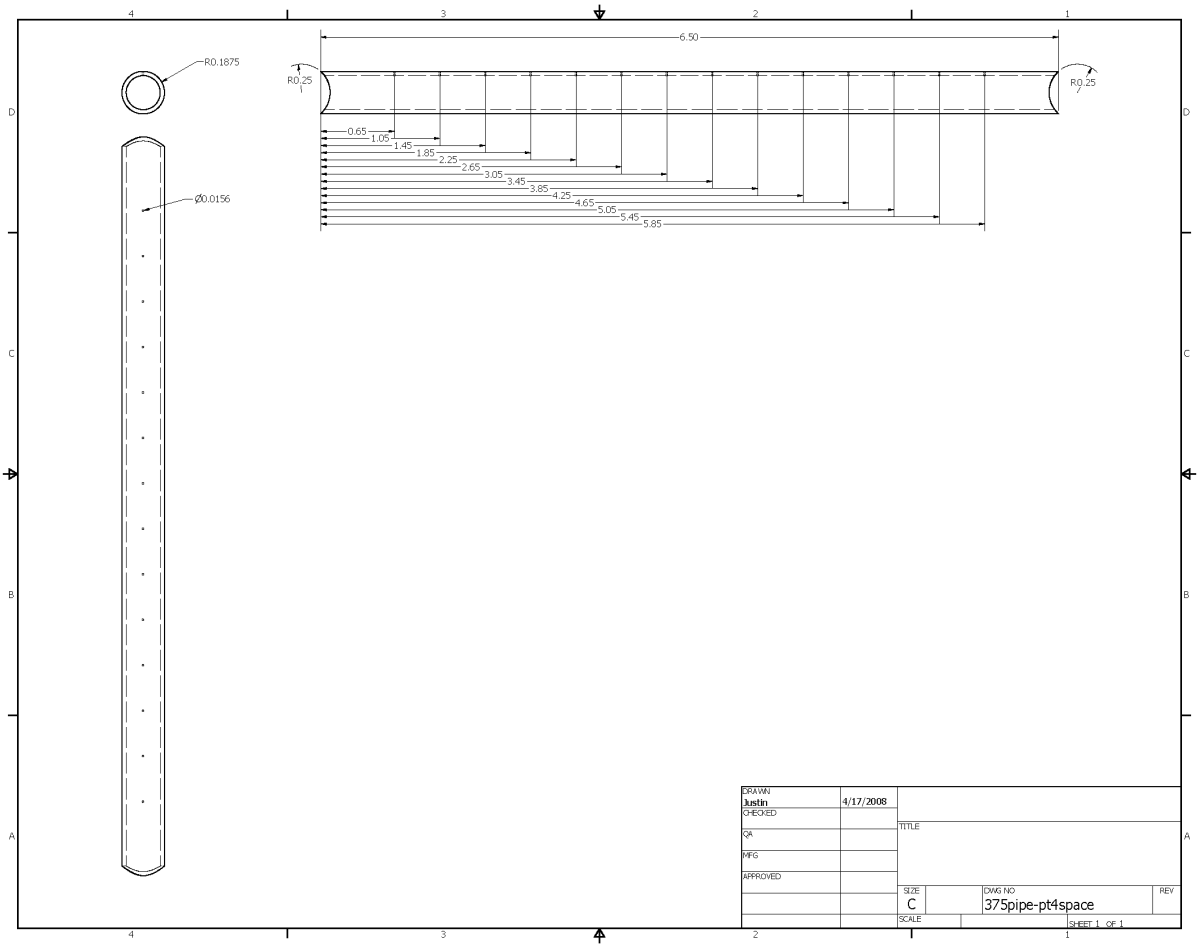

Figure B.9: One of the two orifice tubes of sub burner 4

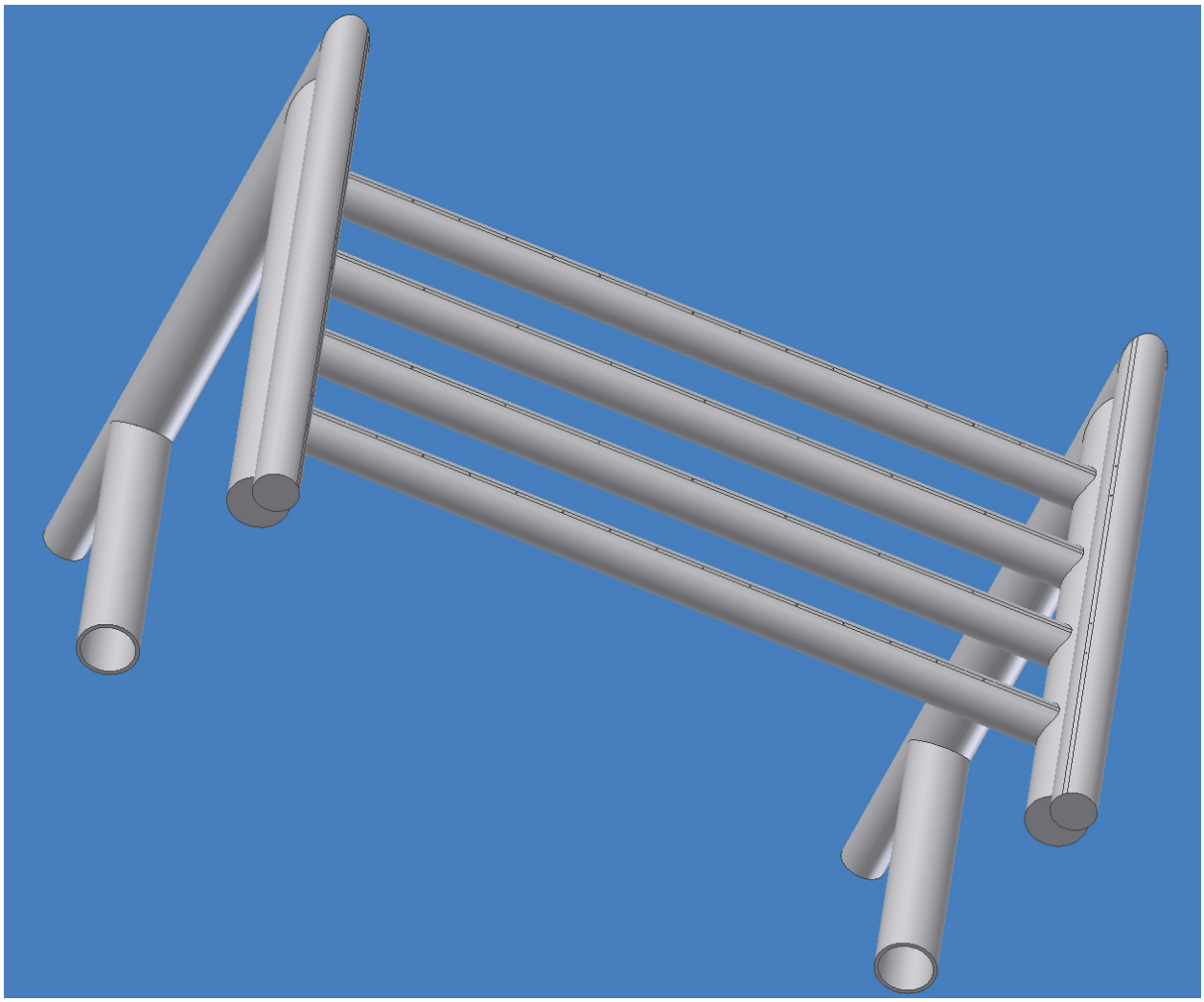

Figure B.10: Full Assembly

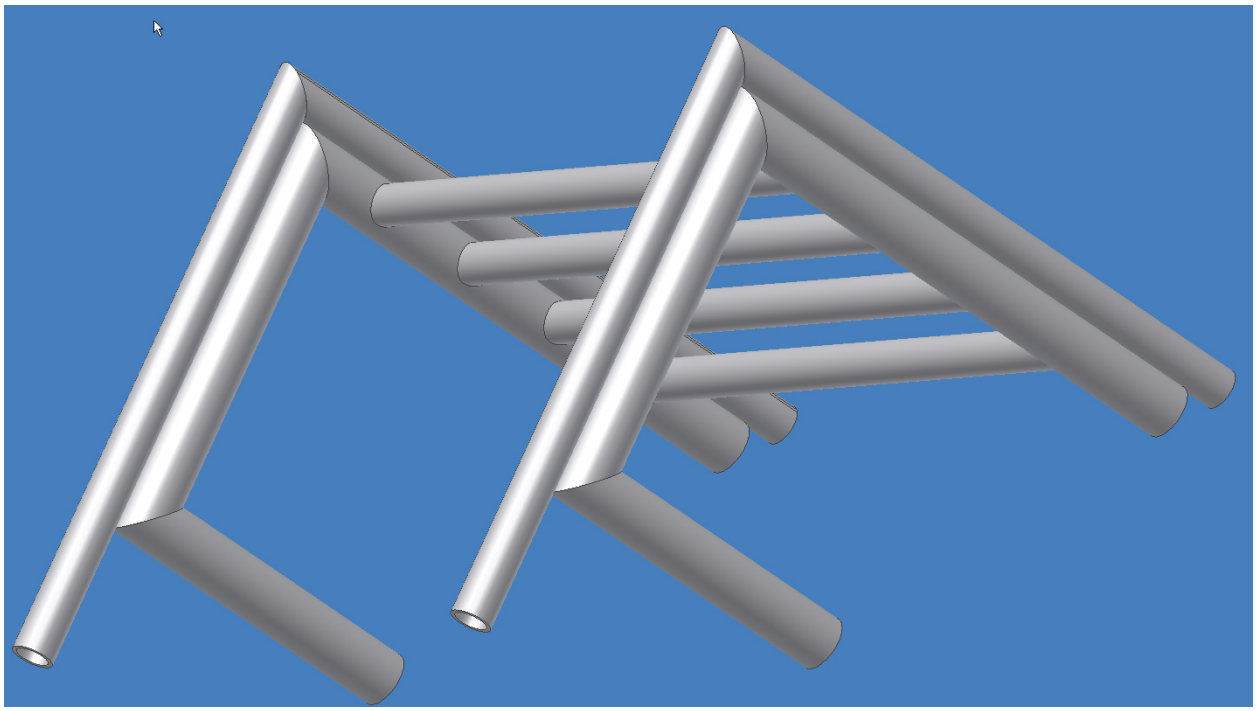

Figure B.11: Full Assembly

APPENDIX C

WATER HEATER TEST RESULTS

C.1 0.25 psig at 63.1 cc/s

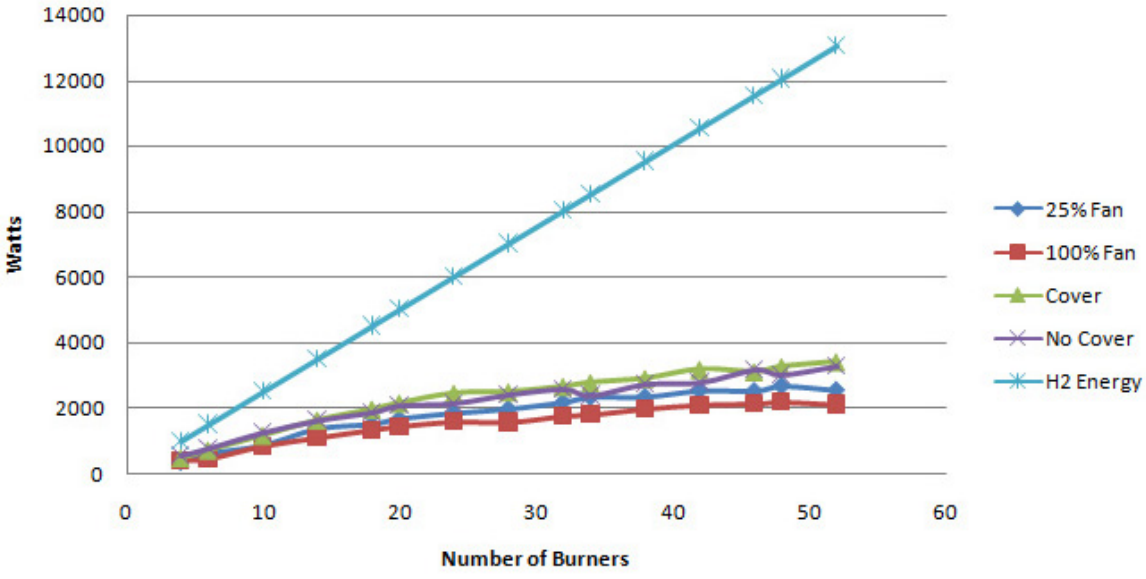

Figure C.1: Absorbed Energy Graphed with Hydrogen Energy Content from Burner

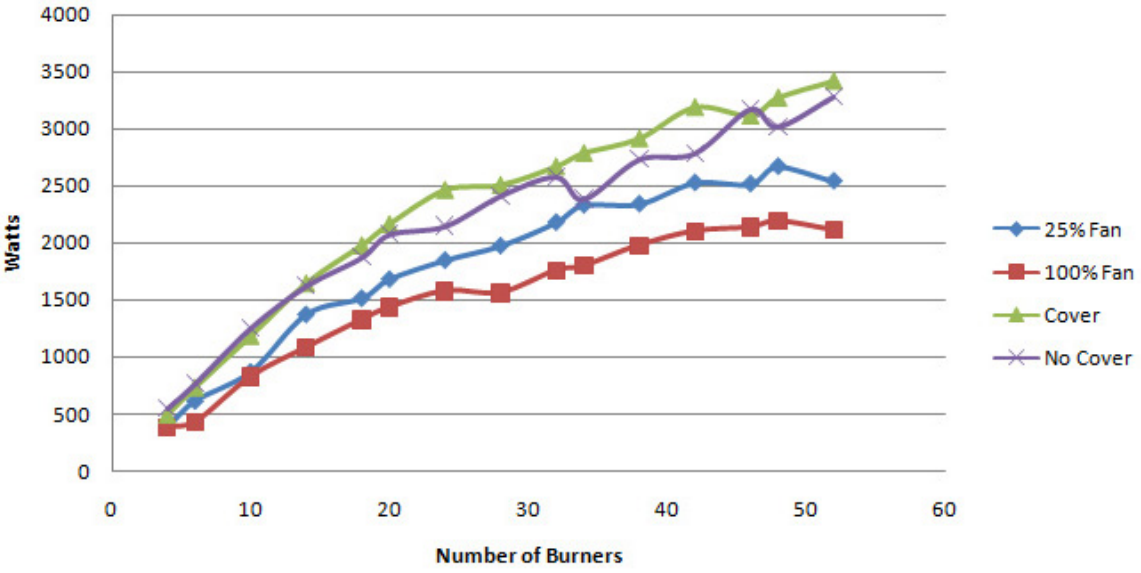

Figure C.2: Absorbed Energy Graphed from Burner

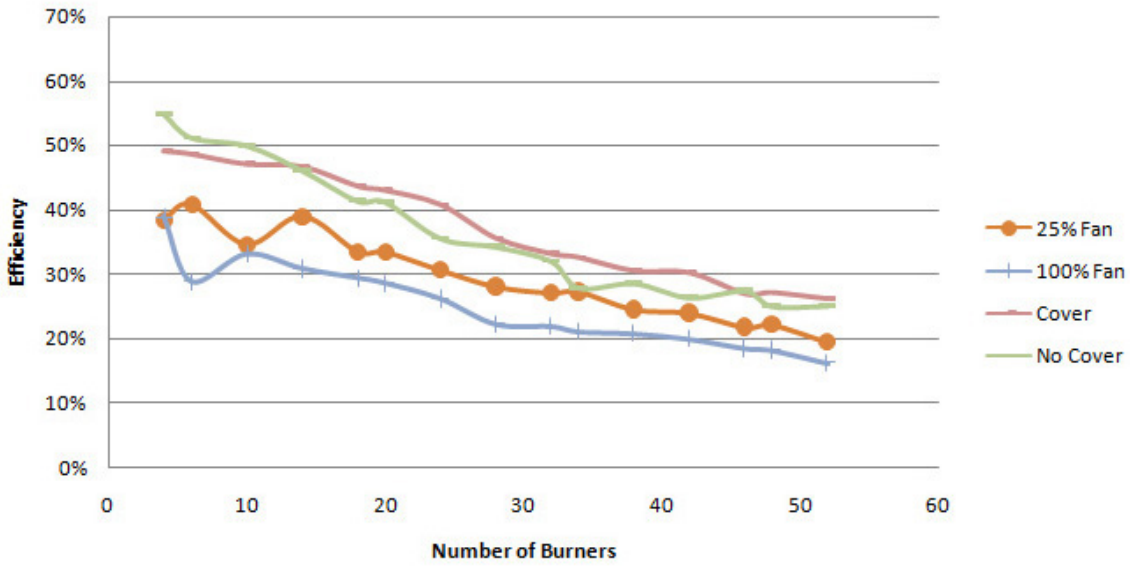

Figure C.3: Burner Efficiency

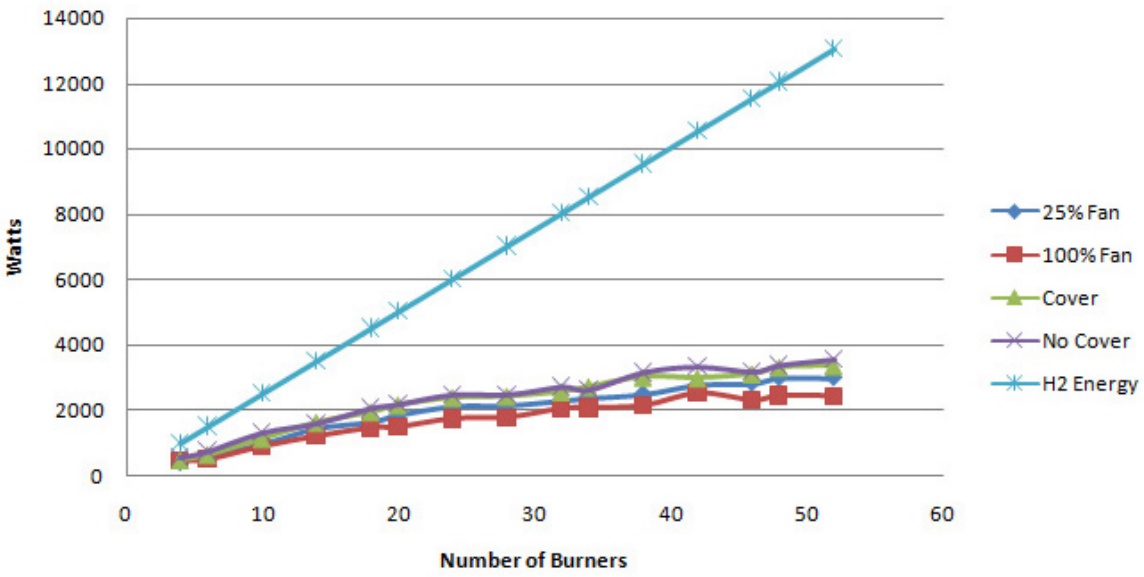

Figure C.4: Absorbed Energy Graphed with Hydrogen Energy Content from Burner

C.2 0.25 psig at 126.2 cc/s

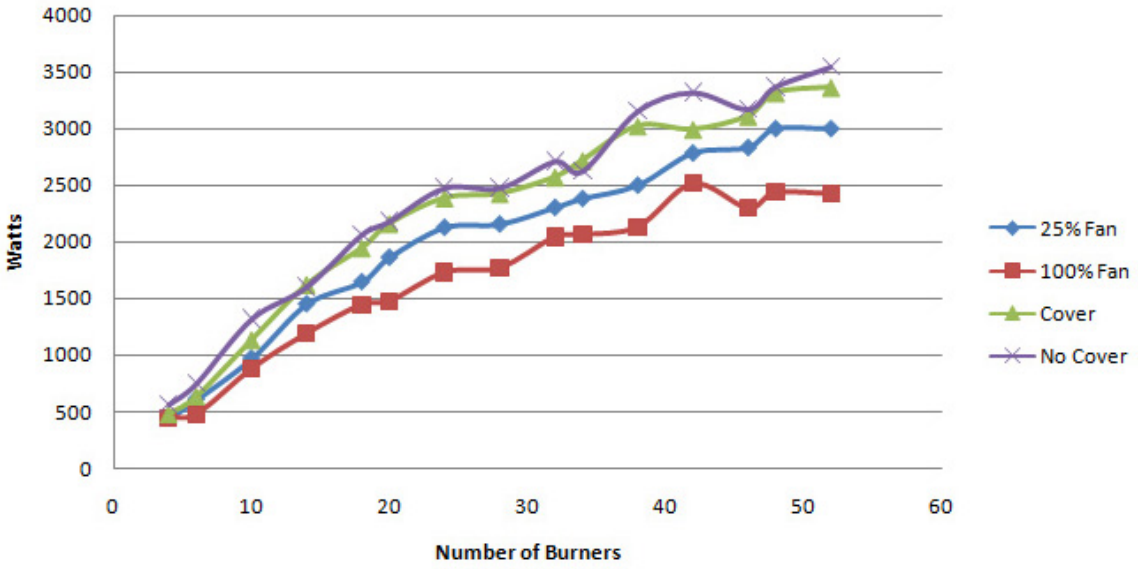

Figure C.5: Absorbed Energy Graphed from Burner

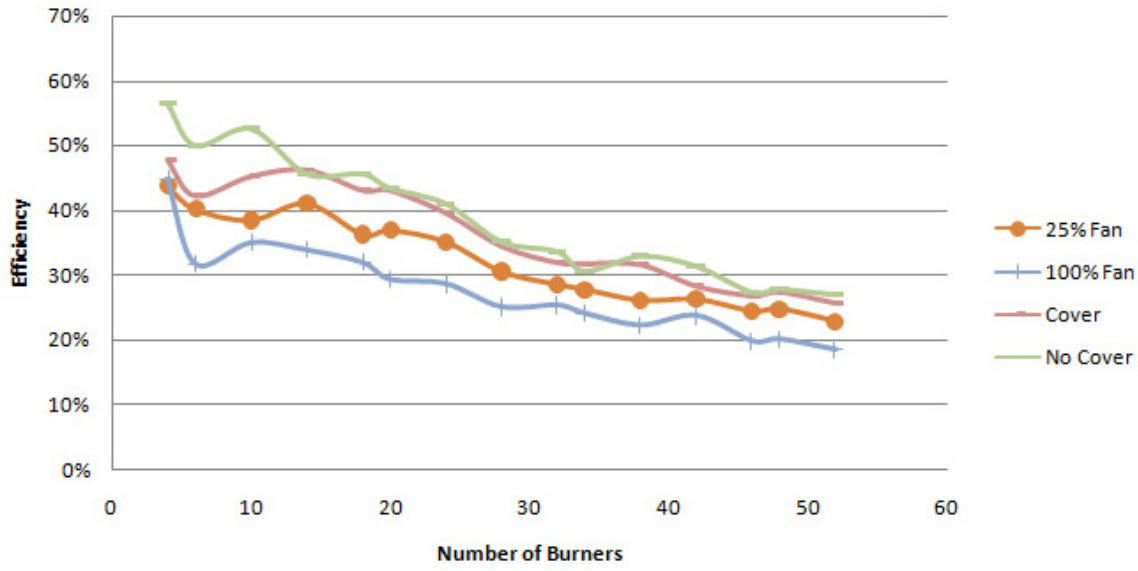

Figure C.6: Burner Efficiency

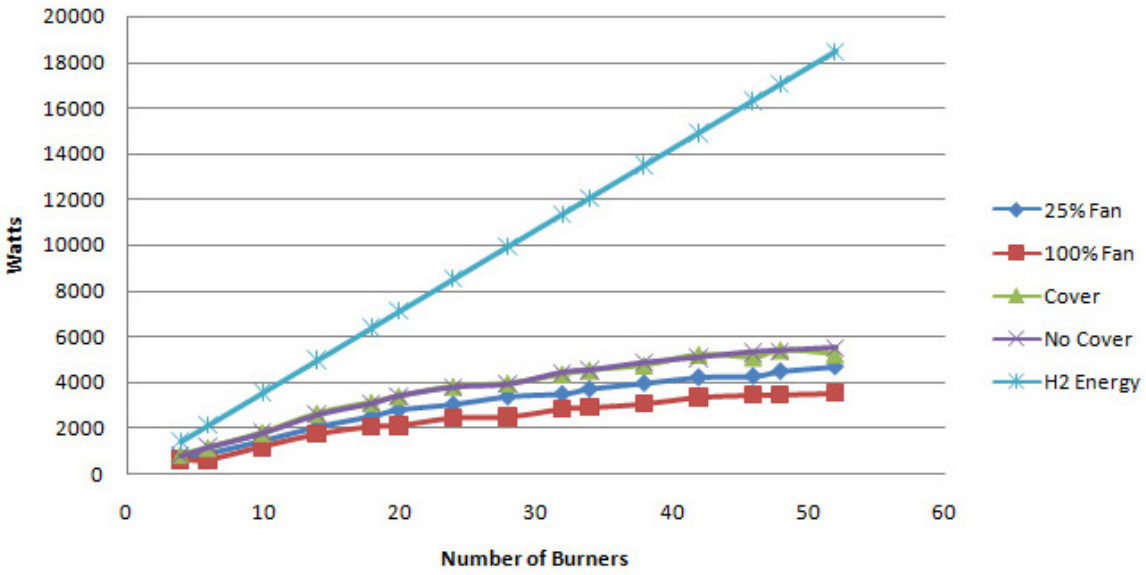

Figure C.7: Absorbed Energy Graphed with Hydrogen Energy Content from Burner

C.3 0.5 psig at 63.1 cc/s

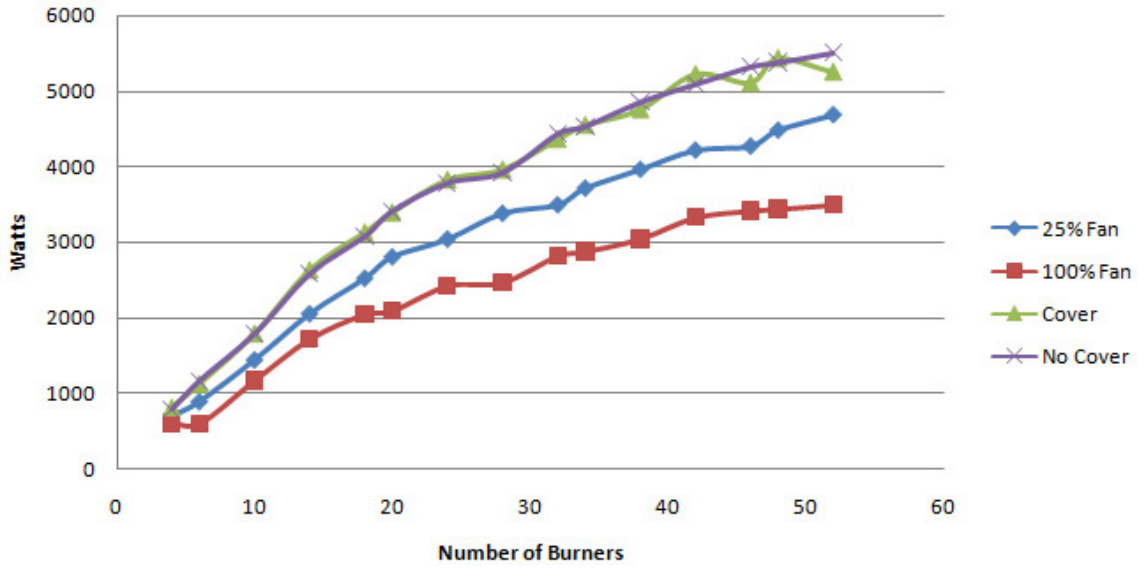

Figure C.8: Absorbed Energy Graphed from Burner

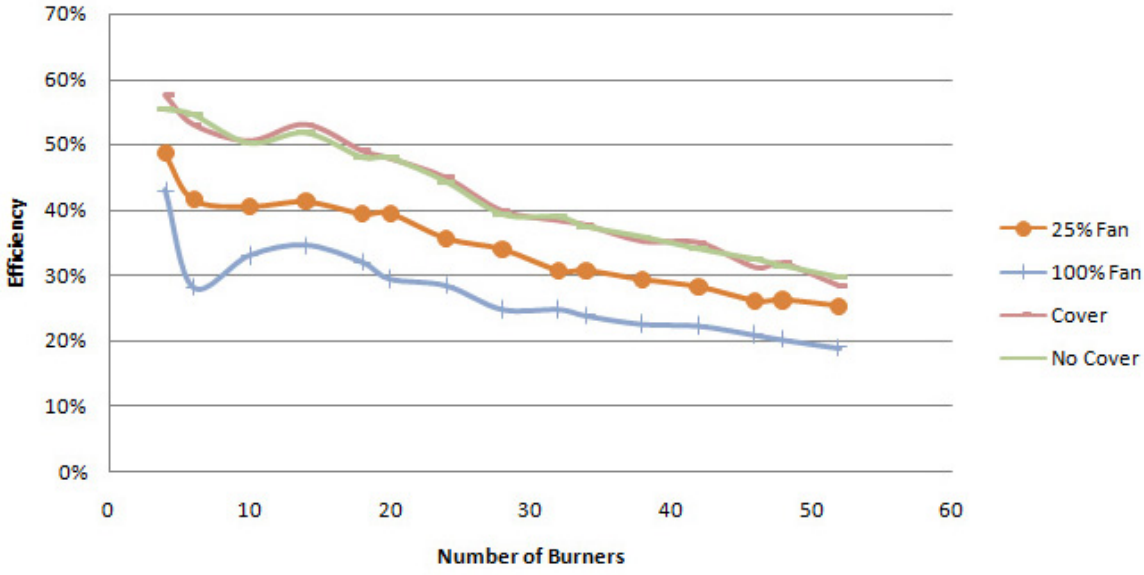

Figure C.9: Burner Efficiency

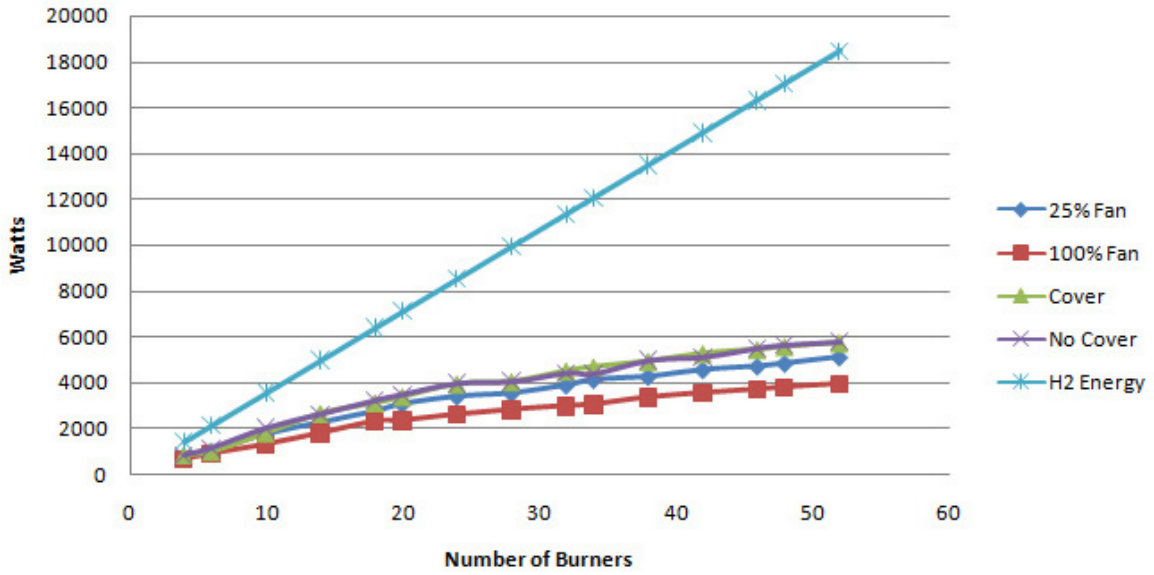

Figure C.10: Absorbed Energy Graphed with Hydrogen Energy Content from Burner

C.4 0.5 psig at 126.2 cc/s

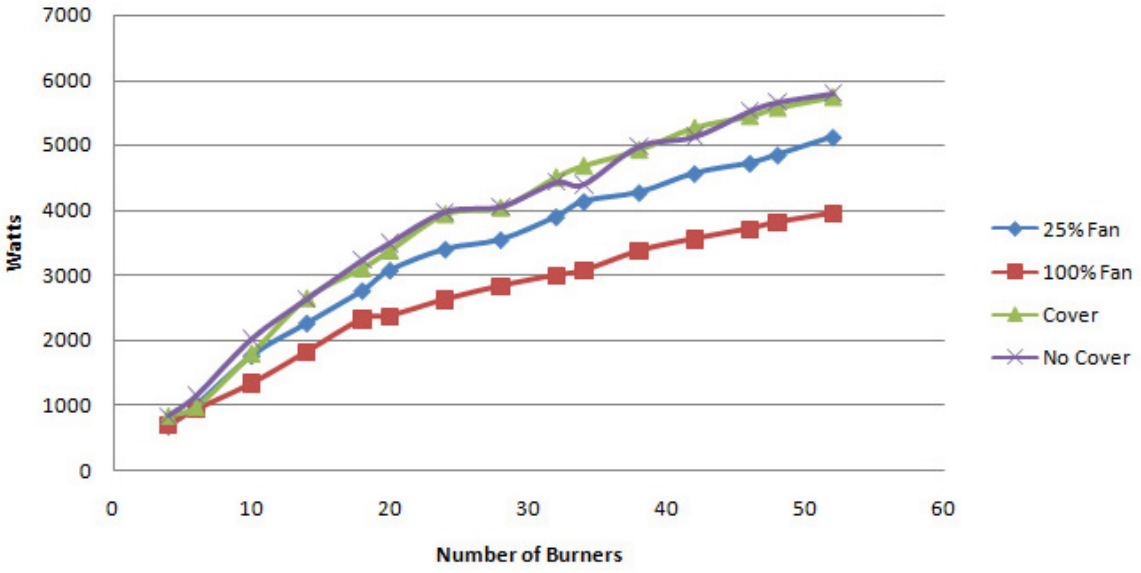

Figure C.11: Absorbed Energy Graphed from Burner

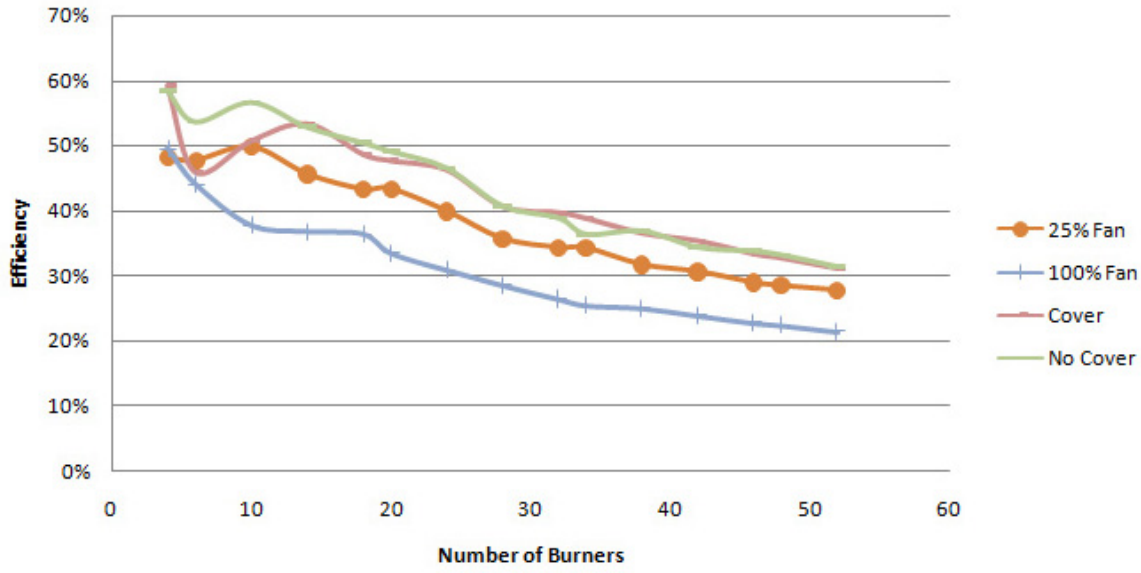

Figure C.12: Burner Efficiency

REFERENCES

[1] OECD/IEA. World energy outlook, 2004. (document), 1.3

[2] J.W.Tester. Sustainable energy, 2005. (document), 1.4

[3] Home energy ratings, 2008. http://www.fsec.ucf.edu/en/consumer/buildings/homes/ratings/improve.htm. (document), 1.6

[4] Energy Information Administration. Official energy statistics from the u.s. government. http://www.eia.doe.gov/emeu/international/contents.html. 1

[5] *BP Statistical Review of World Energy*, June 2008. 1

[6] Average retail fuel prices in the u.s., July 2008. http://www.eere.energy.gov/afdc/data/fuels.html. 1

[7] Intergovernmental Panel on Climate Change. Climate change 2007, 2007. 1

[8] Peter B. Woodbury, Linda S. Heath, and James E. Smith. Carbon sequestration in the u.s. forest sector from 1990 to 2010. *Forest Ecology and Management*, 241:14–27, 2007. 1

[9] T.M. Parris and R.W. Kates. Characterizing and measuring sustainable development. *Annu. Rev. Environ. Resour.*, 28:559–586, 2003. 2

[10] United states green building council. http://www.usgbc.org/. 2, 2

[11] William McDonough and Michael Braungart. *cradle to cradle*. North Point Press, New York, 2002. 2

[12] Structural insulated panel system association. http://www.sips.org/. 2.3

[13] Nas study, 2008. 3.1

[14] Stephen R. Turns. *An Introduction to Combustion*. McGraw-Hill Higher Education, Boston, Massachusetts, second edition, 2000. 3.1, 3.1

[15] A. Bain. Colorless, non-radiant, blameless: A hindenburg disaster study. *Gasbag Journal/Aerostation*, 39, March 1999. 3.1

[16] H.F. Calcote. Spark ignition: Effect of molecular structure. *Ind. Eng. Chem.*, 44:2656–2661, 1952. 3.1

[17] D. Kretschmer and J. Odgers. Fuel correlations for combustion purposes: a summary of progress within the past fifteen years. II. In *Proceedings of the 31st Intersociety*, volume 3, pages 1975–1980. Energy Conversion Engineering Conference, 1996. 3.1

[18] R.W. Schefer, W.G. Houf, B. Bourne, and J. Colton. Spatial and radiative properties of an open-flame hydrogen plume. *International Journal of Hydrogen Energy*, 31:1332–1340, August 2006. 3.1

BIOGRAPHICAL SKETCH

Justin Strahm Kramer was born on July 23, 1983, in Melbourne, Florida, to Kim and Teresa Kramer. In 2006, he received his Bachelors in Mechanical Engineering from Florida State University. He started his graduate studies under Dr. Anjaneyulu Krothapalli and Dr. Brenton Greska immediately after graduation in pursuit of his Masters in Sustainable Energy Engineering.